EVALUATION OF SENSORS FOR ON-LINE MONITORING OF AUTOCLAVE PROCESSING OF POLYMER COMPOSITES

BY

YANG ZHANG

A Thesis Submitted to
the Faculty of Graduate Studies
in Partial Fulfillment of the Requirements for the Degree of

MASTER OF SCIENCE

DEPARTMENT OF MECHANICAL AND MANUFACTURING ENGINEERING

UNIVERSITY OF MANITOBA

WINNIPEG, MANITOBA

THE UNIVERSITY OF MANITOBA

FACULTY OF GRADUATE STUDIES

*****

COPYRIGHT PERMISSION

"Evaluation of Sensors for On-Line Monitoring of Autoclave Processing of Polymer Composites"

BY

Yang Zhang

A Thesis/Practicum submitted to the Faculty of Graduate Studies of The University of Manitoba in partial fulfillment of the requirement of the degree

Of

MASTER OF SCIENCE

ABSTRACT

Conservative and costly cure cycles for processing thermoset composites currently used in aerospace industries ensure that parts are completely cured regardless of the materials used in different parts in a batch and locations of parts cured in an autoclave. Cure cycle optimization is therefore expected to reduce the processing time while maintaining the part quality in order to improve the productive efficiency and reduce the production cost. Material parameters, such as viscosity, gel point, degree of cure, residual strain/stress and modulus, are required to be monitored to control the cure procedure and ensure final part quality. Reliable sensors that can measure these properties of interest accurately and quickly are required for on-line optimization of cure cycles. The objective of this thesis was to evaluate the suitability of the most prospective sensors available in the market that have the potential for use in on-line monitoring of curing process, including the ultrasonic sensor, dielectric sensor, and fiber Bragg grating sensor. A processing mold was designed and fabricated to simulate the autoclave processing environment. Sensors were tested during different cure cycles using both the neat resin and the composite specimens. The response of each type of the sensor was studied and compared with the material parameters measured by additional independent experiments. The sensors have been found to be promising – yet, further development is required before they can be used in on-line monitoring of autoclave processing of polymer composites. Firsthand knowledge and experience on sensors, their installation, data acquisition, data processing, and data analysis have been generated through this study. Based on this knowledge, the advantages and limitations of sensors were evaluated and various issues that should be considered before using these sensors in real industrial environment were discussed.

ACKNOWLEDGEMENTS

Thank you to all my fellow students who encouraged and supported me. Special thanks to:

- Anand Birur for his constant encouragement and support as a labmate.
- Michael Hudek, R. Mark Shead, Madhava Koteshwara and M. A. Balachander for their time in demonstrating the experiment equipment and answering questions on thermal experiments and their thesis.

Many thanks to the employees of the project partners:

- Loren Hendrickson for his help in obtaining the materials used in research work and his knowledge of composites.

I would also like to thank:

- John Van Dorp for his help in setting up experiment equipment.
- Kim Majury for his support for setting up the computer and software.
- Irwin Penner for machining the processing mold and Paul Krueger for his advice in pressure fittings.
- Evangeline Rivera for all her time, help and knowledge in experiments of evaluation of FBG sensors.
- Darryl Stoyko for lending the ultrasonic couplants.
- Robot, Dr. Cheng-kuei Jen of NRC, Quebec and Ahmad Chahbaz of Rd-Tech for their help in answering the technical questions about the ultrasonic monitoring equipment.
- Dave Shepard of Micromet Inc. for his help in answering the technical questions on dielectric monitoring equipment.
- Erica Grice of Sonotech Inc. for providing the ultrasonic couplant samples.
- Dr. Xianwei Zeng in Advanced Composites Processing Lab for his help in answering my technical questions.

Thank you to NSERC, NRC, Boeing Canada Technology, Winnipeg Division and the University of Manitoba for their financial support of this project.

Thank you to my thesis examining committee members: Dr. Gary Wang from the Department of Mechanical and Manufacturing Engineering and Dr. Dimos Polyzois from the Department of Civil Engineering.

Special thanks to:

- Dr. Raghavan Jayaraman, my advisor, for providing me with the opportunity in this program, his valuable guidance and financial support in this project.
- My family, my uncle's family and friends for their encouragement and support during the past years. Without you this project would have been very difficult.

TABLE OF CONTENTS

ABSTRACT i

ACKNOWLEDGEMENT ii

TABLE OF CONTENTS iii

LIST OF FIGURES viii

LIST OF TABLES xiii

LIST OF SYMBOLS xiv

CHAPTER 1 INTRODUCTION 1

1.1 Introduction 1

1.2 Issues in Selection of On-line Sensors 7

1.3 Thesis Objective 11

1.4 Thesis Outline 12

CHAPTER 2 LITERATURE REVIEW 13

2.1 Introduction 13

2.2 Ultrasonic Sensor 14

2.2.1 Principle of Ultrasonic Sensing 14

2.2.2 Application of Ultrasonic Sensors in Cure Monitoring 18

2.3 Dielectric Sensor 24

2.3.1 Principle of Dielectric Sensing 24

2.3.2 Application of Dielectric Sensors in Cure Monitoring 35

2.4 Fiber Bragg Grating (FBG) Sensor 41

2.4.1 Principle of FBG Sensors 41

2.4.2 Application of FBG Sensors in Cure Monitoring 47

2.5 Application of Multi-Sensors in Cure Monitoring 51

2.6 Scope of Thesis 53

CHAPTER 3 EXPERIMENTAL DETAILS 56

3.1 Introduction 56

3.2 Simulation of Autoclave Environment 56

3.3 Materials 62

3.4 Experimental Set-up 65

3.4.1 Ultrasonic Monitoring Test Set-up 65

3.4.2 Dielectric Monitoring Test Set-up 72

3.4.3 Fiber Bragg Grating Sensor Sensing Test Set-up 76

3.5 Experimental 79

3.5.1 Specimen Preparation 79

3.5.1.1 Near Resin Specimen Preparation 79

3.5.1.2 Composite Specimen Preparation 80

3.5.2 Sensor Embedment 83

3.5.2.1 Sensor Embedment in Neat Resin Specimens 83

3.5.2.2 Sensor Embedment in Composite Specimens 84

3.6 Cure Cycles 86

CHAPTER 4 RESULTS 90

4.1 Introduction 90

4.2 Cure Monitoring with a Single Sensor 91

4.2.1 Ultrasonic Cure Monitoring 91

4.2.1.1 Ultrasonic Response of Neat Resin Specimen (Cure Cycle 3, R934 T-05) 91

4.2.1.2 Ultrasonic Response of Composite Specimen (Cure Cycle 8, HMF T-22) 100

4.2.1.3 Ultrasonic Monitoring Data for Neat Resin and Composite Specimens 104

4.2.1.4 Modulus Measurement Using Ultrasonic Sensor 107

4.2.2 Dielectric Cure Monitoring 112

4.2.2.1 Dielectric Response of Neat Resin Specimen (Cure Cycle 1, R934 T-01) 112

4.2.2.2 Dielectric Response of Composite Specimen (Cure Cycle 10, HMF T-24) 120

4.2.2.3 Dielectric Monitoring Data for Neat Resin and Composite Specimens 121
4.2.2.4 Dielectric Response of Neat Resin Specimens in Isothermal Experiments 123
4.2.3 FBG Sensor Cure Monitoring 128
4.3 Sensor Evaluation Using a Combination of Sensors 137
4.3.1 Ultrasonic and dielectric monitoring results for neat resin specimen .. 137
4.3.2 Ultrasonic and dielectric monitoring results for composite specimen .. 138
4.4 Summary of Monitoring Results 140

CHAPTER 5 DISCUSSION 143
5.1 Introduction 143
5.2 Monitoring Result Analysis 143
5.2.1 Degree of Cure and Viscosity 143
5.2.2 Viscosity Minimum 145
5.2.3 Gelation 145
5.2.4 End of Cure 146
5.2.5 Glass Transition Temperature (T_g) and Vitrification 147
5.2.6 Modulus 149
5.2.7 Process Induced Residual Strain 149
5.3 Issues Related to Industrial Applicability of Sensors 150
5.3.1 Issues in Using Ultrasonic Sensor 150
5.3.1.1 Sensor and Installation Issues 150
5.3.1.1.1 Clamping Pressure 150
5.3.1.1.2 Ultrasonic Couplant 151
5.3.1.1.3 Ultrasonic Transducer Selection 152
5.3.1.1.4 Issues Related to Change in Ultrasonic Wave Velocities ... 154
5.3.1.2 Experimental Issues 155
5.3.1.2.1 Specimen Quality 155
5.3.1.2.2 Specimen Thickness 158
5.3.1.3 Data Processing Issues 159

5.3.1.3.1 Issues Related to Identification of Maxima/Minima or Inflection Values 159
5.3.1.3.2 Data Processing 160
5.3.2 Issues in Using Dielectric Sensor 161
5.3.2.1 Sensor and Installation Issues 161
5.3.2.1.1 Sensor Selection 161
5.3.2.1.2 Comparison of Ultrasonic and Dielectric Sensors 162
5.3.2.2 Experimental Issues 164
5.3.2.2.1 Influence of Resin Flow on Dielectric Monitoring 164
5.3.2.2.2 Fundamental Relationship 164
5.3.2.3 Data Processing Issues 165
5.3.2.3.1 Result Analysis 165
5.3.2.3.2 Data Processing 166
5.3.3 Issues Related to Use of FBG Sensor 167
5.3.3.1 Sensor and Installation Issues 167
5.3.3.1.1 FBG Sensors 167
5.3.3.1.2 Alignment of FBG Sensor 167
5.3.3.1.3 Effects of Transverse Strains and Thermal Response of FBG Sensors 168
5.3.3.1.4 The Advantages and Limitations of FBG Sensors 169
5.3.3.2 Data Processing Issues 170

CHAPTER 6 CONCLUSIONS AND RECOMMENDATIONS 171
6.1 Introduction 171
6.2 Conclusions 171
6.3 Recommendations 174

REFERENCES 177

APPENDIX A THEORY OF OPERATIONAL PRINCIPLES FOR VARIOUS SENSORS 184
A.1 Ultrasonic Sensors 184

A.1.1 Frequency, Period, Wavelength and Velocity of Ultrasonic Wave ... 184
A.1.2 Types of Ultrasonic Waves 184
A.1.3 Attenuation of Ultrasonic Waves 186
A.1.4 Acoustic Impedance 186
A.1.5 Reflection and Transmission of Ultrasonic Waves at a Boundary 187
A.1.6 Generation of Ultrasonic Waves 190
A.2 Dielectric Sensors 191
A.2.1 Classic Debye Equations of Dielectric Response 191
A.2.2 Division of Dielectric Sensors 198
A.3 Optical Fiber Sensors 199
A.3.1 Mode of Optical Fibers 199
A.3.2 Classification of Optical Fiber Sensors 200
A.3.3 Sensor Interrogation Techniques 202

APPENDIX B MORE INFORMATION FOR EXPERIMENTAL DETAILS .. 204
B.1 FEM Analysis Results for Processing Mold 204
B.2 Determination of Ultrasonic Time Delay and Amplitude Using Sensing Data 205
B.2.1 Ultrasonic Time Delay 205
B.2.2 Ultrasonic Amplitude 207

APPENDIX C MORE MONITORING RESULTS 208
C.1 Ultrasonic Cure Monitoring 208
C.1.1 Ultrasonic Response of Neat Resin Specimen 208
C.1.2 Ultrasonic Response of Composite Specimen 212
C.2 Dielectric Cure Monitoring 218
C.2.1 Dielectric Response of Neat Resin Specimen 218
C.2.2 Dielectric Response of Composite Specimen 220
C.2.3 Dielectric Response of Neat Resin Specimens in Isothermal Experiments 221
C.3 FBG Sensor Cure Monitoring 234

LIST OF FIGURES

Figure 1.1 Typical autoclave used in the manufacturing of composite 3

Figure 1.2 Prepreg and vacuum bag lay-up for autoclave processing 4

Figure 1.3 A vacuum bagged uncured composite in an autoclave 4

Figure 1.4 A typical cure cycle 5

Figure 1.5 The resin before and after cross-linking reaction 6

Figure 1.6 Viscosity data of a composite specimen 9

Figure 2.1 Principle of ultrasonic sensing 15

Figure 2.2 Fundamental dielectric measurement scheme 25

Figure 2.3 The Cole – Cole plot or arc diagram 31

Figure 2.4 The effect of the ionic conductivity to the Cole – Cole plot 33

Figure 2.5 Boundary layer effects 35

Figure 2.6 The extrapolation method used to determine the vitrification point 38

Figure 2.7 Structure of an optical fiber with Bragg grating 42

Figure 2.8 Extrinsic and intrinsic systems 44

Figure 2.9 Bragg grating principle operation 45

Figure 3.1 The processing mold 57

Figure 3.2 Experimental Setup 60

Figure 3.3 Pressure fitting used in experiments 61

Figure 3.4 Ultrasonic monitoring set-up 68

Figure 3.5 CUB ultrasonic immersion inspection system 69

Figure 3.6 Ultrasonic signal of a cured composite laminate 71

Figure 3.7 Ultrasonic amplitude data for a resin specimen 71

Figure 3.8 IDEX fringe measurement sensors 73

Figure 3.9 Dielectric and ultrasonic monitoring test set-ups 75

Figure 3.10 log Permittivity data for a composite specimen 76

Figure 3.11 FBG sensor 77

Figure 3.12 SHM 5100A system 78

Figure 3.13 Vacuum bagging and sensor embedment (cured composite specimen) .. 82
Figure 3.14 Sensor embedment for neat resin specimens 84
Figure 3.15 Sensor embedment composite specimens 86
Figure 3.16 The manufacturer recommended cure cycle (MRC) 87
Figure 4.1 Part temperature and predicted degree of cure for cure cycle R934 T-05 . 92
Figure 4.2 Predicted viscosity for cure cycle R934 T-05 90
Figure 4.3 Waveforms obtained from the resin specimen in cure cycle R934 T-05 ... 94
Figure 4.4 Ultrasonic signals recorded in the A-Scan mode at various discrete process time 95
Figure 4.5 Time delay and attenuation obtained from the resin specimen in cycle R934 T-05 98
Figure 4.6 Modulus of the neat resin specimen during curing in cycle R934 T-05 ... 99
Figure 4.7 Ultrasonic response of fiberglass resin specimens cured isothermally at room temperature 100
Figure 4.8 Part temperature and predicted degree of cure for cure cycle HMF T-22 . 101
Figure 4.9 Predicted viscosity for cure cycle HMF T-22 101
Figure 4.10 Time delay and attenuation obtained from the composite specimen in cycle HMF T-22 103
Figure 4.11 Modulus of the neat resin specimen during curing in cycle HMF T-22 .. 103
Figure 4.12 Ultrasonic response of composite specimens with 6 and 12 plies of laminas 104
Figure 4.13 Part temperature and degree of cure of neat resin and composite specimens (R934 T-05 and HMF T-17) 106
Figure 4.14 Ultrasonic attenuation data of neat resin and composite samples (R934 T-05 and HMF T-17) 107
Figure 4.15 Part temperature and predicted degree of cure in cycle R934 T-01 113
Figure 4.16 log Loss Factor at 500 Hz for cure cycle R934 T-01 115
Figure 4.17 log Permittivity at 500 Hz for cure cycle R934 T-01 115
Figure 4.18 log Loss Factor for cure cycle R934 T-01 116
Figure 4.19 log Permittivity for cure cycle R934 T-01 116
Figure 4.20 log Ionic Conductivity obtained in cycle R934 T-01 117
Figure 4.21 The comparison between the ionic viscosity and mechanical viscosity in cycle R934 T-01 119
Figure 4.22 log Ionic Viscosity and dlog IV/dt data for cycle R934 T-01 119
Figure 4.23 Part temperature and predicted degree of cure for cycle HMF T-24 120

Figure 4.24 log Ionic Viscosity and dlog IV/dt data for cycle HMF T-24 121
Figure 4.25 Part temperature and degree of cure of neat resin and composite specimens (R934 T-05 and HMF T-13) 122
Figure 4.26 log Ionic Conductivity and dlog IV/dt data of neat resin and composite specimens (R934 T-05 and HMF T-13) 123
Figure 4.27 Isothermal experiments with 934 neat resin system 125
Figure 4.28 log Loss Factor data for cycle R934 T-08 127
Figure 4.29 log Permittivity data for cycle R934 T-08 127
Figure 4.30 Part temperature and predicted degree of cure for cycle HMF T-25 129
Figure 4.31 Sensitivity of FBG sensors to temperature 130
Figure 4.32 Total strain measured in cycle HMF T-15 131
Figure 4.33 Thermal expansion of FBG sensor (constant sensitivity coefficient to temperature) 132
Figure 4.34 Total strain measured in cycle HMF T-25 vs. cure temperature 133
Figure 4.35 Variation of sensor response with temperature in cooling stage in cycle HMF T-25 134
Figure 4.36 Modeling of the composite sample used in experiments 135
Figure 4.37 Ultrasonic and dielectric response of neat resin sample in cycle R934 T-05 138
Figure 4.38 Ultrasonic and dielectric response of composite samples in cycle HMF T-12 and HMF T-13 139
Figure 4.39 Part temperature and degree of cure of composite specimens (HMF T-12 and HMF T-13)..... 139
Figure 5.1 Time delay and attenuation for the resin specimen in cycle R934 T-05 ... 144
Figure 5.2 Weakened ultrasonic signals after several experiments 152
Figure 5.3 Ultrasonic response of combined mode transducer to aluminum plate ... 153
Figure 5.4 Comparison of the ultrasonic response of specimens with and without caul plate (Cycle 7 (HMF T-17) and Cycle 8 (HMF T-22)) 158
Figure 5.5 The dielectric sensor embedded in a composite specimen 162
Figure 5.6 The FBG sensor embedded in a composite specimen 168
Figure A.1 Longitudinal wave 185
Figure A.2 Transverse wave 185
Figure A.3 Reflection and transmission of ultrasonic waves at a boundary 188
Figure A.4 Reflection and transmission of an ultrasonic wave at oblique incidence . 190
Figure A.5 Model of a polymeric material under test 192

Figure A.6 The Debye response as a function of $\omega\tau$ 197
Figure A.7 The Cole – Cole plot or arc diagram 197
Figure A.8 Bulk and fringe measurement sensors 199
Figure A.9 Three basic types of optical fiber waveguides 201
Figure A.10 Classification of optical fiber sensors 202
Figure B.1 FEM analysis for top plate 204
Figure B.2 FEM analysis for bottom plate 205
Figure B.3 Determination of ultrasonic time delay 206
Figure B.4 Determination of ultrasonic amplitude 207
Figure C.1 Specimen temperature and predicted degree of cure for cure cycle R934 T-04 208
Figure C.2 Predicted viscosity for cure cycle R934 T-04 209
Figure C.3 Time delay and attenuation obtained for the resin specimen in cycle R934 T-04 210
Figure C.4 Time delay and attenuation vs. DOC for the resin specimen in cycle R934 T-04 211
Figure C.5 Variation of the main bang with the cure temperature in cycle R934 T-04 212
Figure C.6 Part temperature and predicted degree of cure for cycle HMF T-12 213
Figure C.7 Time delay and attenuation obtained from the composite specimen in cycle HMF T-12 214
Figure C.8 Part temperature and predicted degree of cure for cure cycle HMF T-16. 215
Figure C.9 Time delay and attenuation obtained from the composite specimen in cycle HMF T-16 216
Figure C.10 Part temperature and predicted degree of cure in cycle HMF T_17 217
Figure C.11 Time delay and attenuation obtained from the composite specimen in cycle HMF T-17 218
Figure C.12 log Ionic Viscosity and dlog IV/dt obtained in cycle R934 T-05 219
Figure C.13 Part temperature and predicted degree of cure for cure cycle HMF T-13 220
Figure C.14 log Ionic Viscosity and dlog IV/dt data for cycle HMF T-17 221
Figure C.15 log Ionic Conductivity data obtained in isothermal experiments with 934 neat resin system 223
Figure C.16 dlog IV/dt data obtained in isothermal experiments with 934 neat resin system 223
Figure C.17 Permittivity vs. log frequency of a DGEBA polymer in an isothermal experiment 225

Figure C.18 Method of estimating the time when the loss peak occurred at each frequency 226
Figure C.19 Cole-Cole plot at different process time of cycle R934 T-08 227
Figure C.20 log Loss Factor after EPC by software for cycle R934 T-08 228
Figure C.21 log Permittivity after EPC by software for cycle R934 T-08 228
Figure C.22 Parameters for electrode polarization correction 231
Figure C.23 log Loss Factor after EPC by calculation for cycle R934 T-08 231
Figure C.24 Permittivity after EPC by calculation for cycle R934 T-08 232
Figure C.25 Cole-Cole plot after EPC by calculation for cycle R934 T-08 233
Figure C.26 Permittivity vs. log frequency after EPC for cycle R934 T-08 234
Figure C.27 Actual strain obtained after compensating for the thermal effect of the sensor 235
Figure C.28 Cure shrinkage of the composite part in cycle HMF T-25 237

LIST OF TABLES

Table 1.1 Sensors and parameters measured in this project 10

Table 3.1 Summary of the results of Material Characterization 63

Table 3.2 Control parameters for ultrasonic sensing 70

Table 3.3 The specification of the dielectric sensors 73

Table 3.4 The specification of FBG sensors 77

Table 3.5 Cure cycles applied in experiments 88

Table 4.1 The measured mechanical and acoustic properties for the fiberglass resin specimens after curing 109

Table 4.2 Theoretical mechanical and acoustic properties for polyester resin 109

Table 4.3 The measured ultrasonic wave velocity and modulus for the aluminum and composites 111

Table 4.4 The theoretical mechanical and acoustic properties for the aluminum and composites 111

Table 4.5 Summary of monitoring results 141

Table 4.6 Isothermal experiment results of 934 neat resin 142

LIST OF SYMBOLS

Symbol	Description
α	Degree of cure
α_{gel}	Gel point
t_{gel}	Gel time
t_{hold}	Hold time
t_{min}	Process time corresponding to viscosity minimum
T_g	Glass transition temperature
Δt	Ultrasonic time delay
A	Ultrasonic wave amplitude
c	Ultrasonic wave velocity
c_L	Longitudinal wave velocity
c_S	Transverse wave velocity
h	Specimen thickness
α	Ultrasonic wave attenuation
p	Ultrasonic sound pressure
E	Young's modulus
G	Shear modulus
ρ	Density of material under test
υ	Poisson's ratio
L	Longitudinal modulus
K	Bulk modulus
M	Storage modulus
λ	Ultrasonic wavelength
$v(t)$	Input time varying voltage
$i(t)$	Response current
$q(t)$	Net charge
ϵ'	Permittivity

ϵ''	Loss factor
θ	Phase angle
$\tan \delta$	Tangent loss
ω	Angular frequency of excitation sinusoidal voltage $v(t)$
τ	Relaxation time
ϵ_o	Permittivity of free space
σ	Ionic conductivity
A	Area of parallel plate electrode
D	Separation of parallel plate electrodes
$G(\omega)$	Frequency dependent conductance
ϵ_∞	Unrelaxed permittivity
ϵ_s	Relaxed permittivity
ϵ'_x	Experimentally measured permittivity
ϵ''_x	Experimentally measured loss factor
L	Plate separation
t_b	Blocking layer thickness
T	Temperature
$\log(cond)$	log (ionic conductivity)
λ_B	Bragg wavelength
n_{eff}	Effective core refractive index
Λ	Pitch of grating
p_e	Effective photoelastic coefficient
α_o	Attenuation coefficient
ξ	Thermo-optic coefficient
η_o	Young's modulus coefficient
C	Temperature sensitivity of optical fiber sensor
$\frac{d\alpha}{dt}$	Rate of degree of cure
H	Total heat of reaction
E	Activation energy

z	Pre-exponential factor
n	Reaction order
k	Reaction rate constant
R	Gas constant
$\Delta\alpha$	Increment of degree of cure
Δt	Increment of process time
α_{11}, α_{22}, α_{33}	Coefficient of thermal expansion of composite
ϵ_{11}, ϵ_{22}, ϵ_{33}	Coefficient of cure shrinkage for composite
t	Process time
η_{min}	Viscosity minimum
log IV	log (ionic viscosity)
dlog IV/dt	Derivative of log (ionic viscosity) by process time
ϵ_{total}	Total strain measured during curing
ϵ_{actual}	Actual strain (cure induced residual strain)
$\epsilon_{sensor\ thermal\ expansion}$	Thermal expansion of FBG sensor
T	Period
f	Frequency
τ_p	Attenuation coefficient
I	Ultrasonic wave intensity
d	Propagation distance
Z_{ac}	Acoustic impedance
Z	Characteristic impedance
J	Ultrasonic wave energy
R	Coefficient of reflection
D	Coefficient of transmission
α_e, α_d, α_r	Incident, reflected and refracted wave angles
C_1	Capacitor modeled for induced dipoles
C_2, R_2	Capacitor and resistor modeled for permanent dipoles
R_3	Resistor modeled for ionic conductivity

$Y(\omega)$	Electrical admittance
V	Complex amplitude of $v(t)$
I	Complex amplitude of $i(t)$
V_0	Amplitude of $v(t)$
I_0	Amplitude of $i(t)$
$Z(\omega)$	Electrical impedance
C^*	Complex capacitance
C_o	Capacitance of free space
ϵ^*	Complex permittivity
β	Distribution parameter of relaxation time
λ_0	Light wavelength in vacuum
r	Fiber core radius
V	Dimensionless standardized structure constant
n_{co}	Refractive index of inner core
n_{cl}	Refractive index of cladding
M	Number of modes
pts	Number of points
ϵ'_o	Low frequency dielectric constant
R	R value
ϵ_t	Thermal expansion of composite
ϵ_c	Cure shrinkage of composite

CHAPTER 1

INTRODUCTION

1.1 Introduction

A composite is a mixture of two or more distinct constituents or phases, usually a matrix and reinforcement. A matrix is the constituent that is continuous and its volume fraction may be less, equal or more than the reinforcing medium. The main functions of the matrix include transferring the load to the reinforcing phase (fibers), keeping the fibers in place, maintaining the integrity of the composite, and protecting the surface of the fiber from an adverse environment and mechanical abrasion encountered during fabrication. Reinforcement is the constituent that enhances the properties of the matrix and is harder, stronger and stiffer than the matrix. Its function is to share the major portion of the applied load. With proper selection of matrix, fiber and their size, shape and orientation, the properties of the composite can be tailored to desired levels. High performance composite materials are used increasingly in aerospace, automobile industries etc. due to their high specific strength and specific stiffness compared to conventional metals, alloys, plastics and ceramics, which results in weight reduction and cost reduction (1). The composites used in aerospace industries are polymer matrix composite materials, reinforced with continuous fibers.

The share of polymer matrix composites has slowly increased to about 10-12% in the latest commercial planes such as Boeing 777, MD 12X, and Airbus 340. Business jets such as Beech Starship have 21% of total weight made up of composites. The current

application of the composites include empennage, wing components, body components, fuselage, landing gear and engine components such as cowls, thrust reverser, fan exit guide vanes, turbine rotor containment system, outer compressor ducts, and fan blades. Recently, Airbus 380 and Boeing 7E7 Dreamliner have started to use composites in primary structures such as fuselage and wings. In the latest military aircraft such as F-22, 35% of the weight of the aircraft is made up of composites. 51% of the structural weight of the modern helicopters such as AH-66 is composites. In space application such as satellites and launchers, composites are mainly used as truss members and other components such as dish reflectors, deployment arms, struts, and solar array panels (1). This share of the application of composites is expected to increase in the future.

Several manufacturing methods are currently available to fabricate thermoset polymer composite parts. Autoclave processing is the most widely used manufacturing process in aerospace industries. Autoclave shown in Figure 1.1 is a cylindrical pressure cooker where heat and pressure (pressurized nitrogen) can be simultaneously applied to a part. The composite part is shaped manually using ready-to-use prepregs. A prepreg is a single layer of continuous fibers impregnated with polymer matrix, purchased from material suppliers. The fibers in the prepreg can be parallel or woven. The resin content by weight is about 35 – 42% and fiber content by weight is 65 – 58%. Commonly, the prepreg purchased from the supplier is cured to about 5% (B-stage cure) for ease of handling and lay-up. To fabricate a composite part the prepregs are cut to desired size and shape normally by a computer controlled ultrasonic cutting system. These cut prepreg layers (known as lamina) are laid-up manually on a tool that is shaped like the part. The part –

tool assembly is enclosed in a vacuum bag as shown in Figure 1.2. The purpose of the application of vacuum bag is to remove any volatile gases and moisture that evaporated from the prepreg during curing, and to prevent pressurization gas (nitrogen) used in the autoclave to come in contact with the composite part resulting in voids. The tool is coated with a non-stick coating. The peel ply, in contact with either side of the laminate, is used to obtain smooth surface. The release film is used for easier removal of the part from the tool and prevents the part from being stuck to the breather or bleeder cloth. The breather provides the least resistance path for gases to escape to the vacuum port. Bleeder is used to adjust the resin content in the cured composite. A vacuum bagged uncured composite part in an autoclave is shown in Figure 1.3. A cure cycle as shown in Figure 1.4 is applied inside the autoclave to cure the part. The cure cycle is supplied by the prepreg material supplier.

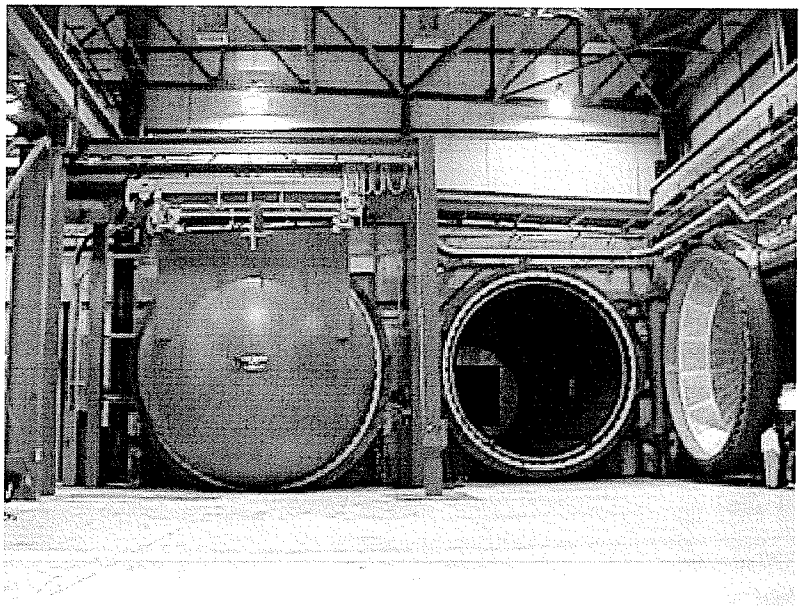

Figure 1.1 Typical autoclave used in the manufacturing of composite

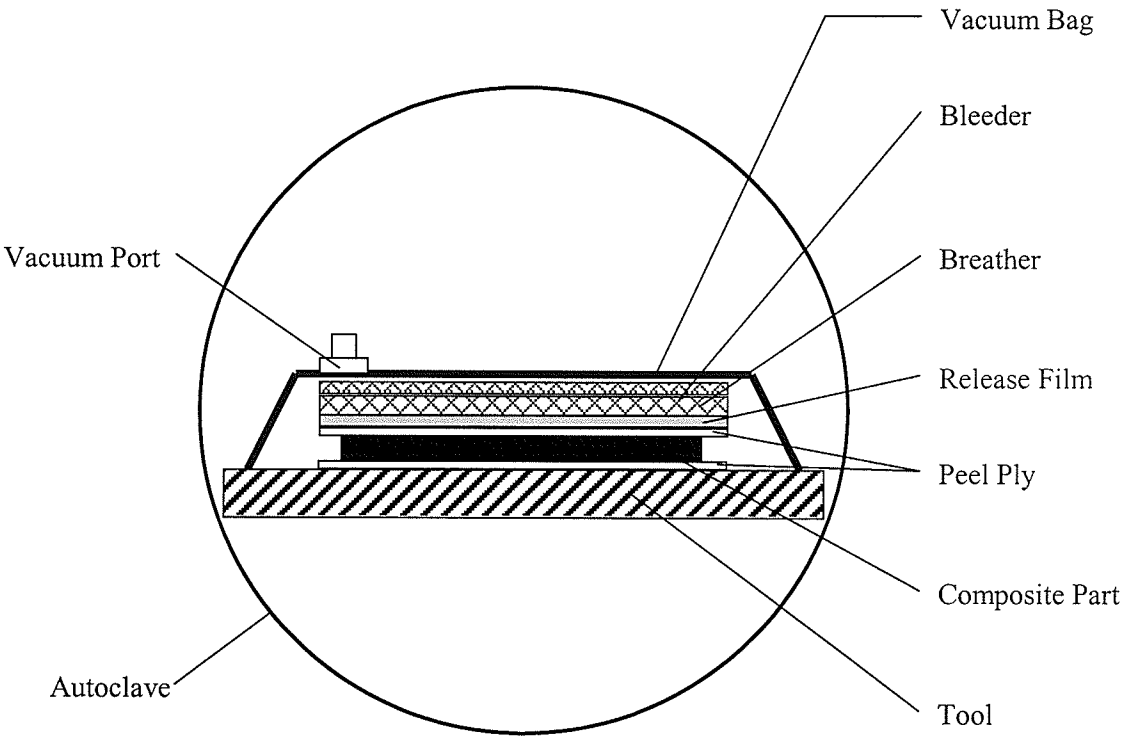

Figure 1.2 Prepreg and vacuum bag lay-up for autoclave processing

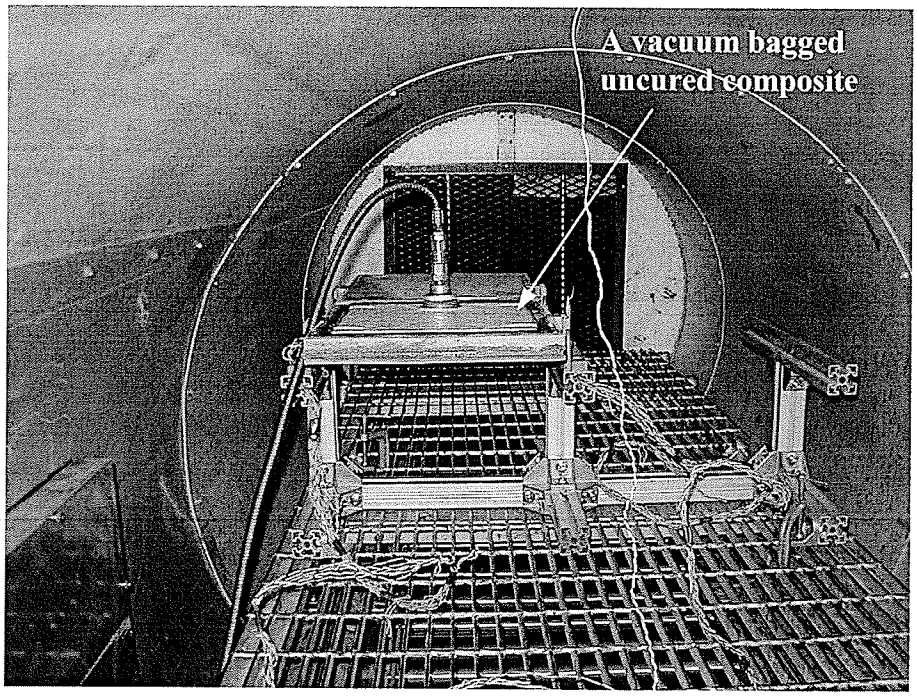

Figure 1.3 A vacuum bagged uncured composite in an autoclave

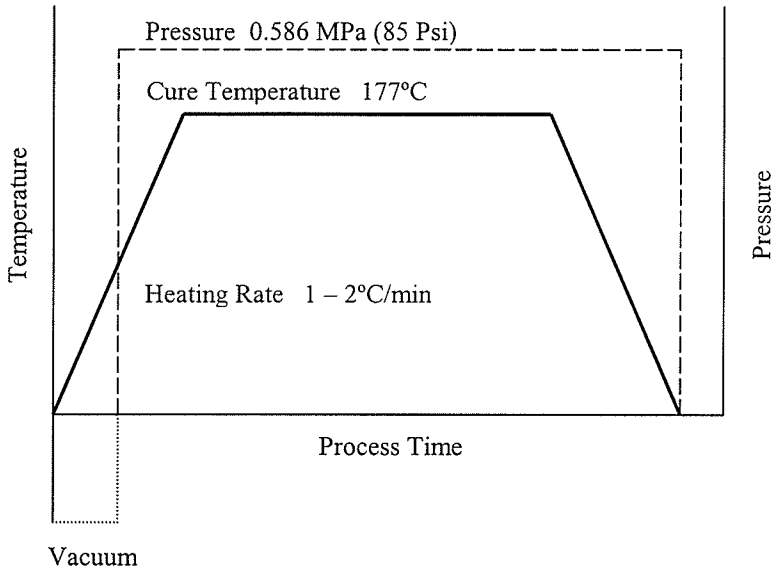

Figure 1.4 A typical cure cycle

Before curing, a polymer composite part will be in an uncured state with poor mechanical properties. During processing in an autoclave, the part transforms from an uncured state to a cured state with required properties. The process of curing is described as follows. The matrix of an uncured composite is a mixture of monomers (building unit of a polymer), cross-linking monomers (hardener), and a catalyst. Under heat and pressure in an autoclave, the monomers join together to form giant-organic chains and this process is known as polymerization. From this, these long chains are connected together by hardeners, and this process is known as cross-linking, as shown in Figure 1.5. This entire process of polymerization and cross-linking is known as curing. This curing process causes the viscosity of the resin to continually increase during processing, and the material changes from a liquid to a gel, and finally to a solid. The modulus of the composite part increases with the degree of cure (the amount of cross-linking) and reaches a constant value when the part is completely cured.

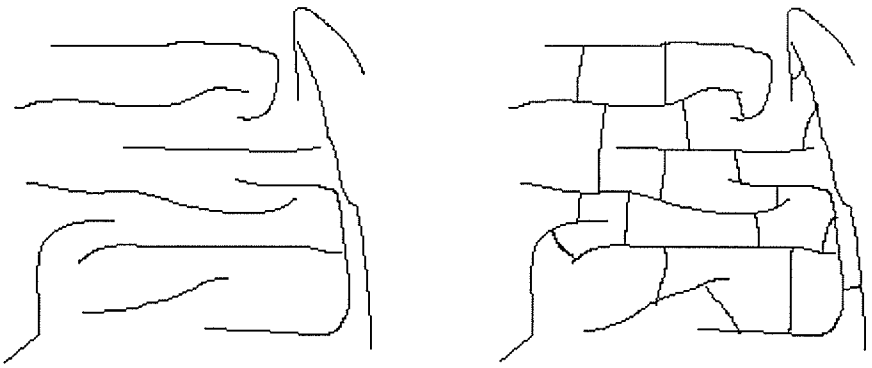

Figure 1.5 The resin before and after cross-linking reaction

The cure cycle shown in Figure 1.4 is dependent on the composite matrix resin and is usually provided by the prepreg suppliers. However, in order to ensure that components made using different composite resin materials with similar cure cycles are accommodated within the same batch load, OEMs (Original Equipment Manufacturer) modify the manufacturer suggested cure cycles by trial-and-error into a very conservative cure cycle. This conservative cycle ensures that parts are completely cured regardless of material type and location within an autoclave and hence, have required properties. Therefore, currently, there is enough room for optimization to reduce cycle time while maintaining part quality in order to improve efficiency, and reduce production costs and the capital investment required for large equipment such as autoclaves. In addition, optimization of cure cycle for minimization of warpage and residual stress in a component is important to industry as it could lead to reduction in costly part rejection, elimination of costly tool trial-and-error design, and reduction in part dimensional variation from batch to batch. However, such optimization is yet to be developed.

Cure cycle optimization can be done at two levels: off-line optimization and on-line optimization. Off-line optimization results in a cure cycle for a part or a batch load, which is subsequently inputted into the autoclave controller. On-line optimization involves re-optimization of off-line optimized cure cycle on the fly when a deviation from the desired process window/properties is sensed during manufacturing. Both levels of optimization require:

(i) A science based process model for relating process and material parameters to properties of interest such as degree of cure, modulus, residual stress, warpage etc.

(ii) Optimization software that optimizes the cure cycle and interfaces with the process model, sensors and autoclave controller

(iii) Reliable sensors that can measure the properties of interest accurately and quickly

Advanced Composite Structures Research Group at the University of Manitoba has already developed (i) and (ii). Details of these can be found in references (2), (3) and (4). This study has focused on requirement (iii). Sensors are important to both validate the process model prediction to develop optimal process cycle off-line and to monitor deviation during processing and to activate on-line optimization software.

1.2 Issues in Selection of On-line Sensors

Process parameters such as temperature and pressure, and material parameters, such as viscosity, gel point, state of cure (degree of cure), residual strain/stress and modulus, are required to be monitored and controlled to ensure final part quality. Cure kinetics

information can be used to determine the time required to achieve complete curing at a given temperature. The degree of cure α, which is the amount of cross-linking, is one of the most important material parameters. Material parameters, such as viscosity, glass transition temperature and moduli are the function of degree of cure.

The viscosity of the resin matrix is very important to obtain proper flow, consolidation and to eliminate voids and dry spots. Variation of viscosity with temperature is shown in Figure 1.6, which was obtained in a cure cycle studied in this project. The viscosity decreases with increase in temperature during ramping to the cure temperature. The degree of cure increases during the heating up procedure. The net effect is that a minimum value in viscosity is obtained. The process time corresponding to the viscosity minimum can be used to determine when to cut the vacuum and apply the pressure in a cure cycle. It also determines the temperature for the hold procedure to ensure proper flow before ramping the part to the cure temperature in a two-step cure cycle. Beyond this minimum, the viscosity increases rapidly due to the rapid increase in degree of cure. The degree of cure α when the viscosity approaches infinity is the gel point (α_{gel}). The time corresponding to α_{gel} is the gel time (t_{gel}) and it decreases with the increase in temperature during isothermal curing. Gel time is used to determine the hold time at hold temperature and ensure that $t_{hold} < t_{gel}$. After gel time is reached, the moduli of the composite part start to build up significantly. The end of cure state determines when the composite part is completely cured and the curing process should be stopped. It is a crucial parameter to determine the minimum cycle time required for composite manufacturing with the desired material properties.

Residual stresses are introduced in composite parts during fabrication due to the mismatch in thermal properties of the constituents. Residual stresses influence significantly the dimensional accuracy and strength, and lead to defects to the composite structures and therefore are highly undesirable.

The modulus of the composite part increases with the increase in degree of cure. It is an important parameter to ensure the quality of the cured part.

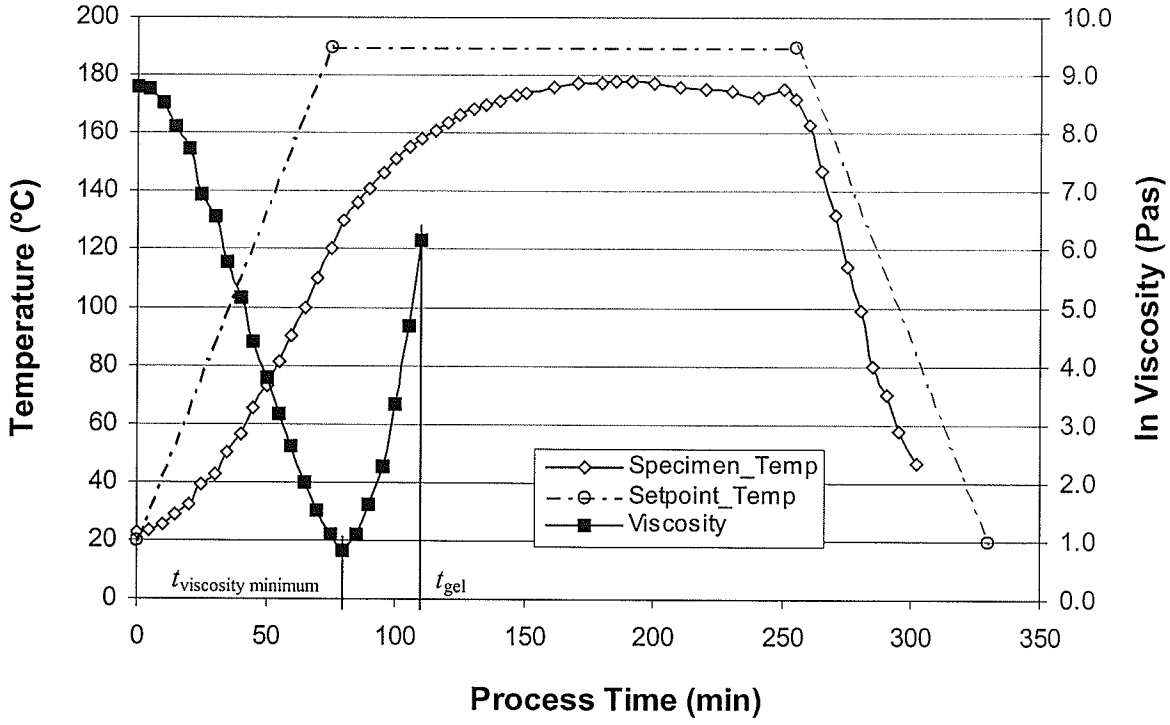

Figure 1.6 Viscosity data of a composite specimen

Parameters that are crucial to the manufacturing process are listed in Table 1.1. These parameters must be monitored by the relevant sensors. There are two types of sensors: direct sensors and indirect sensors. In "indirect" sensors, the relationship between

measured data and the required material properties are established by indirect correlation. In "direct" sensors, the relationship could be established by physical models. Direct sensors are highly desired. Different kinds of sensors have been either developed or under development which could be used to monitor various parameters.

A number of commercially available on-line sensors that have the potential to be used for monitoring of autoclave curing process have been reported in the literature by either individual researchers or companies that developed them, including ultrasonic sensors, dielectric sensors, and fiber Bragg grating (FBG) sensors. The sensors have been reported to be capable to measure one or more of the parameters of interest listed in Table 1.1. As no sensor is available to directly measure the material parameters, such as degree of cure, gel time etc., these sensors are indirect sensors. The material parameters of interest are indirectly correlated to the sensor response.

Table 1.1 Sensors and parameters measured in this project

Potential Sensors	**Parameters to be Measured**	**Process Parameters and Material Properties to be Correlated**
Ultrasonic Sensor	Time delay Attenuation	Process parameters: Temperature, pressure – measured by thermocouple and pressure transducer Material properties: Viscosity minimum, gel point, end of cure state, degree of cure, residual strain/stress and Moduli
Dielectric sensor	Permittivity Loss Factor Tan δ	
Fiber Bragg grating sensor	Wavelength shift	

However, there is no single sensor that is able to monitor all the required parameters. A sensing system with multi-sensing ability is highly desirable. Requirements regarding on-line sensor selection were reviewed in reference (5). Two most important issues that need to be addressed are:

(1) There is no mature routine to interpret signals obtained by on-line sensors during curing. The sensing response is mostly interpreted by researchers with a certain level knowledge of the sensors and it lacks rigor. The sensing data interpretation is based on indirect empirical correlation rather than sound physical models. Experimental results obtained by different types of sensors were seldom compared to verify the correlation between sensor responses to material parameters.

(2) There is lack of knowledge on issues related to the application of the sensors, such as information on limitation of these sensors, the sensor accuracy, reliability, survivability and lifetime during and after fabrication and embedment, the sensor installation and configurations, such as equipment, handling, and wire connections etc. Generation of the knowledge of sensors is required and is a goal of this study.

1.3 Thesis Objective

The objective of this thesis is to evaluate the suitability of the most prospective sensors available in the market (ultrasonic sensor, dielectric sensor and fiber Bragg grating sensor) that have the potential for on-line monitoring using the material property prediction model developed in reference (3), by addressing the above mentioned issues in

using them for on-line monitoring.

1.4 Thesis Outline

A brief introduction to the project, the background of this project, on-line sensing systems and the objective of this thesis are provided in Chapter 1. Chapter 2 presents the literature review, background and details on on-line sensor monitoring techniques, including ultrasonic sensors, dielectric sensors and fiber Bragg grating sensors. Some results of multi-parameter sensing systems are also reviewed. Chapter 3 discusses the experimental configurations in this project, including the sensors, equipments, materials, and cure cycles etc. used in experiments. Chapter 4 presents and compares the experiment results from all the three types of sensors. Chapter 5 discusses the issues appeared in the experiments which should be considered before using these sensors in the real manufacturing applications. Performance of the sensors in experiments was reviewed in this chapter. Chapter 6 presents the conclusions drawn for this research work and the author's recommendations for future work.

CHAPTER 2

LITERATURE REVIEW

2.1 Introduction

As mentioned in the first chapter, material parameters, such as degree of cure, viscosity minimum, gel point, the end of cure state, modulus and process induced residual stresses are very important parameters to trace the curing procedure and control the final part quality. These parameters can be characterized off-line by many traditional testing methods: The cure kinetics data can be generated using a Differential Scanning Calorimeter (DSC). The viscosity as well as gel point can be determined using a Rheometer. Moduli and glass transition temperature (T_g) can be determined using a Dynamic Mechanical Analyzer (DMA). However, there is no mature method to measure the process induced residual stress in composite.

These testing methods are employed offline and cannot provide real time data during composite processing. Details about these off-line characterizations of composite materials are beyond the scope of this investigation and will not be described in this thesis. Currently, there are no mature process sensors for on-line monitoring of composite curing. Hence, sensors with ability to monitor the parameters on-line are highly desirable by composite manufacturing industries.

A review of the previous work on sensors for on-line monitoring of these parameters during composite processing is presented in this chapter. The fundamental operation principle for each type of sensor is first introduced, followed by a review of research

work completed using that sensor. Only three types of sensors including ultrasonic sensor, dielectric sensor and fiber optical (fiber Bragg grating) sensor were available in the market. Hence, only these three sensors are used in this research. The chapter ends with the scope of this project.

2.2 Ultrasonic Sensor

2.2.1 Principle of Ultrasonic Sensing

Ultrasonic waves are the sound waves with frequencies above the human hearing range (typically 20 KHz). In industries, the commonly used frequency range for non-destructive testing (NDE) is 100 KHz to 50 MHz. The longitudinal and transverse waves are the most important and commonly used waveforms in ultrasonic engineering. The definition of these waves is presented in Appendix A.

Ultrasonic waves are transmitted and received by appropriate transducers. The waves travel through the curing material and their properties change when the material's mechanical properties change. Typical ultrasonic monitoring experimental configurations are shown in Figure 2.1.

The sensor can be setup in two modes. In pulse/echo mode, part of the sound waves generated by the ultrasonic transducer (UT) is reflected back from the transducer/specimen interface, while the rest travels into the specimen. A part of this is again reflected back from the specimen's surface. The reflected waves from both surfaces of the specimen are received by the same transducer. They arrive at the transducer at the

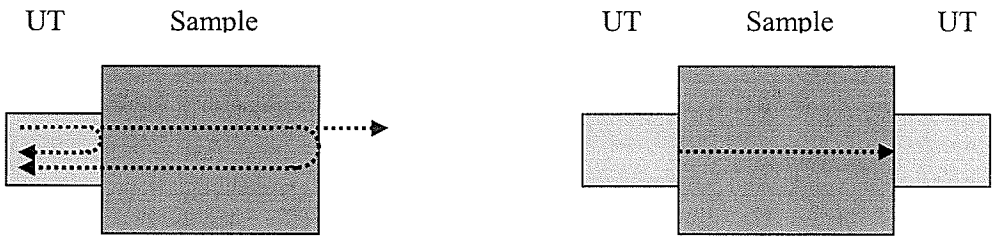

Figure 2.1 Principle of ultrasonic sensing

different time. This difference between the arrived time of the two reflected waves is the time delay. In transmission mode, two transducers are aligned on either side of the sample. Sound waves are generated by one transducer, while they are received by the second transducer after traveling through the specimen. The advantages of the pulse/echo mode include easier alignment and lower cost due to requirement of one transducer. The limitations are: (1) the two surfaces of the specimen should be even, smooth and parallel to each other. Otherwise, the waves will be scattered rather than being reflected back leading to poor noise to signal ratio; (2) Attenuation of ultrasonic energy is normally higher, due to travel of waves twice through the sample thickness. This will normally reduce the thickness of the specimen that can be monitored in the pulse/echo mode.

When an ultrasonic wave is incident normal to the specimen surface, part of its energy will be reflected back and part will be transmitted across the surface along the same direction as the incident wave. Generally, if there is a significant difference between the impedance of the two mediums (i.e. transducer and specimen), the complete reflection

will occur at the boundary between the specimen and transducer. Ultrasonic couplant is used at the interface between the ultrasonic transducer and material in order to fill in any air gaps to ensure that maximum energy can be transmitted in to the material. The details about the effect of acoustic impedance on reflection and transmission of ultrasonic waves at boundary can be found in Appendix A.

Two wave properties of interest during ultrasonic monitoring of composite properties are the time delay (Δt) and amplitude (A). They are subsequently used to determine sound velocity (c) and attenuation (α). The sound velocity can be expressed for pulse/echo mode as:

$$c = \frac{2h}{t} \tag{2.1}$$

where h is the thickness of the specimen, and t is the time delay.

As defined in J. Krautkrämer et al. (6), the attenuation (α) is expressed as

$$\alpha = 20\frac{1}{h}\log\frac{p_0}{p} \text{ dB/mm} \tag{2.2}$$

where p_0 and p are the pressures of incident and reflected sound waves, respectively. h is the specimen thickness. The Sound Pressure is the force (N) of sound on a surface area (m^2) perpendicular to the direction of the sound. The SI-units for the Sound Pressure are N/m^2 or Pa.

The cause of the attenuation is very complicated to interpret. The sound pressure of ultrasonic waves decreases with the increase in the traveling distance in a medium. The attenuation can be induced by (1) geometrical factors, and (2) energy absorption or

scattering mechanisms. The first mechanism is related to the size of the sound source, wavelength and nearby reflecting surfaces. The second mechanism is the absorption and scattering of ultrasonic waves by the medium in which the sound waves are traveling. The energy loss in liquids is related to viscosity, and molecular relaxation absorption. When inhomogeneities exist, the scattering becomes significant. Attenuation in solids is more complicated and difficult to analyze. The attenuation will increase with the increase in frequency. Attenuation in polycrystalline materials is due to thermoelastic relaxation effects within individual grains, scattering at grain boundaries, absorption due to induced movements of lattice imperfections, hysteresis losses of ferromagnetic and ferroelectric origin, and scattering from inclusions, dispersed phases, or voids.

Transverse waves have much stronger attenuation than longitudinal waves, particularly in plastics. This is because the viscoelastic losses are stronger for a change in position (shear) than for a change in volume (compression and dilatation). In anisotropic materials, e.g. fiber reinforced composites, Kim and Park reported that the attenuation is stronger in composites than in isotropic materials (7). The attenuation in fiber reinforced composites is mainly due to the viscoelastic losses in the epoxy matrix rather than scattering losses at the fibers. The authors also concluded that the transverse waves are attenuated more than longitudinal waves regardless of frequency.

Attempts were made to correlate the material parameters, such as minimum viscosity, gel point and the end of cure state qualitatively to the changes in ultrasonic velocity and attenuation. Theoretically, the moduli evolution during curing can be determined

quantitively, if all the necessary parameters including specimen thickness and density changes during processing can be obtained. If both the longitudinal and transverse waves can propagate in the medium, the modulus of the material can be determined using the following equations:

$$E = \frac{c_L^2 \rho (1+\nu)(1-2\nu)}{1-\nu} \tag{2.3}$$

$$G = c_S^2 \rho \tag{2.4}$$

and

$$\nu = \frac{1-2\left(\frac{c_S}{c_L}\right)^2}{2-2\left(\frac{c_S}{c_L}\right)^2} \tag{2.5}$$

where c_L and c_S are ultrasonic sound velocities for longitudinal and transverse waves, respectively, ν is the Poisson's ratio, ρ is the density of the material, E is the Young's modulus and G is the shear modulus.

2.2.2 Application of Ultrasonic Sensors in Cure Monitoring

N. Mard, et al. (8) used a specially designed sensor, similar to the one used in this study, which consisted of 5 MHz broadband piezoelectric ultrasonic transducer (UT), a clad stainless steel buffer rod, and a gel-type high temperature couplant. The pressurized water was used to cool the transducer from the processing temperature of 176°C to a temperature below 60°C. Unidirectional Hercules AS4/3501-6 laminates, $[0_{16}]$ and $[0_{24}]$, were cured using the manufacturer's recommended cure cycle. The authors presented that before the gel point was reached, the echo reflected back from the specimen surface was too weak to be detected. When gelation occurred, the echo could be recorded. In their

work, the end of cure state of the specimen was determined to be the time corresponding to the plateau in time delay data. Two sensors were applied at two different locations. However, the researchers did not present any data obtained using other experiment methods to verify their qualitative measurement results. The attenuation was not applied to correlate material parameters in their work.

J.-Y.Chen et al. (9) used a similar experimental configuration as in (8). They used both pulse/echo and transmission/reflection modes. The AS4/3501-6 prepregs were used. Similar to observations in reference (8), the echo reflected back from the top surface of the composite specimen in the initial stage (from the beginning of the experiment to about 160 minutes) was too weak to be detected. They suggested that the sharp decrease in the time delay could be attributed to the gelation of the prepreg. At the end of curing, the specimen debonded from the tool plate causing a discontinuity in the signal. They concluded that the end of cure was reached when the time delay reached a plateau value. They also reported that when gelation occurred, the ultrasonic attenuation reached a maximum value, and dropped sharply during the gelation period. After that the attenuation gradually decreased and approached a plateau value, corresponding to the end of cure state. In their research work, they described the evolution of the ultrasonic response of the composite specimen during curing and qualitatively related material parameters such as gel point and the end of cure state to ultrasonic signals, but the validity of the qualitative correlations was not mentioned.

Paul J. Biermann et al. (10) developed a sensor for monitoring the compression molding processing procedure. The transducers were built onto the tool and caul plate. Graphite/Fiberite 934 resin was used in their experiments. Only sound velocity was measured to correlate the curing process. They qualitatively determined that the dip in sound velocity early during curing corresponded to the viscosity minimum. They also found that the transducer response had a good repeatability in a series experiments. They did not provide any criterion for determination of the gel point and the end of cure state, and no data was presented to verify their conclusion that dip in sound velocity correlated to minimum viscosity point.

M. Rath et al. (11) studied process monitoring of moulding compounds in a compression mould. Typical moulding compounds including epoxies-EP etc. were used in processing. The RTM equipment and ultrasonic transmission mode was used. The thickness of the part was monitored during processing. The authors presented that ultrasonic measurement was sensitive to polymer chain segment motions, and the corresponding relaxation modes. They reported that the glass transition caused a maximum in the ultrasonic attenuation. The influence of different cure parameters was also discussed, including the different types of moulding compounds, artificial thermal weathering on the moulding compound, moisture content, the amount of hardener etc. Only the resin sample with a very short cure cycle (around 250 seconds) was discussed.

Tony Saliba et al. (12) used transmission mode to monitor the autoclave processing of graphite/epoxy and graphite/Bismaleimides composite specimens. They found the results

to be repeatable in experiments. They tried to correlate the attenuation data to the viscosity before the gelation using a sixth order polynomial equation with a root mean square error of 0.32. However, no physical model was established between these two parameters. In their experiment, they did not correlate the gel point as well as the end of cure state to the sensing data. Similar modeling work was also conducted by J.N. Prassianakis et al. (13) and Susan S. Saliba et al. (14).

Donald E. Yuhas et al. (15) configured a through-transmission ultrasonic measurement system for measuring the moduli of composite specimens. In their experiments, a 2.25 MHz ultrasonic transducer and receiver with buffer rods were aligned at both sides of the sample. A mechanical coupling force was applied to the sensors to maintain contact between the sensors and the sample. The thickness change of the sample during heating was monitored by a thickness sensor. Based on the longitudinal and shear wave velocities obtained in five independent measurements from different sample orientations, the material elastic constants were determined. The data showed good agreement with values reported in literatures with 15% errors for the Young's and shear moduli, and 40% errors for the Poisson's ratio. This method can also trace the modulus changes in elevated temperatures. However, as five independent measurements in different directions were required for this work, it could not be possible to apply this sensing system in an autoclave processing environment and perform the on-line monitoring tasks.

M. Frigione et al. (16) applied a set of equations for calculating the properties of isotropic materials to quantitatively monitor the evolution of mechanical properties of epoxy

adhesives for civil applications at ambient temperature environment. These equations are listed as:

$$L^* = L' + iL'' \tag{2.6}$$

$$L' = K' + 4/3G' \qquad L'' = K'' + 4/3G'' \tag{2.7), (2.8}$$

$$M' = \frac{\rho V^2\left[1-\left(\frac{\alpha\lambda}{2\pi}\right)^2\right]}{\left[1+\left(\frac{\alpha\lambda}{2\pi}\right)^2\right]^2} \qquad M'' = \frac{2\rho V^2\left(\frac{\alpha\lambda}{2\pi}\right)}{\left[1+\left(\frac{\alpha\lambda}{2\pi}\right)^2\right]^2} \tag{2.9), (2.10}$$

$$L = \rho V_L^2 \qquad G = \rho V_s^2 \tag{2.11), (2.12}$$

$$E = \frac{3G}{1+\frac{G}{3K}} \tag{2.13}$$

where L^* the complex longitudinal modulus

L' and L'' the storage and loss bulk longitudinal moduli, respectively

K' and K'' bulk moduli

G' and G'' storage and loss components of shear moduli, respectively

V the ultrasonic longitudinal velocity (V_L) or shear velocity (V_s)

α the ultrasonic attenuation

M the storage (M') and loss (M'') components of the complex moduli

ρ the material density

λ the ultrasonic wavelength

L and G the longitudinal modulus and shear modulus

E Young's modulus

The experiments were performed using a 10 MHz ultrasonic transducer in both pulse-echo mode and transmission mode. A thin sheet of specimen (2 mm) was used in pulse-echo mode. The isothermal experiments were performed at 25°C and 30°C. A DMA with 1 to 10 Hz scanning rate was used to monitor the moduli changes during curing. Researchers found that when the resin approached its gel point, there was a significant increase in ultrasonic velocities, reflecting the buildup of the longitudinal and shear moduli. They also observed two attenuation peaks occurred during curing. The first (weaker) was attributed to gelation and the second (stronger) to the glass transition state (vitrification). The time for the first peak corresponded with the time when the velocity showed a sharp increase. While the second peak was observed to happen much earlier at 10 MHz, while the physical vitrification tested by DMA at 1 Hz occurred after longer time. The moduli calculated by the 10 MHz ultrasonic sensing data were much higher than the values measured by DMA with the low frequency (1-10 Hz). The authors interpreted the results assuming a viscoelastic behavior of the resin in a broad frequency range in DMA and ultrasonic measurements. However, they did not account for the effects of the specimen thickness and density changes. Whether these equations are applicable for composite applications need to be verified.

Summary

Ultrasonic sensors have been used in cure monitoring of thermoset resin and composite materials. Material parameters, such as the viscosity minimum, gelation and end of cure state were qualitatively correlated to the ultrasonic response. However, there is lack of reliable criterion to determine these parameters using ultrasonic sensing data due to lack

of independent experimental data obtained by other methods to verify these correlations. This is even an issue for specimens cured at manufacturer recommended cure cycles as it is more difficult to use DSC and rheometer to simulate these nonisothermal curing processes on-line. Researchers also tried to quantitatively determine the evolution of specimen moduli during curing. However, due to lack of apparatus that can work properly in the autoclave processing environment, the experimental results are not satisfied. The research in this direction needs to be further conducted. No fundamental relationship between material parameters, such as the degree of cure, and ultrasonic response is established.

2.3 Dielectric Sensor

2.3.1 Principle of Dielectric Sensing

Dielectric analysis, or dielectrometry, is a technique that can be used to investigate the relaxation in polymers. There have been attempts in the past to correlate the measured dielectric properties to material properties, such as the state of cure, minimum viscosity, gel point and the end of cure state. Dielectric analysis is performed by placing the dielectric materials between the two electrically conducting parallel plates (electrodes), applying a time-varying voltage $v(t)$ between the electrodes, and measuring the response current $i(t)$ and the phase difference between $v(t)$ and $i(t)$, as shown in Figure 2.2.

When a time-varying voltage $v(t)$ is applied to a dielectric material, a corresponding time-varying electric field $e(t)$ will be established between the electrodes, and the dielectric

material becomes electrically polarized. It will show two electric responses, i.e. its capacitive (the ability to store charges) and conductive (the ability to pass charges). The

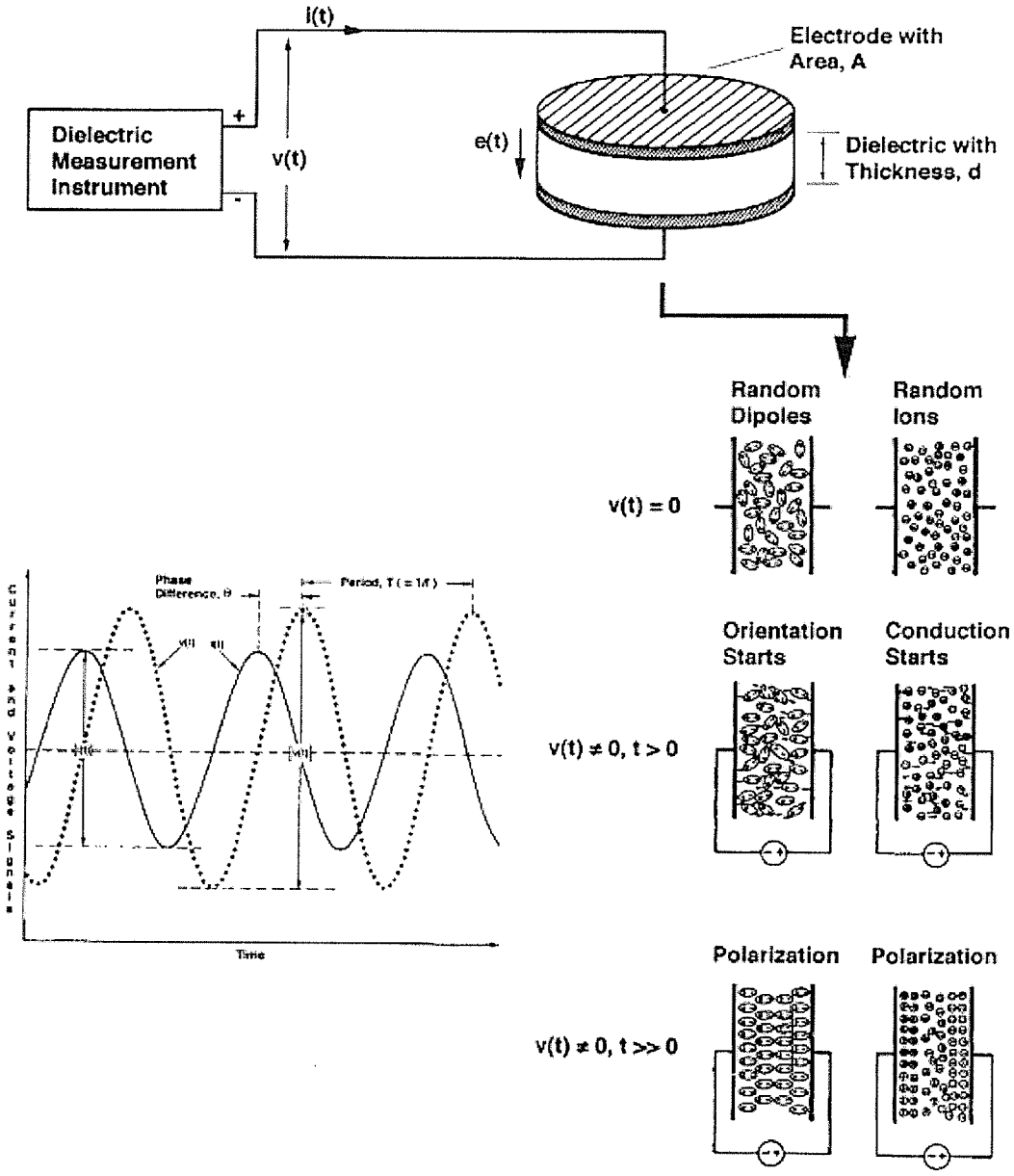

Figure 2.2 Fundamental dielectric measurement scheme (17)

dipoles contributing to capacitive response in the material tend to reorient themselves due to the electric field. The mobile ions (since polymers are non-conductors, the measured conductivity is due to impure ions induced during manufacturing) will move in opposite direction to the electric field. The overall contribution of the dipole polarization and ion migration will generate a net charge $q(t)$, and thus a time-varying current $i(t)$ (the time integral of $q(t)$). The capacitive and conductive responses can be expressed by the dimensionless quantities:

ϵ' = relative permittivity

ϵ'' = loss factor.

and $\tan \delta = \epsilon''/\epsilon'$ (2.14)

where $\delta = 90^{\circ} - \theta$, θ is the phase angle. (2.15)

Changes in a material's degree of electrical dipole alignment and its ion mobility (i.e. ϵ' and ϵ'') can be used to qualitatively infer the material properties, such as viscosity, gel point, the end of cure state etc.

As mentioned above, when an electric field is applied to a polymeric material, the atomic and molecular charges are displaced from their equilibrium positions, and the material is polarized. There are several mechanisms within a polymeric material that contribute to dielectric response, including dipole polarization, ionic conduction, electrode polarization, electronic conduction and inhomogenieties (interface/interphase polarization).

1. Electronic polarization and atomic polarization (induced dipole polarization)

Electronic polarization and atomic polarization are formed by the induced dipoles. When the electric field is applied, the electrons will be displaced from their equilibrium positions in an atomic nucleus, thus generate the electronic polarization. The electronic polarization has an extremely short relaxation time with a resonant frequency in the ultraviolet or visible range of the electromagnetic spectrum (18). Another kind of induced dipole polarization is caused by the non-polar bonds in molecules. Two different kinds of atoms with different electron distribution in a molecule generate a nonsymmetrical distribution of charges. The external electric fields will deflect the ions from their equilibrium positions, and they are frequency independent. This is called atomic polarization. The resonant frequency of the atomic polarization is in the infrared region. Both the electronic and atomic polarization have a low dielectric loss in the frequency range from 10^{-4} to 10^{11} Hz, which is the commonly used frequency range of dielectric monitoring techniques. Because of the frequency independence of both polarization mechanisms, they provide the background values (baseline) in dielectric measurements.

2. Dipole polarization

In addition to the induced dipoles caused by external electric field, the polymeric materials contain permanent dipoles (static dipoles), i.e. charge distribution in the molecule. The applied electric field pushes the permanent dipoles move toward the direction of electric field thus generate dipole polarization. Unlike electron and atom vibrations, the movement of permanent dipoles requires cooperative motion of various

molecules within the polymeric chain. This dipole polarization cannot be completed instantaneously when the electric field is applied. Instead, a certain time is needed to orient the dipoles. It is a time and frequency dependent procedure. Delayed reorientation of dipoles after removal of the electric field is called dipole relaxation.

3. Ion migration

There are always ions present in polymeric materials, induced as impurities during the manufacturing of polymers, the residual reactants, and absorbed moisture. Ions move with a limited speed under the influence of an external electric field, and it is a frequency independent polarization mechanism.

4. Electrode polarization

When the ion level is high, especially at the beginning stage of curing, ions accumulate at the interface between the electrodes and the polymer. The blocking ion layer acts as an electrochemical potential barrier, which significantly affects the absolute measurement values.

5. Interfacial polarization

The interfacial polarization is caused by the building up of ions at the interface/interphase between the different components of a heterogenous polymeric system, such as reinforcement/polymer interface. The dielectric response of such a system could be very complicated and unknown at the current stage.

The dipole polarization and ion migration are the two most important contributions to the dielectric response of a material. Electrode polarization is always encountered during the curing of the polymers. Using measured $i(t)$ and phase, and input $v(t)$, ϵ' and ϵ'' can be calculated using the following classic Debye equations:

$$\varepsilon' = \varepsilon_\infty + \frac{\varepsilon_s - \varepsilon_\infty}{1 + (\varpi\tau)^2} \tag{2.16}$$

$$\varepsilon'' = \frac{\sigma}{\varpi\varepsilon_o} + \frac{(\varepsilon_s - \varepsilon_\infty)\varpi\tau}{1 + (\varpi\tau)^2} \tag{2.17}$$

and the loss tangent is

$$\tan\delta = \frac{\varepsilon''}{\varepsilon'} = \frac{(\varepsilon_s - \varepsilon_\infty)\varpi\tau}{\varepsilon_s + \varepsilon_\infty(\varpi\tau)^2} \tag{2.18}$$

where

ϵ' is the permittivity (or dielectric constant) of the material under test

ϵ'' is the loss factor of the material under test

ω is the angular frequency of the excitation sinusoidal voltage $v(t)$

ϵ_0 is the permittivity of the free space

τ is the relaxation time

$\sigma = \frac{D}{AR} = \frac{1}{G(\varpi)}$ is the bulk ionic conductivity($ohm^{-1}m^{-1}$). $G(\omega)$ is the frequency dependent conductance (2.19)

ϵ_∞ is the unrelaxed permittivity measured at very high frequency. At this frequency, the permanent dipoles and ions will not be able to respond to the varying electric field in such a short time interval, and only the induced dipoles will contribute to the measured dielectric permittivity. The induced dipole

polarization provides the background values (baseline) for the dielectric monitoring.

ϵ_s is the relaxed permittivity measured at low scanning frequency. Since sufficient time is available for all dipoles to orient, a maximum permittivity value will be measured at this frequency. Both the induced dipoles and permanent dipoles contribute to the relaxed permittivity.

Additional details on deriving of the classic Debye equations of dielectric response can be found in Appendix A.

The dielectric loss factor ϵ'' in the above equations is a measure of the energy absorbed or lost in aligning dipoles and moving ions during the curing of dielectric materials. Both permittivity ϵ' and loss factor ϵ'' will change during the curing process. For the loss factor, the contribution of the dipole alignment could be relatively less when compared to the contribution from ionic conductivity. From the equation 2.19, it can be seen that the loss factor ϵ'' is inversely proportional to the scanning frequency ω. i.e. if the frequencies are low enough, the ionic conduction contribution will dominate the loss factor. During the dielectric analysis, a series of frequencies are scanned, and the ionic conductivity data will be extracted from the data recorded at these frequencies.

Since the ionic conductivity is a measure of the ionic mobility in dielectric materials, it is closely related to the polymeric chain movement in the curing procedure. Qualitatively, it could be related to the viscosity of dielectric materials up to gelation occurred, and rigidity after gelation. Hence the ionic conductivity could be a useful dielectric parameter

in the monitoring of polymer composites to correlate the material parameters such as minimum viscosity, gel point and the end of cure state.

A commonly used representation of dielectric data is the Cole-Cole plot or the arc diagram, shown in Figure 2.3, which is a plot of ϵ'' as a function of ϵ'. If the ionic conductivity could be neglected, the Debye equation is represented by a semicircle. The maximum point of the arc is corresponding to where $\omega\tau = 1$. At $\omega = 0$, the curve will intersect the x-axis, and the corresponding permittivity is the relaxed permittivity ϵ_s, which is often related to the chemical structure of the dielectric material. The left intercept of the arc with x-axis is the unrelaxed permittivity ϵ_∞. During a dielectric experiment, the relaxed and the unrelaxed permittivity can never be measured directly. These two values are often determined by extrapolation.

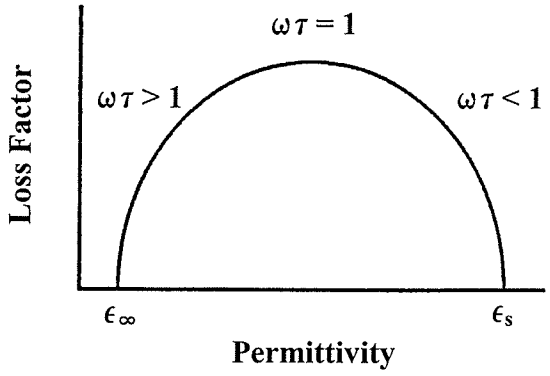

Figure 2.3 The Cole – Cole plot or arc diagram

The above plot in Figure 2.3 is for ideal condition with the assumption that there is just one single dipole relaxation time (τ) for the material. In most of polymeric systems, the

relaxation time will change as dipole mobility changes, which depend on molecular weight, and the surrounding environment. There have been a number of research done in the past on a more precise relaxation time distribution based modeling of dielectric data. Because of this distribution in the relaxation time, the Cole-Cole plot is often squashed or skewed.

The above discussion is based on the assumption that the ionic conductivity is negligible. However, there is always ionic conduction caused by mobile ions present in a polymeric system, especially at the beginning stage of the reaction. The Debey equations of loss factor is

$$\varepsilon'' = \underbrace{\frac{\sigma}{\varpi\varepsilon_o}}_{\text{Conductivity Component}} + \underbrace{\frac{(\varepsilon_s - \varepsilon_\infty)\varpi\tau}{1+(\varpi\tau)^2}}_{\text{Dipole Component}} \qquad (2.20)$$

Dominate above T_g Dominate below T_g

The loss factor includes both the ionic conductivity and dipole polarization contributions. At the limiting low frequencies, the ionic conductivity contribution will dominate the loss factor, and could mask the contribution from dipole polarization. When the ion mobility is small enough, the conductivity would not be the dominating factor. Figure 2.4 shows the effect of ionic conductivity in the Cole-Cole plot.

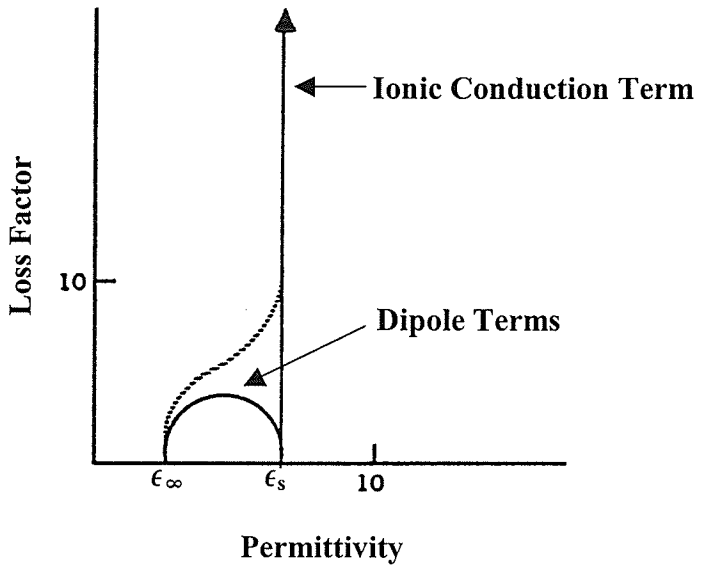

Figure 2.4 The effect of the ionic conductivity to the Cole – Cole plot

Electrode Polarization

As discussed above, in the curing of polymeric materials, along with the dipole polarization and ion migration, there is always electrode polarization happening when the ion level is high, especially at the beginning stage of the reaction, which will interfere the measurements at the low frequencies. The blocking layer act as adding two large capacitors to the ends of the modeling circuit. For a curing process monitored by a parallel plate electrode sensor, the polarization effect can be accounted in a model (19):

$$\varepsilon'_x = \varepsilon'(\frac{L}{2t_b})\left[\frac{(\tan\delta)^2 + \frac{L}{2t_b}}{(\tan\delta)^2 + (\frac{L}{2t_b})^2}\right] \tag{2.21}$$

$$\varepsilon''_x = \varepsilon''\left(\frac{L}{2t_b}\right)\left[\frac{\frac{L}{2t_b}-1}{(\tan\delta)^2+\left(\frac{L}{2t_b}\right)^2}\right] \tag{2.22}$$

$$\tan\delta_x = \frac{\varepsilon''_x}{\varepsilon'_x} = \tan\delta\left[\frac{\frac{L}{2t_b}-1}{(\tan\delta)^2+\frac{L}{2t_b}}\right] \tag{2.23}$$

where $\tan\delta = \frac{\varepsilon''}{\varepsilon'}$ (2.24)

ϵ'_x is the experimentally measured permittivity

ϵ''_x is the experimentally measured loss factor

ϵ' is the actual permittivity

ϵ'' is the actual loss factor

L is the plate separation

t_b is the blocking layer thickness

The equations are also applicable for the correction of electrode polarization of Inter-Digitated Electrode (IDEX) sensors, where L is the electrode spacing.

Electrode polarization will cause a large semicircular response in the Cole-Cole plot. It has significant effect to the permittivity, loss factor and tangent loss as shown in Figure 2.5.

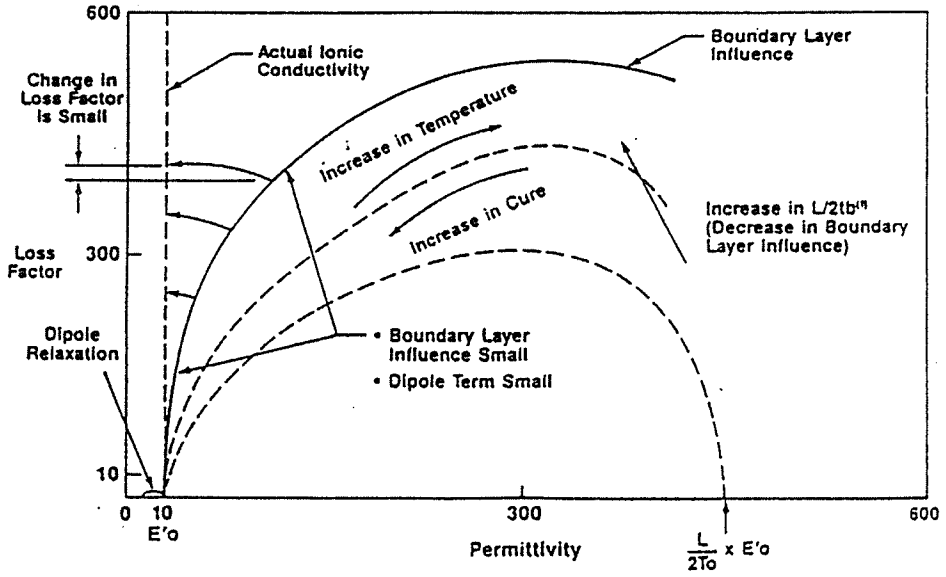

Figure 2.5 Boundary layer effects (19)

2.3.2 Application of Dielectric Sensors in Cure Monitoring

David R. Day et al. (20) applied Micromet Instruments' System III Microdielectrometer and the IDEX sensor with filters in this research work. Materials included a Fiberite 934 graphite epoxy, a USP graphite PMR-15, and a Hexcell 8-297 graphite epoxy. They tried to use the ionic conductivity information to quantitatively simulate the evolution of the cure state. To eliminate the influence of temperature on ionic conductivity, the relationship of ionic conductivity to temperature was established and accounted for, which determined the cure index as:

$$\text{Cure Index} = \frac{LogConductivity - (A(0\%)T + B(0\%))}{(A(100\%)T + B(100\%)) - (A(0\%)T + B(0\%))} * 100\% \qquad (2.25)$$

where A, B are coefficients obtained from linear fitting of temperature dependence of the ionic conductivity corresponding to 0% and 100% cured samples, T is the temperature in a given instant. The cure index increased monotonically with cure state, similar to the

degree of cure. However, there was still a relatively large deviation between the cure index and actual degree of cure values.

In another work in reference (21), they applied the similar experimental setup to trace the evolution of the glass transition temperature T_g for the epoxy resin system: diglycidylether of bisphenol-A (DGEBA-EPON828) with a diamino diphenyl sulfone (DDS) curing agent. They determined the T_g by removing the temperature dependence for the ionic conductivity using the equation reported in reference (20) as:

$$T_g = \frac{\log(cond) - 0\% \log(cond)}{100\% \log(cond) - 0\% \log(cond)} \times (T_g 100\% - T_g 0\%) + T_g 0\% \qquad (2.26)$$

where 0% and 100% log (cond) and 0% and 100% T_g are the temperature dependence of ionic conductivity and T_g measured at 0% and 100% cure. The predicted T_g values are close to the measured data. Similar work was reviewed in J. Mijović et al. (18).

The authors also tried to quantitatively determine the reaction end point of Hercules 3501-6 composites curing process as reported in reference (22). To eliminate the sensitivity to the change in ionic concentration level from batch to batch, the slope of log ionic viscosity, i.e. the first derivative of log IV (Ionic Viscosity) by time (dlog IV/dt) was considered. A series of isothermal experiments at different curing temperatures were performed. A dlog IV/dt value close to 0 (0.04, 0.01 and 0.001) was set as the criterion to determine the reaction end point. Good reproducibility was obtained for the time to reach the critical slope and measured T_g. A strong linear relationship between dlog IV/dt and T_g regardless of curing temperatures was also observed. An empirical equation was developed to calculate T_g based on the temperature and dlog IV/dt values. They

concluded that the accuracy appeared to be reasonable to predict the T_g evolution. However, more data is needed to verify this observation. Similar work completed can be found in D. Abraham et al. (23). All the above models are only empirical correlations and are not based on fundamental physical model since ions are not part of the polymeric network.

F.Stephan et al. (24) used the DGEBA/DDA/imidazole resin system to investigate the processing of epoxy composite. First, isothermal curing at different temperatures were examined by DSC. Dielectric measurements were performed in a frequency range of 1 Hz to 100 kHz. In their work, they were not able to identify the dipolar relaxation peak when vitrification occurred at lower curing temperatures. A viscosity of 20,000 Pa.s was chosen to determine the gel point. They defined that the occurrence of gelation would correspond to the inflection point in ionic conductivity data. However, the gel point extracted from the ionic conductivity data were quite different from the experimental value determined using a rheometer. They also developed an empirical model based on ionic conductivity that accounted for the temperature effect to quantitatively predict the degree of cure of the specimen. The predicted curve was very close to the data measured by thermal methods except for the specimens cured at a lower temperature in isothermal and nonisothermal experiments.

George M. Maistros et al. (25) investigated the curing of a carbon fiber composite with the Fibredux 924 resin matrix by dielectric monitoring. A series of isothermal experiments were performed using the neat resin. They observed that the inflection point

of the log ionic conductivity curve qualitatively corresponded to the gel point of the resin. They reported that the vitrification time could be quantitatively correlated to the value when the dipolar loss peak was extrapolated to a frequency of 1 Hz. Because dipolar loss peaks were masked by the high conductivity level, the researchers applied classical Debey theory, in which the frequency of the dielectric loss peak is defined as the frequency at which permittivity is half-way between the static and infinite frequency values. They selected approximate values for static and infinite permittivity, and linearly extrapolated the midpoints of the permittivity of all the scanning frequencies to 1 Hz and defined the results as the vitrification points, as shown in Figure 2.6.

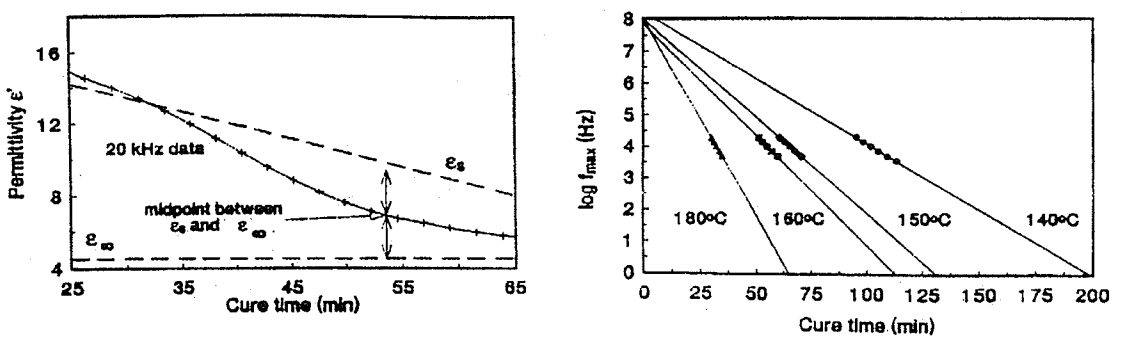

Figure 2.6 The extrapolation method used to determine the vitrification point

However, they did not verify their results using the data from Rheometer and DSC. Using the same method, they obtained the vitrification points of the composite specimens. This method of determining the vitrification by the dipolar contribution instead of ionic conductivity contribution is valuable and requires further investigation. However, it cannot be applied to measure the material parameters such as T_g, hence its application could be limited in the cure monitoring.

In another work in reference (26), the authors studied the curing of Dow DER 332 epoxy resin and blends containing liquid CTBN rubber. They developed a model to describe the evolution of dielectric behavior during curing using established principles concerning chemical kinetics, viscosity-conversion-temperature relationships, and dielectric relaxations. The overall dielectric response of a curing sample was obtained by combining numbers of contributory factors. The authors concluded that the model gave good agreement with experimental results. However, as empirical equations and fit values were used for modeling the cure kinetics, viscosity and dielectric response, this work still cannot establish the fundamental relationships between the dielectric response and material properties. Similar modeling work was conducted by A. Ajji et al. (27) and J. O. Simpson et al. (28).

Besides the dielectric monitoring technique at low frequencies, the applications of microwave dielectric monitoring, which is performed in the frequency range of 1 to 10 GHz in curing process is under development, such as in research work of J. Jow et al. (29) and S. Carrozzino et al. (30). They reported that at low frequencies, it was difficult to relate the measured dielectric data to the degree of cure. However, at high frequencies in the microwave region, the contribution from electrode polarization and ionic conductivity is negligible, and the dipole polarization is the only contributor. The authors presented that the mechanism of microwave dielectric cure monitoring is that the uncrosslinked molecules (high dielectric loss) will absorb more microwave energy than the corsslinked molecules (low dielectric loss). Hence the loss factor becomes the measurement of energy dissipation in the material. They reported that the dielectric

response in the microwave range is dominated by the disappearance of dipolar groups. The loss factor could be used to directly model the material properties, such as the degree of cure. J. Jow et al. (29) applied microwave cavity technique with single frequency at 2.45 GHz to monitor the curing of Epoxy/Amine (DER332/DDS) resin. It was shown by quantitative measurement results that the relationship between dielectric loss factor and the degree of cure for thermal and microwave cured specimens is the same at constant temperature and frequency.

S. Carrozzino et al. (30) used a time domain reflectometer (TDR) and a microwave bridge to monitor the EPON 828/EDA mixtures in the frequency range of 10^7 to 10^{10} Hz. It was shown that at a certain frequency, the quantitative model developed by the authors based on the loss factor data and the degree of cure data measured using DSC were in excellent agreement. There was only slight deviation observed at the end of cure stage. The authors reported that the model fitted to the data was better than that the low frequency range monitoring results. However, a wide band of trial experiments at different frequencies are needed to determine the most appropriate frequency for the microwave dielectric monitoring work. Due to the special requirements of equipment at this time, this technique cannot be applied for on-line monitoring of autoclave processing of composites.

Summary

Similar to the application of ultrasonic sensors in cure monitoring, material parameters, such as viscosity minimum, gelation and end of cure state were qualitatively related to

dielectric response. However, reliable criterion to determine these parameters using dielectric data is required to be established. Researchers have tried to model the material parameters using dielectric data by empirical equations. However, the fundamental models capable of describing the variation of measured dielectric response during curing, and the subsequent use of models to obtain fundamental correlations between dielectric response and material parameters, thus utilizing the dielectric signals to control the process is still in research stage.

2.4 Fiber Bragg Grating (FBG) Sensor

2.4.1 Principle of FBG sensors

Fiber optic technology was originally developed for high speed digital communications in the mid-fifties. In the mid-sixties it was applied in sensing applications. Since the fiber optic technology provides numerous advantages, such as fiber optical sensors can directly sense the chemical state of the material, they are readily adaptable to remote sensing applications and they can be embedded in the curing specimen. Development of sensors for the composite fabrication and health monitoring applications was undertaken since mid-eighties (31).

Optical fibers are a bundle of transparent, glass or plastic fibers that can carry light. The fibers, whose ends are ground, polished and bound together with epoxy, are bundled to form light guides. The fibers can provide a low cost, low dispersion transmission medium to carry the light from one region to another.

An optical fiber consists of an inner core lightwaves guide (usually made by silica), a surrounding cladding (silica), a coating and a protective jacket (polymeric or metallic coating), as shown in Figure 2.7. The refractive index of the inner core n_{co} is made large than that of the cladding n_{cl}, and thus the light is kept within the core and propagated. The optical fiber can be classified as single mode and multimode. The details for the mode of the sensor and its determination can be found in Appendix A.

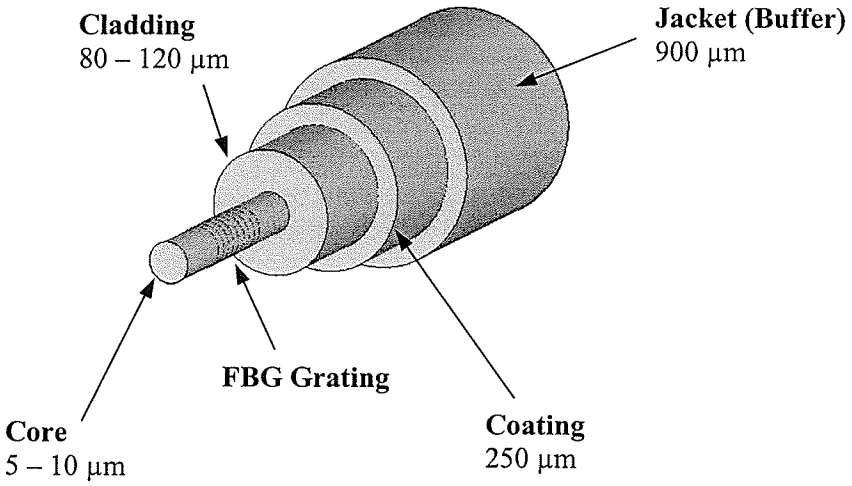

Figure 2.7 Structure of an optical fiber with Bragg grating

Optical fibers have been fabricated as sensors and widely used in various applications because of their attractive features, such as small size, low weight, immunity to electromagnetic and radio frequency interference, low cost, solid-state reliability, geometric versatility and flexibility, resistance to corrosion and high temperature.

Optical fiber sensors can be used to measure various physical parameters, including temperature, pressure, displacement, corrosion etc. When the sensors are embedded into

materials, they can be used in on-line monitoring of manufacturing process. The external environment parameters, such as temperature, pressure, humidity, displacement/rotation/bending etc. will affect the light traveling in the optical fiber. Demodulating and comparing the changes in intensity or phase of the output light to the input light, the environment parameters can be evaluated.

Optical fiber sensors can be divided into extrinsic and intrinsic systems, as illustrated in Figure 2.8. In extrinsic (indirect) system, the sensor element measures the light intensity change in response to physical parameters. The optical fibers act only as a light-transmitting medium. The sensor element does not need to include the fibers. Extrinsic Fabry-Perot Interferometer (EFPI) is an extrinsic sensing system, which has been embedded into materials to measure the strain and vibration variables. In intrinsic (direct) systems, optical fibers act as both the sensor element and the light-transmitting medium. When the environment condition under monitoring changes, the light propagation properties of the fiber also change, resulting in determination of the physical parameters. Because of the closed optical path, the intrinsic system is immune to dirty environments. The sensors include the Intrinsic Fabry-Perot Interferometric sensor (IFPI) and fiber Bragg grating sensor (FBG), which can be used to measure the temperature and strain parameters. Intrinsic sensors are usually smaller in diameter as they do not need any specific transduction mechanism and are easier to implant into material under test with less intrusiveness to the host structure.

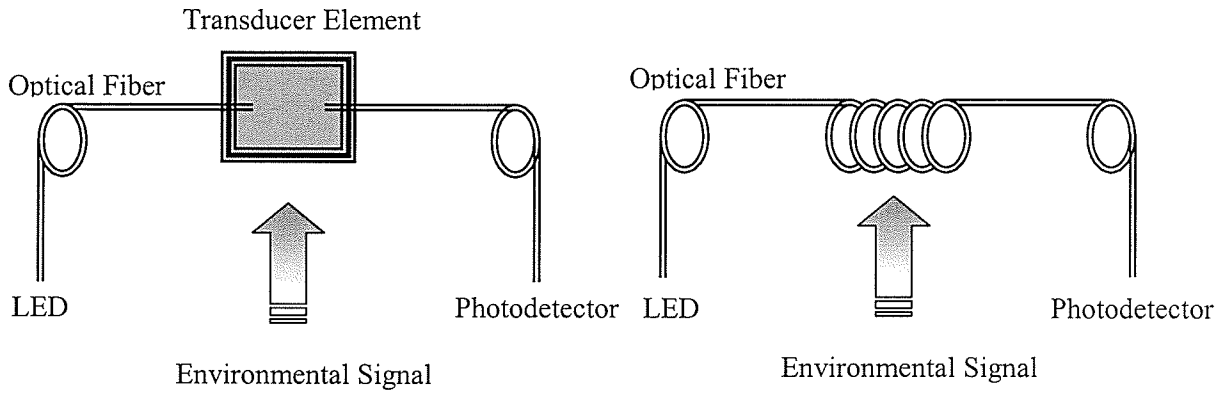

Figure 2.8 Extrinsic and intrinsic systems

Fiber Bragg grating technology was first discovered by Hill in1978 (31). FBG sensor is a single mode fiber with a short length of gratings written in the inner core. The grating was produced by transverse illumination with an interference pattern created by a pair of strong UV beams, thus a permanent periodic modulation of the refractive index is formed in the core of the optical fiber. The gratings permanently change the physical properties of the optical fiber, and act as a wavelength selective mirror. When a broadband light propagates through the FBG sensor, a portion of the incident light is reflected back by the grating. The reflected light consists of a narrow spectral band, which has the center wavelength defined as the Bragg wavelength. The remaining part of the light is transmitted through the grating and lost, as shown in Figure 2.9. The Bragg wavelength λ_B of the reflected light is expressed as

$$\lambda_B = 2n_{eff}\Lambda \tag{2.27}$$

where n_{eff} is the effective core refractive index (average refractive index) of the grating, and Λ is the pitch of the grating.

In a multiplexed sensor, a series of gratings are fabricated in the core of the sensors. The incident light will be reflected back or transmitted through the gratings along the fiber, as shown in Figure 2.9.

Both the changes in pitch length and effective refractive index will affect the response of the FBG sensor. When a strain is applied to the FBG sensor, the pitch of the grating will be changed due to the stretch and the effective refractive index will also change due to the strain-optic effect (32). Hence, the Bragg wavelength will shift

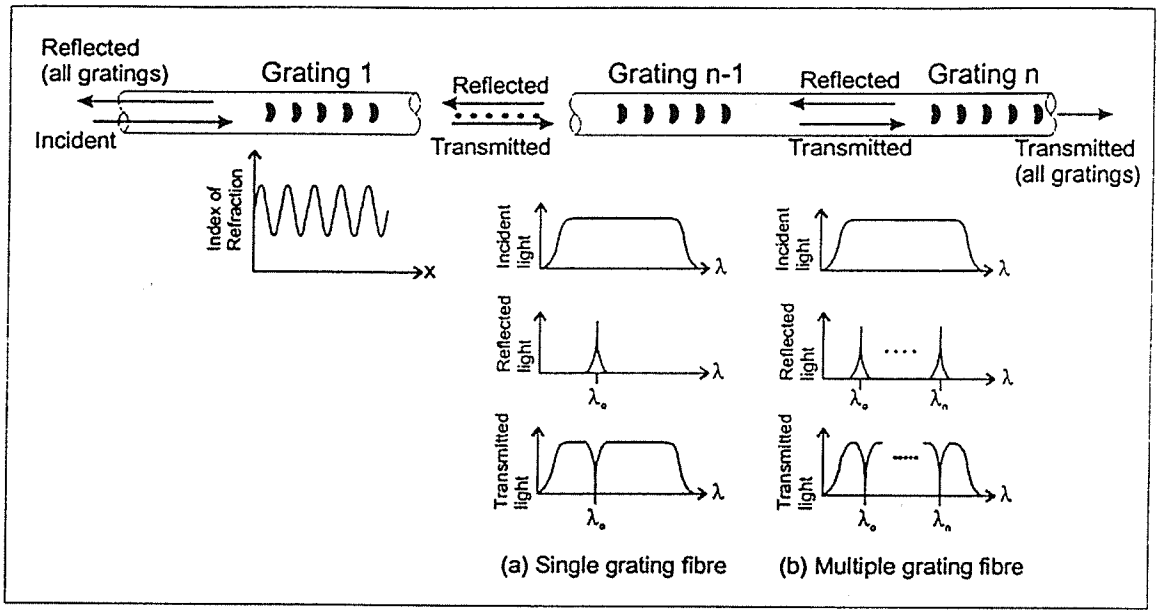

Figure 2.9 Bragg grating principle operation (31)

because of the changes in both n_{eff} and Λ. The environment temperature will also cause the shift of the Bragg wavelength, since the grating pitch will change due to thermal expansion of the fiber and the refractive index is also temperature dependent. The sensor response can be expressed as

$$\delta\lambda / \lambda_0 = (1 - p_e)\varepsilon + (\alpha_o + \xi)\Delta T + \eta_o \Delta P \tag{2.28}$$

where p_e, α_o, ξ and η_o are the effective photoelastic, attenuation, thermo-optic, and Young's modulus coefficient of the fiber material, respectively (31).

The minimum detectable strain and temperature depends on the properties of the light source, demodulation scheme and signal-to-noise ratio requirements. The transverse stress/strain will also affect the sensor response. However, limited studies have been done on this subject. The FBG sensor is able to perform the absolute measurement because of its wavelength interrogation mechanism. The demodulation system can be switched off at any time and the relevant parameters can be measured again after reconnecting, without a need for calibration etc.

Residual stress induced in composite manufacturing process is one of the most significant problems that will affect the quality of composite parts. The residual stress is caused by thermal stress formed in curing process due to different thermal expansion coefficients of constituents and curing shrinkage of the matrix material. The residual stress will cause warpage, and significantly reduce the strength of composite parts. Experimental determination of residual stress is difficult. The most commonly used testing method is the destructive techniques or non-standard measurement method. The specimen containing the residual stress is sliced into thin pieces. The warpage of the pieces, due to imbalance of equilibrated residual stress, is measured and related to the residual stress. Such method is not applicable to measure the residual stress during curing. Non-destructive methods such as X-ray diffraction, neutron diffraction, photoelasticity, Raman

spectroscopy and optical fluorescence etc. are also under development. Strain gauge also has problems when it is embedded into the material. It will significantly decrease the integrity of composite structures due to the relatively large size, and increase the weight of the host material because of the weight of the sensor itself and connecting wires. FBG sensor could be a relatively mature and feasible technique to quantitatively monitor the evolution of residual strain thus determining the residual stress. The potential ability for FBG sensor to qualitatively determine the press parameters such as gel point, the end of cure state etc. also attractive and requires to be verified.

It is necessary to make a brief comparison of FBG and FPI, because both of them show the ability to be used in monitoring of the cure process. Both sensors provide a well defined gauge length and sufficient strain resolution. They can be manufactured to be thermally insensitive. FPI sensors possess the advantages such as easier to manufacture, implant and compensate for the thermal effect, insensitivity to transverse strain measurement. While FBG sensors have a smaller sensor size and better multiplexing abilities (31). Sensor dimension could be a very important factor in real industrial applications.

2.4.2 Application of FBG sensors in Cure Monitoring

K. T. Slattery et al. (33) performed the composite cure monitoring with FBG sensors and tried to determine the residual stress quantitatively. Two sensors were imbedded into the fiberglass/epoxy cross-ply composite. One sensor was placed in the midplane of the composite panel, while another one was implanted near the tool surface. It was observed

that during the initial ramping, FBG sensors showed a pure thermal expansion response. As the resin gelled, the sensors became bonded to the composite and indicated the contraction of the resin during curing. A micromechanical finite element model was established to verify the monitoring results. After curing, when the temperature was cooled down to the room temperature, the modeling results were consistent with the values obtained by FGB data. However, in their experiments, the sensors were not reported to be compensated for the thermal effect during curing. The response came from both the thermal and mechanical strain contributions.

In the research work of C. M. Lawrence et al. (34), two EFPI sensors and one FBG sensor were applied in a $[0_5/90_5]_s$ HyE6049U carbon fiber/epoxy composite specimen. The FBG sensor was embedded at the same location and direction as one of the EFPI sensors between two 90° layers and along the fiber direction. Another EFPI sensor was placed between 0° layers and along the fiber direction. To compensate for the temperature induced response, the calculation was used as:

$$\varepsilon_{actual} = \varepsilon_{measured} - \varepsilon_{thermal} \tag{2.29}$$

$$\varepsilon_{thermal} = C(T - T_0) \tag{2.30}$$

where $\epsilon_{thermal}$ is the thermal apparent strain, C is the temperature sensitivity of the sensor given by the manufacturer; T and T_0 are the curing temperature and room temperature, respectively. It was illustrated that in a 260°F curing process, both the EFPI sensors and FBG sensor showed a trend that reflected the build-up of the residual strains during curing. As expected, the two EFPI sensors had similar strain magnitudes. Very small strain was observed during the ramp-up period. The FBG sensor showed an apparent

deviation from EFPIs data. The authors concluded that this was caused by the sensitivity of the FBG sensor to the transverse strains. During the cooling stage, a nearly linear relation between the strain and temperature was obtained by the FBG sensor. Similar research was performed by J. S. Leng et al. (35).

V. Dewynter-Marty et al. (36) used two FBG sensors in their experiments. One was implanted into a composite sandwich structure made up of a glass/epoxy skin and foam core, another one was placed outside the composite but close to it in an autoclave to compensate for the temperature effect. The sensors had a center wavelength difference of 5 nm, and were fabricated and interrogated in series. They observed that the pressure applied in the autoclave affected both response of the strain sensor and temperature sensor. The strain sensor was able to trace the strain evolution as the combination from thermal expansion and curing shrinkage. At the end of experiment, there was a worsening of the signal-to-noise ratio, which could have been caused by the optical power decrease induced by the stress on the sensor.

Efforts were made to separate strain and temperature effects by using a single FBG sensor. H. K. Kang et al. (37) applied the single FBG/EFPI hybrid sensor to simultaneously monitor the fabrication strain and cure temperature. The sensor characteristic matrices were derived analytically. The sensors were embedded into CU-125 NS GR/EP unidirectional, symmetric cross-ply and fabric composite laminates both in longitudinal and transverse directions. A two step cure cycle was applied to cure samples in an autoclave. The temperature measured by sensors showed good agreement

with the temperature measured by the thermocouple. Similar studies were conducted by some other researchers. M. G. Xu et al. (38) superimposed two FBG sensors with different wavelengths at 1300 nm and 850 nm, respectively. B. O. Guan et al. (39) spliced joint two types of optical fibers made of different materials with the same diameter together to increase the temperature sensitivity and decreased the strain sensitivity. P. Sivanesan et al. (40) applied the first and the second order FBG spectra to simultaneously measure the temperature and cure strain using a single sensor. However, most of the above sensors have not been applied in composite manufacturing, and have no sufficient data to support their suitability for on-line sensing purpose.

C. M. Lawrence et al. (41) tried to quantitatively correlate the measured strain to residual stress using an elastic and viscoelastic model of laminates for cured composites. Hercules AS4/3501-6 graphite/epoxy composite laminates, and EFPI sensors that are not sensitive to temperature and transverse loading changes, were applied. Two sensors were placed in both the longitudinal and transverse directions into a $[0_5/90_5]_s$ laminate. The residual stress buildup in this cross-ply sample was calculated using the model based on the measured strain values. To perform the calculation, (1) the chemical and thermal shrinkage strains, i.e. non-mechanical strains of a unidirectional laminate with the same number of layers (i.e. $[0_{20}]$ laminate, which was also monitored by the embedded FBG sensor), and (2) the degree of cure as a function of time must be known. The calculated result showed good agreement (with 20% and 10% errors, respectively), with the results of the experimental peel-ply test and viscoelastic finite element analysis. It was demonstrated that the magnitude of residual stress at the end of holding period was small

enough and negligible. In the experiment with non-symmetric laminate, the calculated curvature also showed reasonable agreement with the model predicted value.

Summary

FBG sensors have been used in cure monitoring of composite laminates. Researchers have found that FBG sensors can be used to trace the evolution of fabrication strains during curing. However, very limited work has been done to verify the monitoring results using the data obtained by other experimental methods. No relationship between the FBG sensor response and material parameters, such as degree of cure, is provided.

2.5 Application of Multi-Sensors in Cure Monitoring

Researches also tried to apply multi-sensors for composite cure monitoring. M. J. O'Dwyer et al. (42) embedded dielectric sensor, FBG sensor and a thermocouple into Fiberdux 934 composite coupons to monitor the curing process. The FBG sensor was fabricated by the research group. The minimum viscosity and gel point were qualitatively determined by the maximum value and inflection point of the ionic conductivity data respectively. The authors concluded that the plateau in the ionic conductivity curve following gelation was associated with vitrification. However, they cannot determine the vitrification and the endpoint of the reaction with accuracy. The strain measured by the FBG sensor at the end of cure cycle was observed for different cure cycles. However, no data was provided to verify the measured FBG response.

David D. Shepard et al. (43) used both dielectric and ultrasonic sensors to monitor the curing of the epoxy-fiberglass prepreg. The sound speed and resistivity, which was defined as the inverse of ionic conductivity, were measured simultaneously during compression molding. It was observed that at the holding temperature, the sound speed and log resistivity curves had an excellent correlation. However, during the ramp-up, the log resistivity showed a faster decrease than the ultrasonic velocity. The authors interpreted that this was because the sound speed traveling through the liquid resin did not change significantly with temperature as did the mobility of an ion. In isothermal experiment, a good correlation between the sound speed and the resistivity was obtained. The comparison was based on the shapes of the two sensor response curves. Hence the correlation is empirical.

J. -Y. Chen et al. (44) applied ultrasonic sensor and Extrinsic Fabry-Perot Interferometric (EFPI) sensor to monitor the curing of AS4/3501-6 graphite/epoxy prepregs. It was observed that both the EFPI fiber-optic and ultrasonic sensors can qualitatively sense the gelation of the prepregs and the detachment of the composites from Al mold plate. The researchers reported that the sudden decrease in the ultrasonic attenuation curve corresponded to the gel point. When the gelation occurred, the bonding between the EFPI sensors and the laminate became strong enough to effectively transfer the load. During cooling stage, the strain measured in $[90_3/SG1/90_3/0_2/SG2/0_2/90_6]$ panel (SGi represented the embedded EFPI strain sensors) decreased at a linear rate of 0.26 and 3.87 $\mu\epsilon/^{o}C$, while the calculated values using the classical lamination theory were 0.72 and 4.74 $\mu\epsilon/^{o}C$, respectively. They also reported that the ultrasonic sensor can sense the end of

cure, which was defined as the process time when the ultrasonic time delay or attenuation reached a plateau, while EFPI fiber-optic sensor could not sense the end of cure state.

Some research work was performed using other kinds of sensors and techniques, such as piezoelectric sensor in reference (45), FTIR (Fourier Transform Infrared) sensor in reference (46) etc., which will not be reviewed here.

Summary

Limited research work was conducted using multi-sensors. No literature is available using the ultrasonic, dielectric and FBG sensors simultaneously in on-line monitoring of curing process of polymer composites. There is lack of sensing data from different kinds of sensors obtained in one cure cycle or similar cycles that can be compared and used for the purpose of evaluation of sensors.

2.6 Scope of Thesis

Based on the literature summary and market availability, these sensors, namely ultrasonic sensor, dielectric sensor, and fiber Bragg grating sensor, have been chosen for this study to evaluate their industrial suitability for on-line monitoring of autoclave processing. Although these sensors have been studied before by researchers, a number of issues, critical in deciding their industrial suitability, need to be addressed. They are:

(i) In prior studies, interpretation of signals from these sensors has been qualitative and has not been confirmed quantitatively with independent experiments. For example, events in the sensor signals have been interpreted

to be corresponding minimum viscosity, gelation, end of cure, and vitrification. However, such interpretation has not been validated through independent measurement of time for minimum viscosity, gelation, end of cure and vitrification and comparison with process time corresponding to these events in the data signals. Such validation is necessary to verify the reliability of these sensors in sensing the critical values in the material properties, which are important during autoclave processing.

(ii) In prior studies involving ultrasonic and dielectric sensors, the measured signals were not material properties and the correlation between them was made qualitatively by comparing the shape and trend in the data. In addition, efforts were made to correlate the critical events in the signals as discussed in (i). However, direct correlation between signals and material properties is highly desirable in industrial applications and is not available currently.

(iii) Another critical requirement on industrial applications of these sensors is the ease with which the acquired data signals can be processed into a desired output format that can be easily analyzed and interpreted correctly for further action by the autoclave controller. Information in this aspect is lacking and is very important if these sensors have to be interfaced with autoclave instrumentation.

(iv) Finally, no comprehensive knowledge is available on critical issues related to practical aspects of applying these sensors in an industry such as sensor installation and operating condition, and their impact on data quality and

interpretation, geometry and quality of samples on data quality and interpretation, etc.

Hence, the objective and scope of this thesis is to study the above-mentioned issues and generate the required and related knowledge that would enable the objective evaluation of industrial suitability of these sensors for on-line monitoring of autoclave processing of polymer composite structures.

CHAPTER 3

EXPERIMENTAL DETAILS

3.1 Introduction

This chapter describes the mold, materials, equipment and procedure used in this experimental component of the study carried out in order to evaluate the suitability of various sensors for on-line monitoring of autoclave processing of polymer composites.

3.2 Simulation of Autoclave Environment

The parameters of interest and the corresponding signals to be measured by each sensor during curing of the neat resin and composites have been listed in Table 1.1. To simulate the autoclave curing environment, a processing mold, as shown in Figure 3.1, was designed and machined at the University of Manitoba. The mold was designed to be able to take high curing temperature, pressure and vacuum simultaneously. It was equipped with feed-through passages for sensors, vacuum and pressure tubes. The mold was machined with a suitable size and weight for easy handling and placement within the oven chamber.

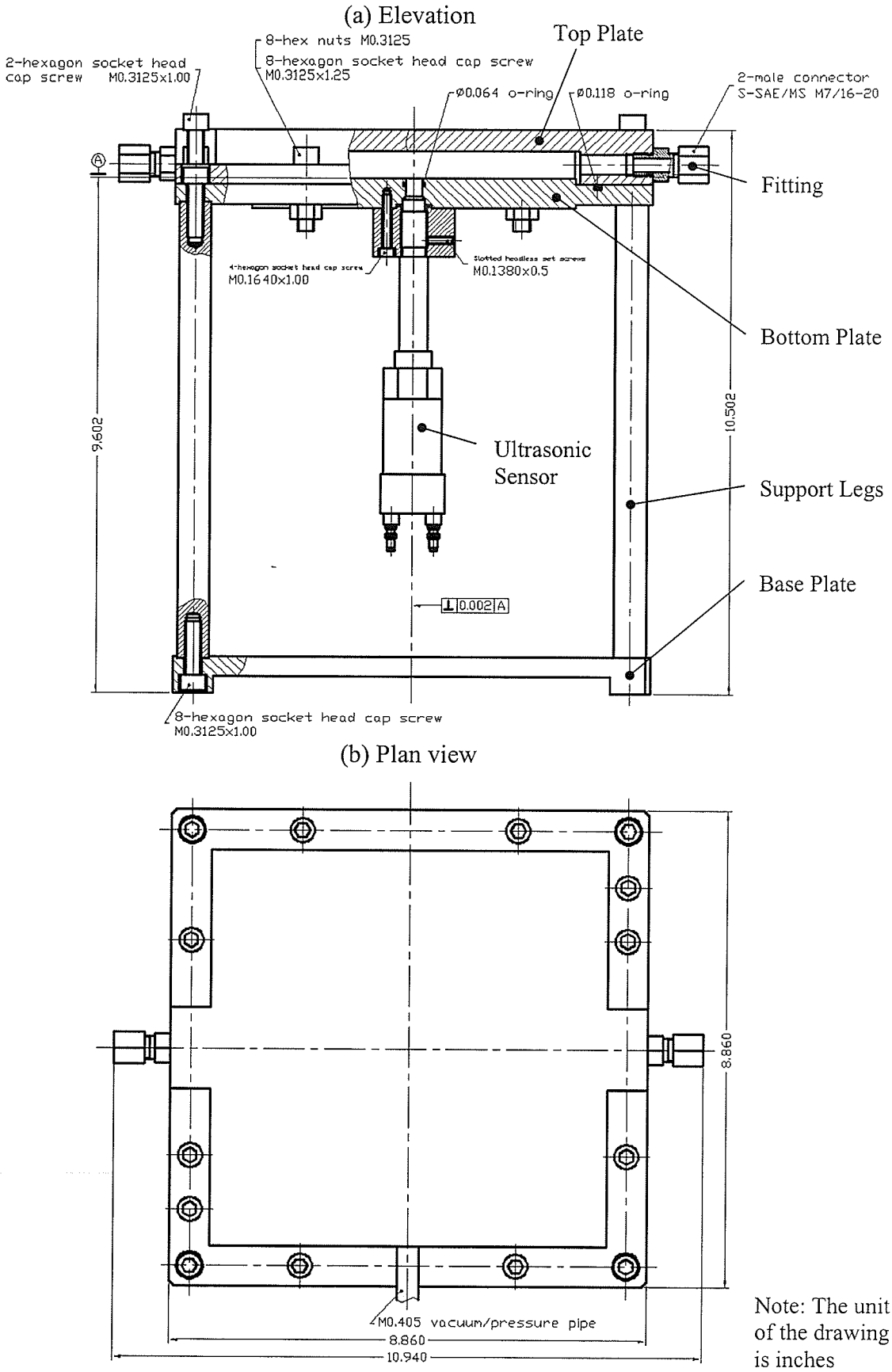

Figure 3.1 The processing mold

The mold was made of mild steel. It consisted of three components: the top plate, bottom plate and support legs. The top plate was designed as a cover with a dimension of 225×225 mm (8.86"×8.86") and enclosed a processing chamber between itself and the bottom plate. Three ports were machined on the top plate. One was on the front wall for connecting a 6.35 mm (¼") copper tube used to apply the nitrogen gas pressure. The other two ports were located on the sidewalls with standard stainless fittings. These fittings were used as feed throughs for sensor cables and thermocouple wires. To minimize the bending of sensor cables and wires, especially for FBG sensors, the centerline of input/output ports were designed close to the top surface of bottom plate.

A 152.4×152.4 mm (6"×6") raised platform was machined on the bottom plate. A hole was drilled at the center of the platform to firmly mount the buffer rod of the ultrasonic sensor. A small O-ring was placed inside the hole to prevent the resin from leaking out. Another hole was drilled at one corner of the bottom plate and connected with a copper tube. This port was used to apply the vacuum. To seal the mold, a groove was machined along the edge of the bottom plate. A 3 mm diameter O-ring was placed in the groove. By assembling the bottom plate with the top plate, a chamber with a dimension of 152.4×152.4×12.7 mm (6"×6"×0.5", length×width×height) was formed. The two parts were assembled together and sealed by an O-ring, eight bolts and nuts.

The ultrasonic sensor was mounted on the mold through the center hole at the bottom plate using a threaded connector. The end of the buffer rod was flush with the top surface

of platform in the bottom plate in order to yield a good contact between the specimen and the buffer rod. The entire mold was supported by four 216 mm (8.5") long legs.

The height of the mold was about 266.7 mm (10.5"), and the weight was about 12.1 Kg (26.7 lb). Finite element analysis was performed to confirm that that the mold was capable of withstanding the applied pressure. The analysis results can be found in Appendix A.

The processing mold was heated in a programmable oven (CW-6680-E-MP550) from GS Blue M Electric. The oven was equipped with a RPO-550 controller, and a 508×508×508 mm (20"×20"×20") chamber. The level of the mold was adjusted using the screws on its support legs. The height of the mold fittings was adjusted to be at the same level as the oven feed through ports on the sidewalls of the oven, so that the cables, wires, and tubes could be connected to the mold from outside with less bending.

As shown in Figure 3.2, the ultrasonic sensor and the dielectric sensor cables, the FBG sensor and thermocouple wires were fed through the oven port and connected to the mold using standard feed-through connectors. In order to prevent the leakage of gas, a small Teflon plastic part was machined and inserted into the connector to replace the steel ferrule. Three small holes were drilled through the Teflon part to fit the diameter of cables and wires. During processing, the unused holes were blocked. In addition, three pieces of high temperature rubber and an aluminum plate were inserted together with the

Teflon part into the fitting as shown in Figure 3.3 to obtain good sealing. The Teflon and rubber parts had to be changed after several experiments.

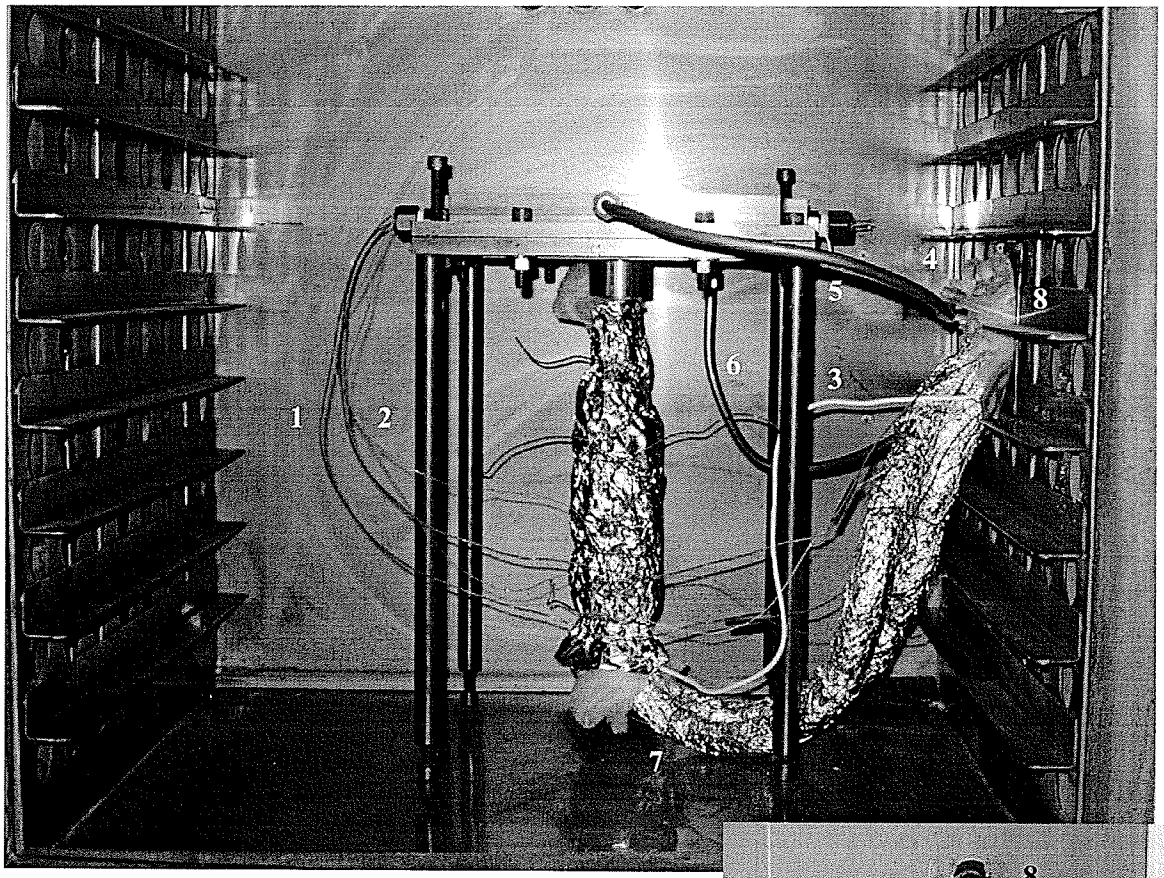

1. Dielectric sensor wires
2. Thermocouples
3. Ultrasonic sensor cable
4. FBG sensor
5. Pressure tube
6. Vacuum tube
7. Compressed air tubes
8. Input/output port of the oven

Figure 3.2 Experimental Setup

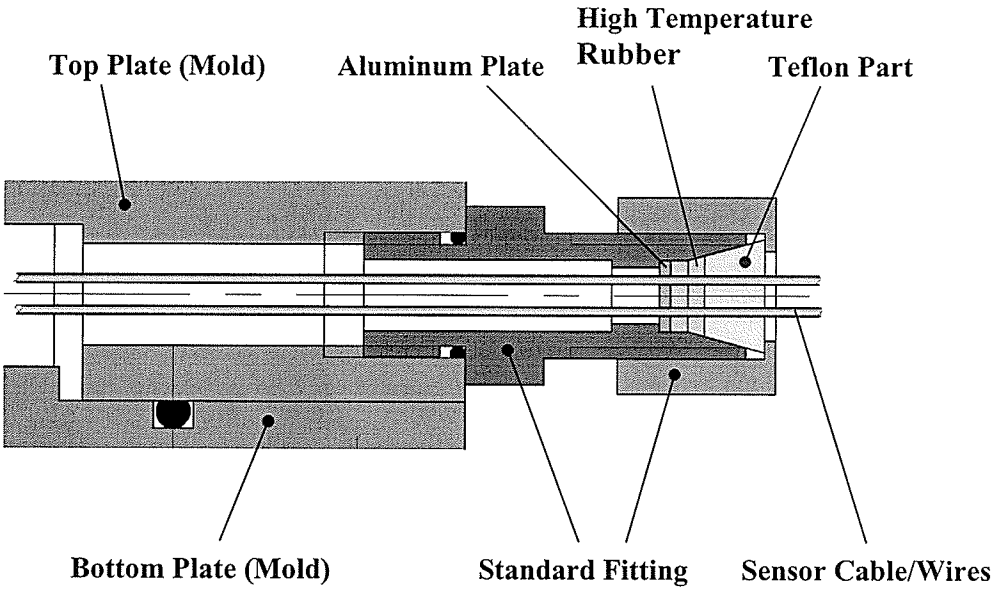

Figure 3.3 Pressure fitting used in experiments

A 6.35 mm (¼") copper tube was connected to the pressure port on the top plate. Nitrogen gas at 0.586 MPa (85 psi) was applied through the tube. Vacuum was applied by a vacuum pump through another 6.35 mm (¼") copper pipe connected to the vacuum port on the bottom plate. The ultrasonic sensor was cooled by the compressed air at 0.69 MPa (100 psi) and at room temperature using two Teflon tubes. The sections of Teflon tubes inside the oven were wrapped in 2 to 3 mm thick fiberglass insulation and a thin aluminum foil to minimize the heating of the compressed air. The same insulation structure was applied to the buffer rod as shown in Figure 3.2. Using this set-up, the outlet air temperature after cooling the sensor was about 41°C, which was 7 to 9°C lower than the condition without thermal insulations.

3.3 Materials

To evaluate the sensors, a high temperature curable neat resin system, a composite composed of this neat resin as matrix, and a room temperature curable resin system were used in the experiments. The high temperature curable resin was Cytec-Fiberite 934 system. The composite was Cytec-Fiberite HMF 5-322/34C composite made up of Cytec-Fiberite 934 resin and Toray T300 carbon fibers as reinforcement. The fiber was in a plain weave fabric form. The volume fraction of carbon fiber in the prepreg was 57.3%. Both the resin and composite were stored in a freezer at a temperature of –18°C. The resin was stored in small vials and a small quantity of prepreg was kept in airtight bags. Before experiments, the materials were allowed to thaw to room temperature before being removed from the vial/bag to avoid condensation of moisture. The 934 neat resin system had 3% acetone to decrease the viscosity of the resin. If the acetone is not removed, it could get entrapped in the cured resin as air bubbles and could affect the experiment results. Hence the thawed materials were subsequently dried in vacuum oven/ desiccators from several hours to a week to remove as much acetone in the resin as possible, as well as any entrapped moisture air bubbles. The required cure kinetics, thermal-physical, rheological and mechanical properties of the materials have been measured and modeled by Koteshwara (3). The summary of results of material characterization can be found in Table 3.1.

Table 3.1 Summary of the results of Material Characterization

Classification	Properties	Measured Values
Physical	Density Fiber volume fraction	Resin: 1300, Fiber: 1760 57.3 %
Cure Kinetics	Total heat of reaction (kJ/kg °C) Activation energy (kJ/mol) Log Z (1/min) Reaction order (n)	$H = 483.1$ $E = 34.88$ 3.11 $n = n_o + A/(1+\exp(-(T-T_o)/B))$ $n_o = 14.953$, $A = -13.244$, $T_o = 139.218$, and $B = 9.951$
Thermo-Physical	Specific heat capacity (J/kg °C) Thermal conductivity (W/m^2 K) CTE of composite × 10-6 / °C Coefficient of cure shrinkage for composite	Resin: $Cp = 2.7\ T + 200.0$ Fiber: $Cp = 1.1\ T + 1560.0$ $K_{11} = 5.27 + 0.0389\ T$ $K_{22} = K_{33} = 2.567 + 0.0123\ T$ $\alpha_{33} = \alpha_{22} = 36.5$ $\alpha_{11} = 3.5$ $\epsilon_{33} = \epsilon_{22} = -0.0249$ $\epsilon_{11} = -0.000485$
Rheological	Viscosity Gel point Glass transition temperature (T_g)	$\mu = \mu_\infty \exp(k\alpha) \exp(U/RT)$ $\mu_\infty = 8.858\text{E-}16$ Pas, $k = 28.264$ $U = 103.309$ kJ/mol $T = 177.4^\circ$C, $\alpha = 0.4$ $T_g = 19.538\exp(2.4617\ \alpha)$
Mechanical	Modulus of composite GPa	For, $0 \le \alpha \le 0.32$, $E_{11} = 57$GPa & $E_{22} = 1.83$GPa, For, $0.32 \le \alpha \le 1.0$, $E_{11} = 38.571\ \alpha + 87.963$ $E_{22} = 2.448\ \alpha + 3.624$ $G_{12} = 0.112\ \alpha - 0.0126$, $0.32 \le \alpha \le 0.86$ $G_{12} = 31.7\ \alpha - 27.1$, $0.86 \le \alpha \le 1.0$

A brief account of calculation of the degree of cure using the prediction model is given below. The cure kinetics parameters such as heat of reaction (H), Arrhenius constant (k), reaction order (n), activation energy (E), and pre-exponential factor (Z) for resin and

composite were obtained using TA instruments 2910 Modulated Differential Scanning Calorimeter (MDSC). Isothermal scans were performed at peak temperature 190°C and at range of temperatures between 100°C and 190°C. The dynamic scan data was used along with isothermal data to solve equation 3.1, in isothermal kinetics, to obtain the Arrhenius constant and reaction order at various cure temperature.

$$\frac{d\alpha}{dt} = k(1-\alpha)^n \tag{3.1}$$

where $d\alpha/dt$ rate of degree of cure

α degree of cure

n reaction order

k reaction rate constant (1/min)

The temperature dependence of the reaction rate constant is given by:

$$k = ze^{(-E/RT)} \tag{3.2}$$

where E activation energy (J/mol)

R gas constant (8.314 kJ/kg K)

T absolute temperature (T)

z pre-exponential factor (1/min)

The temperature dependence of the reaction order was modeled as:

$$n = n_0 + \frac{A}{1+e^{\left(\frac{-(T-T_0)}{B}\right)}} \tag{3.3}$$

where n_0, A, T_0 and B model constants

T Temperature

In this study, the degree of cure was expressed as:

$$\Delta\alpha = k(1-\alpha)^n \Delta t \tag{3.4}$$

The uncured specimen was assumed to have an initial degree of cure value of 0.05. The values of k and n were calculated using equations 3.2 and 3.3 at each recorded process time and temperature. Applying the process time increment Δt, the increment of degree of cure $\Delta\alpha$ was calculated using equation 3.4. By adding each $\Delta\alpha$ to the α value calculated at last recorded process time, the final level of degree of cure was thus determined. The parameters such as viscosity, moduli and cure shrinkage were hence able to be determined as the function of degree of cure.

The room temperature curable fiberglass resin did not require cold storage and it was only used to assist for this study. To make a specimen, the resin that contains polyester resin and styrene monomer, and the MEKP liquid hardener was mixed to a certain ratio in a crucible. The weight ratio used in this study for resin and hardener is 13.7:1, at which the specimen can be cured in 6 hours without bubbles. The resin and hardener was quickly mixed and stirred, and the mixture was poured into the processing mold.

3.4 Experimental Set-up

3.4.1 Ultrasonic Monitoring Test Set-up

The ultrasonic monitoring test set-up consisted of an ultrasonic sensor and a pulser/receiver controlled by a computer. The ultrasonic sensor was made up of a transducer at one end and the buffer rod at the other end as shown in Figure 3.4. The sensor was supplied by NRC, Quebec. A 10 MHz longitudinal wave transducer V112-SM

manufactured by Panametrics Inc., USA was used in the sensor. The transducer was mounted in place within the sensor using mechanical clamping pressure, which ensured good contact with the buffer rod. An ultrasonic couplant was used between the transducer and the buffer rod to ensure loss-free transmission of ultrasonic waves. The sensor has a microdot connector, which made contact with the transducer at one end. The other end was connected to the pulser/receiver through a BNC cable.

The buffer rod acted like a wave guide and protected the transducer from high temperature processing environment. The buffer rod consisted of a steel core and a thermal-sprayed stainless steel inner cladding surrounded by a bronze outer cladding. To ensure that the maximum amount of ultrasonic energy was transmitted into the test specimens, the surface of the buffer rod in contact with the ultrasonic transducer was machined to be perfectly flat. Otherwise, ultrasonic waves would be reflected and scattered in all directions even with the presence of a couplant, and both the intensity and propagation distance of ultrasonic waves would weaken significantly. The top end of the sensor, which holds the transducer, was connected to the buffer rod using four screws.

A Sensor-Safe Red HI-TEMP gasket maker (high temperature silicon sealant), which could take the temperature up to 345°C, was used to seal the gap between the top end and buffer rod. The operating temperature of the piezoelectric ultrasonic transducer was 60°C, which was much lower than the curing temperature of the composite materials, 177~200°C. To ensure that the temperature of the transducer was below its allowable value, a spiraled groove had been machined in the wall of the sensor by the manufacturer.

Compressed air at 0.69 MPa (100 psi) was applied to the sensor through this groove to cool the transducer to a temperature below 50°C.

Several ultrasonic couplants were tested by the author, including Shear Gel, HIGH Z (low viscosity and high viscosity version), SONOTEMP, SONO 600 and Ultragel II. All the couplants were manufactured by SONOTECH Inc., USA. Shear Gel could support both longitudinal and transverse waves, while the others could be used to carry longitudinal wave only. The HIGH Z couplant with high viscosity was found to be the most stable couplant in the testing environment.

The sensor was flush-mounted with platform of the bottom plate of the processing mold as shown in Figure 3.4. Teflon tubing was connected to the sensor inlet and outlet ports for air cooling, which helped to keep the transducer as well as the couplant below the designed operating temperature of 60°C.

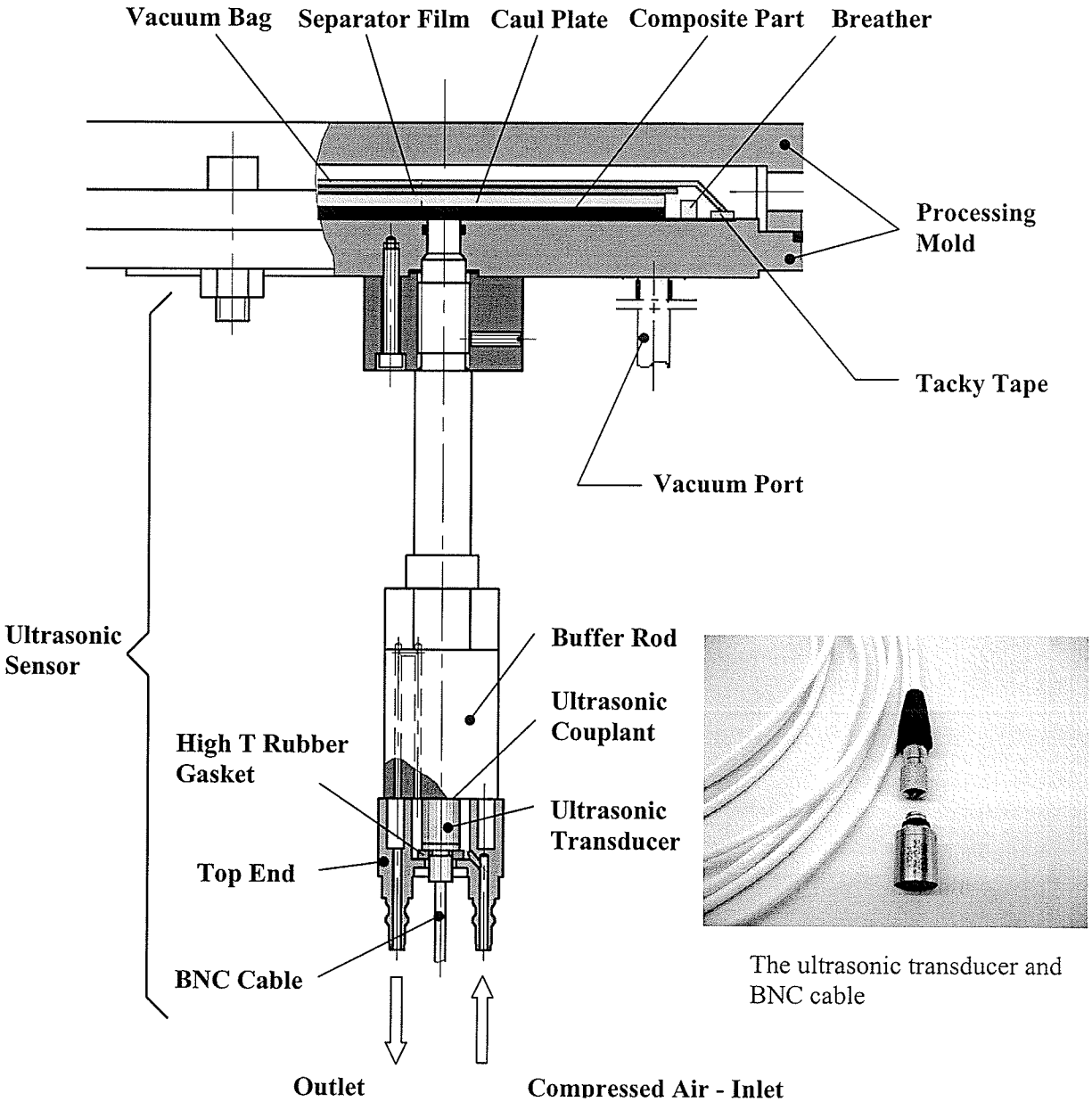

The ultrasonic transducer and BNC cable

Figure 3.4 Ultrasonic monitoring set-up

The pulser/receiver used in this study was a part of the CUB Ultrasonic Immersion Inspection System from TEKTREND (Rd-Tech), Quebec, as shown in Figure 3.5.

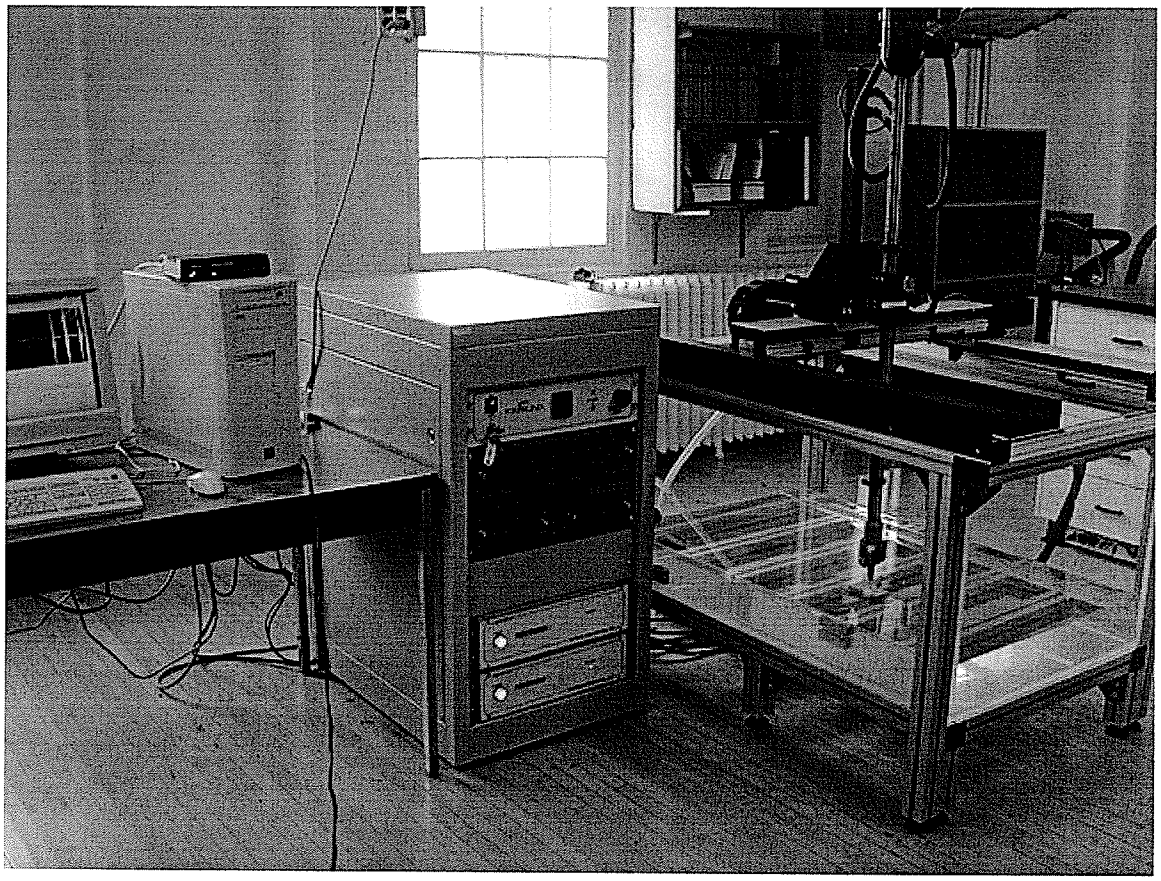

Figure 3.5 CUB ultrasonic immersion inspection system

CUB is a multi-axis immersion ultrasonic inspection system. The PRC35 ultrasonic pulser/receiver installed in the inspection system was used to supply the exciting voltage and receive echo signals. Ultrasonic waveforms were recorded by STR 8100 digitizer with 50 MHz sampling rate and 1 min time intervals. ARIUS IV software system was used to manage the entire process of ultrasonic testing and result analyzing. The scanning images could be displayed on-line by the software.

The control parameters set for STR 8100 and PRC35 are listed in Table 3.2.

Table 3.2 Control parameters for ultrasonic sensing

Digitizer – STR 8100		**Pulser/Receiver – PRC35**	
Sampling Rate	50 MHz	Gain	40 dB
Input Voltage	1 V	Energy	60 μJ
Peak Mode	THR XING	Damping	15
Signal Type	RF	LP Filter	35.0 MHz
Averaging	16 – 32	HP Filter	5.0 MHz

The pulse/echo mode was applied in this study, as shown in Figure 2.1.

Two parameters measured in the experiments were the time delay and attenuation. The time delay was measured as the time period between the main bang and the first echo from the specimen/caul plate (air) interface, as illustrated in Figure 3.6.

The attenuation was calculated using the equation:

$$\alpha = 20\frac{1}{h}\log\frac{A}{A_0}\ \text{dB/mm} \tag{3.5}$$

In this study, A_0 was defined to be the maximum value of the signal amplitude recorded in an experiment, as shown in Figure 3.7, which was a constant. A was the amplitude in any instant (the current amplitude) of process time.

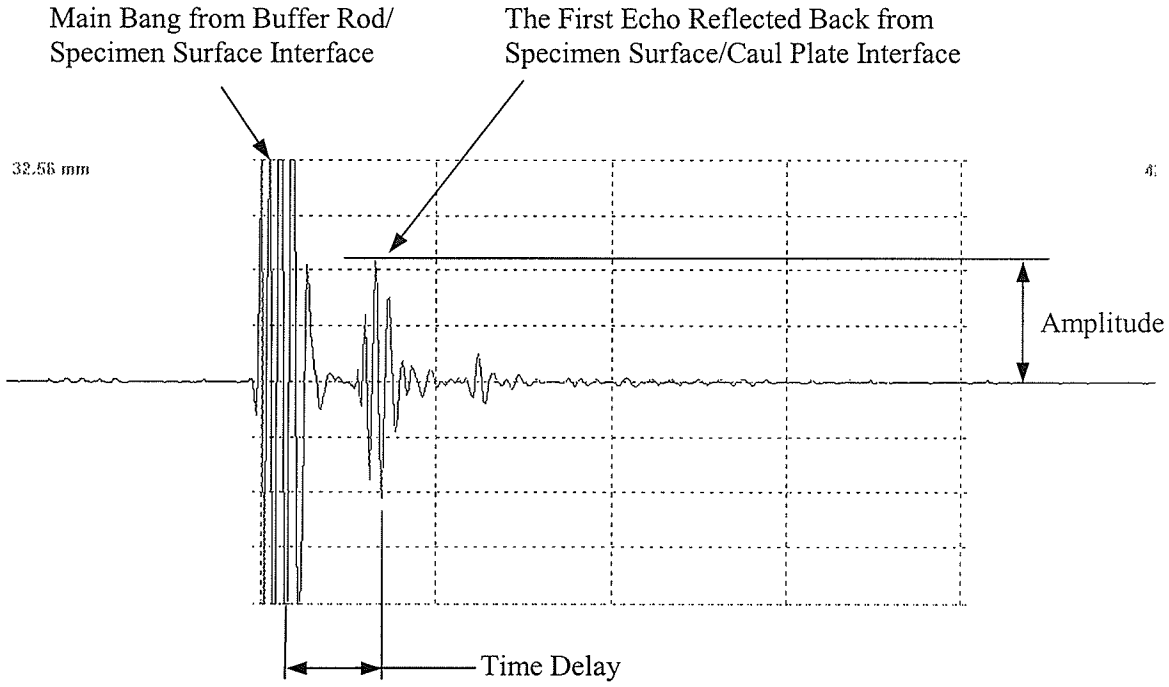

Figure 3.6 Ultrasonic signal of a cured composite laminate

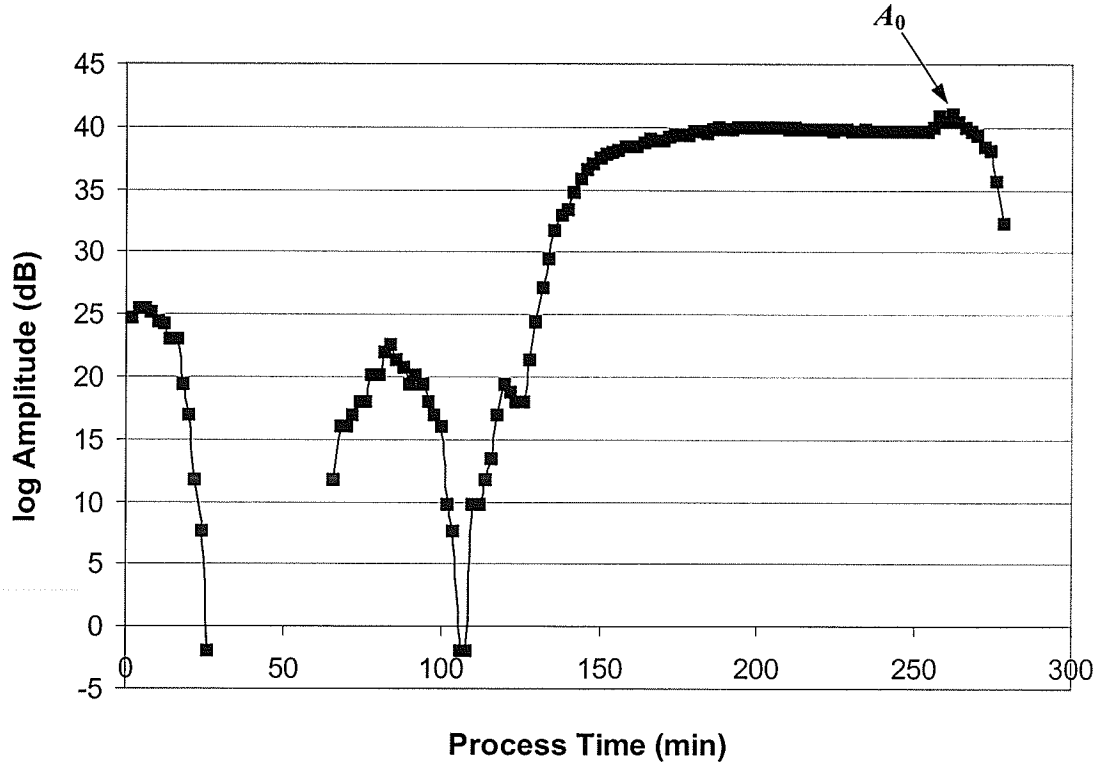

Figure 3.7 Ultrasonic amplitude data for a resin specimen

The sensing data was acquired and stored by the ARIUS IV software system in a special format. The software converted and displayed the data in real time in A-Scan mode (the time – amplitude plots) during curing. The raw data of the ultrasonic response cannot be directly used for analysis after monitoring. The other software programmed using MATLAB and provided by the manufacturer of the CUB system was modified in this study to receive and convert the sensing data from raw data files to a usable format. The processed data is plotted in Figure 3.6. The time corresponding to the main bang and the first echo reflected back from the specimen/caul plate (air) interface, and amplitudes of the first echoes were read manually in A-Scan Analysis Mode of ARIUS IV software system to calculate the time delay and attenuation. This is a time consuming work and it cannot be used in on-line monitoring and control of the curing process. Hence an intelligent algorithm is required for this purpose.

3.4.2 Dielectric Monitoring Test Set-up

The implantable Inter-Digitated Electrode (IDEX) fringe measurement sensors (068S series and 069S series) from Micromet USA, were used in the experiments and are shown in Figure 3.8. Both sensors had an electrode spacing of 0.013 cm (0.005"), and pre-wired Teflon coated wires that connected the sensor head to the instrument. The difference between the two sensors is that 069S sensors were covered with layers of glass felt and glass cloth, while the 068S sensor did not contain such layers. The filter layers prevented the sensors from shorting due to contact with the conductive carbon fibers. However, they allow the resin to flow through to reach the sensing grid. The specifications of the sensors are listed in Table 3.3.

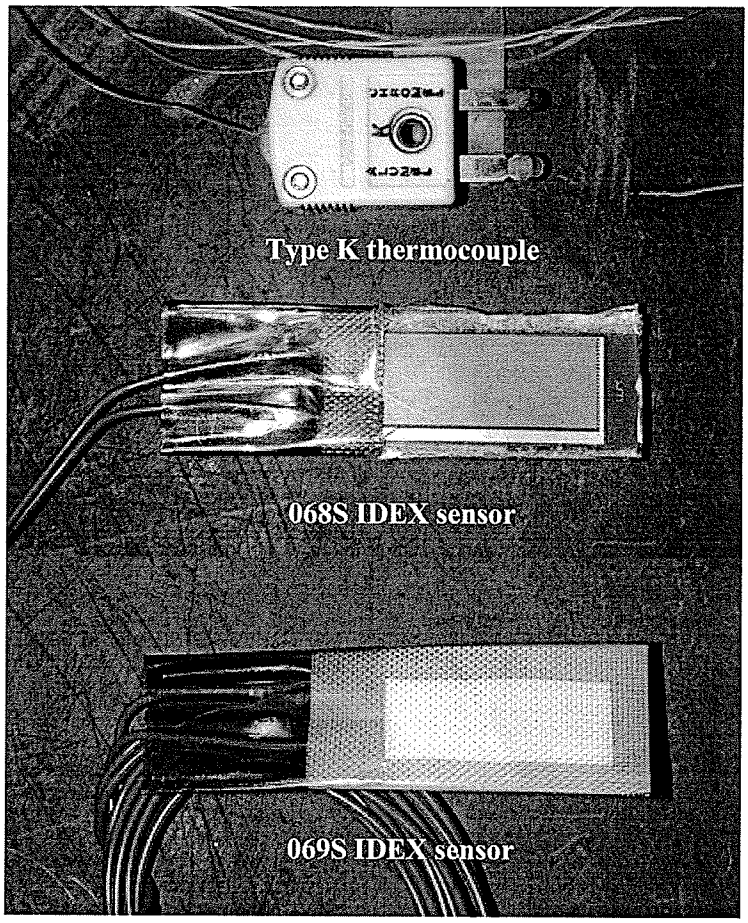

Figure 3.8 IDEX fringe measurement sensors

Table 3.3 The specification of the dielectric sensors

Parameter	**Specification**
Sensor Dimensions	35.56 x 0.953 x 0.015 cm (14" x 0.375" x 0.006")
Active Face Dimensions	2.54 x 0.826 x 0.015 cm (1" x 0.325" x 0.006")
Electrode Spacing	0.013 cm (0.005")
Operating Frequency Range	0.1 to 100,000 Hz in Mid Conductivity mode 0.001 to 100,000 Hz in High Conductivity mode
Measurement Values	
Log Conductivity (Siemens/cm)	-13 to -4 in Mid Conductivity mode -11 to -2 in High Conductivity mode

Log Ion Viscosity (Ohm-cm)	4 to 13 in Mid Conductivity mode 2 to 11 in High Conductivity mode
Log Loss Factor	1 to 4 in Mid Conductivity mode 1 to 6 in High Conductivity mode
Permittivity	1 to 10^5 in Mid Conductivity mode None in High Conductivity mode
Operating Temperature Range	-150° C to 375° C (-283° F to 707° F)
Pressure Limitations	66.7 kg/cm^2 (1000 psi)
Distance from DEA	Up to 20 m (60')

DEA 230/1 cure monitor as shown in Figure 3.9 from Micromet was used to perform the dielectric monitoring work. To monitor the temperature in real-time, DEA 230/1 is equipped with a Type J thermal couple jack. In this study, the equipment was re-configured to use Type K thermocouples.

The Mid Conductivity measurement mode was used in the monitoring work. It permits measurements of dielectric loss factor and permittivity to be performed on materials with bulk conductivities ranging from 10^{-13} to 10^{-3} Siemens/cm. 12 scanning frequencies in the range from 0.1 Hz to 100 KHz (0.1, 1, 10, 50, 100, 200, 500, 1,000, 5,000, 10,000, 50,000, 100,000 Hz) and 20 second time intervals were used to record the dielectric data.

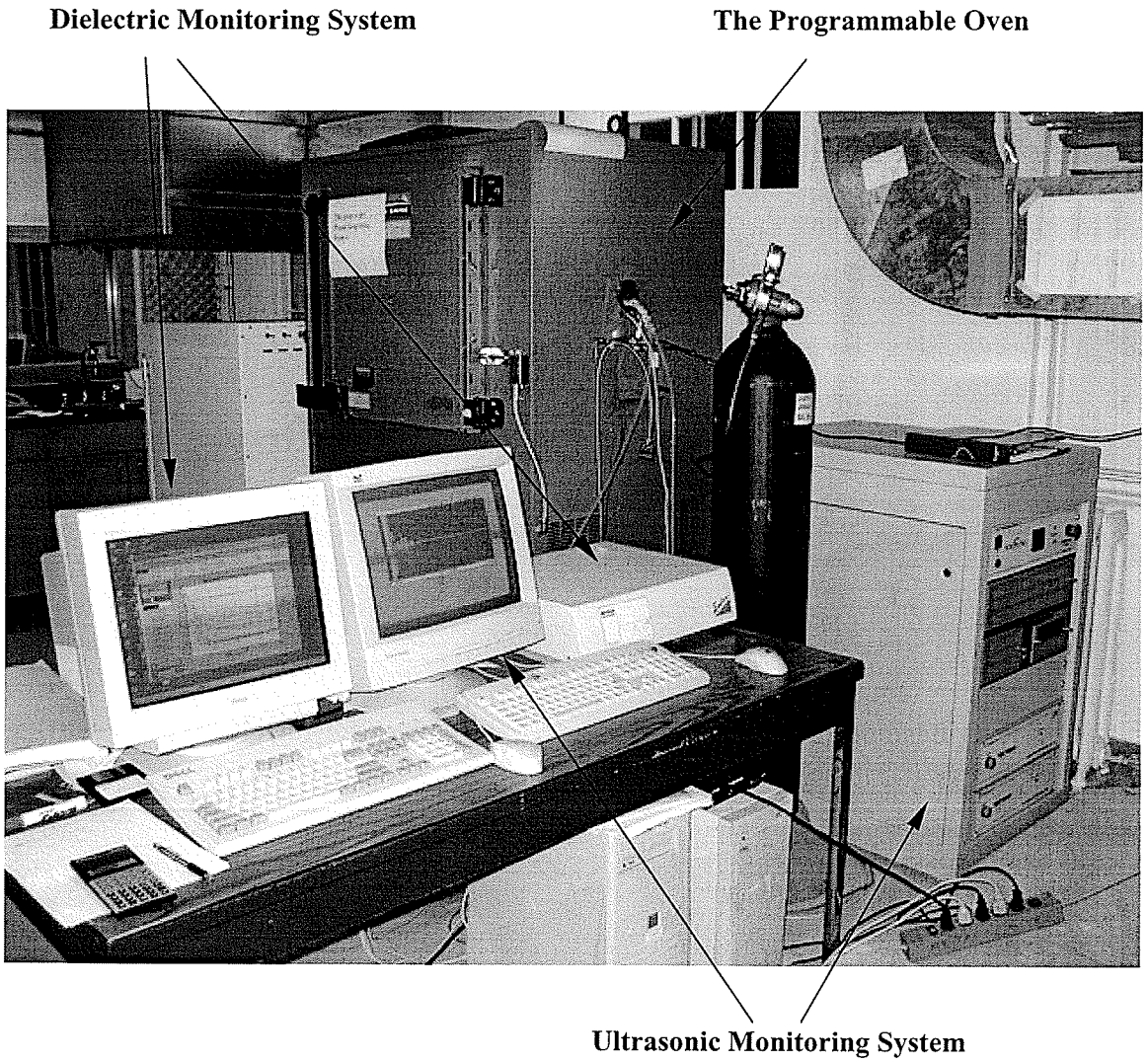

Figure 3.9 Dielectric and ultrasonic monitoring test set-ups

The sensing data was acquired and stored by the Eumetric software system in ASCII format. Parameters including the response voltage, current and phase difference were measured by the equipment. The permittivity, loss factor, log Ionic Viscosity and dlog IV/dt etc. were calculated and displayed by the software based on the sensing data in real time during curing. These parameters can also be transferred to an Excel file format by the software after monitoring, allowing for this data analysis performed separately. Because only one frequency was scanned at any instant of time, the recorded data was

shown in Figure 3.10 with missing data at certain time. A VBA program was developed to determine the missing data using linear interpolation.

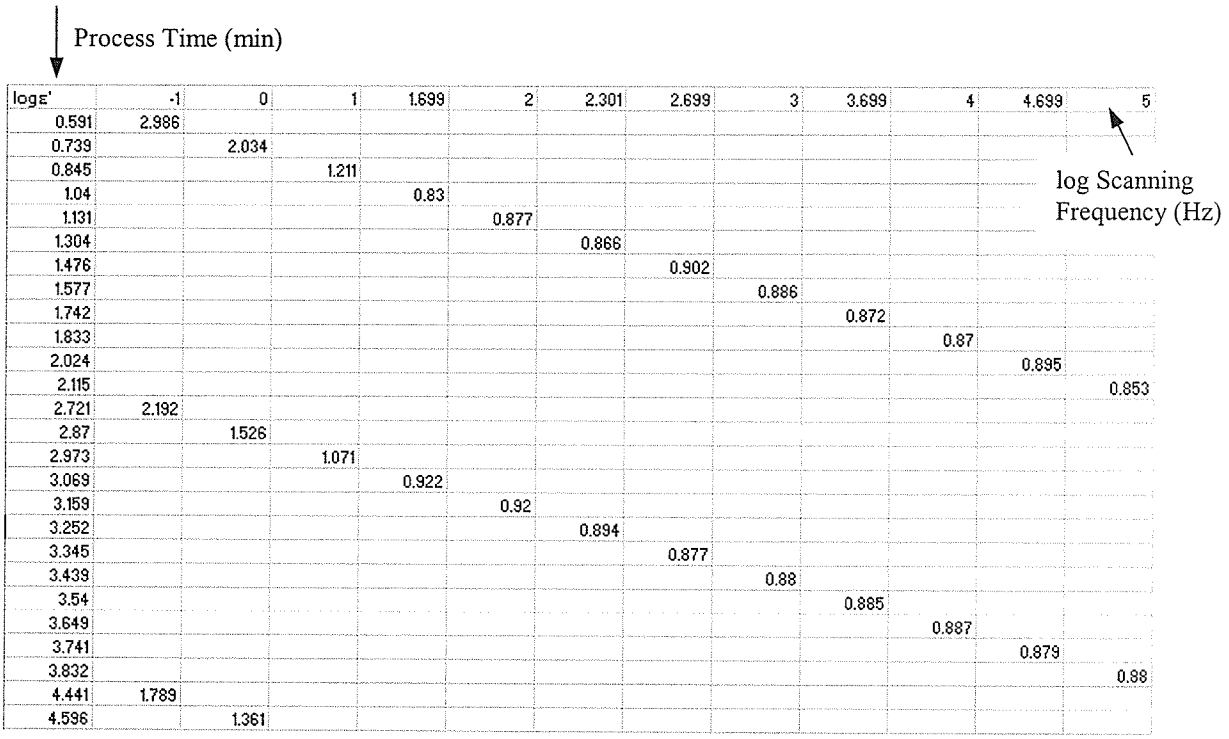

logε'	-1	0	1	1.699	2	2.301	2.699	3	3.699	4	4.699	5
0.591	2.986											
0.739		2.034										
0.845			1.211									
1.04				0.83								
1.131					0.877							
1.304						0.866						
1.476							0.902					
1.577								0.886				
1.742									0.872			
1.833										0.87		
2.024											0.895	
2.115												0.853
2.721	2.192											
2.87		1.526										
2.973			1.071									
3.069				0.922								
3.159					0.92							
3.252						0.894						
3.345							0.877					
3.439								0.88				
3.54									0.885			
3.649										0.887		
3.741											0.879	
3.832												0.88
4.441	1.789											
4.596		1.361										

Figure 3.10 log Permittivity data for a composite specimen

3.4.3 Fiber Bragg Grating Sensor Sensing Test Set-up

The FBG sensors used in experiments were manufactured by O/E Land Inc., in Quebec. Because the cure temperature could be as high as 200°C, the optical fiber was coated with high temperature polyimide for protection from breaking during handling. However, the sensor was still relatively thin and brittle, and must be dealt with very carefully. The sensor is shown in Figure 3.11.

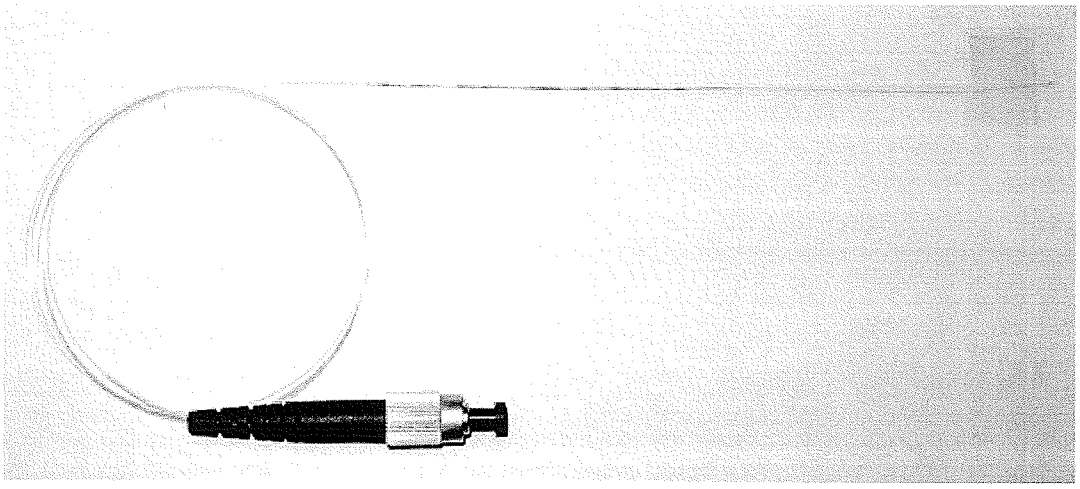

Figure 3.11 FBG sensor

The specification of the sensors is presented in Table 3.4.

Table 3.4 The specification of FBG sensors

Parameter	**Specification**
Wavelength	1539 –1540 nm
Bandwidth @ 3dB	0.17 – 0.2 nm
Reflectivity	>= 90%
Fiber Type	SMF-28
Grating Length	10 mm
Fiber Length	3048 mm (10 ft)
Grating Emplacement	End
Recoating	Polyimide
Connectorization	FC/APC
Bare Fiber Length	30mm

The SHM (Structural Health Monitoring) 5100A system from IDERS Inc., Winnipeg, was used to interrogate the FBG sensors. SHM 5100A as shown in Figure 3.12 generates

and feeds the light to the optical fiber containing the Bragg grating, and receives the light reflected from the grating. The wavelength shift due to straining of the grating is measured and converted to determine the strains built in the specimen during curing.

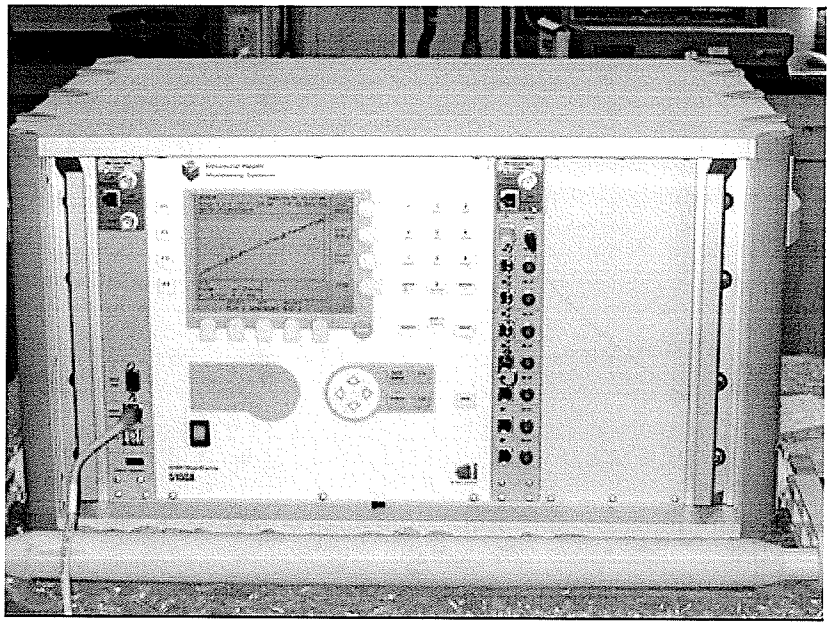

Figure 3.12 SHM 5100A system

While light with center wavelength at 1539 nm was transmitted to the sensor. The measurement range for this study was configured to be -200 to +1000 microstrain.

The SHM 5100A was connected to the computer via a RS-232 or RJ-45 networking cable. The Shmget software system was developed by the manufacturer for communication between the computer and the SHM 5100A. The sensing data was first stored in the data-log memory in SHM 5100A, and then was downloaded to the computer in data files every 5 minutes (this time interval can be changed by the operator). The sampling rate was set at 50 or 100 Hz. Each data file contained 5000 sampled data in a

special format and could not be retrieved and analyzed directly. The manufacturer also provided the other software to convert the raw data files to Text or Excel files. All the converted files were impacted into one Excel file manually (a VBA program was developed in this study to perform this job) and thus the measured strains could be analyzed. An intelligent algorithm is required to automatically convert and pick up the sensing data for analysis during curing.

3.5 Experimental

3.5.1 Specimen Preparation

3.5.1.1 Neat Resin Specimen Preparation

To cure 934 neat resin specimens in the mold using manufacturer recommended processing procedure, a dam was built by laying up several layers of high temperature tacky tape on the platform of the bottom plate. The height of the dam was about 10 mm. The thawed and dried resin at room temperature was poured from a vial into the dam. After that, the mold was enclosed and placed in the oven. The vacuum was not applied and the vacuum port was blocked to prevent the flow of the resin. 0.586 MPa (85 psi) pressure was applied to the mold to remove any bubbles entrapped in the resin and obtain a cured part with good surface quality.

In isothermal experiments, it was not possible to heat the mold to a pre-determined temperature in a very short period because of the thermal lag. The empty mold was preheated in the oven to the cure temperature. When the mold temperature reached the setpoint value, the resin at room temperature was poured into the dam and the oven was

closed within half a minute. The mold was left open within the oven during curing and neither vacuum nor nitrogen pressure could be applied. The specimens of fiberglass resin were prepared similar to 934 resin.

3.5.1.2 Composite Specimen Preparation

The fabric prepreg was cut into 89×89 mm (3.5"×3.5") pieces. 64×64 mm (2.5"×2.5") prepregs were used in experiments involving simultaneous evaluation of all the sensors, because of the limited size of the mold. The cut pieces were packaged in a vacuum bag and stored in the freezer until use. Individual pieces (lamina or ply) were laid manually to obtain 6-ply or 12-ply composite laminate specimens and the fiber directions were same in all plies. Air-gap between plies was removed by manual compaction using a plastic tool. The laminate was debulked in a vacuum to assist in the removal of entrapped air after laying up the lamina layers. The laid-up laminate was vacuumed in a vacuum bag on a steel caul plate for 3 to 5 minutes to obtain good contact between the lamina. After completing lay-up, the laminate was again debulked in vacuum for 5 minutes before use.

The laid-up composite laminate was placed and vacuum bagged on the platform of the mold, as shown in Figures 3.4 and 3.13. The vacuum bag was applied to cover the composite part during processing in an autoclave to prevent its exposure to the pressurization gas used in the autoclave. The vacuum bag is also used to help consolidate the plies by applying a vacuum of -1 atmosphere on the part. Inside the vacuum bag, the composite laminate is covered with various bagging materials. In this study, these

bagging materials along with the outer bag material are referred to as a "vacuum bag". The procedure of vacuum bagging is as follows: the laid-up composite laminate was placed on the platform of the bottom plate of the processing mold, which was pre-coated with the non-stick coating. A steel caul plate was placed above the specimen. A single layer of tacky tape was laid on the platform surrounding the composite panel, so that about 10 to 15 mm gap was left between the specimen and tape dam. This gap was used for placing the breather strips and to limit excessive resin flow. A Teflon separator film was placed above the specimen and the caul plate to separate the vacuum bag from the cured specimen. Thin strips of breather cloth were placed around the edges of the laminate, and strips of glass fibers connected the laminate to the breather, to provide an air path. Thus, the volatilized gases generated during curing could be channeled from the laminate to the vacuum port via glass fibers and the breather. The excessive resin squeezed out from the laminate was absorbed by the breather cloth strips. Finally, a nylon film covered the entire set-up and its edges were stuck to the tacky tape dam using a plastic tool to obtain a good sealing effect. This film prevented the nitrogen gas from entering the bag.

The vacuum bag enclosed the 6.35 mm (¼") vacuum port. During experiments it was found that the nylon film was punctured at the vacuum port because of contact with the rough edge of the port. To avoid this, a small section of copper tube was inserted into the vacuum port. The copper tube was bent to a right angle at the position just above the vacuum port such that a section of the tube was parallel and close to the platform. A small piece of high temperature rubber was placed between the end of the tube and nylon

film to prevent the vacuum bag from being punched by the sharp edge of the tube. The tube end was elevated to prevent it from contacting with the platform. Thus, the resin was prevented from being sucked into and blocking the vacuum port.

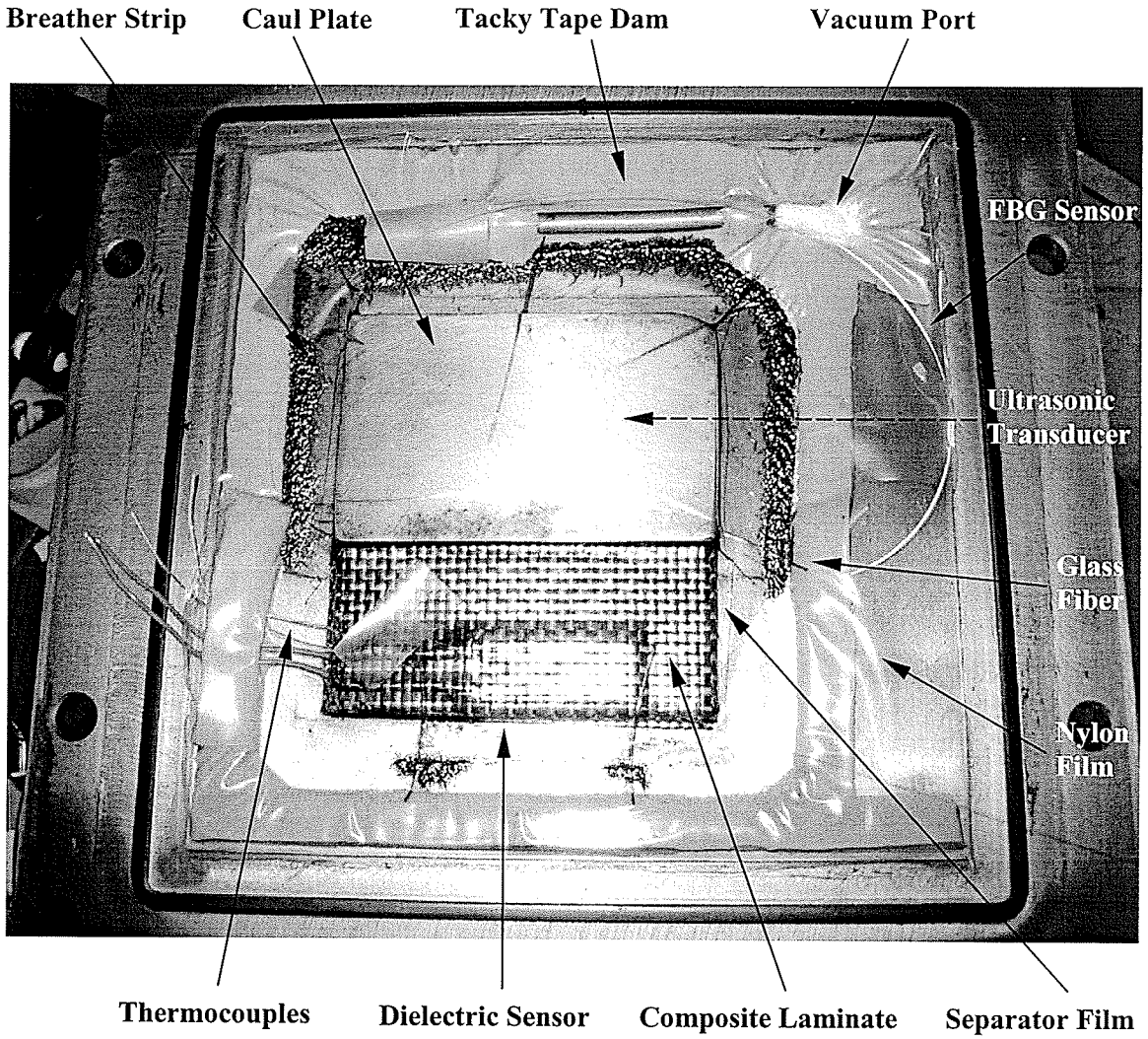

Figure 3.13 Vacuum bagging and sensor embedment (cured composite specimen)

3.5.2 Sensor Embedment

Sensors used in this study included an ultrasonic sensor, a dielectric sensor, a FBG sensor and thermocouples. All the sensors were evaluated simultaneously in one experiment. One or two types of sensors were tested at the same time in most experiments.

3.5.2.1 Sensor Embedment in Neat Resin Specimens

The embedment of sensors in neat resin specimens is shown in Figure 3.14. Since too much resin would attenuate the waves, only sufficient amount of resin that would just immerse the buffer rod end (1 to 2 mm) was used in the experiments. The IDEX dielectric sensor was attached to the platform of the mold using the high temperature tape with the sensing surface immersed in the resin. The FBG sensor was placed with the sensing section (the 10 mm grating) immersed in the resin. However, it was prevented from contacting the platform, so that the sensor would respond to the temperature and strain changes in the specimen rather than that of the mold. Two thermocouples made of TT-K-36-SLE K Type thermocouple wires from Omega Engineering Inc., USA, with a cross-section size of .48×.76 mm (.019"×.030") were placed close to the dielectric sensor to measure the resin temperature during curing. One thermocouple was connected to the thermocouple jacket in DEA 230/1, and the temperature data was measured automatically. The sensing data from the other thermocouple was recorded manually using a multimeter. Pressure was applied only during experiments using modified manufacturer recommended cure cycles. No vacuum and pressure was applied during isothermal experiments.

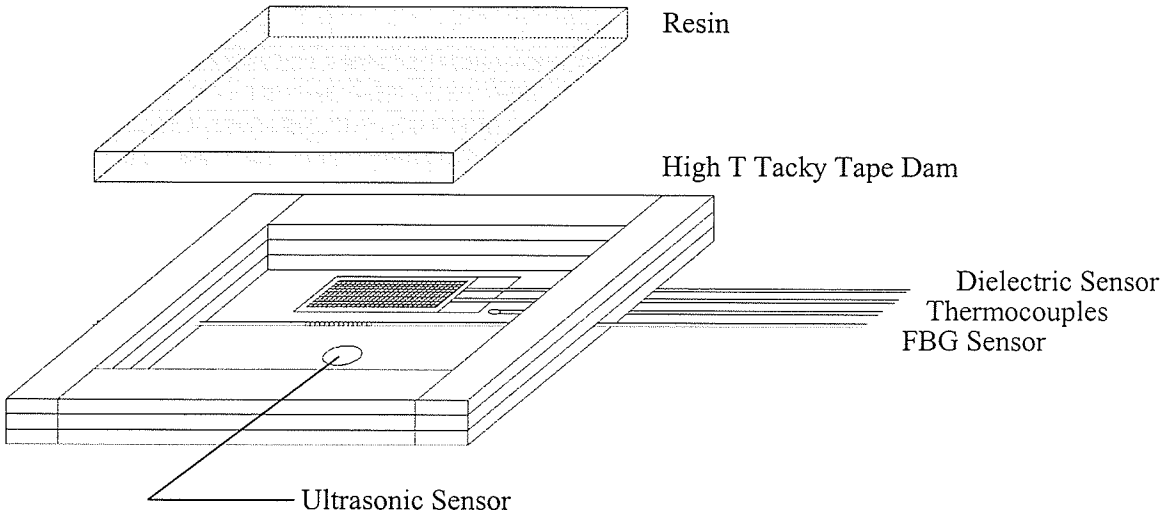

Figure 3.14 Sensor embedment for neat resin specimens

3.5.2.2 Sensor Embedment in Composite Specimens

The embedment of sensors in composite specimens is shown in Figure 3.15. The end of the buffer rod of the ultrasonic sensor was flush with the platform on the bottom plate of the mold, which ensured that the sensor contacted with the bottom surface of the specimen. A small amount of 934 resin was applied between the end surface of the buffer rod and the laminate as the ultrasonic couplant. Thus, even at the beginning of experiment, when the temperature was low and prepreg was in solid state, the signals could still be obtained. A steel caul plate was placed above the laminate to apply evenly the mechanical pressure to the specimen. This resulted in good consolidation surface quality, which was necessary for obtaining strong echoes. The resin was also applied between the caul plate and the top surface of the specimen to act as an ultrasonic couplant. The steel plate did not cover the area of the specimen where the dielectric

sensor and thermocouples were embedded. A set-up without steel plate was also used to investigate the influence of using the steel caul plate.

The IDEX dielectric sensor was embedded between the 3rd and 4th ply in the laminate, close and parallel to the edge of the composite laminate. The dielectric sensor with glass filter was used. Two thermocouples were placed near the dielectric sensor to monitor the specimen temperature during cure. Since the thermocouple jacket of DEA 230/1 was not grounded, the sensing head of the thermocouple was prevented from contacting the carbon fibers using a small piece of high temperature tape.

The FBG sensor was embedded between the 3rd and 4th ply in the laminate along the 0° fiber direction. The grating of the FBG sensor was placed in the middle section of the composite laminate and was well separated from the dielectric sensor. Tight radii of curvature in FBG fiber were avoided to minimize signal loss. Cables and wires of the sensors were fed through the tacky tape dam and port.

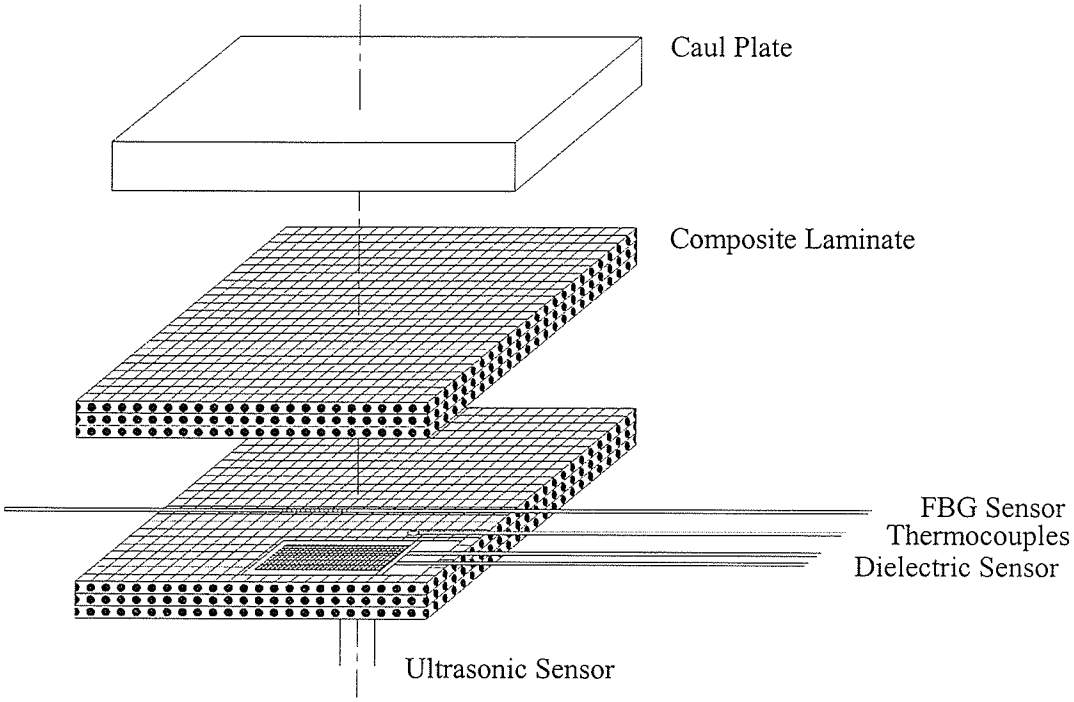

Figure 3.15 Sensor embedment composite specimens

3.6 Cure Cycles

The temperature and pressure cycles used to cure the composite parts is known as the cure cycle. A manufacturer recommended cure cycle for Cytec-Fiberite HMF 5-322/34C is shown in Figure 3.16.

In this manufacturer recommended cure cycle, the autoclave is heated from room temperature to 177°C at a rate of 2.2°C/min. Then the temperature is held at 177°C for 120 minutes. Post-curing at 200°C for 1 hour, after holding at 177°C, is also applied in certain experiments. After the hold period, the autoclave is cooled down to room temperature at a rate of 2.2°C/min. Nitrogen gas pressure at 0.586 MPa (85 psi) is applied at the beginning of the cure cycle and is removed when temperature reaches room temperature. Vacuum is applied at the beginning of the cycle and removed before the

composite part reaches its minimum viscosity state, which is determined from the rheological data for composites.

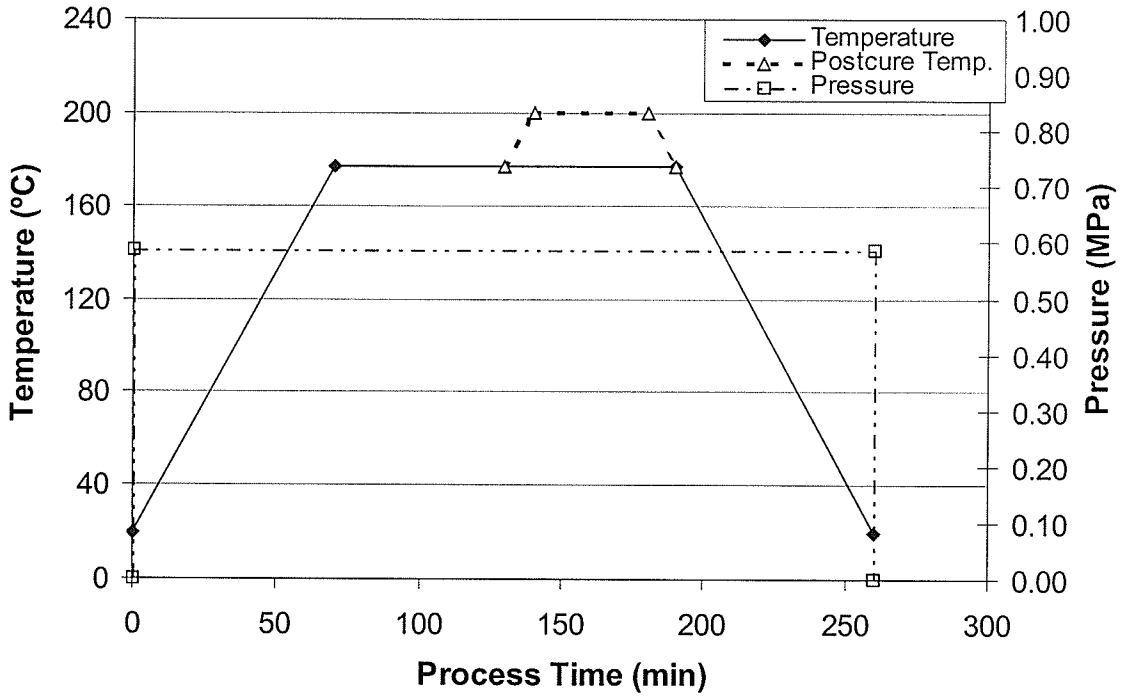

Figure 3.16 The manufacturer recommended cure cycle (MRC)

The above mentioned manufacturer recommended cure cycle was slightly modified in this study. The oven chamber was heated up to 177°C ~ 190°C depending on specific experiment conditions at the rate of 2 ~ 2.5°C/min. The cooling rate was not controlled. The mold was cooled down to room temperature by a fan or compressed air to reduce the cooling time. To prevent excessive resin being squeezed out from the specimen, the pressure was not applied until the vacuum was cut off instead of applying at the beginning. The vacuum was switched off when the temperature of the specimen reached 90°C. The specimen reached its minimum viscosity state at T = 127 ~ 130°C. After removing the vacuum, the N_2 gas pressure was applied to the mold chamber. In some experiments, after holding at about 177°C for 120 minutes, the oven was heated up with

the same heating rate to 200°C and held at this temperature for another 60 minutes. The application of a postcure procedure increased the degree of cure of the specimen to almost 100% ($\alpha = 1$). The postcure procedure was used to evaluate the ability of sensors to detect the end of cure state.

In isothermal experiments, the mold was pre-heated in the oven to the desired temperature, which was set at 164, 176 and 190°C, respectively. The resin was poured into the dam within half a minute, and then the oven was closed. The resin was cured for 3 to 6 hours and then cooled down to room temperature.

The cure cycles applied in the experiments are listed in Table 3.5. The ramp rates and hold temperatures listed are control parameters for the programmable oven.

Table 3.5 Cure cycles applied in experiments

Cure Cycle	**Run Code**	**Type of Specimen**	**Details**
Cycle 1	R934 T-01	Resin	Heating to 177°C at 2.24°C/min – Holding for 2 hrs – Cooling
Cycle 2	R934 T-04	Resin	Heating to 177°C at 3.9°C/min – Holding for 110 minutes – Cooling
Cycle 3	R934 T-05	Resin	Heating to 177°C at 2.24°C/min – Holding for 2 hrs – Heating to 200°C at 2.24°C/min – Holding for 1 hr – Cooling
Cycle 4	HMF T-12	Composite	Heating to 177°C at 2.24°C/min – Holding for 2 hrs – Cooling
Cycle 5	HMF T-13	Composite	Heating to 177°C at 2.24°C/min – Holding for 2 hrs – Heating to 200°C at 2.24°C/min – Holding for 1 hr – Cooling
Cycle 6	HMF T-16	Composite	Heating to 177°C at 2.24°C/min – Holding for 2 hrs – Heating to 200°C at 2.24°C/min – Holding for 1 hr – Cooling

Cycle 7	HMF T-17	Composite	Heating to 190°C at 2.24°C/min – Holding for 3 hrs – Cooling
Cycle 8	HMF T-22	Composite	Heating to 190°C at 2.24°C/min – Holding for 3 hrs – Cooling
Cycle 9	HMF T-23	Composite	Heating to 190°C at 2.24°C/min – Holding for 3 hrs – Cooling
Cycle 10	HMF T-24	Composite	Heating to 190°C at 2.24°C/min – Holding for 3 hrs – Cooling
Cycle 11	HMF T-25	Composite	Heating to 177°C at 2.24°C/min – Holding for 4 hrs – Cooling

CHAPTER 4

RESULTS

4.1 Introduction

Material properties, such as viscosity minimum, gelation, state of cure, cure induced strains and moduli are important parameters for on-line monitoring of curing process, and were measured using the ultrasonic, dielectric and FBG sensors in this study. These parameters are indirectly correlated to the sensor response since no sensor is able to measure them directly.

The response of the sensors during curing of neat resin and composite are presented and discussed in this chapter. A number of experiments involving either a single sensor or a combination of sensors were completed. Various experimental run codes are identified in Table 3.4. For each experiment, a number of trials were completed. Data from one trial is discussed in this chapter. Results of other trials are presented in Appendix C.

Results of sensing using a single sensor are discussed first. Subsequently, data from runs using combination of sensors is presented. Finally a summary of monitoring results is presented.

4.2 Cure Monitoring with a Single Sensor

4.2.1 Ultrasonic Cure Monitoring

Ultrasonic time delay and attenuation were measured during curing. Material parameters, such as the minimum viscosity and gelation are quantitatively related to the measured time delay and attenuation.

4.2.1.1 Ultrasonic Response of Neat Resin Specimen (Cure Cycle 3, R934 T-05)

The resin temperature and predicted degree of cure are plotted in Figure 4.1. The oven was heated to 177°C in 70 minutes, and held for 120 minutes. Subsequently, it was heated to 200°C and held for 60 minutes to post-cure the resin. After the postcure procedure, the resin was cooled down to room temperature. A pressure of 0.586 MPa (85 psi) was applied during the entire cycle. At the end of curing process, the resin's degree of cure approached 0.96, which can be deemed to be a complete cure. Significant thermal lag among mold temperature, the actual specimen temperature, and the setpoint values was observed. The actual specimen temperature was used to predict the degree of cure.

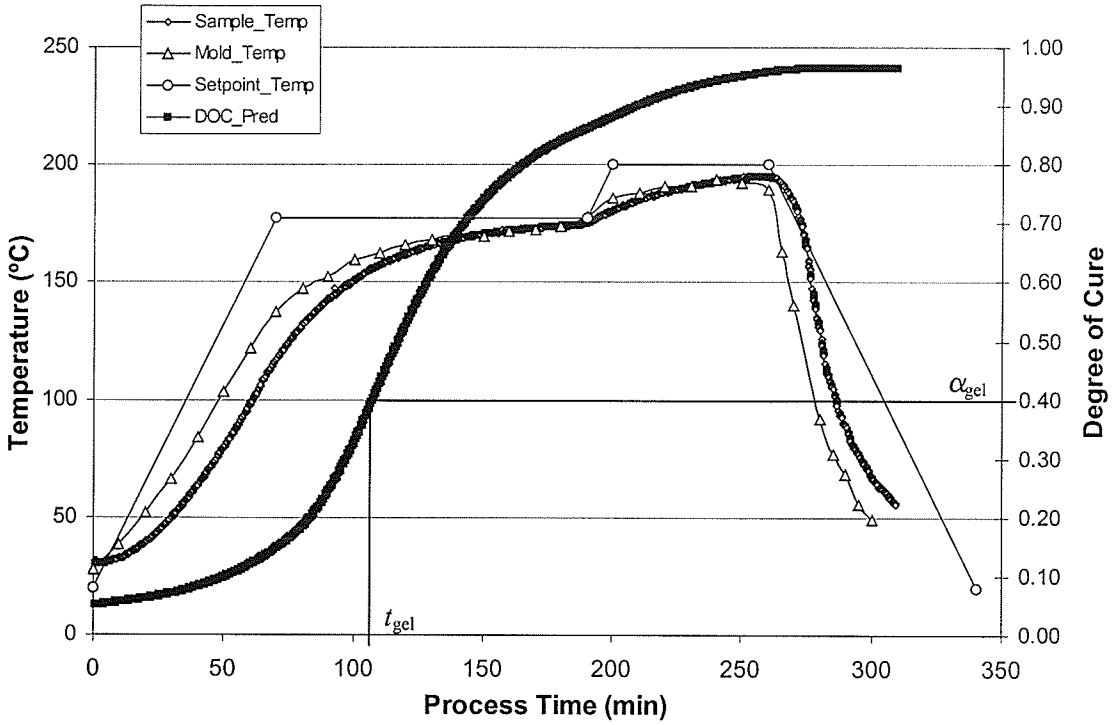

Figure 4.1 Part temperature and predicted degree of cure for cure cycle R934 T-05

Figure 4.2 shows the viscosity of the specimen, which was predicted using the model developed in reference (3) for this resin. The viscosity of the resin decreased with increase in the specimen temperature until a minimum value. The time corresponding to this minimum viscosity at a heating rate of 2.2°C/min is about t = 76.4 minutes. As the process time increased, viscosity started to increase due to the significant curing. The degree of cure, for which the material transformed from a viscous fluid to an infinite-viscosity semi-solid is known as the gel point and was determined to be 0.4 using a rheometer (3). This gelation of the resin occurred at t = 107.3 minutes for this imposed cure cycle. After gelation, the model cannot be used to predict the viscosity of the specimen and hence is not shown in the figure.

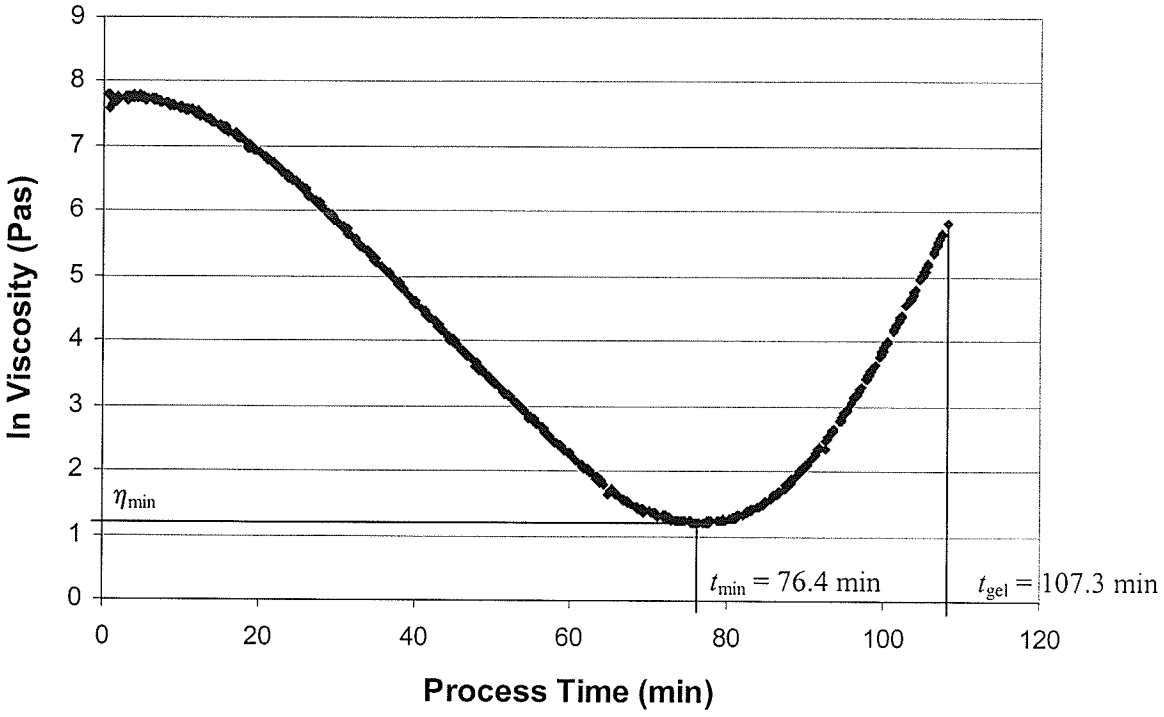

Figure 4.2 Predicted viscosity for cure cycle R934 T-05

The ultrasonic signals were recorded in the A-Scan mode. The waveform at t = 75 minutes is shown in Figure 4.3. The number of points of digitized sample on the acquired analog waveform, since the generation of ultrasonic waves to the traveling of the waves through the specimen thickness direction and being reflected back from the specimen surface, is plotted in x-axis. The ultrasonic time delay is calculated using this number of points and the sampling rate. The amplitude of the ultrasonic wave is plotted along the y-axis, and is calculating the ultrasonic attenuation using equation (3.2). Determination of the time delay and amplitude can be found in Appendix B.

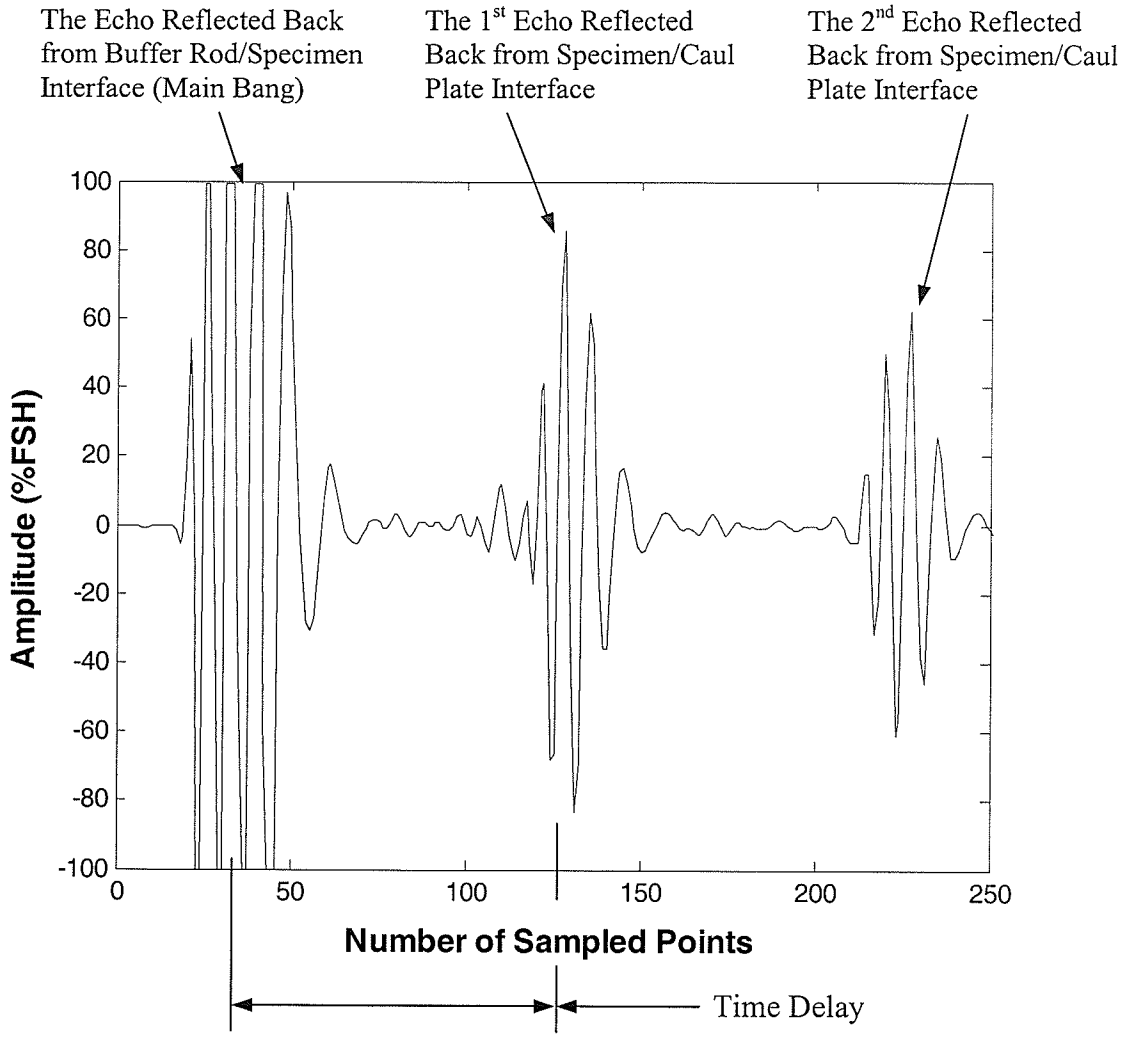

Figure 4.3 Waveforms obtained from the resin specimen in cure cycle R934 T-05

The ultrasonic signals recorded at various discrete process time is plotted in Figure 4.4. The numbers on the right hand side of the figure are the process time. The signals are displayed at a time interval of 5 minutes.

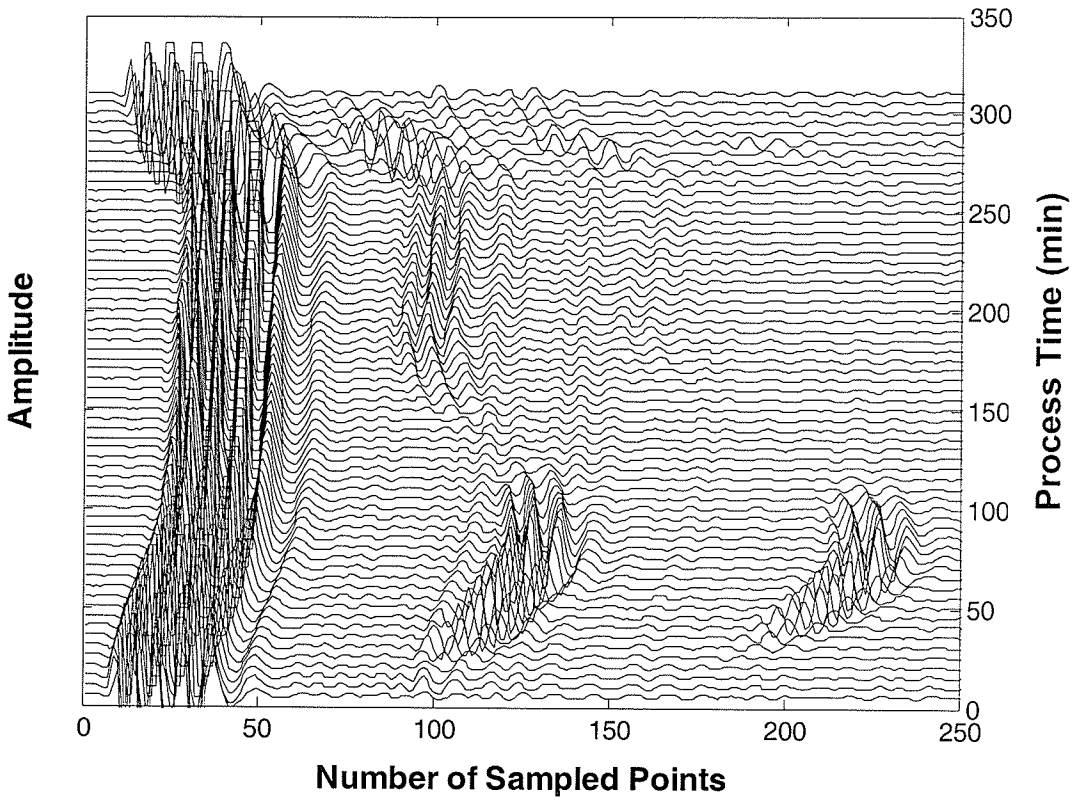

Figure 4.4 Ultrasonic signals recorded in the A-Scan mode at various discrete process time

Time Delay

With increase in temperature, the viscosity of the resin decreased initially, as shown in Figure 4.2. Consequently, the modulus also decreased. Because the sound wave propagates faster in a material with a higher modulus, the time delay shown in Figure 4.5 increased until the resin reached its minimum viscosity point. The process time corresponding to the maximum in time delay is $t = 66 \sim 78$ minutes. In this time period, the time delay remained constant, but not a single maximum point. The process time corresponding to minimum viscosity is $t = 76.4$ minutes. Thus, the peak in time delay

data correlates well with minimum in viscosity. Beyond this maximum, the time delay started to decrease due to increase in modulus of the specimen caused by curing.

The process time close to the time for inflection in the time delay curve corresponded to gel time of 107.3 minutes. Beyond that, the time delay continuously decreased, which indicated that the modulus was increasing continuously. At about t = 175 minute, the time delay reached a plateau value. This suggested that the moduli of the specimen are close to the maximum values. The predicted moduli of composite at this time is E_{11} = 120 GPa and E_{22} = 5.6 GPa, which are 96% and 94% of the values of fully cured specimen (E_{11} = 125 GPa and E_{22} = 5.98 GPa, α = 0.96), as shown in Figure 4.6.

The longitudinal, transverse and shear moduli of the composite as a function of degree of cure have been measured in reference (3). They are plotted versus the process time in Figure 4.6. It was observed that the moduli increased with the increase degree of cure. The longitudinal modulus (E_{11}) of the unidirectional composite was found to be a linear function of the degree of cure in the measuring range of 0.32 to 1.0 (corresponding to the time period of t = 99 minutes to the end of experiment). The longitudinal modulus below 0.32 degree of cure was assumed to be a constant value of 57 GPa. The transverse modulus (E_{22} and E_{33}) was a linear function of degree of cure in the measuring range of 0.32 to 1.0. Below that, it was calculated using the rule of mixture as 1.83 GPa. As cure proceeded, the moduli of the material increased with increase in viscosity. As the moduli were built up evenly and approached their maximum values, the time delay ceased to decrease and reached a plateau value. However, the degree of cure was 0.83 and it

continued to increase beyond the process time corresponding to the time delay plateau, the material had not reached its end of cure state. Hence the process time corresponding to the plateau in time delay can be correlated to the built-up of specimen's moduli. However, this process time cannot be used as the criterion to determine the end of cure state.

Near the end of the postcure procedure, a slight increase in time delay was observed. This is believed to be due to the slight increase in the thickness of the specimen due to thermal expansion. During the cooling stage, the specimen thickness decreased with the decrease in temperature leading to a decrease in time delay.

Attenuation

For the neat resin, it is believed that the attenuation is due to the energy loss related to viscous deformation (47). At the beginning of the experiment, as the temperature and pressure were applied simultaneously to the specimen, the attenuation dropped initially and then increased sharply until reaching a peak value at t = 19 minutes. Similar trend was also observed during curing of the composite specimen. The reason for this is unknown at this time. After this first peak, the attenuation decreased and reached a minimum value at $t = 66 \sim 78$ min, which correlated well to the time for minimum viscosity at $t = 76.4$ min.

Beyond this minimum, the attenuation increased. When the gel point was reached, the attenuation started to increase sharply and was close to a peak value. Beyond this, it

dropped again rapidly. The attenuation curve reached a plateau at t = 194 minutes with a degree of cure value of $\alpha = 0.87$, which suggested that the specimen was close to the end of cure state. However, it can be observed in Figure 4.1 that the degree of cure of the specimen was still increasing even after the attenuation reached a plateau, which suggested that the plateau in attenuation does not correspond to the end of cure state. During the postcure procedure, the attenuation increased at a slow rate due to the change in thickness of the specimen. At the beginning of the cooling stage, the attenuation decreased because of the decrease in specimen thickness, similar to the time delay. The reason for the sudden increase in attenuation at t = 280 minute is not understood at this time.

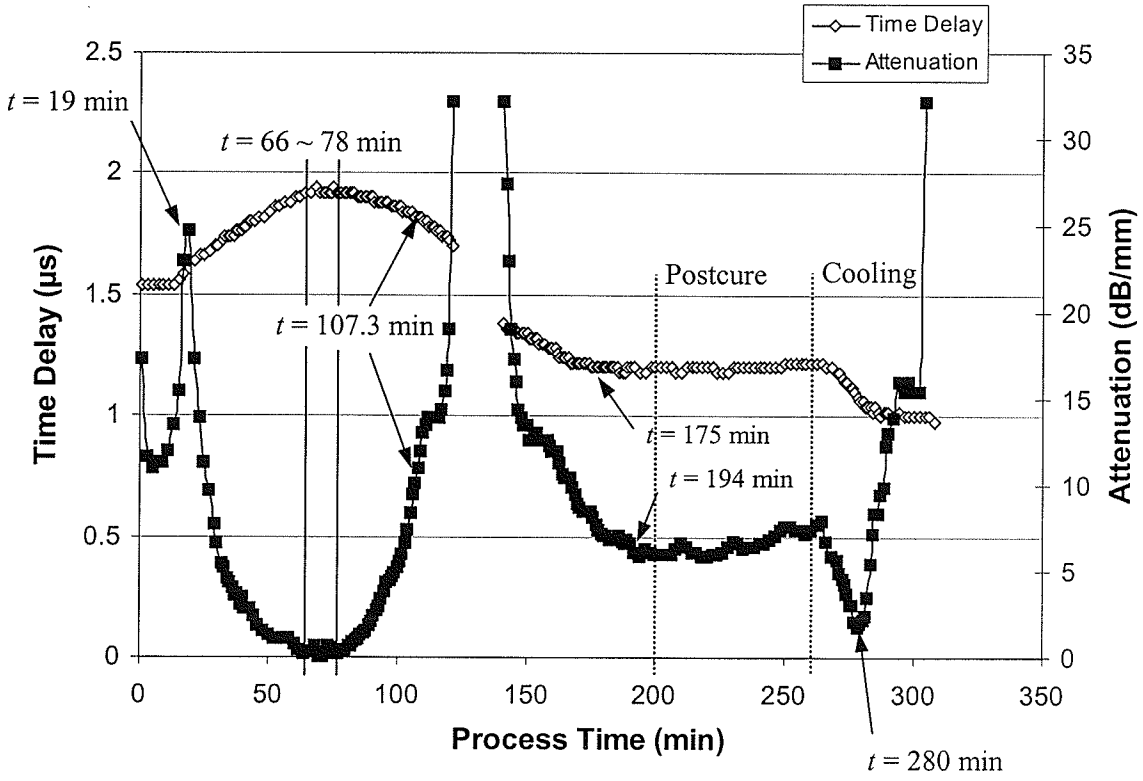

Figure 4.5 Time delay and attenuation obtained from the resin specimen in cycle R934 T-05

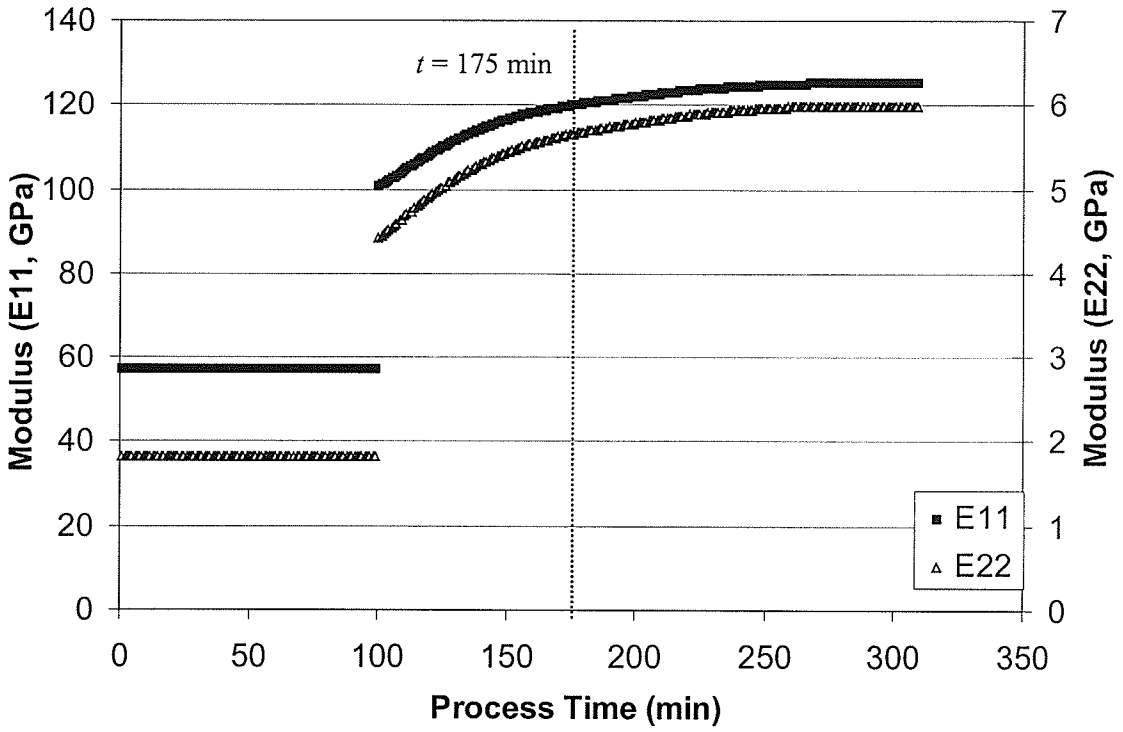

Figure 4.6 Modulus of the neat resin specimen during curing in cycle R934 T-05

A gap in the attenuation and time delay data just after gelation corresponds to a process time period of t = 121 to 141 minutes, when the ultrasonic signals became too weak to be detected. In order to understand this, additional ultrasonic cure monitoring experiments were carried out at room temperature using room temperature curing fiberglass resin. As shown in Figure 4.7, the thicker the specimen, the longer the transmission path length for ultrasonic waves, leading to more energy absorption.

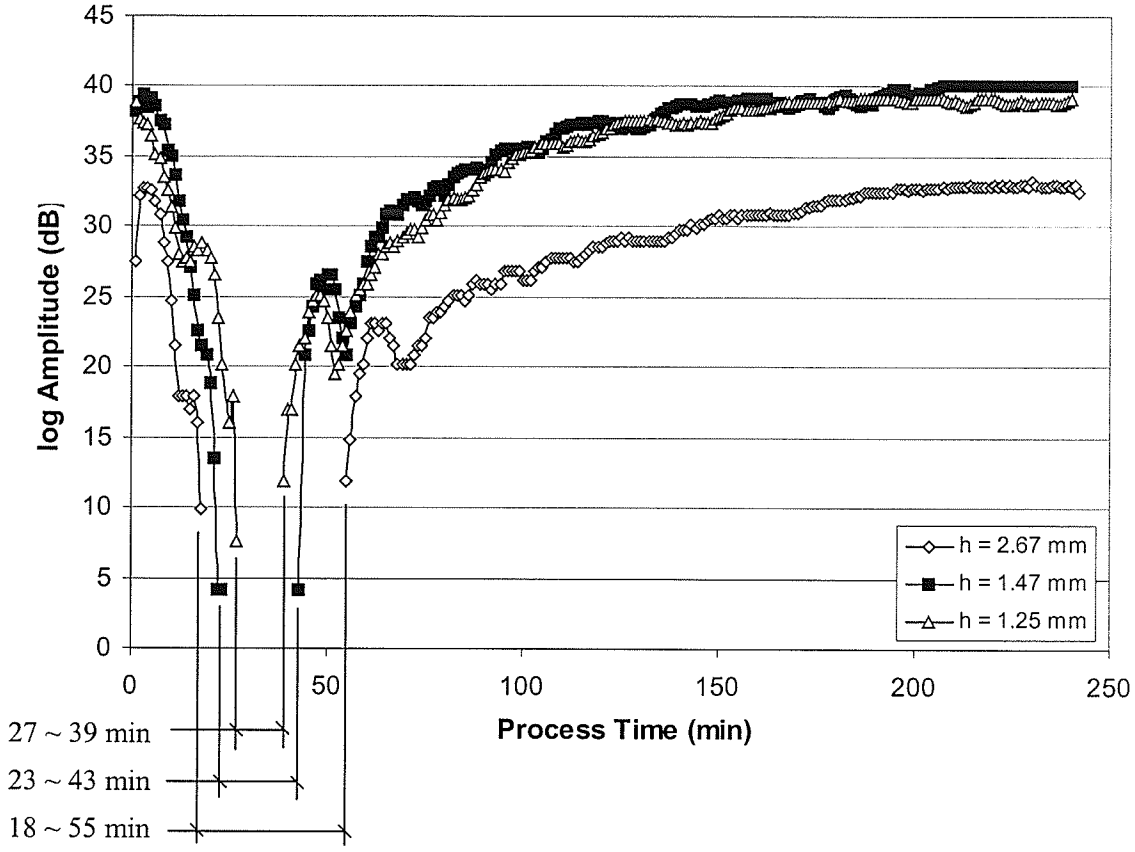

Figure 4.7 Ultrasonic response of fiberglass resin specimens cured isothermally at room temperature

4.2.1.2 Ultrasonic Response of Composite Specimen (Cure Cycle 8, HMF T-22)

The 6-ply composite specimen was cured at 190°C for 180 minutes as shown in Figure 4.8. The vacuum was removed when the specimen temperature reached 90°C at t = 60 min in order to avoid the resin being sucked out by the vacuum pump. After removing the vacuum, 0.586 MPa (85 psi) pressure was applied till the end of the cycle. The specimen reached its minimum viscosity at t = 82 minutes and gelation at t = 106 minutes, as shown in Figure 4.9. The degree of cure by the end of processing was as 0.97.

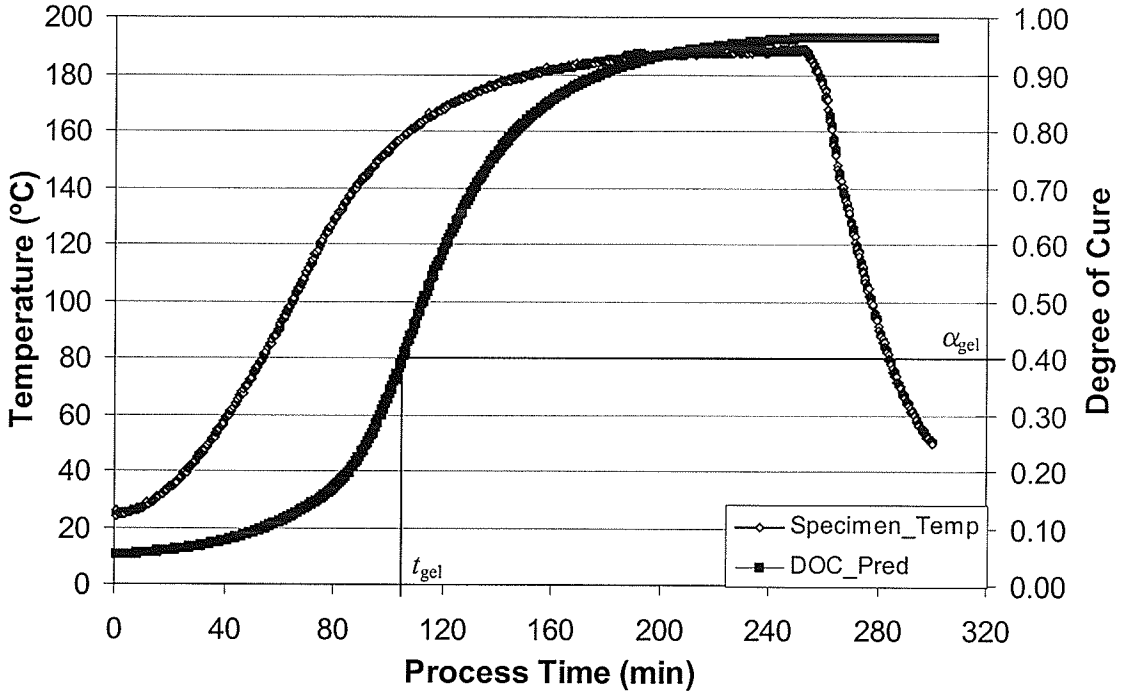

Figure 4.8 Part temperature and predicted degree of cure for cure cycle HMF T-22

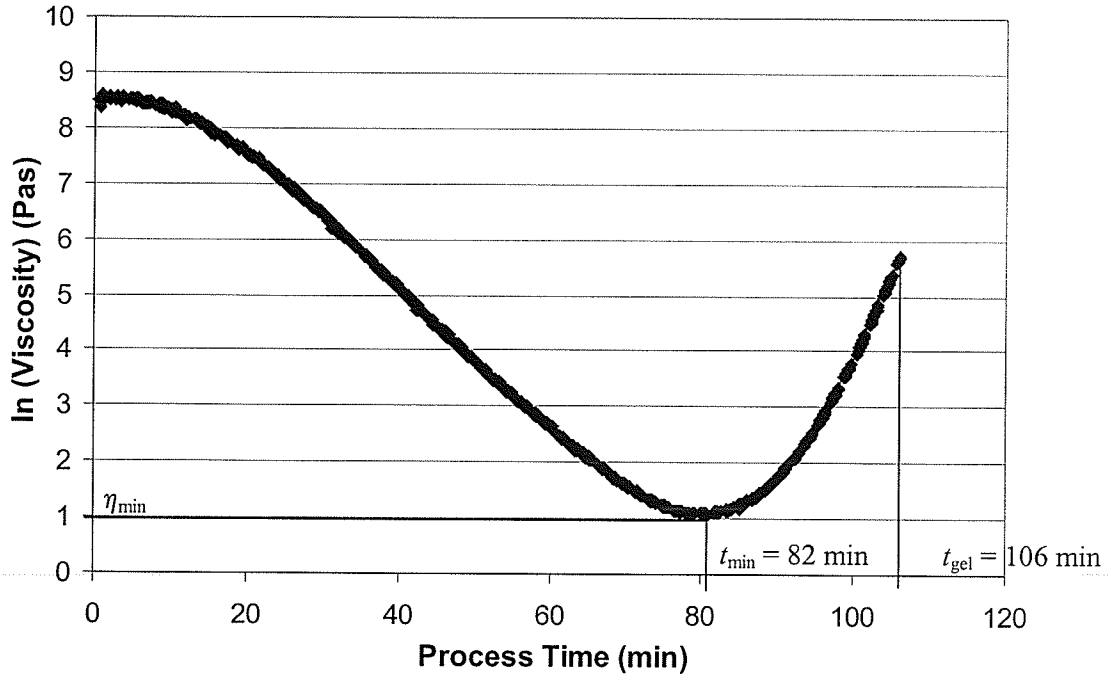

Figure 4.9 Predicted viscosity for cure cycle HMF T-22

Time Delay

As shown in Figure 4.10, the composite specimen had an ultrasonic response similar to the neat resin specimen. The maximum in time delay at t = 84 ~ 94 min corresponded well to the minimum viscosity at t = 84 min. When the gelation occurred at t = 106 minutes, the time delay curve approached its inflection point. As the cure proceeded, the time delay reached a plateau value at t = 150 minute. The predicted moduli of the specimen at this time is E_{11} = 120 GPa and E_{22} = 5.6 GPa, as shown in Figure 4.11. However, as the degree of cure of the material was 0.82 at this time, the plateau in time delay does not correspond to the end of cure state.

Attenuation

The ultrasonic attenuation reached a minimum value at the same time as the minimum viscosity at t = 84 min. When gelation occurred, the attenuation reached a peak value at t = 106 min. Beyond this peak in attenuation at gel point, a second peak was observed at t = 124 minutes, which was much smaller in magnitude. The cause for this second peak is still unclear. The attenuation decreased until it reached a plateau value at t = 188 minutes. The degree of cure at this time was 0.92. During the cooling stage, a trend similar to that observed with neat resin was recorded and the signals were lost at t = 278 minutes.

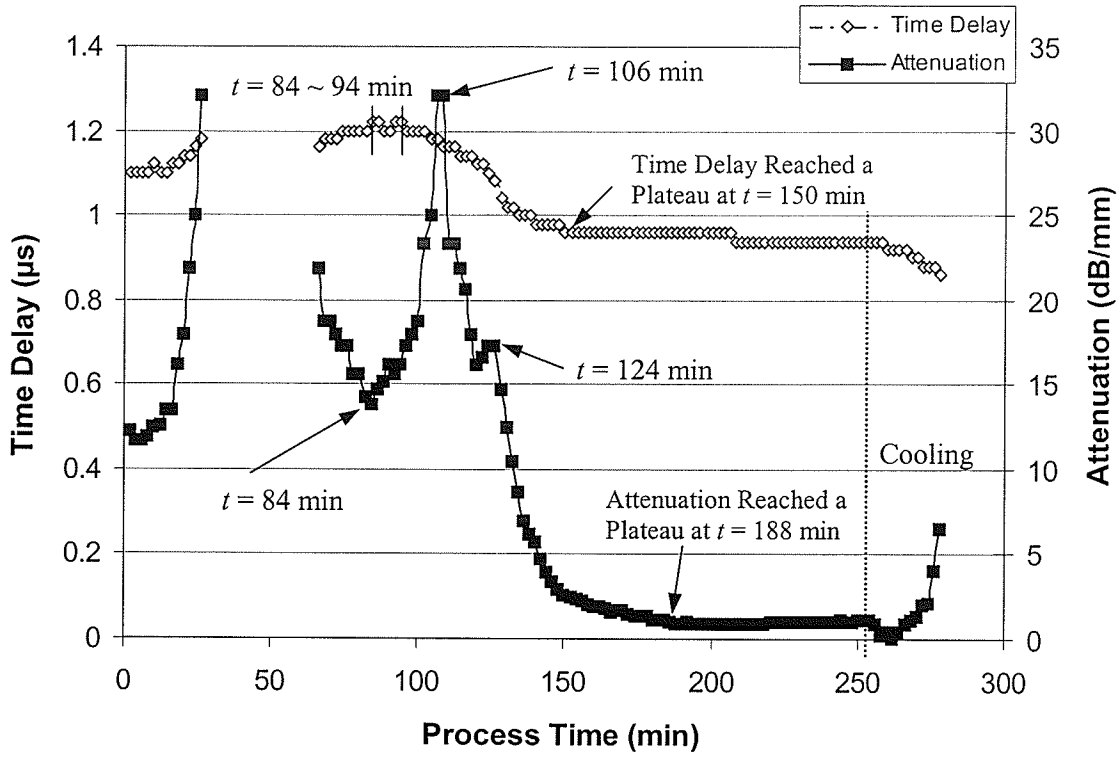

Figure 4.10 Time delay and attenuation obtained from the composite specimen in cycle HMF T-22

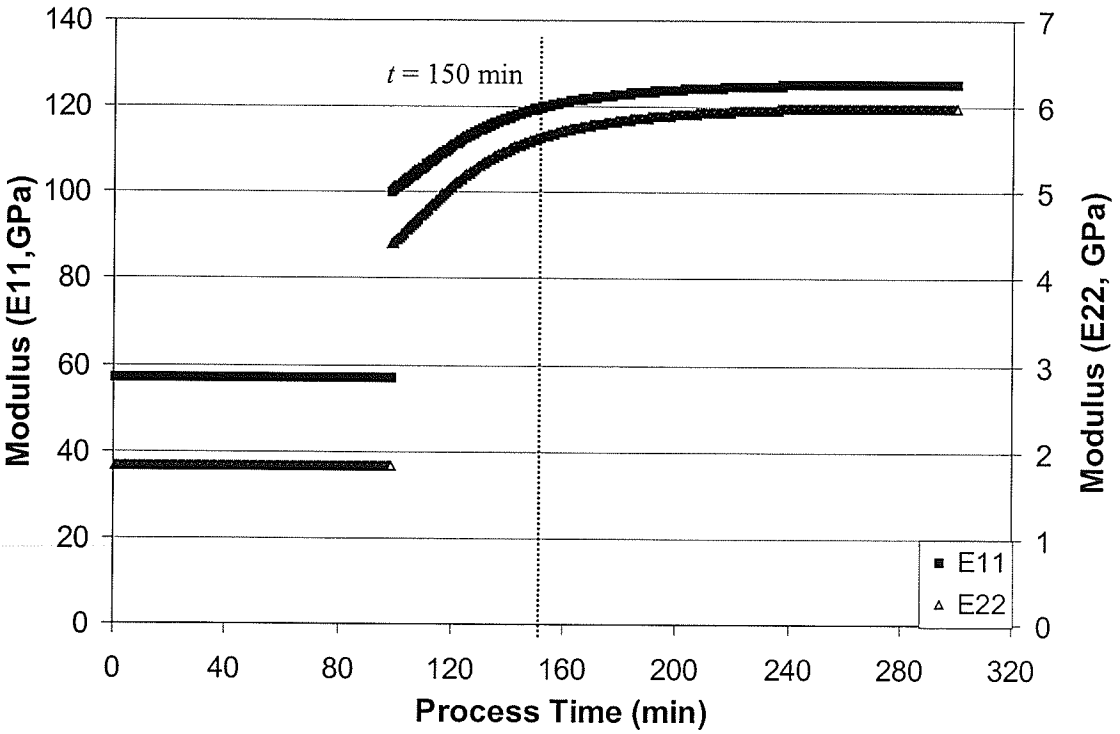

Figure 4.11 Modulus of the neat resin specimen during curing in cycle HMF T-22

The thickness of the composite also significantly affected the results. As observed in Figure 4.12, the ultrasonic signals were lost from the beginning of the cure cycle to t = 124 minutes during monitoring of composite specimen made of 12 plies of prepreg, while the data for 6-ply composite was recorded from the beginning of the cure cycle. Hence, selection of an optimum thickness of composite parts is important in ultrasonic monitoring.

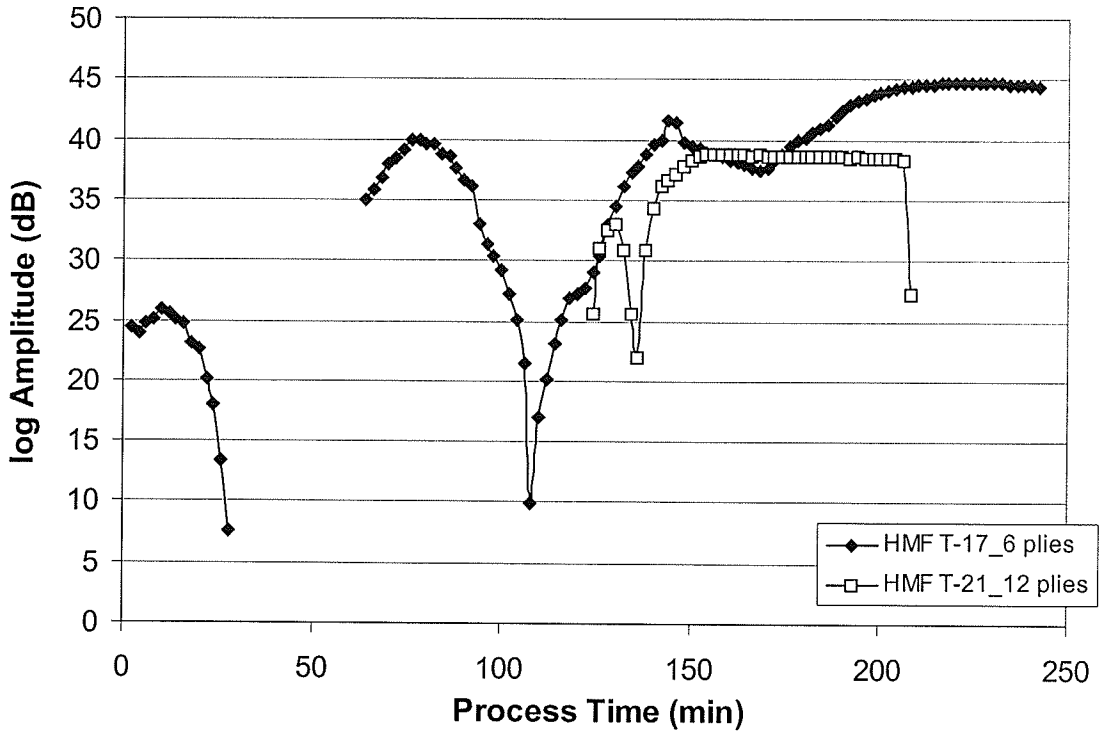

Figure 4.12 Ultrasonic response of composite specimens with 6 and 12 plies of laminas

4.2.1.3 Ultrasonic Monitoring Data for Neat Resin and Composite Specimens

Figures 4.13 and 4.14 compare the cure cycles and ultrasonic monitoring data of neat resin and composite specimens in experiments R934 T-05 (Cure Cycle3) and HMF T-17 (Cure Cycle 7). Processed using similar cure cycles (HMF T-17 dose not have postcure

procedure), there was slight difference in specimen temperature and degree of cure profiles.

The predicted process time for neat resin and composite to reach minimum viscosity are at t = 76.4 minutes and t = 80 minutes, respectively. The minimum value of the attenuation for both specimens corresponded well to the time for minimum viscosity. One difference between the ultrasonic response of neat resin and composite specimens is that for composite, the gel time correlated exactly to the process time corresponding to the peak in attenuation curve and the inflection point in the time delay curve at t = 108 minutes. However, for neat resin, predicted gelation occurred earlier than the time for the attenuation peak and the inflection in the time delay curve at t = 107.3 minutes. The attenuation peak and time delay inflection for the neat resin occurred at the time period of t = 121 ~ 141 minutes. This is believed to be due to the facts that the viscosity of resin was determined using experimental data generated for the composite, while the degree of cure, used to determine gel point, was determined using the experimental data generated for the resin. Hence, error in the determination of gel point for this resin could lead to such a difference. The time delay reached plateau values at t = 175 minutes and t = 142 minutes (the longitudinal and transverse moduli of the composite specimen at this time is 117 GPa and 5.5 Gpa). At t = 192 minutes and t = 212 minutes, the attenuation of both specimens reached plateau values.

It is observed that the signals around the attenuation peak were not lost in composite in contrast to neat resin. During ramping, at the beginning of the cure, the attenuation in

composite specimen started to increase until the ultrasonic signals became too weak to be detected and totally lost for a period from $t = 29$ to $t = 63$ minutes. The attenuation signal appeared again at $t = 64$ minutes when the vacuum was removed and pressure was applied as shown in Figure 4.14. Whereas no signal was lost before the viscosity minimum was reached in resin specimen. The reason is still unknown at this time.

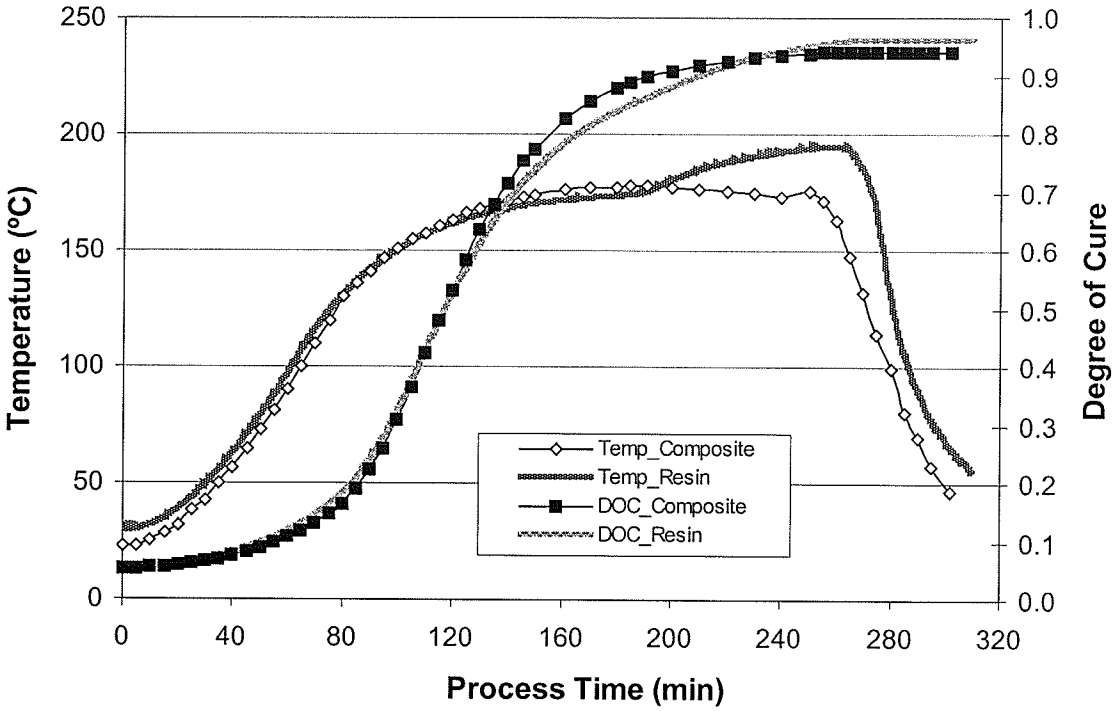

Figure 4.13 Part temperature and degree of cure of neat resin and composite specimens (R934 T-05 and HMF T-17)

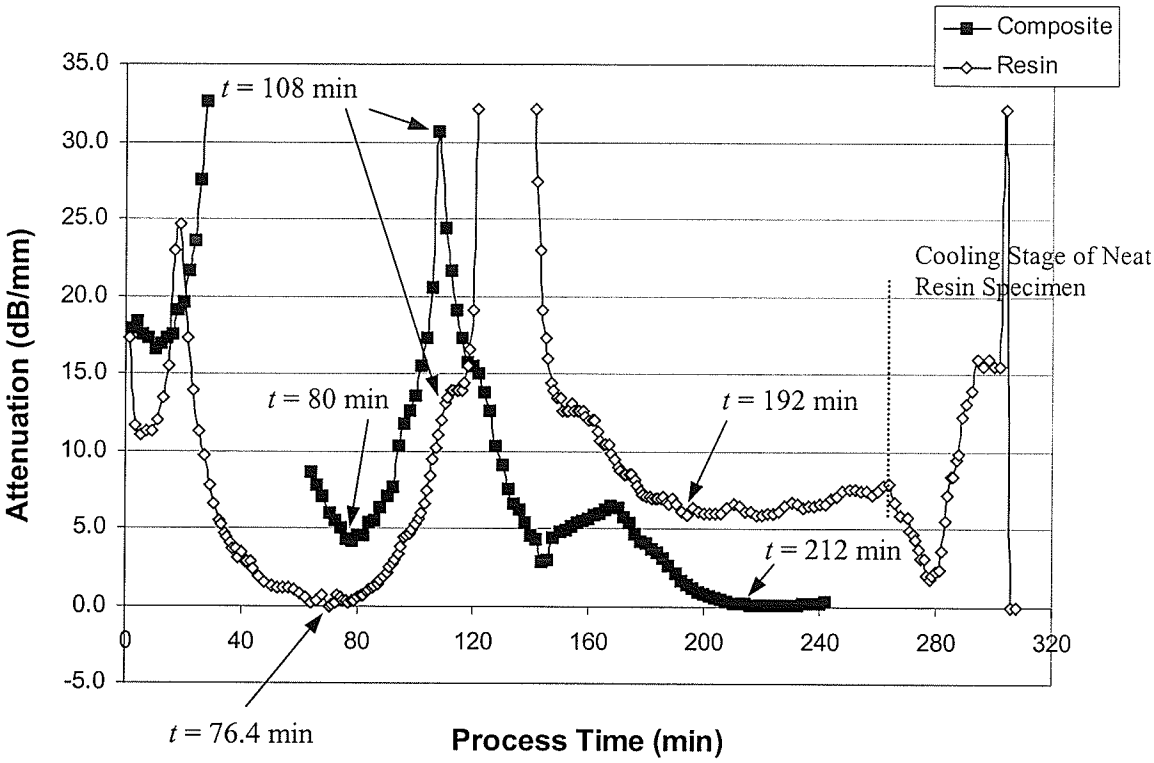

Figure 4.14 Ultrasonic attenuation data of neat resin and composite samples (R934 T-05 and HMF T-17)

4.2.1.4 Modulus Measurement Using Ultrasonic Sensor

Moduli of several types of materials were measured using ultrasonic sensors in room temperature to evaluate the ability of the sensor to monitor the modulus during processing. The materials tested were room temperature curable fiberglass resin, composite and aluminum.

The fiberglass resin, used in modulus measurement, has been discussed in Chapter 3. The transverse wave signals cannot be obtained during curing of the fiberglass resin at room temperature in this study. This is believed to be due to the difficulties in sensor alignment, high damping property of the material and the large thickness of the specimen.

The time delay for the longitudinal wave, wave traveling distance, and density of the specimen were measured after curing. The longitudinal modulus L was calculated using equation (2.11). To compare the test results with the Young's modulus of the material, which has been reported in other literatures, the longitudinal modulus was converted into Young's modulus using the equations:

$$K = \frac{E}{3(1-2\nu)} \tag{4.1}$$

and

$$G = \frac{E}{2(1+\nu)} \tag{4.2}$$

Hence, the Young's modulus of the specimen was calculated by substituting equations (4.1) and (4.2) into equation (2.7):

$$E = \frac{(1+\nu)(1-2\nu)}{(1-\nu)} L \tag{4.3}$$

The test results for eight fiberglass resin specimens were listed in Table 4.1 (assuming that the Poisson's ratio of the resin is 0.27).

The mechanical properties of this resin are unavailable. The Young's modulus value for polyester resin is obtained from reference (48) and is listed in Table 4.2.

Table 4.1 The measured mechanical and acoustic properties for the fiberglass resin specimens after curing

Specimen Number	Parameters Measured						Parameters Calculated		
	Weight Ratio of Resin to Binder	Thickness of Propagation (m)	Volume of specimen (m^3)	Mass (Kg)	Density (Kg/m^3)	Time Delay (s)	Longitudinal Velocity (m/s)	Longitudinal Modulus (GPa)	Young's Modulus (Gpa)
001	NA	0.00187	8.00E-07	9.24E-04	1.16E+03	1.58E-06	2.37E+03	6.47	5.18
003	13.73 : 1	0.00267	9.50E-07	1.16E-03	1.22E+03	2.36E-06	2.26E+03	6.24	4.99
004	17.39 : 1	0.00316	1.00E-06	1.22E-03	1.22E+03	2.80E-06	2.26E+03	6.22	4.98
005	34.55 : 1	0.00388	1.15E-06	1.36E-03	1.18E+03	3.42E-06	2.27E+03	6.07	4.86
006	13.73 : 1	0.00149	1.85E-06	2.23E-03	1.20E+03	1.40E-06	2.13E+03	5.46	4.37
007	17.42 : 1	0.00157	2.50E-06	3.12E-03	1.25E+03	1.48E-06	2.12E+03	5.61	4.49
009	13.20 : 1	0.00127	1.55E-06	1.77E-03	1.14E+03	1.22E-06	2.08E+03	4.94	3.95
015	13.73 : 1	0.00210	2.10E-06	2.59E-03	1.23E+03	1.98E-06	2.12E+03	5.55	4.44

Table 4.2 Theoretical mechanical and acoustic properties for polyester resin

	Specific Gravity	Young's Modulus (GPa)
Polyester (thermoset)	1.04-1.46	2.07-5.34

The modulus of the aluminum plate/block and composite panels was also measured in room temperature. The results are shown in Table 4.3. The values of theoretical mechanical moduli of aluminum are taken from reference (6). Two kinds of composite specimens were tested. One of the composite panel was made using F263/T300 prepregs from Hexcel, which were laid up as an unidirectional laminate in $[0]_6$ sequence. The modulus measurement was performed using a completely cured specimen. The mechanical properties of this composite panel are taken from M. A. Balachander's Master's thesis in the University of Manitoba (49) and listed in Table 4.4. Another angled composite plate was made using the Cytec-Fiberite HMF 5-322/34C woven prepregs used in this study. Both the longitudinal and transverse waves were obtained for aluminum and F263/T300 composite. Only longitudinal waves were obtained for angled HMF 5-322/34C composite plate due to the large thickness of the specimen. The longitudinal modulus of this composite plate was converted into the Young's modulus using equation (4.3).

Table 4.3 The measured ultrasonic wave velocity and modulus for the aluminum and composites

Specimens Measured	Parameters Measured		Parameters Calculated					
	Density (kg/m^3)	Thickness (mm)	Longitudinal Velocity (m/s)	Transverse Velocity (m/s)	Longitudinal Modulus L (GPa)	Young's Modulus (GPa)	Shear Modulus (GPa)	Poisson's Ratio
F263/T300, $[0]_6$	1.57E+03	1.02	2926.83	1558.44	13.45	9.93	3.81	0.30
F263/T300, $[0]_6$ (position 2)	1.57E+03	1.20	3243.24	1558.44	16.51	10.29	3.81	0.35
Aluminum panel	2.71E+03	3.07	6395.83	3164.95	110.86	72.63	27.15	0.34
Aluminum block	2.71E+03	19.05	6392.62	3175	110.75	73.01	27.32	0.34
Cytec-Fiberite HMF 5-322/34C	1.23E+03	3.72	3110.09	NA	11.85	8.76		

Table 4.4 The theoretical mechanical and acoustic properties for the aluminum and composites

Materials	Elastic Modulus (GPa)	Shear Modulus (GPa)	Poisson's Ratio
$[0]_6$ Composite	9.09 (E_{22})	5.0 (G_{12})	0.19 (ν_{12}) 0.019 (ν_{21})
Aluminum and Its Alloy	70-79	26-30	0.33
Cytec-Fiberite HMF 5-322/34C	6.07	3.54	

It is observed that the ultrasonic sensor can be used to measure the modulus of the resin and composites off-line. With a proper experimental set-up, it is expected to be used in the on-line control of the part quality of the composites. Due to lack of the ultrasonic couplant that can transmit transverse waves in the autoclave processing environment, and the equipment that can monitor the changes in thickness and density of the materials during curing, based on the current experimental configurations, the moduli were not measured during cure experiments in this study.

4.2.2 Dielectric Cure Monitoring

The dielectric permittivity and the loss factor were measured during curing, and quantitatively correlated to the material parameters, such as viscosity and gel point etc.

4.2.2.1 Dielectric Response of Neat Resin Specimen (Cure Cycle 1, R934 T-01)

The process cycle is plotted in Figure 4.15. The oven was heated to 177°C in 70 minutes, held at 177°C for 120 minutes, and then it was cooled down to room temperature. The resin specimen was poured into the mold before the start of the experiment. Vacuum and pressure were not applied. Because the mold was opened during the entire experiment, there was negligible thermal lag between the specimen and mold. The predicted minimum viscosity appeared at t = 49.3 minutes, and the gelation occurred at t = 63 minutes. The degree of cure of the specimen reached 0.95 by the end of the process cycle.

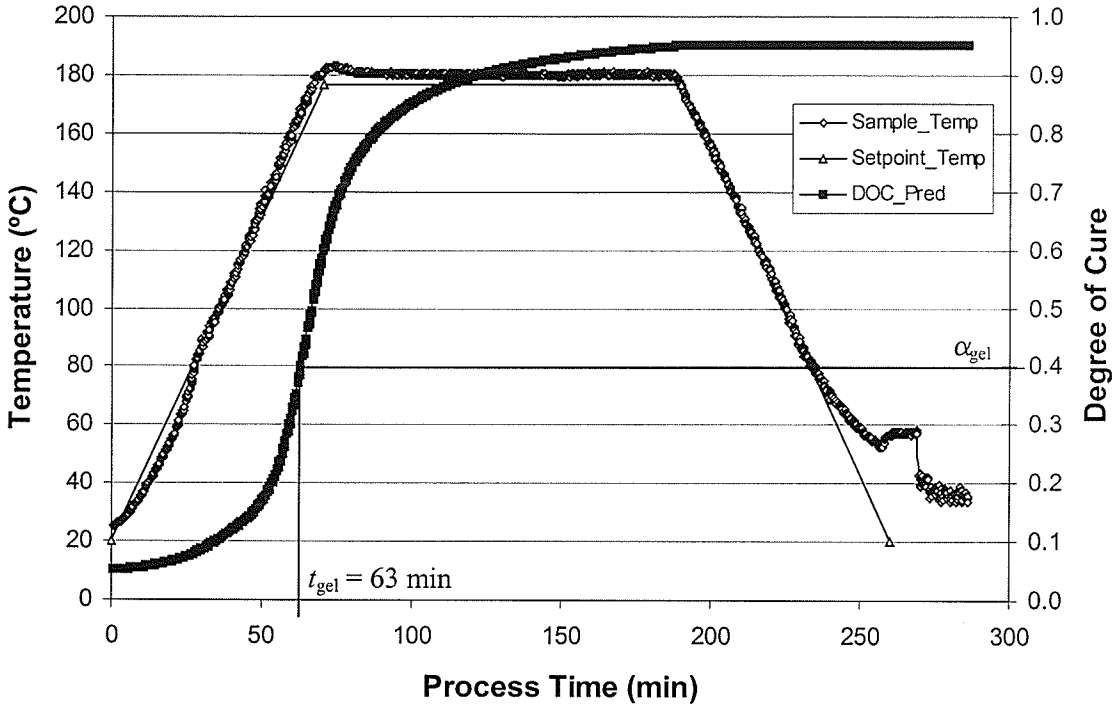

Figure 4.15 Part temperature and predicted degree of cure in cycle R934 T-01

Permittivity (ϵ') and Loss Factor (ϵ'') data

Figures 4.16 and 4.17 show the log permittivity and the log loss factor measured at a frequency of 500 Hz. The permittivity and loss factor data was used by the software that comes with the instrument to calculate the ionic conductivity. The dashed lines show the permittivity and loss factor data measured under ideal condition, in which the ionic conductivity contribution is negligible. However, in reality, both the permittivity and loss factor increased until a peak value was reached at the beginning of cure. Beyond that, both of them decreased and reached plateau values. During the cooling stage, the loss factor decreased with decrease in temperature, while the permittivity remained constant.

The reason for this non-ideal behavior is as follows: as discussed in previous chapters, the permittivity (capacitive response) is related to the ability to align dipoles, and loss factor (conductive response) is related to the energy dissipated in attempting to align. In reality, both the dipole polarization and the free charge migration (i.e. migration of impurity ions) occurred simultaneously. In addition, electrode polarization due to building-up of ions at the electrodes also occurred. During the initial stage, the viscosity was low, which resulted in the high degree of free ion mobility and a significant ionic conductivity contribution to the measured permittivity and loss factor. At limiting low frequencies, the ionic conductivity dominated the dielectric loss. The conduction also contributed to ϵ' and caused a large increase in permittivity in the low frequency region during the early stage of cure, because of the accumulation of blocked charges at the electrodes, i.e. the electrode polarization. Because of the dominance of conductance effects, any dipolar loss peaks are masked by the high conductivity level. As the reaction proceeded, the viscosity of the resin increased and the ionic and dipole movement was restricted, hence less energy was lost and both ϵ' and ϵ'' fell off to a final nonzero plateau value. This change can be clearly observed in Figures 4.18 and 4.19. Since ionic conduction is more significant during the initial stage of the curing, there have been attempts to use it to correlate to the changes in viscosity, which are discussed in subsequent sections. Experiments at higher frequencies (e.g. microwave frequencies) will yield results free from the influence from free charge migration and the pure dipole response could be possible to obtain (18). However, due to the lack of equipment, this was not pursued in this study.

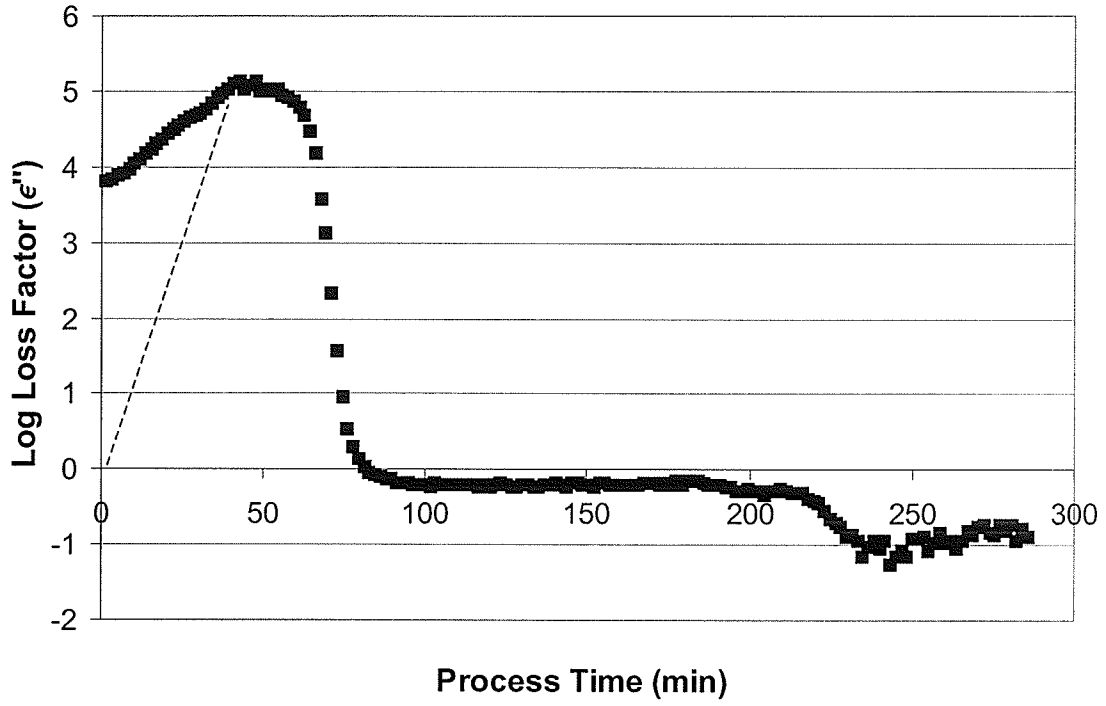

Figure 4.16 log Loss Factor at 500 Hz for cure cycle R934 T-01

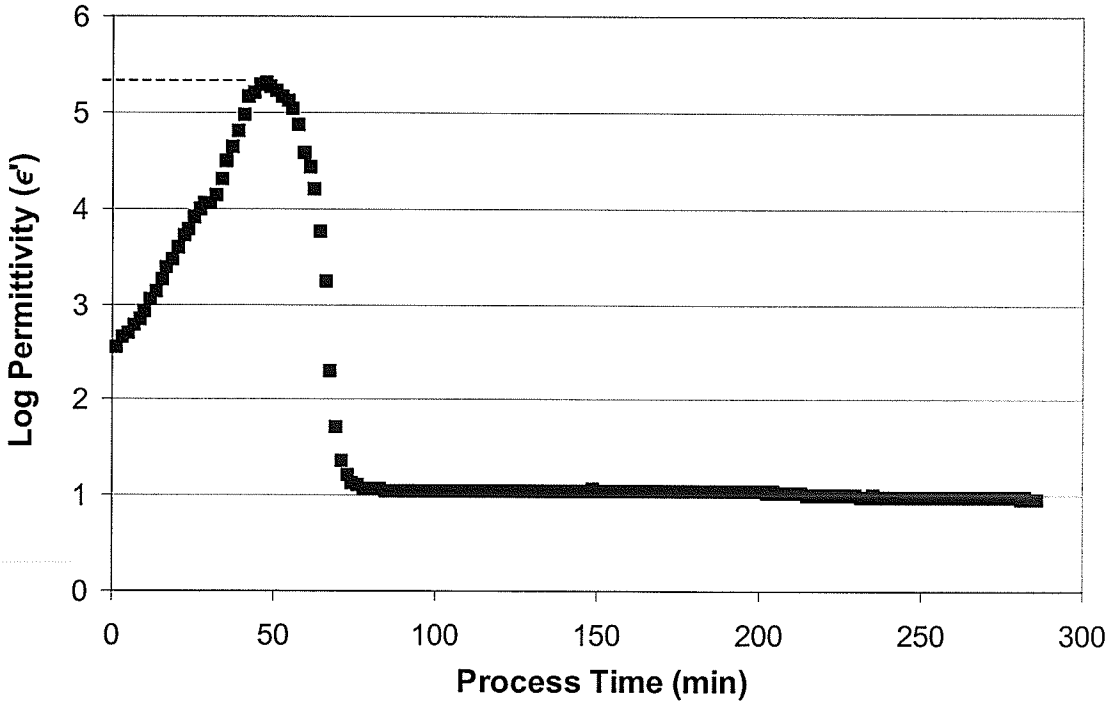

Figure 4.17 log Permittivity at 500 Hz for cure cycle R934 T-01

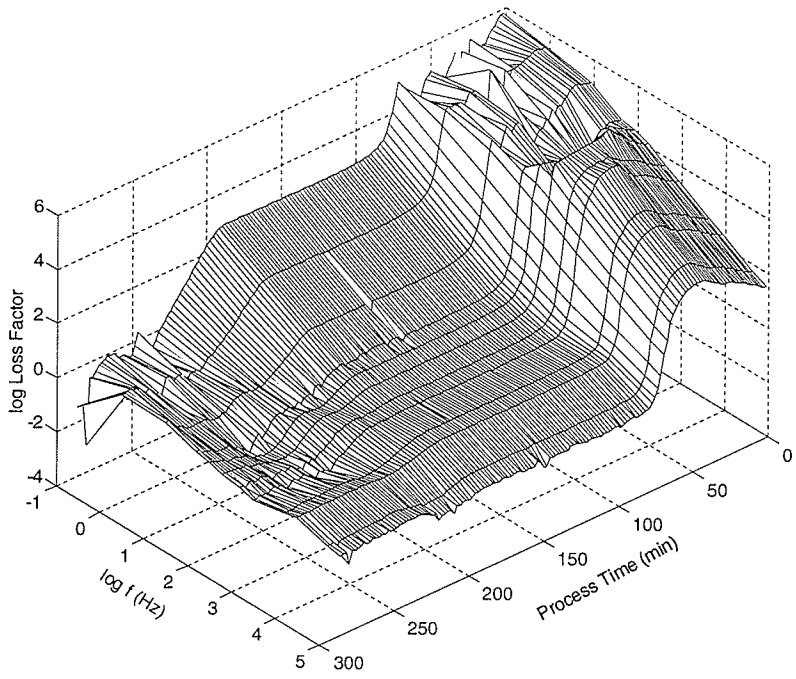

Figure 4.18 log Loss Factor for cure cycle R934 T-01

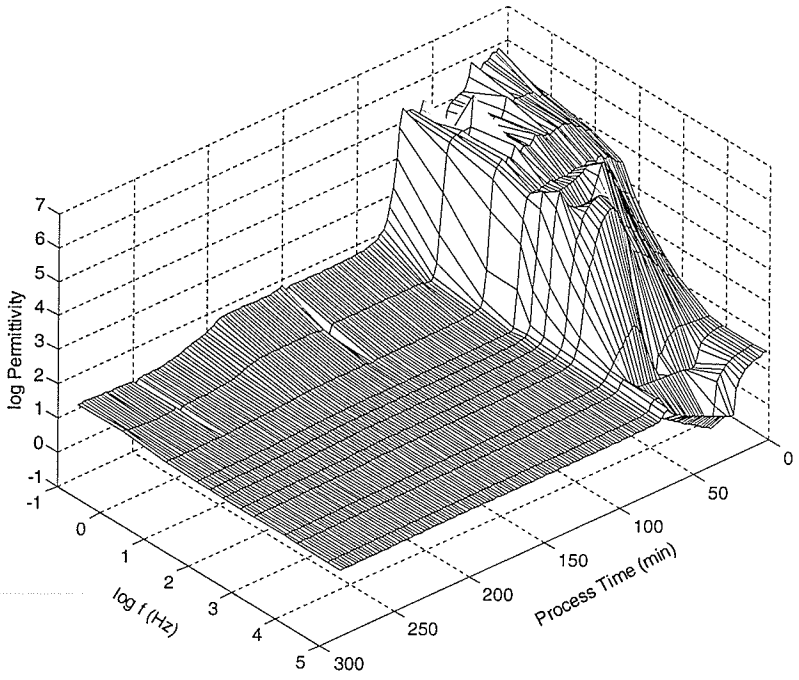

Figure 4.19 log Permittivity for cure cycle R934 T-01

Ionic Conductivity

The calculated ionic conductivity of the resin is plotted in Figure 4.20. During ramping, the synergistic effects of decrease in viscosity and increase in temperature results in overall increase in mobility of the ion in the resin and thus the ionic conductivity. The ionic conductivity increased to a peak value at t = 49.1 min, which corresponds to the process time when minimum viscosity is reached. Beyond this, the viscosity gradually increased due to increase in the degree of cure, and the ion mobility decreased. When the gelation occurred at t = 63 minutes, the ionic conductivity started to decrease sharply. At t = 115 minutes, it reached a plateau value. At the cooling stage, the ionic conductivity decreased as the ion mobility decreased with the temperature. Since ionic conductivity is essentially a measure of the mobility of ions in the resin, it is inversely related to the viscosity prior to gelation.

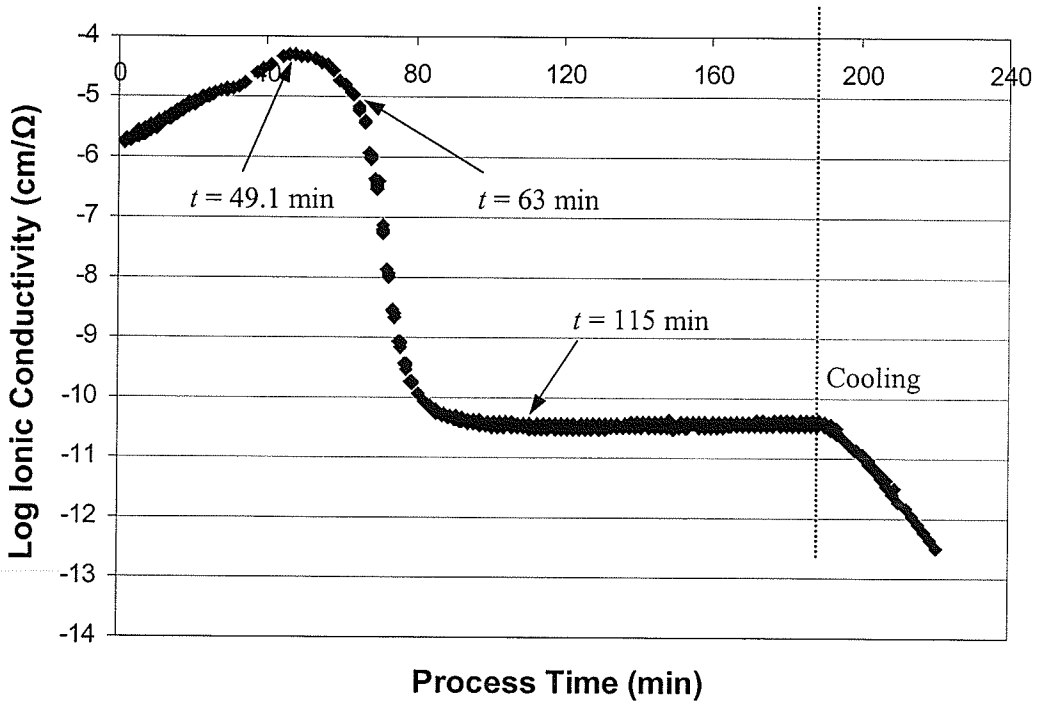

Figure 4.20 log Ionic Conductivity obtained in cycle R934 T-01

log Ionic Viscosity and dlog IV/dt

The inverse of ionic conductivity, i.e. the ionic viscosity (IV) has been used to compare with the viscosity, as reported in reference (22). The dielectric ionic viscosity and mechanical viscosity are compared in Figure 4.21. It can be observed that before gelation occurred, both the two curves have similar shape. However, a fundamental relationship between the dielectric data (the ionic viscosity) and the mechanical viscosity of the resin at a theoretical level is not possible since the ionic mobility is related to the mobility of impurities in resin, and hence, it can hardly be directly correlated to the mechanical viscosity, which is due to mobility of polymer chains.

A derivative of log Ionic Viscosity with process time, dlog IV/dt, can be calculated and used to assist in correlating with parameters of interests, as shown in Figure 4.22. When the mechanical viscosity reached a minimum value at t = 49.3 min, the ionic viscosity also approached its minimum point, and dlog IV/dt was equal to zero. After the minimum viscosity, the ionic viscosity increased sharply when the gelation occurred. dlog IV/dt increased until it reached a maximum value at t = 72.5 min, which corresponds to the process time when a inflection point in ionic viscosity curve was observed. Beyond this it decreased to zero at t = 115 minutes, which corresponded to the time when the ionic viscosity reached a plateau value. The degree of cure of the specimen at this time was 0.89. Since the curing proceeded beyond this, the plateau does not correspond to end of cure state. Hence it cannot be deemed as the criterion to determine the fully cured state as was suggested by research (22). This conclusion shows a disagreement to the work of research in reference (22).

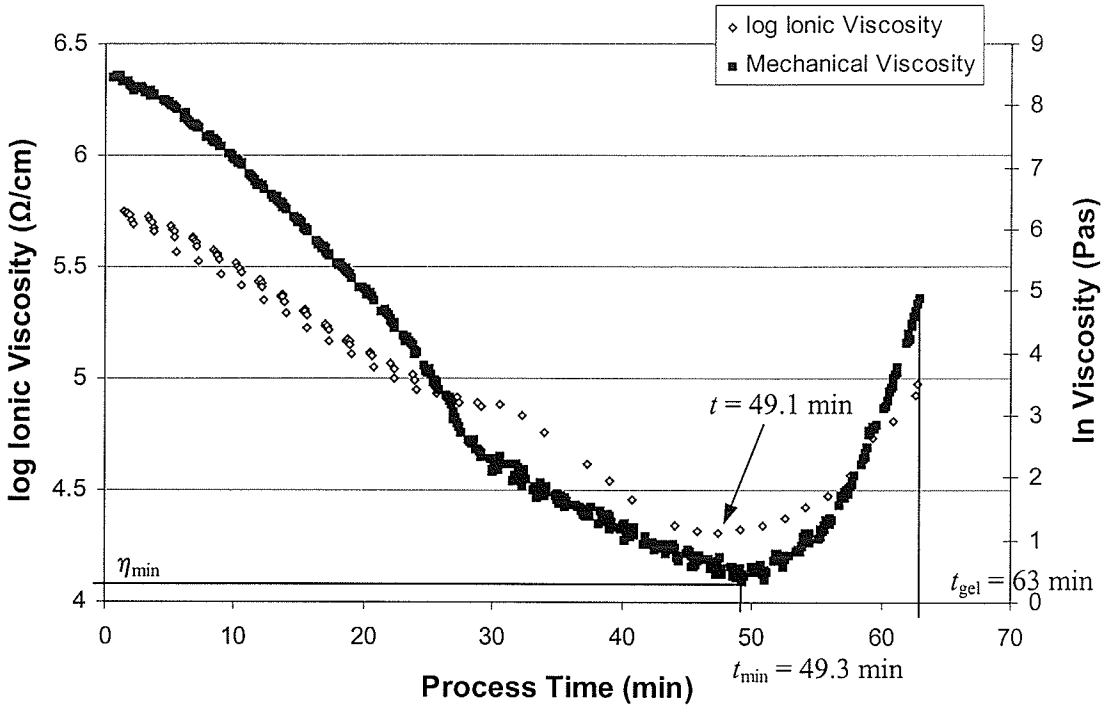

Figure 4.21 The comparison between the ionic viscosity and mechanical viscosity in cycle R934 T-01

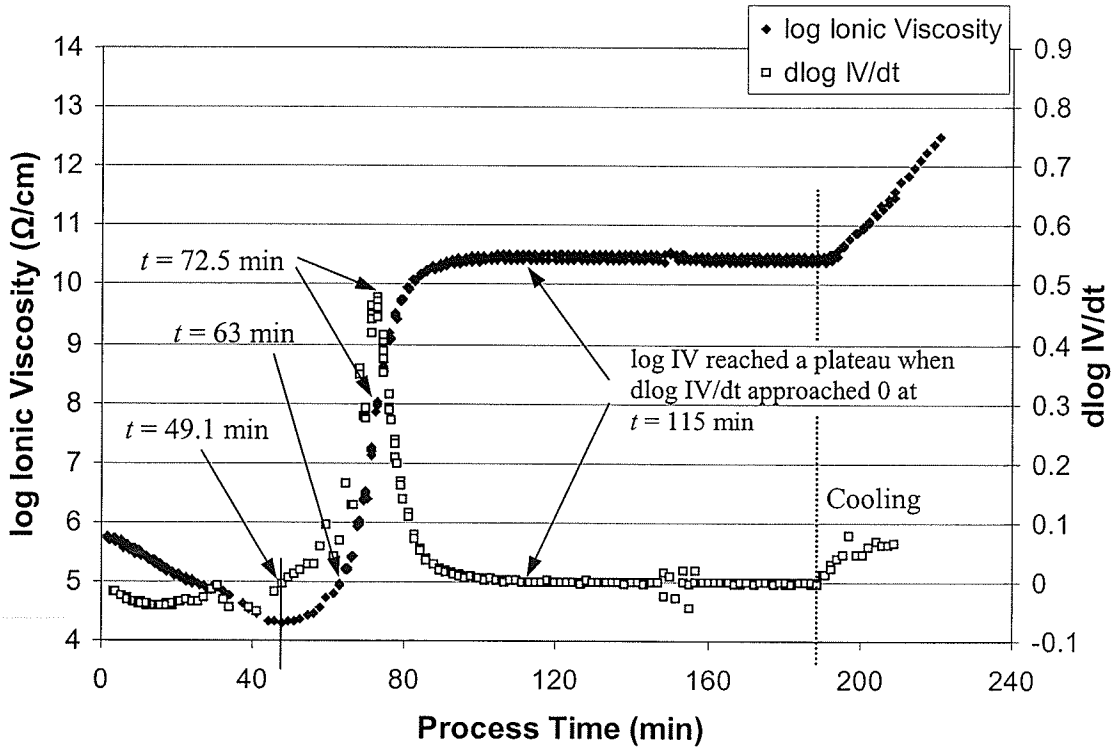

Figure 4.22 log Ionic Viscosity and dlog IV/dt data for cycle R934 T-01

4.2.2.2 Dielectric Response of Composite Specimen (Cure Cycle 10, HMF T-24)

As shown in Figure 4.23, the oven was heated to 190°C in 75 minutes and held for 180 minutes. The vacuum was applied from the beginning of the cure to t = 60 minutes. After removing the vacuum, the pressure was applied till the end of the processing. At the end of the cure cycle, the specimen's DOC was 0.96. The minimum viscosity and gelation occurred at t = 78 minutes and t = 104.5 minutes, respectively.

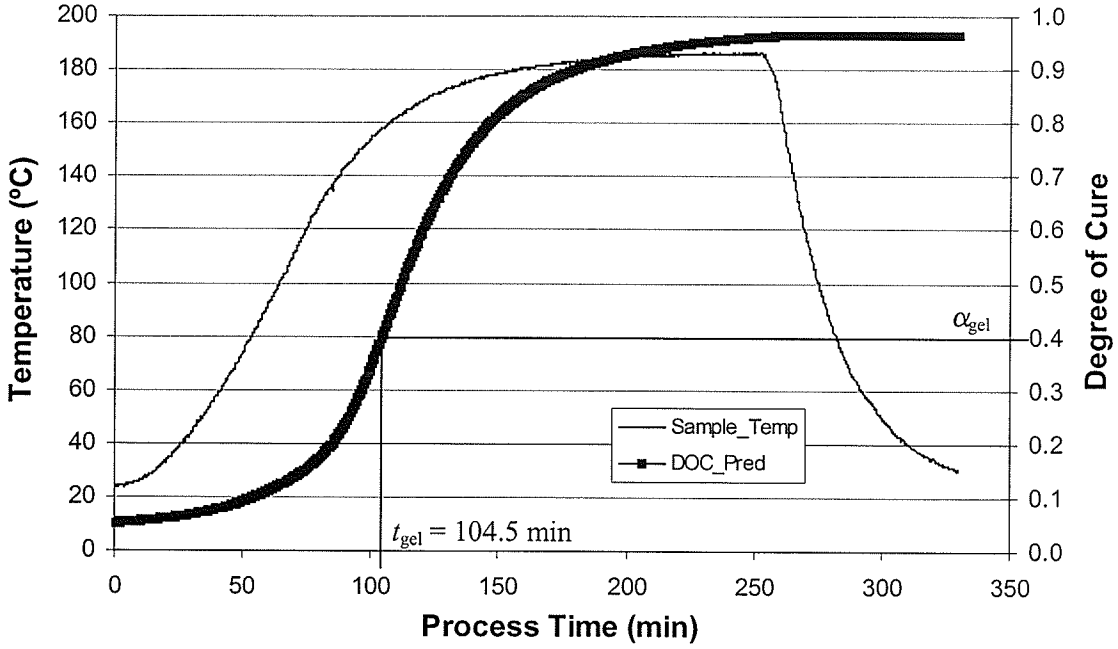

Figure 4.23 Part temperature and predicted degree of cure for cycle HMF T-24

The dielectric response is shown in Figure 4.24. Similar to the neat resin specimen, the ionic viscosity reached its minimum value at t = 78 minutes, which corresponded well to the time for minimum viscosity. It reached the inflection point (the peak value in dlog IV/dt) at t = 112 minutes, while the predicted gelation time was t = 104.5 minutes. This difference was within 1 minute in other experiments, the results for which can be found in Appendix C. Such a correlation cannot be observed in the neat resin. The dlog IV/dt

peak occurred at t = 72.5 minutes as measured in Cure Cycle 1 (R934 T-01), while the predicted gelation occurred at t = 63 minutes. This discrepancy similar to the observations during ultrasonic testing is believed to be due to the fact that the viscosity for resin was determined from the experiment data for composite. dlog VI/dt approached zero value again at t = 162 minutes, when the ionic viscosity reached a plateau value. The degree of cure of the specimen at this time was 0.86.

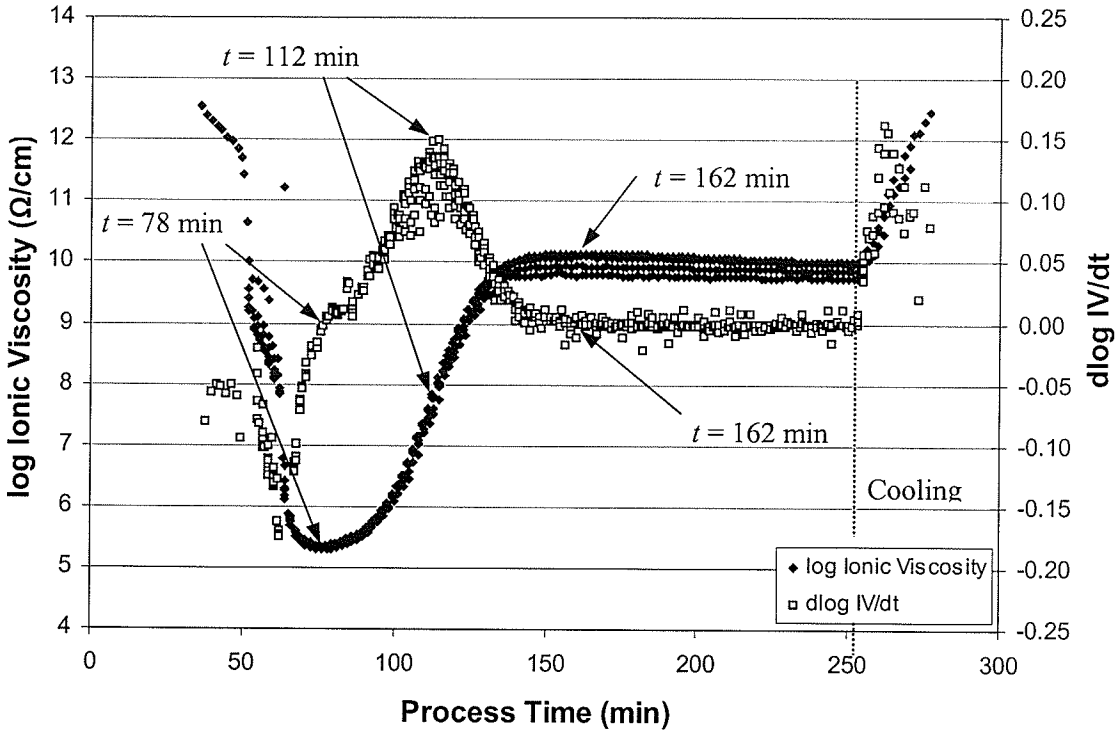

Figure 4.24 log Ionic Viscosity and dlog IV/dt data for cycle HMF T-24

4.2.2.3 Dielectric Monitoring Data for Neat Resin and Composite Specimens

Similar to the ultrasonic response of neat resin and composite, both types of specimens exhibited similar dielectric responses as shown in Figures 25 and 26 (R934 T-05 and HMF T-13). The log Ionic Viscosity of the resin and composite reached minimum values at t = 76.4 minutes and t = 85 minutes, respectively, which corresponded well to the

minimum viscosity. dlog IV/dt approached zero value at t = 192 minutes and t = 189 minutes, respectively, when the ionic viscosity reached plateau values. When gelation occurred at t = 119.2 minutes and t = 107.3 minutes for composite and resin respectively, dlog IV/dt reached a peak value at t = 119.2 minutes for the composite, while for the resin specimen, it corresponded to a process time before the peak value at t = 126 minutes was observed.

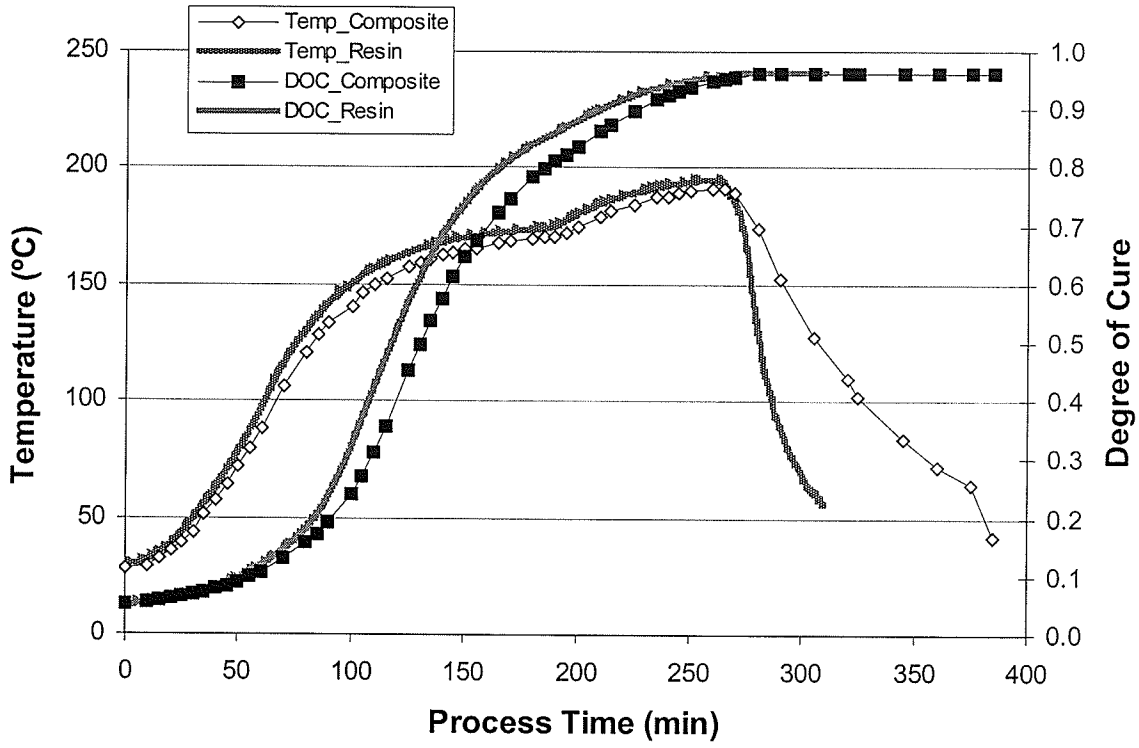

Figure 4.25 Part temperature and degree of cure of neat resin and composite specimens (R934 T-05 and HMF T-13)

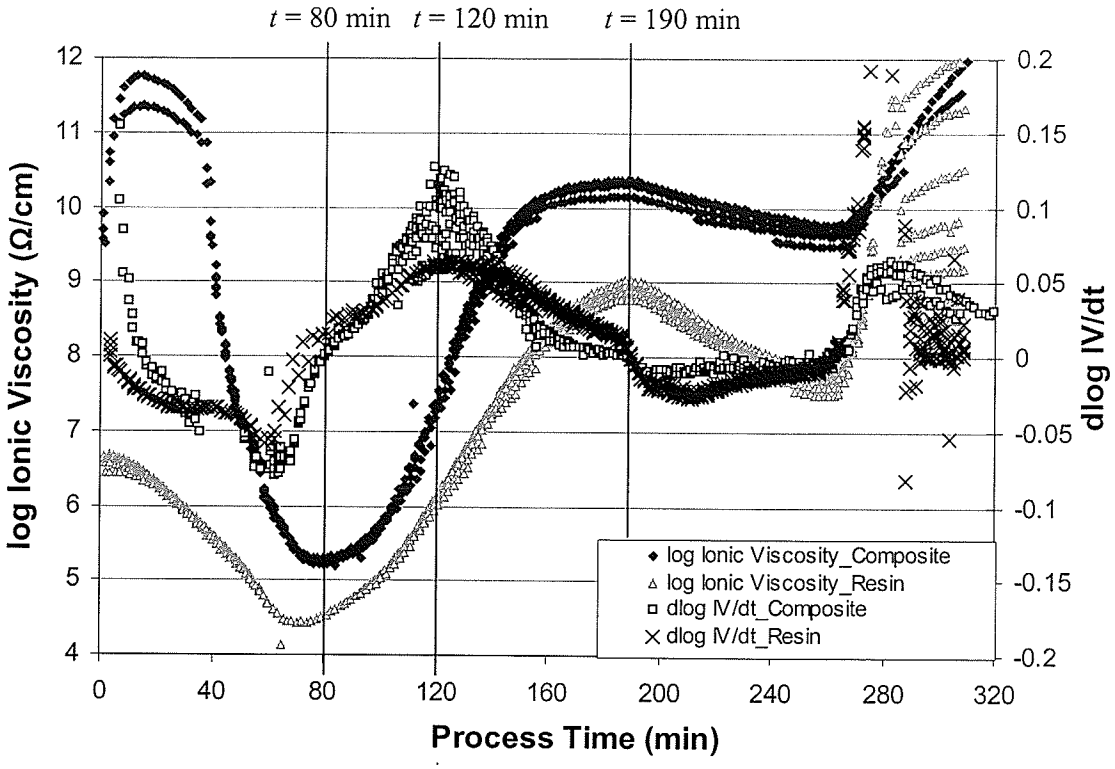

Figure 4.26 log Ionic Conductivity and dlog IV/dt data of neat resin and composite specimens (R934 T-05 and HMF T-13)

4.2.2.4 Dielectric Response of Neat Resin Specimens in Isothermal Experiments

This study is for establishing relationships between the degree of cure or the vitrification time and the dielectric dipole contribution. Vitrification corresponds to the moment at which the glass transition temperature of the resin, which increases as curing proceeded, has reached the cure temperature. Beyond this point, the curing is almost stopped, and it can only proceed at a very lower rate, while the resin behaves like a vitrified solid. When a composite part reaches its vitrification state, the manufacturer should either increase the hold temperature to postcure the part, or to stop curing and cool the part down to save the cycle time. The dielectric response of the resin results from the contributions from dipole

polarization, ion migration and electrode polarization. Temperature also affects the measured dielectric data. Hence, establishing the fundamental relationships between the dielectric response and material parameters, such as degree of cure requires careful experimentation in view of complications that arise due to various factors mentioned above. As discussed in Chapter 2, the dipole contribution can be directly related to the degree of cure and hence the measurement of pure dipole response is highly desired. G. M. Maistros et al. (25) has tried to use the dipolar loss peak data to determine the vitrification of a DGEBA polymer in isothermal experiments. Because few researchers tried to correlate the dipole contribution to material parameters, it is also desirable to verify their observation in this study. Hence a series of isothermal experiments were pursued.

Isothermal experiments at 164, 176 and 190°C were performed. All experiments used the same procedure. The mold was pre-heated to the pre-determined isothermal temperature. The resin was subsequently poured over the sensor bonded to the bottom of the mold and the oven door was closed within half a minute. It took about 5 minutes for the resin to return to the pre-determined temperature. Since the mold had to be left open, to enable pouring the resin, the vacuum and pressure could not be applied. In the experiment conducted at 164°C, the specimen temperature was stable at about 162.5°C and was cured for 5 hours. The predicted degree of cure by the end of the cycle was 0.88. The gelation was predicted to occur at t = 10.3 minutes. Since the resin cured faster at this temperature, the minimum viscosity occurred during the time for stabilizing of the temperature after pouring the resin. Hence signals corresponding to minimum viscosity

were rarely obtained. The results for experiments performed at 176°C and 190°C can be found in Table 4.6. It is observed that the log Ionic Viscosity of the specimens cured at 164°C, 176°C and 190°C reached plateau values at t = 244.6, 78.8 and 35.2 minutes, respectively. It is very close to the process time when the predicted vitrification occurred at t = 244, 78.2 and 57.2 minutes. The DOC of specimens at this time was 0.86, 0.89 and 0.87, respectively. However, as discussed in previous chapters, this cannot be deemed as the criterion to determine the vitrification of the specimens. Log Ionic Viscosity and dlog IV/dt data for these experiments can be found in Appendix C.

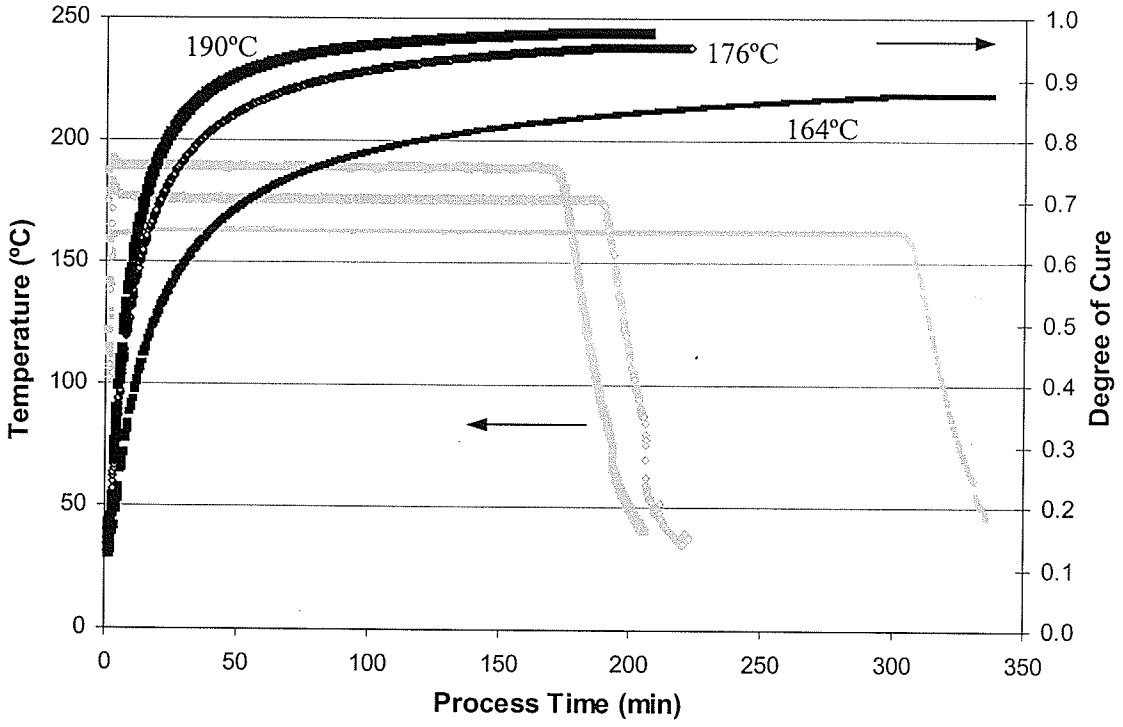

Figure 4.27 Isothermal experiments with 934 neat resin system

Efforts on correlation of vitrification with permittivity data and correction of electrode polarization effect

Log Loss Factor and log Permittivity for the neat resin specimen cured at 164°C are plotted in Figures 4.28 and 4.29, respectively. It is observed that the measured data curves for both the permittivity and loss factor were incomplete. This is due to the fast reaction of the resin at the cure temperatures used in the isothermal experiments. The dashed lines show the permittivity and loss factor would be obtained under ideal condition. In the experiment performed at 164°C, the resin was cured for 5 hours with the degree of cure of 0.88. At lower temperatures, it would take much longer time to cure the specimens. However, due to the unavailability of DEA 230/1, which was leased from Micromet Inc., it was not possible to do any more experiments at lower temperatures before it was returned to the manufacturer. Although the temperature effect was eliminated by performing isothermal experiments, the high level of ion conductivity contribution and electrode polarization still had significant effects on the measured dielectric response and brought difficulties in data analysis and interpretation. Efforts were made in this study to correlate the dipole contribution to the material parameters by using the method reported in reference (25), and correcting the electrode polarization effect on the dielectric response. However, as the difficulties mentioned above, vitrification and other material parameters, such as degree of cure could not be obtained using the experiment data. The details for efforts on correlation of vitrification with permittivity data and correction of electrode polarization effect can be found in Appendix C. Isothermal experiments at lower temperatures should be performed in the further work.

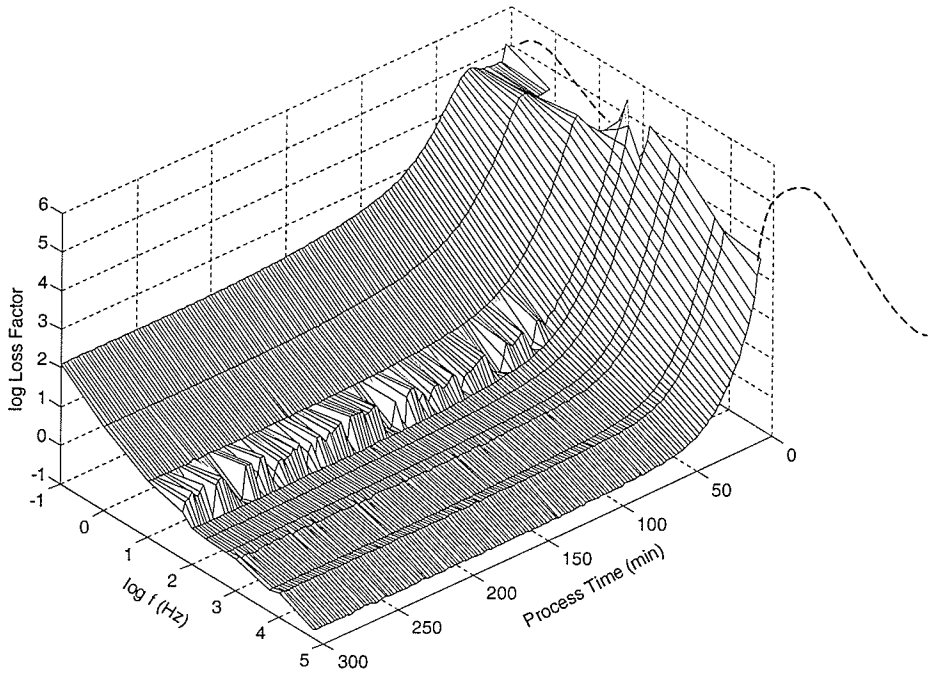

Figure 4.28 log Loss Factor data for cycle R934 T-08

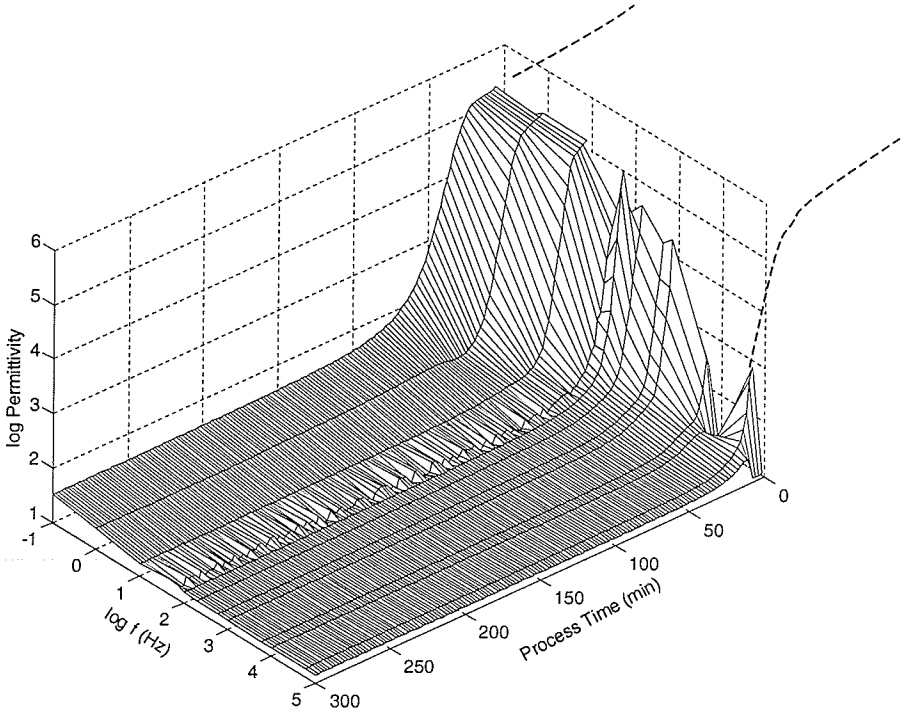

Figure 4.29 log Permittivity data for cycle R934 T-08

4.2.3 FBG Sensor Cure Monitoring

A FBG (Fiber Bragg Grating) sensor can be used to quantitatively measure the residual strain/stress. The changes in Bragg wavelength were monitored during curing and used in calculating the cure induced strains. While cure shrinkage is not the focus during on-line monitoring but the cured induced residual strain is. However, no separate data for the residual strain for the materials used in this study are available, and the residual strain cannot be measured using this indirect method. On the other hand, cure shrinkage of the resin and composite had been measured in reference (3), which could be used separately to confirm the measured results. Hence, the cure shrinkage is expected to be calculated using the monitoring data from a FBG sensor and compared with the value taken from reference (3). Because of the brittle nature of the sensors, only a single sensor was fed into the mold and embedded in the specimen (Cure Cycle 11, HMF T-25).

As shown in Figure 4.30, the oven was heated to 180°C and held for 240 minutes. Vacuum and pressure were applied successively at the beginning of the curing and at t = 65 minutes. Due to the lack of suitable fittings for the sensor, the pressure leakage was inevitable. The flowing nitrogen cooled the specimen and prevented the specimen temperature from increasing beyond 160°C before t = 195 minutes. Since this would result in a low DOC, the pressure was cut off after a hold period of 120 minutes. This allowed the specimen temperature and DOC to be increased to 173°C and 0.91 respectively. The minimum viscosity and gelation were predicted to occur at t = 80 minutes and t = 122 minute, respectively.

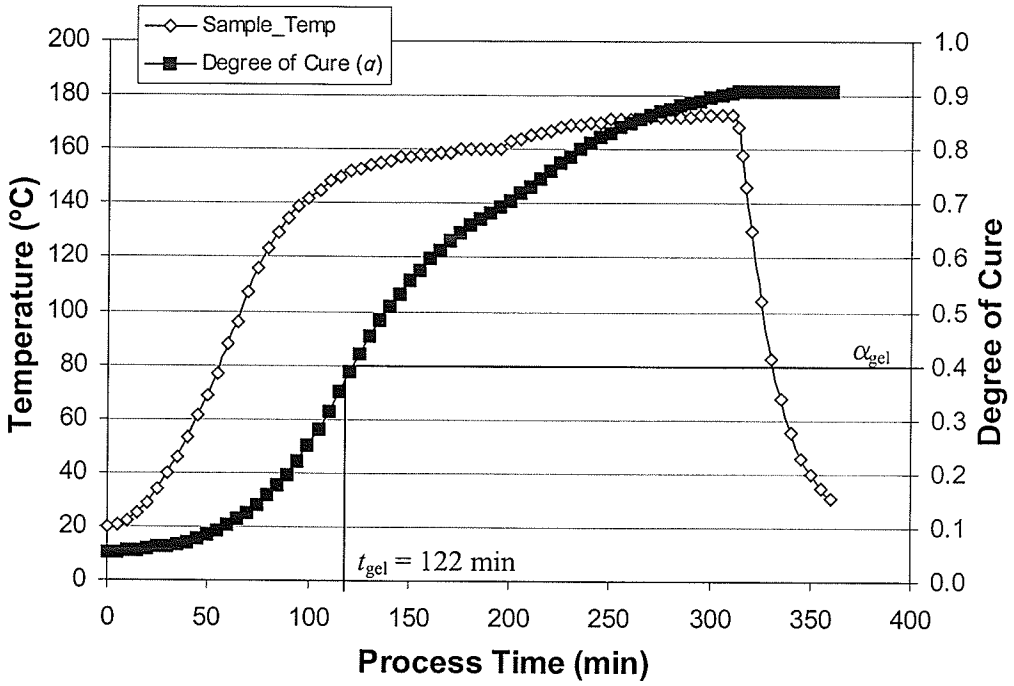

Figure 4.30 Part temperature and predicted degree of cure for cycle HMF T-25

The sensitivity coefficient of the sensor to temperature due to thermal expansion/contraction of the optical fiber was determined before it was embedded in the specimen. The sensor was fixed to the bottom of the mold using a tacky tape. No specimen was used during this experiment. The sensing section was lifted to leave a certain clearance from the bottom plate so that only response of the sensor to the air temperature inside the mold was monitored. This data was used to compensate for the thermal expansion of the sensor. The sensitivity coefficients of two FBG sensors to temperature were plotted in Figure 4.31. One of them was obtained using the sensor used in cure cycle 11 (HMF T-25).

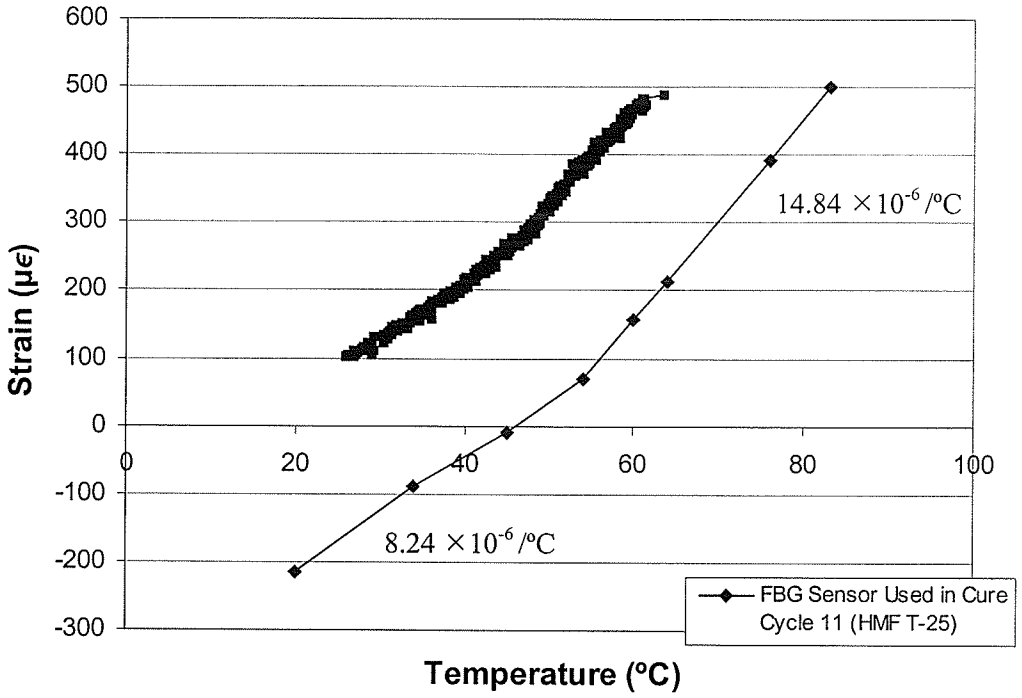

Figure 4.31 Sensitivity of FBG sensors to temperature

A slope of 11.25×10^{-6} /°C was obtained in the entire testing temperature range and was used for compensating the thermal expansion of the sensor. However, two slightly different slopes of 8.24×10^{-6} /°C and 14.84×10^{-6} /°C were observed in sensor response. The reason for this change in shape is unknown.

Figure 4.32 shows the total strain recorded during processing. The total strain followed the imposed temperature profile. The strain drop of 206 με at the beginning of the experiment was caused by the application of vacuum. When vacuum was removed and the pressure was applied at t = 65minutes, the strain dropped by 52 με. During the hold period, the pressure was removed at t = 195 minutes and the strain decreased by 67 με.

Beyond t = 340 minutes, when the specimen temperature had cooled down to 55°C, the strain was not recorded further since it was out of the measuring range of the equipment.

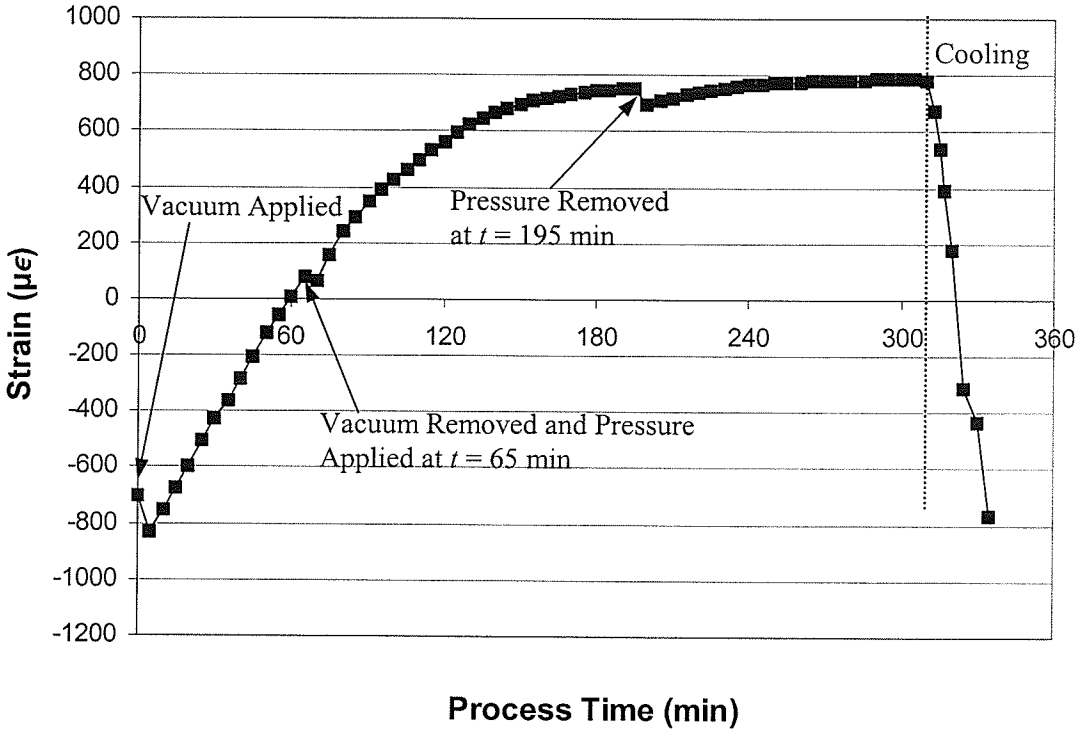

Figure 4.32 Total strain measured in cycle HMF T-15

Figure 4.33 shows the thermal expansion of the sensor calculated using its measured temperature sensitivity coefficient of 11.25×10^{-6} /°C. The data curve has been shifted to start from the zero value.

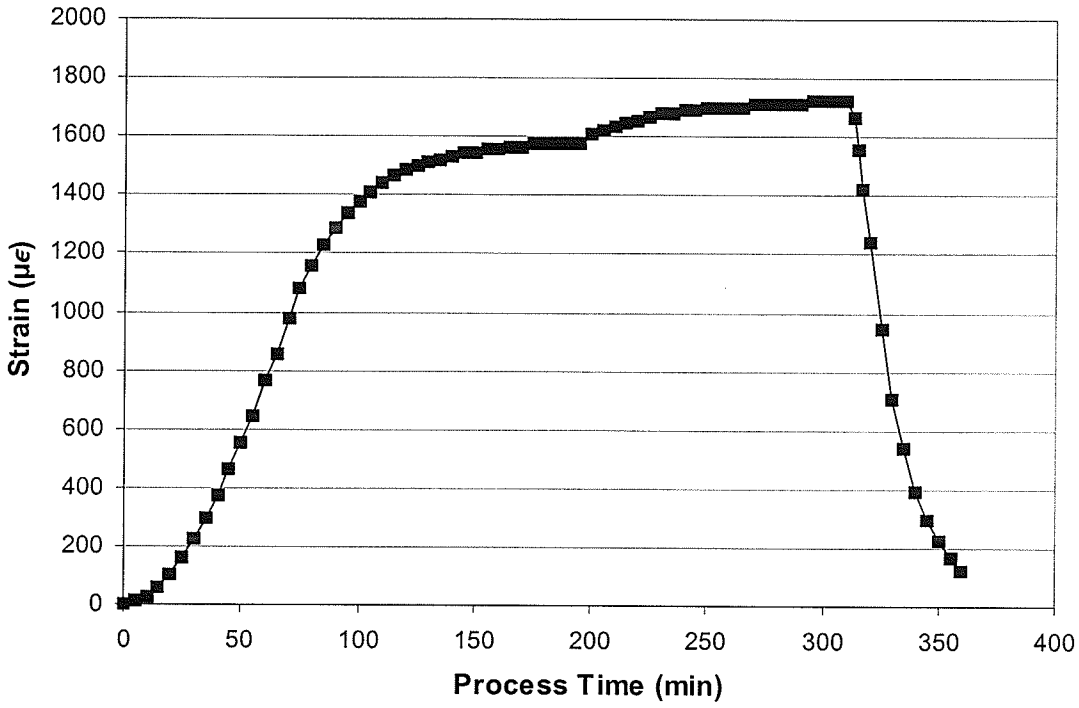

Figure 4.33 Thermal expansion of FBG sensor during the cure cycle

The thermal expansion of FBG sensor shown in Figure 4.33 corresponds to a condition of no bonding between the sensor and matrix resin of the composite. However, the sensitivity coefficient of the FBG sensor to temperature could be changing during the entire curing process as the resin gradually bonds to the sensor. This is illustrated in Figure 4.34, where the measured total strain during curing of composite is plotted as a function of temperature. The effects on measured data due to application and removal of the vacuum and pressure have been eliminated by removing these steps in Figure 4.32. During processing, the interface between the sensor and resin changed from no bonding to bonding. The slope of this plot directly yields apparent CTE of composite so that it can be compared with CTE of bare sensor. The apparent CTE of composite in different zones from I to V as shown in Figure 4.34 are 9.28×10^{-6} /°C, 10.49×10^{-6} /°C, 22.05×10^{-6} /°C, 9.14×10^{-6} /°C, and 14.26×10^{-6} /°C, respectively. A substantial change in CTE is

observed near the gel point (t = 115 minutes, T = 150°C). In order for the sensor to accurately measure the strain in the composite, a good bonding between the sensor and the composite is essential. The CTE of composite in zone I and II is almost equal to that of the bare sensor suggesting that there was no bonding between the sensor and the composite. The apparent CTE of composite above gel point is greater than that below gel point suggesting that the bond condition changed drastically through gel point. Hence, no effort was made in this study to subtract values in Figure 4.33 from Figure 4.34 to obtain the cure induced strain. In addition, the apparent CTE of composite in region III is greater than that in zones I and II even the temperature tends to reach constant value, and the apparent CTE of composite during cool down (region V) is less than that in region III above gel point. This is thought to be due to the fact that there is contribution from cure shrinkage in region III and IV when compared to no such contribution in region V.

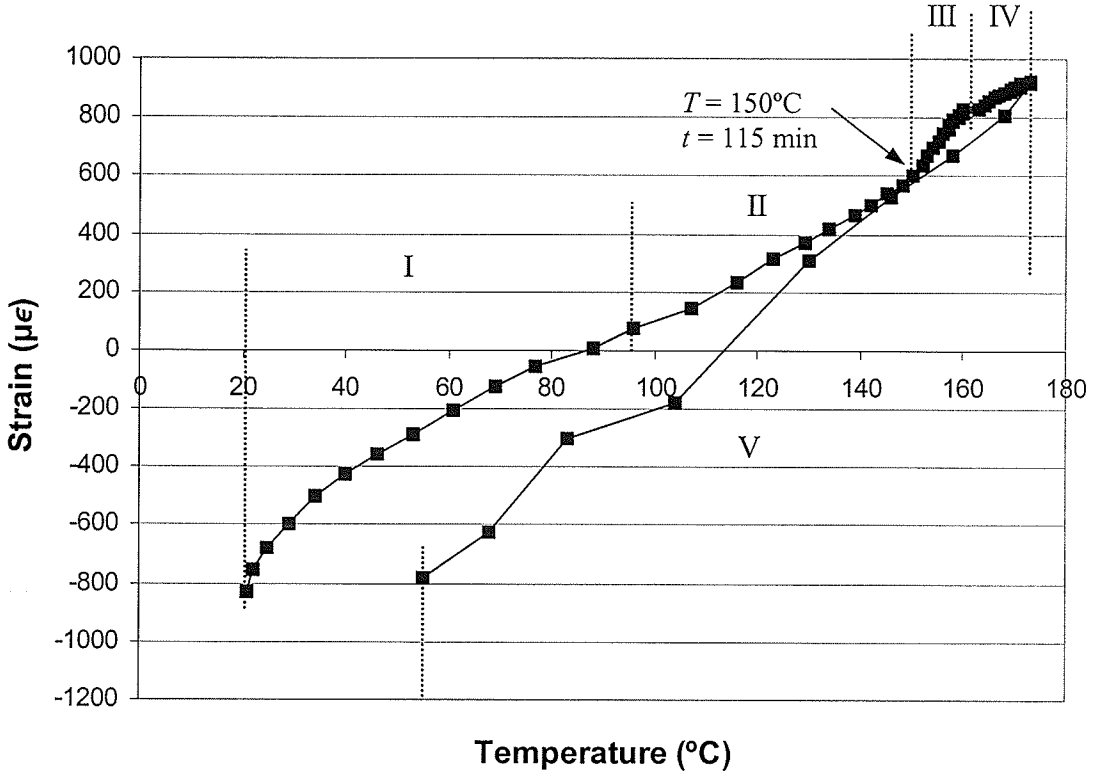

Figure 4.34 Total strain measured in cycle HMF T-25 vs. cure temperature

At the cooling stage, the FBG sensor had been bonded to the resin. The cure shrinkage was negligible and hence the measured strain was due to the thermal contraction of the specimen. A slope of 14.26×10^{-6} /°C was observed as shown in Figure 4.35. This slope is different from the value of 11.25×10^{-6} /°C for the bare optical fiber. This also significantly deviates from the coefficient of thermal expansion (CTE) of the composite laminate.

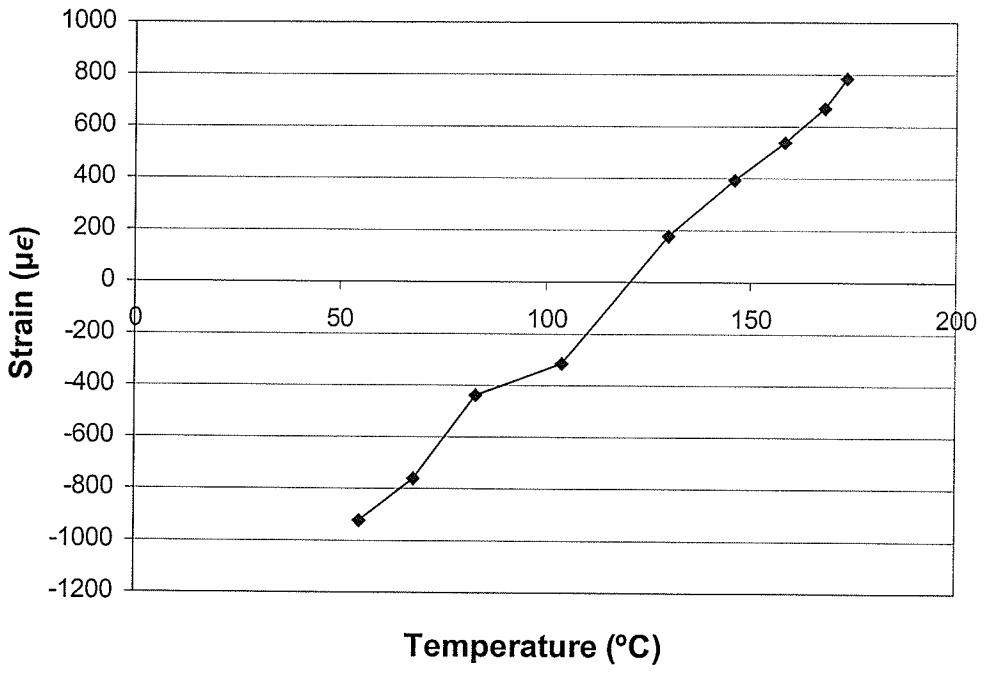

Figure 4.35 Variation of sensor response with temperature in cooling stage in cycle HMF T-25

The CTE of the unidirectional lamina used in this study has been measured by M. P. Koteshwara (3) to be nearly independent of degree of cure and temperature. The average CTE was found to be:

$$\alpha_{11} = 3.5\times10^{-6}/°C \tag{4.4}$$

$$\alpha_{22} = \alpha_{33} = 36.5\times10^{-6}/°C \tag{4.5}$$

The prepreg used in the experiment was plain weave fabric form, which contained reinforcing fibers woven in 0° and 90° direction as shown in Figure 4.36 (a). Since calculation of CTE of woven prepreg is difficult, it was modeled as a laminate laid up using four layers of unidirectional prepregs in $[0/90]_s$ sequence as illustrated in Figure 4.36 (b).

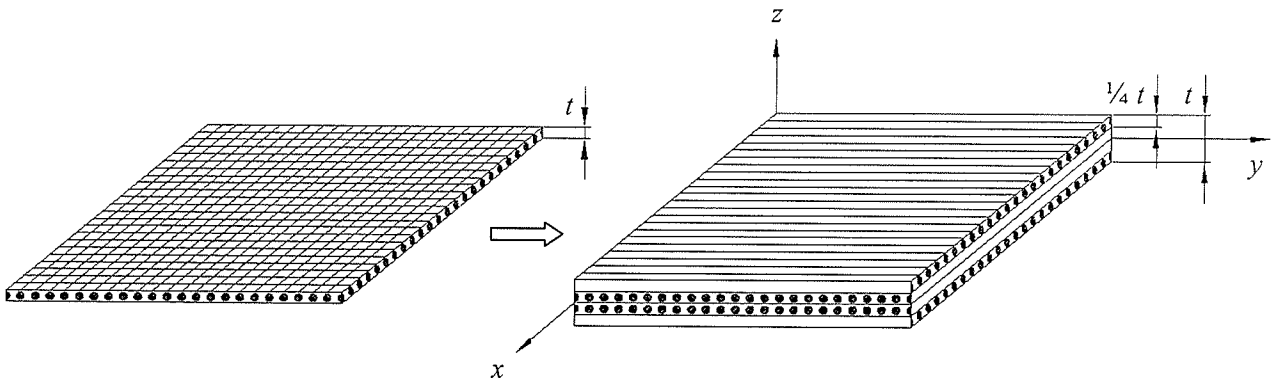

(a)
Fabric Prepreg

(b)
Modeled $[0/90]_s$ Laminate

Figure 4.36 Modeling of the composite sample used in experiments

Using the lamination theory and the unidirectional α value, the CTE of the woven prepreg was calculated to be:

$$\alpha_{11} = \alpha_{22} = 5.354 \times 10^{-6} /°C \qquad (4.6)$$

Assuming that the strain measured by FBG sensor is the global strain in the composite, the measured coefficient of thermal expansion for the composite during cooling should be close to 5.354×10^{-6} /°C. However, a much higher value of 14.26×10^{-6} /°C was recorded.

The reasons for this deviation could be:

1. During processing, the resin matrix of the composite would normally flow, gel and solidify on the tool plate. Normally, adhesion (the chemical or mechanical) occurs due to this between the tool and the composite. Since CTE of tool is normally much higher than that of the composite, there will be contribution due to this tool-part interaction to the measured strain. Currently, this effect is unknown and hence is thought to be the reason for the observed discrepancy.
2. FBG sensor has a diameter 10 to 14 times larger than that of the carbon fibers. When the sensor is embedded into a composite structure, a resin rich region as shown in Figure 5.6 will be generated around the optical fiber. Since a fabric prepreg ply has woven carbon fibers in both 0° and 90° directions, this problem would be more significant. In this resin rich layer, the volume fraction of carbon fibers (zero) is different from other locations. Hence, whether the FBG sensor is measuring the global strain in the composite or the local strain in the resin rich region near the sensor should be distinguished.

Other minor factors that might have affected the results are:

1. Error in the alignment of the FGB sensor with respect to fiber in the specimen;
2. The effect of transverse strains due to vacuum and pressure on the sensor;
3. The accuracy of modeling of the fabric prepreg.

As mentioned at the beginning of this section, if both the total strain and strain component due to thermal expansion of the sensor could be obtained, the actual strain

(cure induced strain) can be calculated using the assumption that the effects of strain and temperature could be separated by:

$$\varepsilon_{total} = \varepsilon_{actual} + \varepsilon_{sensor\ \ thermal\ \ expansion} \tag{4.7}$$

However, based on the facts discussed above, $\epsilon_{\text{sensor thermal expansion}}$ cannot be compensated directly using the data presented in Figure 4.33. Because so many factors affect the strain component due to thermal expansion of FBG sensor, it cannot be determined in this study. Hence, the correct cure induced strain and cure shrinkage cannot be decided. To demonstrate the potential of the sensor in cure monitoring, the cure shrinkage was still calculated using the data presented in Figure 4.33. As expected, the calculated cure shrinkage showed a significant error in both absolute value and shape of the data curve when compared with the values predicted using the material property model. The calculation of the cure shrinkage can be found in Appendix C.

4.3 Sensor Evaluation Using a Combination of Sensors

4.3.1 Ultrasonic and dielectric monitoring results for neat resin specimen

Figure 4.37 shows the ultrasonic attenuation and dielectric ionic viscosity data for the neat resin specimen cured in cycle 3 (R934 T-05). The temperature and degree of cure profiles can be found in 4.2.1.1. When the resin reached its minimum viscosity at t = 76.4 minutes, both signals approached their minimum values. When gelation occurred at t = 107.3 minutes, the attenuation started to increase sharply, and the ionic viscosity curve was close to its inflection point. At around t = 192 minutes, the attenuation reached a plateau value, and the ionic conductivity had a local maximum value (dlog IV/dt was equal to zero). The degree of cure at this time was 0.87.

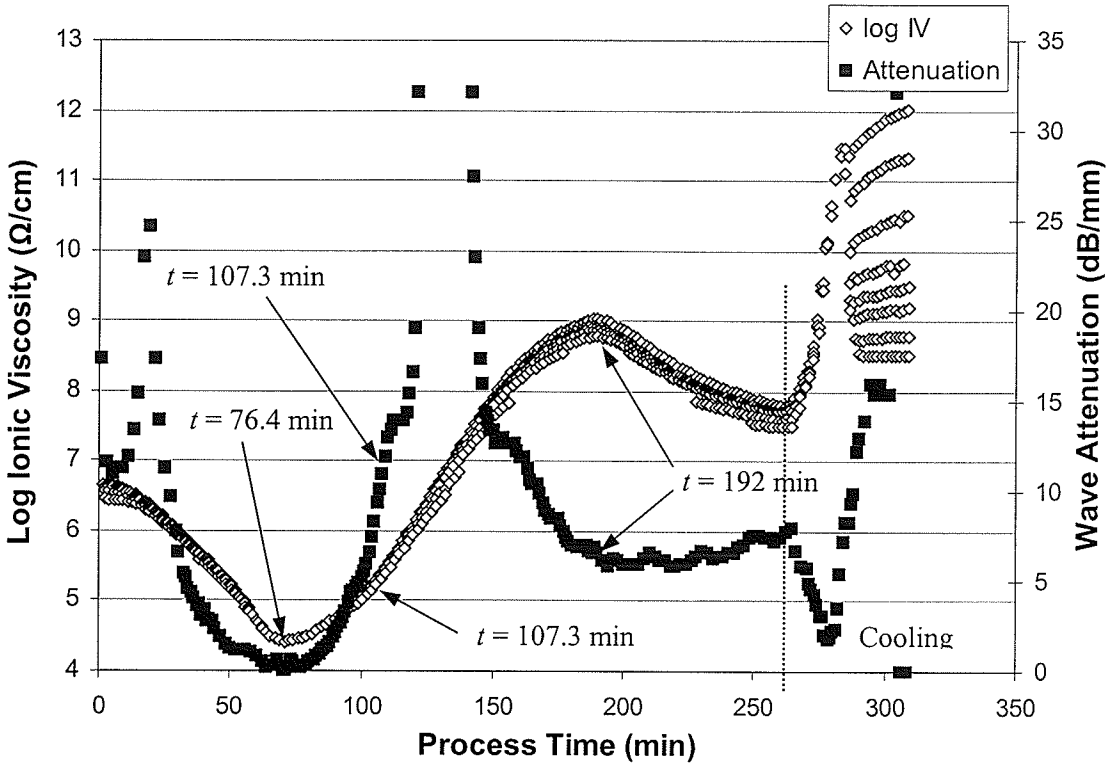

Figure 4.37 Ultrasonic and dielectric response of neat resin sample in cycle R934 T-05

4.3.2 Ultrasonic and dielectric monitoring results for composite specimen

Similar behavior was observed in composite specimens as shown in Figure 4.39. The specimens were cured using similar cycles, except one cycle did not have a postcure procedure, as shown in Figure 4.38. Hence, the sensor responses are displayed till t = 190 minutes. At about t = 80 minutes, the specimen reached its minimum viscosity and both the attenuation and ionic viscosity approached their minimum values. When the gelation occurred at t = 119 minutes, the attenuation reached a peak value and the ionic viscosity approached its inflection point, where dlog IV/dt was equal to zero. At t = 189 minutes, the ionic viscosity reached a plateau value with a degree of cure of 0.81, while the attenuation had a plateau value at around t = 160 minutes.

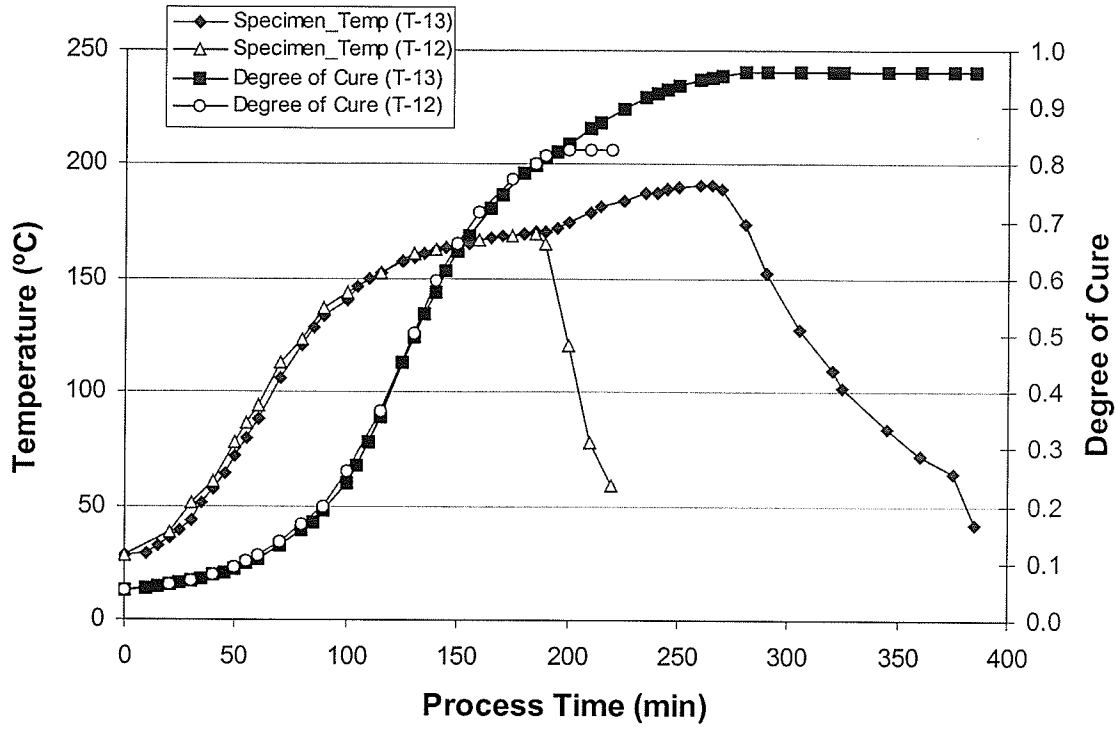

Figure 4.38 Part temperature and degree of cure of composite specimens (HMF T-12 and HMF T-13)

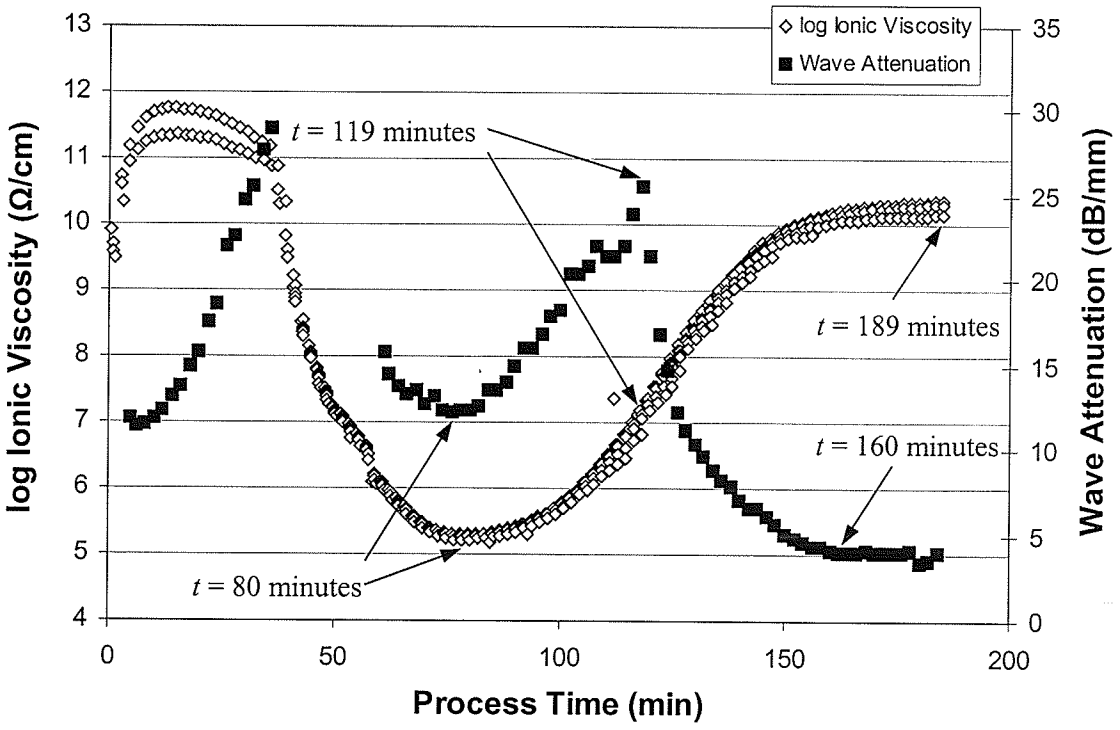

Figure 4.39 Ultrasonic and dielectric response of composite samples in cycle HMF T-12 and HMF T-13

It can be concluded from the comparison of the ultrasonic and dielectric monitoring data for both the neat resin and composite specimens that the sensing data of both sensors can be accurately correlated to the minimum viscosity of the specimens. The time corresponding to the ultrasonic attenuation peak and inflection in ionic viscosity curve (the peak of dlog IV/dt) precisely relates to the gel time for the composite specimens. However, it is not the case for the neat resin. The reason has been discussed in previous sections. When the ultrasonic and dielectric signals reached plateau values, the degree of cure was still increasing. Hence time for reaching the plateau cannot be deemed as the criterion for time to reach the fully cured state.

4.4 Summary of Monitoring Results

Table 4.5 shows the summary of experiment results obtained with neat resin and composite specimens in different cure cycles.

Table 4.5 Summary of monitoring results

Cure Cycle	Sensing Data	Viscosity Min (min)	Gelation Point (min)	Time and Degree of Cure Corresponding to Plateau Values	
				Time (min)	α
Cycle 1 R934 T-01	Predicted	49.3	63	NA	
	Dielectric	49.1	63 72.5*	114~116	0.886~0.890
	Ultrasonic	NA	NA	NA	
Cycle 2 R934 T-04	Predicted	60.4	89	NA	
	Dielectric	NA	NA	NA	
	Ultrasonic	42~62	89 96~114*	NA	
Cycle 3 R934 T-05	Predicted	76.4	107.3	NA	
	Dielectric	72.4~75.9	107.3 126~128*	191.8	0.866
	Ultrasonic	66~78	107.3 121~141*	194	0.87
Cycle 4 HMF T-12	Predicted	80	119	NA	
	Dielectric	NA	NA	NA	
	Ultrasonic	76~78	118	NA	
Cycle 5 HMF T-13	Predicted	85	119.2	NA	
	Dielectric	82	119.2	189.3	0.812
	Ultrasonic	NA	NA	NA	
Cycle 6 HMF T-16	Predicted	85	120	NA	
	Dielectric	NA	NA	NA	
	Ultrasonic	82~95	116	NA	
Cycle 7 HMF T-17	Predicted	80	108	NA	
	Dielectric	NA	NA	NA	
	Ultrasonic	78	108	212	0.919
Cycle 8 HMF T-22	Predicted	82	106	NA	
	Dielectric	NA	NA	NA	
	Ultrasonic	84	106~108	188	0.917

Cycle 9 HMF T-23	Predicted	80	104	NA	
	Dielectric	NA	NA	NA	
	Ultrasonic	80~82	100~128	NA	
Cycle 10 HMF T-24	Predicted	78~83	104.5	NA	
	Dielectric	78	112	162	0.86
	Ultrasonic	NA	NA	NA	
Cycle 11 HMF T-25	Predicted	80	121	NA	
	Ultrasonic	78	118	NA	
	FBG	NA	NA	295	0.891

Table 4.6 shows the isothermal experiment results of neat resin specimens.

Table 4.6 Isothermal experiment results of 934 neat resin

Cure Cycle	Sensing Data	Viscosity Min (min)	Gelation Point (min)	Vitrification		
				Time (min)	T_g (°C)	α
164°C ISO R934 T-08	Predicted	NA	10.3	244	162.4	0.86
	Dielectric	NA	8.8**	244.6	162.5	0.86
176°C ISO R934 T-10	Predicted	NA	5.5	78.2	175.9	0.89
	Dielectric	NA	5.2**	78.8	177.9	0.89
190°C ISO R934 T-09	Predicted	NA	4.4	57.2	188.7	0.923
	Dielectric	NA	5.1**	35.2	170.4	0.87

* Time of ultrasonic attenuation peak or dlog IV/dt peak in neat resin specimen curing process

** Values obtained are uncertain because of the fast reaction speed.

CHAPTER 5

DISCUSSION

5.1 Introduction

The ability of each sensor to monitor the material parameters of interest is discussed first. Subsequently, issues related to the industrial applicability of sensors are discussed.

5.2 Monitoring Result Analysis

The material parameters described in previous chapters are crucial for on-line control of autoclave processing of polymer composites. In this study, the ability of ultrasonic and dielectric sensors that were used to monitor parameters such as minimum viscosity, gelation, and degree of cure was evaluated. The FBG sensor was used to measure the process induced strains during processing. The ability of each sensor to monitor these material parameters is discussed in the following sections.

5.2.1 Degree of Cure and Viscosity

None of the sensors evaluated in this study were able to monitor the evolution of the degree of cure of the specimen during curing. Figure 5.1 shows the ultrasonic time delay and attenuation as a function of degree of cure for a neat resin specimen cured using Cycle 3 (R934 T-05). It is observed that no trend can be found between the time delay, attenuation and degree of cure. Hence, the correlation between the ultrasonic response and degree of cure cannot be established. Researchers tried to use the ionic conductivity data to model the degree of cure as reported in (20). However, as mentioned in previous chapters, the ionic conductivity results from the impurities in the resin, and it cannot be

directly related to the material property changes during curing. Efforts have been made to correlate the dipole contribution to degree of cure and vitrification. However, due to the fast reaction of the material at isothermal experiment temperatures, the permittivity and loss factor data was incomplete. In addition, since it was difficult to extract the dipole contribution from the dielectric monitoring data influenced by high level of ion conductivity contribution and electrode polarization effect, the correct Cole-Cole plot cannot be obtained, and no fundamental relationship between the dielectric response and degree of cure can be established. Due to the same reason, the viscosity of the specimen could not be modeled by the ultrasonic and dielectric monitoring data. The FBG sensor also could not be applied to determine the degree of cure and viscosity during curing.

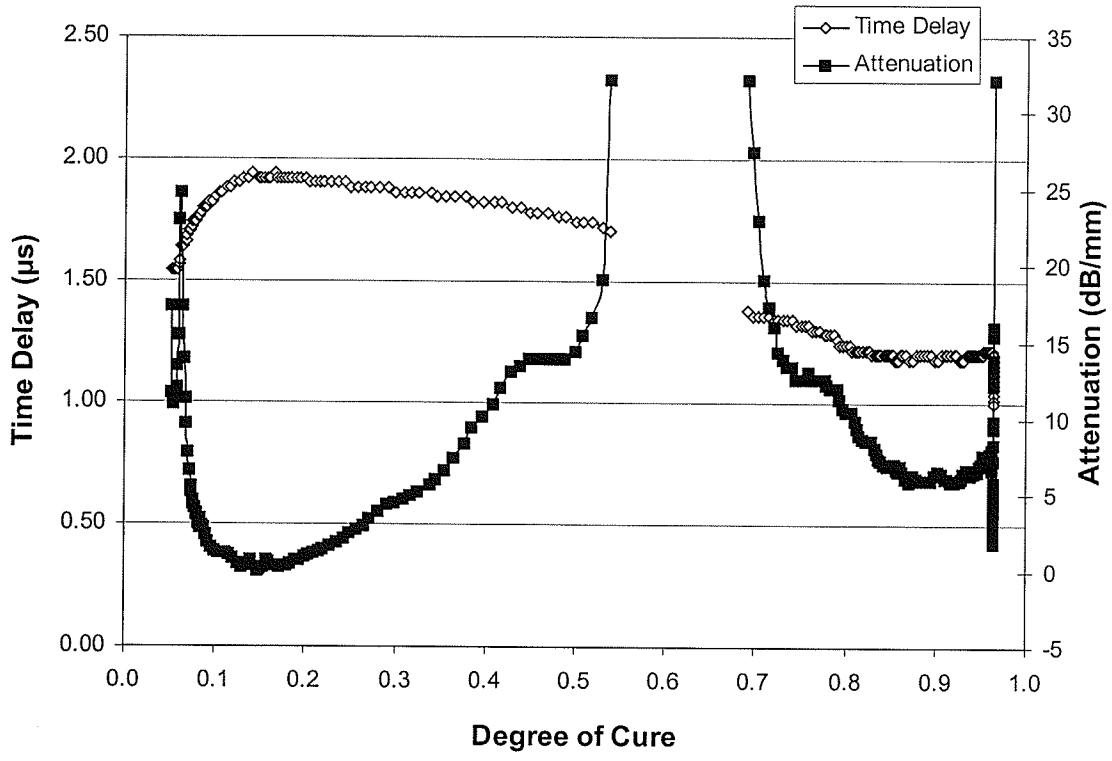

Figure 5.1 Time delay and attenuation for the resin specimen in cycle R934 T-05

5.2.2 Viscosity Minimum

The process time to reach the minimum value in ultrasonic attenuation and the maximum value in time delay correlated to the process time corresponding to the minimum viscosity. In some experiments, the maximum in time delay and minimum in attenuation reached plateau values instead of a single maximum or minimum point. The maximum error in one experiment was 18 minutes. In other experiments, the maximum error was not greater than 10 minutes compared with the predicted time for the viscosity minimum. Because this sensor measured the process time for viscosity minimum was verified by separate experiment results using other testing methods, this correlation is quantitative. Similar response was observed in dielectric monitoring data. The process time corresponding to the minimum value in ionic viscosity (when dlog IV/dt = 0) can be quantitatively correlated to the time for the minimum viscosity with an error not greater than 4 minutes. This observation is consistent with the results observed by other researchers in references (10) and (50). However, few studies reported the correlation between the ultrasonic attenuation and viscosity minimum. Because no fundamental relationships could be established between the ultrasonic/dielectric responses and mechanical viscosity of the specimen, these correlations are empirical.

5.2.3 Gelation

The process time corresponding to the attenuation peak and inflection in time delay can be quantitatively and empirically related to the gel time of the composites within 4 minutes. Similar to the ultrasonic response, the process time corresponding to the zero value of dlog IV/dt, i.e. the inflection in the log Ionic Viscosity curve quantitatively and

empirically correlates to the gel time of the composite specimens within 8 minutes. This conclusion agrees with the observations in the research work such as and (16) and (25). However, in these studies, no data obtained using other experiment methods was presented to prove their monitoring results. Again, there is lack of fundamental relationships between the sensor responses and gelation time.

It was observed that the errors of monitoring of composite specimens gelation were within 8 minutes using both the ultrasonic and dielectric sensors. The error of monitoring of resin specimens could be 23 minutes, which is greater than that of the composites. The predicted gelation for resin occurs earlier than the peak/zero and inflection values in ultrasonic and dielectric curves were reached. The reason has been discussed in Chapter 4: this is believed to be due to the facts that the viscosity of resin was determined using experimental data generated fro the composite, while the degree of cure, used to determine gel point, was determined using the experimental data generated for the resin. Hence, error in the determination of gel point for the resin could lead to such a difference.

5.2.4 End of Cure

As described in Chapter 4, after a certain period of cure, both the ultrasonic and dielectric signals reached plateau values. Beyond that, they would not change even though the degree of cure continued to increase. As the curing proceeded, the moduli of the material increased with the increase in viscosity. As the moduli approached certain values, the time delay ceased to decrease and reached a plateau value. After this plateau, the time delay was not sensitive to the changes in moduli. This is the same condition for the

attenuation data obtained after the plateau in the attenuation. In dielectric response, the mobility of ions decreased with the increase in viscosity. However, no fundamental relationship could be established between the ion contribution and mechanical viscosity. After the ionic viscosity reached a plateau value, it was not sensitive to the changes in viscosity and polymer chains. The degree of cure at the process time corresponding to the ultrasonic and dielectric plateau values was 0.87 ~ 0.92, and it was increasing gradually beyond this time. The moduli of the specimen that were about 90% of that for the fully cured state were also gradually increased. Hence, the process time corresponding to plateau cannot be deemed as the criterion to correlate the end of cure state. The end of cure state could not be determined in this study. This is in the disagreement with most of the research work, such as in (9) and (22), where the process time corresponding to plateau in ultrasonic and dielectric signals was qualitatively related to the end of cure state. The measured cure shrinkage reached a plateau value and built up evenly after the gelation, it is observed to be not sensitive to the degree of cure beyond the time corresponding to this plateau value.

5.2.5 Glass Transition Temperature (T_g) and Vitrification

As shown in Table 3.1, T_g is a function of the degree of cure of the specimen. However, since the degree of cure could not be related to ultrasonic signals, the T_g could not be correlated to the ultrasonic response during curing. Researches in (21) tried to correlate empirically the ionic conductivity data to the T_g of the specimen. However, as discussed in previous sections, the fundamental relationship between the ion contribution and material properties could not be established.

Efforts were made to correlate the dielectric response to vitrification using the method reported in (25). However, the dipole contribution could not be separated from the contributions from ionic conductivity and electrode polarization and hence the correlation to the vitrification could not be made. In this study involving isothermal experiments of 934 resin, the process time corresponding to the plateau values of log Ionic Viscosity data (when dlog IV/dt was equal to zero) is very close to the time for vitrification of the specimens. Whether it is coincidence should be verified by more experiments. Researchers in reference (16) reported that the process time corresponding to the second peak of the ultrasonic attenuation of an epoxy adhesive correlated to the vitrification of the material under test. Although a second peak in attenuation curve was observed in this study for both the resin and the composite specimens, such a correlation could not be obtained. Researchers in reference (11) stated that the glass transition caused a maximum in the ultrasonic attenuation. However, it is proven in this study that the attenuation peak resulted from the gelation, rather than glass transition.

It is concluded that for monitoring the minimum viscosity and gelation, the ultrasonic and dielectric sensors were comparable. Both sensors performed measurements correctly with acceptable errors. Both sensors' data cannot correlate to the end of cure state of specimens in this study. More issues related to use of these sensors need to be considered are discussed in the following sections.

5.2.6 Modulus

Theoretically, the modulus of the specimen can be quantitatively measured by the ultrasonic sensor. Measured modulus for aluminum, cured resin and composite specimens at room temperature is presented in Tables 4.1 and 4.3, which highlights the potential of ultrasonic sensor to be used in measuring the modulus during curing. However, since the changes in thickness and density of the specimen during curing that are crucial in determining the modulus could not be monitored under the current experimental configuration, in addition, the lack of suitable couplant, which is crucial in obtaining strong signals and thus the modulus could not be measured in this study. Details about these issues can be found in 5.3.1.1.4.

5.2.7 Process Induced Residual Strain

The FBG sensor can be used to quantitatively measure the total strain, which is due to the contributions from both the thermal expansion of the FBG sensor and cured induced residual strain. Due to the difficulties in determination of the thermal expansion of the sensor, the residual strain and cure shrinkage were hardly measured. A significant error from the predicted cure shrinkage was observed. The shape of the measured cure shrinkage curve also shows a shift to the predicted shrinkage curve. The possible reasons have been presented in Chapter 4, including the change in the temperature sensitivity coefficient of FBG sensor due to the change in bonding condition between the sensor and the resin; the resin rich region that could present around the sensor; the tooling effect; the errors in sensor alignment; the effect of vacuum and pressure and the accuracy of modeling of the fabric prepreg. More experiment data are required to verify the FBG

sensor response in monitoring of curing process of polymer composites. This study has shown that the FBG sensor could survive after processing. If the composite part with embedded FBG sensor could be safely removed from the autoclave, the sensor could be used in composite structure health monitoring. Design of autoclave fittings to accommodate the FBG sensor is an important issue.

5.3 Issues Related to Industrial Applicability of Sensors

Several issues that significantly affect the sensor results were carefully studied and evaluated in this study in order to evaluate their suitability for industrial use. These issues are categorized as (a) Sensor and Installation Issues, (b) Experimental Issues, and (c) Data Processing Issues.

5.3.1 Issues in Using Ultrasonic Sensor

Several issues observed during these experiments, which can affect the ultrasonic monitoring results, are discussed in the following sections.

5.3.1.1 Sensor and Installation Issues

5.3.1.1.1 Clamping Pressure

The ultrasonic transducer and clad buffer rod should be assembled and installed carefully. As discussed in previous chapters, the surface of the buffer rod in contact with the transducer must be perfectly flat and smooth. Appropriate clamping force is required to obtain a good contact between the transducer and buffer rod. The end of the buffer rod

must be flush with the platform on the bottom plate of the mold. Even a small gap of 120μm caused signal loss during curing.

5.3.1.1.2 Ultrasonic Couplant

In addition to clamping pressure discussed above, an ultrasonic couplant is used to provide the coupling between the transducer and buffer rod. Time delay data for both longitudinal and transverse waves are required to determine the moduli of the specimen. In this study, a mixed-mode ultrasonic transducer capable of generating both longitudinal and transverse waves was initially used. This required a couplant that can transmit both waves. Only limited number of such couplants is available in the market. The shear gel tested in this study could only work continually at room temperature. However, its viscosity drastically decreased at the operating temperature of 50°C encountered during a cure cycle, which reduced its capacity to transmit the transverse wave. In addition, the couplant was easily squeezed out by clamping force when the viscosity decreased and was easily flushed away by the compressive air. This weakened the ultrasonic signals specifically transverse wave significantly. Hence the data for transverse wave could not be obtained. Till now, it has been very difficult to find a couplant whose viscosity would be higher and stable at the operating temperature.

The couplant used in the experiments is the high viscosity version of HIGH Z, a longitudinal wave couplant, which can work at a temperature up to 93°C for a short period (as specified by the manufacturer). It is a relatively stable ultrasonic couplant compared with other couplants tested in this application. However, after five to six

experiments, weakening of the ultrasonic signals was still observed as shown in Figure 5.2. As observed in the tests using shear gel, the decreased viscosity and flushing out of the couplant affected the ultrasonic signals. To obtain the best coupling effect, the transducer and buffer rod were reassembled with a new couplant after every five or six experiments.

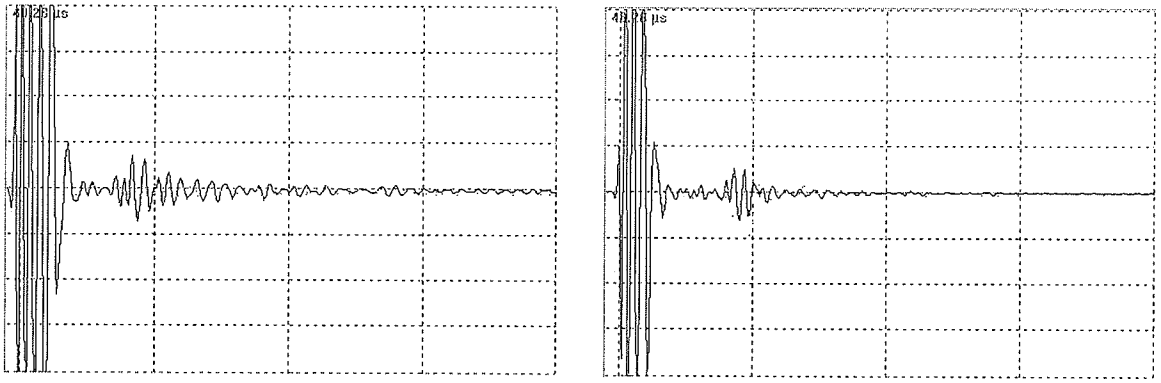

Ultrasonic signals before experiments Ultrasonic signals after five or six experiments

Figure 5.2 Weakened ultrasonic signals after several experiments

The best way to obtain a stable coupling for the sensor is to fix the transducer to the buffer rod permanently by using glue or other adhesives. Using this method, the coupling problem is expected to be eliminated.

5.3.1.1.3 Ultrasonic Transducer Selection

The transducer used in this study has a center frequency of 10 MHz. In theory higher frequencies resulted in a higher loss in energy during propagation through the composite and hence, only specimens with a smaller thickness can be tested. Hence, transducers with lower frequencies are required for testing thicker composite parts.

A 5 MHz transducer that can generate both longitudinal and transverse waves was purchased for this study. However, several factors limited its application. Firstly, there is the lack of a suitable couplant that allowed propagation of both waves at the operating temperature. Secondly, the amplitudes of both waves were weaker than that of waves generated using a single mode transducer. In addition, both the longitudinal and transverse waves were sampled and displayed in the same data window while using a mixed mode transducer. This caused difficult in distinguishing the echo peaks due to the two waves. This is illustrated using test signal from a thin aluminum plate. As shown in Figure 5.3, the velocity of the transverse wave traveling in aluminum is close to half of the longitudinal velocity (c_l = 6.32 km/s, c_t = 3.13 km/s). Therefore, echoes of transverse waves were superimposed with echoes of longitudinal waves. Some cured carbon fiber reinforced polymer composite panels were found to have a similar ultrasonic response to aluminum (e.g. F263/T300 composites). Hence detecting and analyzing the data from echoes of waves generated by a multi-mode transducer would be a challenge during cure monitoring. A solution would be to use two single-mode transducers: one for longitudinal waves and another for transverse waves.

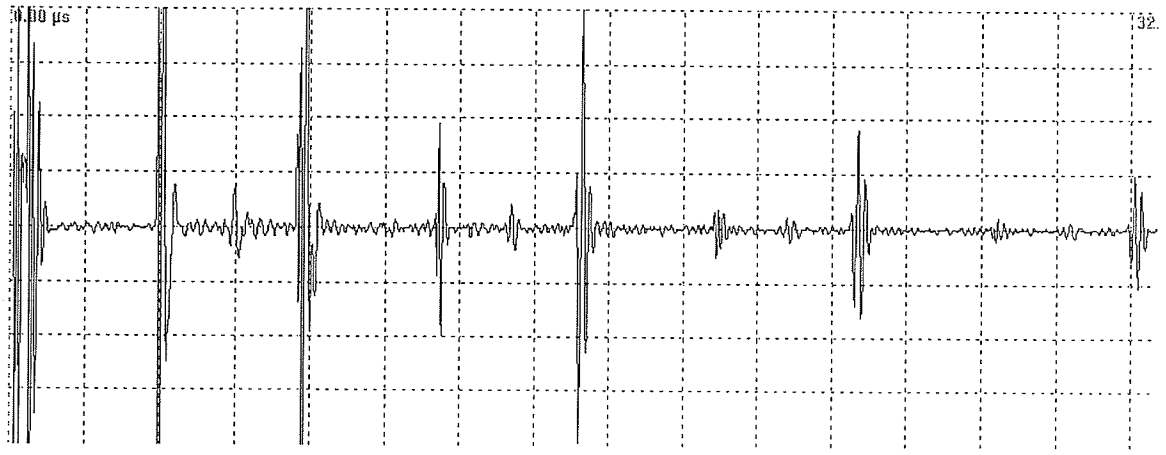

Figure 5.3 Ultrasonic response of combined mode transducer to aluminum plate

5.3.1.1.4 Issues Related to Change in Ultrasonic Wave Velocities

For composite part quality control, moduli evolution during curing must be known. Both longitudinal and transverse waves are required to calculate the Young's modulus, shear modulus and Poisson's ratio. The issues related to using a mixed mode transducer has been described in the previous section. The problems in analyzing the sensing data could not be well solved in this study. Hence to achieve this goal, both longitudinal and shear wave transducers are needed.

In order to calculate the ultrasonic sound velocity and thus the moduli of the specimen, the changes in specimen thickness and density should be monitored during curing. The thickness change is caused by the thermal expansion and cure shrinkage of the specimen. The density will also be slightly changed during curing due to the resin flow caused by the vacuum, pressure and elevated cure temperatures. Accurate thickness and density values cannot be obtained real-time using current experimental test set-up. Hence only ultrasonic time delay was used instead of ultrasonic velocity. Because ultrasonic attenuation was calculated as a relative value, the thickness of the cured specimen was measured and used in the calculation. Limited studies monitored thickness changes of the specimen during curing in their work, such as in reference (11). However, none of them performed their experiments using a vacuum bag. Lack of testing equipment is the most significant problem. Sensors such as LVDT (Linear Variable Differential Transformer), DVRT (Differential Variable Reluctance Transducer) or linear Hall effect sensors etc. can be used to measure the thickness changes, although there could be potential problems for the installation of them in autoclave, such as the coupling force, thermal effect

compensation, installation and sealing etc. It is difficult to find such equipment in the market that is suitable for high temperature and pressure environment, such as in an autoclave. LVDT and DVRT are the most possible sensors to be used for this purpose. However, it would be difficult to install these sensors in real autoclaves. Installing the sensors outside the vacuum bag would cause difficulties in differentiating the thickness change in laminate from those from vacuum bag materials, including the peel plies, release film, breather, bleeder and nylon bag film. If the sensors were installed inside the vacuum bag, the probe has to be fed through the vacuum bag and contact with the specimen. To prevent the probe pitting into the composite by coupling force when the resin flow presents before gelation, the probe might have to be mounted above the caul plate instead of contact with the specimen directly. It would also be difficult to seal the feed-through of the vacuum bag for the probe, which is a moving part of the sensor. In addition, the compensation for the thermal expansion of the sensor itself, the caul plate, and the tool plate, and the effect of pressure and vacuum on the sensor should also be considered. No published work on monitoring change in density was found. However, it should be considered in an actual manufacturing environment.

5.3.1.2 Experimental Issues

5.3.1.2.1 Specimen Quality

Composite part's surface quality significantly affects the quality of the signal. Firstly, good coupling between the bottom surface of the composite and buffer rod end is required for efficient transmission of ultrasonic energy with minimal loss due to scattering at the composite/buffer rod interface. Secondly, the strong reflection of the

wave from the top surface of the composite, i.e. composite/air (caul plate) interface is required. Both require a smooth composite surface, which can be achieved only through good resin flow. During the start of the experiment when resin in the composite does not flow, vacuum and pressure should assist in obtaining good coupling.

Our experiments proved that for a specimen thickness, the more smooth and flat specimen surface, the stronger the ultrasonic signals are. Since a specimen with coarse and uneven surface disperses the incident ultrasonic waves in all directions, no signals can be received by the transducer.

Final level of consolidation is another fact influencing the signal quality. Poor consolidation results in dry spots and delamination, which would weaken the ultrasonic signals. If these dry spot voids across in an area directly above the buffer rod, the poor quality signal would be obtained. To avoid this, multiple transducers at multiple locations may be required.

Alternatively, the surface and consolidation quality should be improved by ensuring good resin flow. Applying a metal caul plate with a smooth surface above the composite part during curing would be helpful in this regard. Using the caul plate results in a better resin flow and consolidation because of the uniform pressure applied to the specimen beneath it. Also, caul plate/composite interface has a higher R (coefficient of reflection) than composite/air interface, which helps in strong reflection of waves. This can be illustrated using a simple calculation. The R is defined as:

$$R = \frac{p_r}{p_e} = \frac{Z_2 - Z_1}{Z_2 + Z_1} \tag{5.1}$$

Let p_e and p_r be sound pressure of incident and reflected waves respectively; Z_1 be the acoustic impedance of material 1, Z_2 be the acoustic impedance of material 2. Details about reflection and transmission of ultrasonic waves at boundary can be found in Appendix A.

The impedance of the aluminum and steel are $Z_{Al} = 17 \times 10^6$ kg/m^{2}s and $Z_{Steel} = 45 \times 10^6$ kg/m^{2}s, respectively. Although the impedance of the composite specimen, Z_{sp}, is not known, it should be a value much lower than that of the aluminum based on the equation

$$Z = \rho c \tag{5.2}$$

and the fact that the impedance of the epoxy resin is $2.7 \sim 3.6 \times 106$ kg/m^{2}s (6). Therefore the reflection coefficients are

$$R_{Sp/Al} = \frac{17 \times 10^6 - Z_{Sp}}{17 \times 10^6 + Z_{Sp}} \tag{5.3}$$

$$R_{Sp/Steel} = \frac{45 \times 10^6 - Z_{Sp}}{45 \times 10^6 + Z_{Sp}} \tag{5.4}$$

The reflection coefficient at specimen/steel interface would be much higher than the value at specimen/aluminum interface.

A comparison of the ultrasonic response of specimens cured with and without caul plate (Cycle 7 (HMF T-17) and Cycle 8 (HMF T-22)) is shown in Figure 5.1 (FSH% is the abbreviation of Full Screen Height, which is a measure of the ultrasonic amplitudes in the software. The determination of the ultrasonic amplitudes can be found in Appendix B). It

can be observed that under the same experimental configurations, stronger amplitudes were obtained from the specimen covered with the steel caul plate.

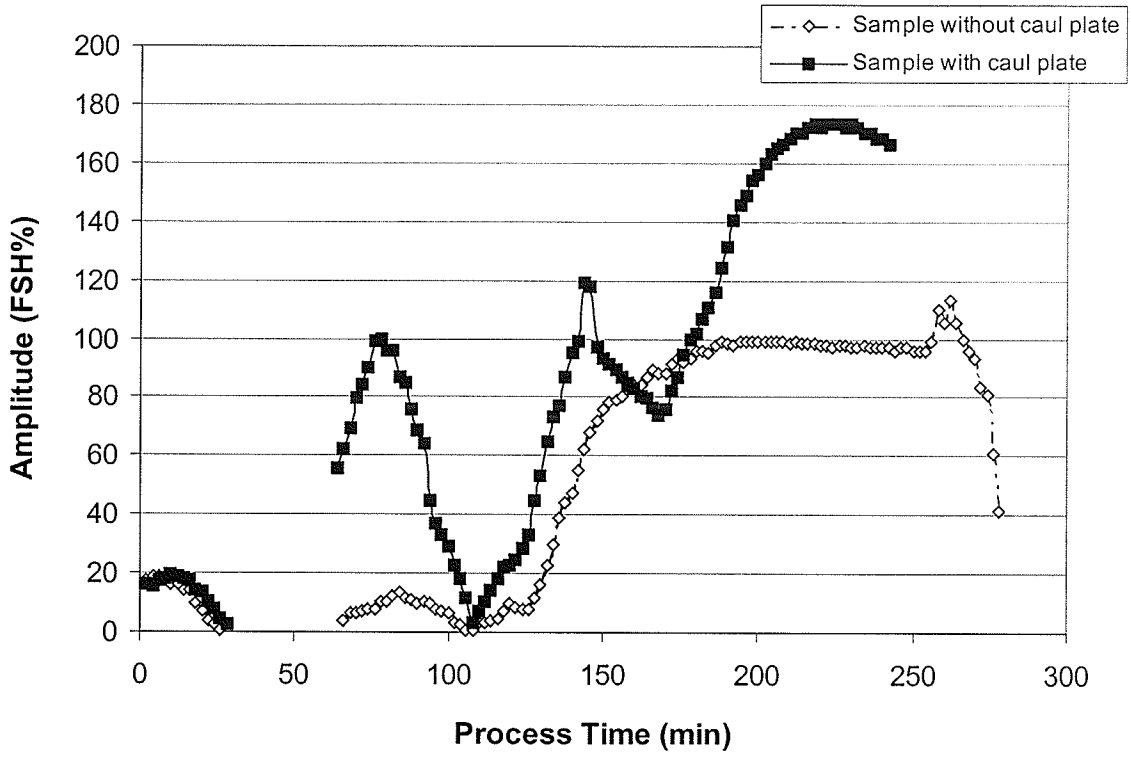

Figure 5.4 Comparison of the ultrasonic response of specimens with and without caul plate (Cycle 7 (HMF T-17) and Cycle 8 (HMF T-22))

5.3.1.2.2 Specimen Thickness

More ultrasonic energy will be lost while traveling through a thicker specimen resulting in weaker signals. As shown in Figure 4.7, for the ultrasonic response of the room temperature curable fiberglass resin system, the thicker the specimen, the more energy was absorbed and more data was lost. The same behavior can be observed in processing of composite specimens. In the curing of 12-ply composite laminates, the amplitudes were too weak to be detected in most of processing periods, as shown in Figure 4.12. Thus it is impossible to monitor curing of thick composite parts using this sensor.

On the other hand, a very thin specimen would result in difficulties in separating signals from the main bang (the waves reflected back from the buffer rod/ specimen interface), the first echo, and following echoes. Hence selecting an optimum specimen thickness in pulse/echo mode is important in ultrasonic monitoring work.

In manufacturing of aerospace composites, the thickness of the parts could be increased due to the inserts and honeycomb cores structures. In addition, these cores inserts introduce inhomogeneity into the composites, which will change the propagation properties of ultrasonic waves. The ultrasonic sensor could not be suitable for monitoring the cored composites and even not applicable in sensing the parts with honeycomb cores. This issue should be considered in the real aerospace industries.

5.3.1.3 Data Processing Issues

5.3.1.3.1 Issues Related to Identification of Maxima/Minima or Inflection Values

As presented in Table 4.1, the process time corresponding to a single minimum value in viscosity can be obtained by the prediction using the model. This is due to the mathematic method used in the calculation. In real measured viscosity data, a data range (flat region) is observed near the viscosity minimum instead of a single minimum value. In ultrasonic time delay and attenuation data, difficulties associated with determining maxima/minima, inflection or plateau due to spread in data were encountered. A plateau could be observed at the time delay or attenuation peak instead of a single point. Theoretically, the peak, inflection and plateau in time delay could be determined by

calculating the first derivative of time delay with process time, similar to dIV /dt used in dielectric response. However, as 1 minute time interval was used to record the ultrasonic sensing data in this study, the applicable d(time delay)/dt data could not be obtained due to the lack of sensing data. This could be solved by either reducing the time interval for data recording or using linear interpolation to determine the missing data. This should be noticed in on-line data processing.

5.3.1.3.2 Data Processing

The ultrasonic monitoring data is acquired and stored by the ARIUS IV software system in a special format. ARIUS IV converts and displays the data in A-Scan mode. The time delay and amplitudes of the main bang and first echoes from the specimen/air (caul plate) interface have to be picked up and recorded manually at each time interval after experiments. The software provided by the manufacturer of the ultrasonic inspection system was modified by the author and used to convert the sampled data to a usable format off-line. The converted data can then be plotted as shown in Figures 4.3 and 4.4. Hence the measured raw data cannot be used directly for analysis. An intelligent program is required to convert the sampled signals into time and amplitude values on-line. It should be able to pick up the amplitude values from the main bang and the first echo to calculate the time delay and attenuation. The algorithm should also have the ability to determine crucial events in ultrasonic signals such as the process time corresponding to the maximum/minimum values of time delay and attenuation, the inflection of time delay curve by calculating its first derivate of process time, the attenuation peak value and

plateau values of both parameters. Such an algorithm is crucial in determining the applicability of this sensor for on-line monitoring.

5.3.2 Issues in Using Dielectric Sensor

5.3.2.1 Sensor and Installation Issues

5.3.2.1.1 Sensor Selection

Implantable dielectric sensors were used in this study. Although the sensor size is small, it still can influence the integrity of composite structures. As observed in Figure 5.4, the sensor has almost the same thickness as the host composite structure. This effect could be not significant when the sensor is embedded in a large composite part. On the other hand, the bonding between the sensor and composite is not good, and the resin rich regions could present near the sensor. Cracks could be generated at and spread along the sensor/composite interface. Due to the small size of the sensor, it can only monitor the material property changes near the sensing element. Bulk properties of the composite could not be obtained using a single sensor. In a real industrial environment, because of the flexible nature of implantable sensors, they can be embedded into the composite part at different locations to form a network to monitor the bulk properties of the part. To avoid destruction to the structures, the sensor should be implanted into the excess material, which will be trimmed off from the part after processing. Tool mount sensor could be more suitable to monitor the small dimension composite parts. Similar to the ultrasonic sensor, it is able to monitor non-destructively, and can be repeatedly used in monitoring work.

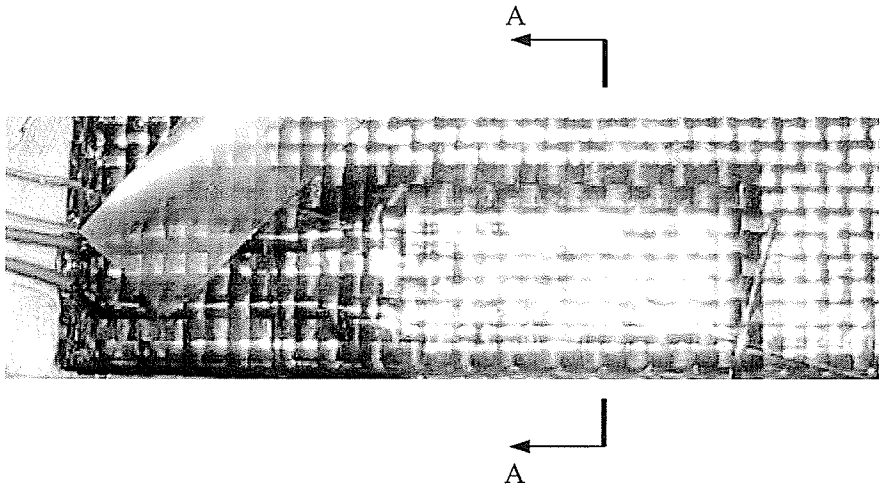

A – A Direction

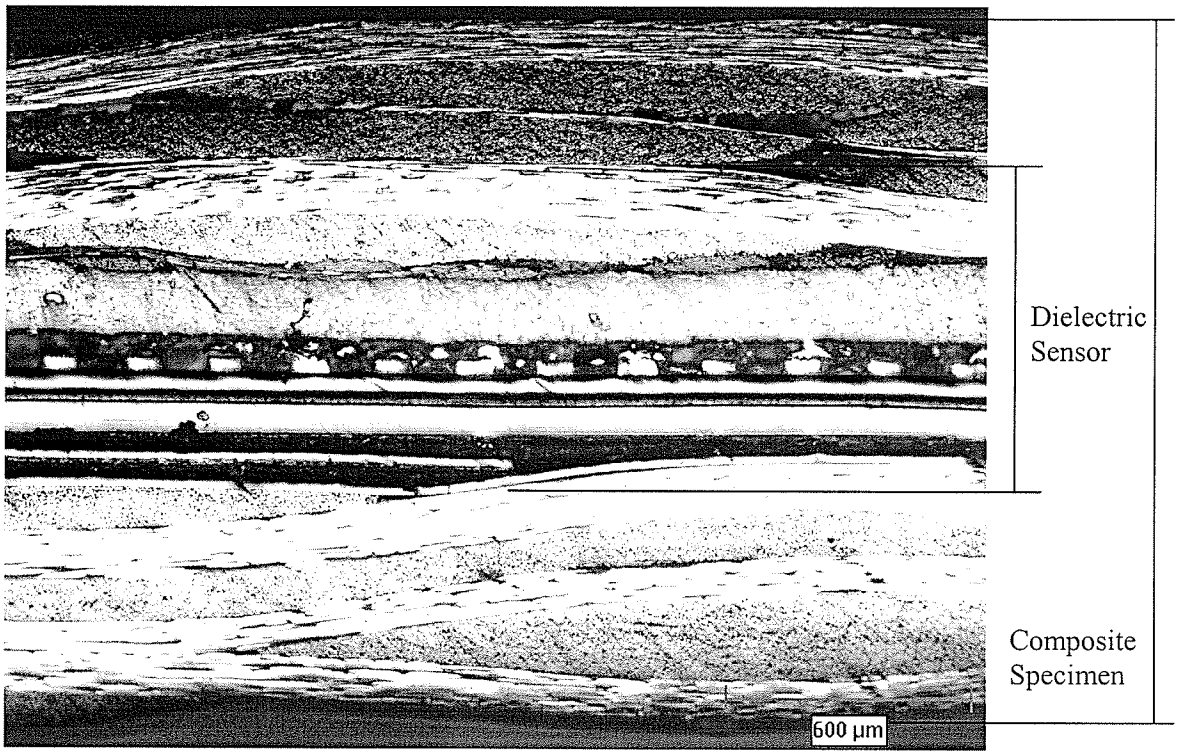

Figure 5.5 The dielectric sensor embedded in a composite specimen

5.3.2.1.2 Comparison of Ultrasonic and Dielectric Sensors

Both sensors were used to measure the material parameters such as time for viscosity minimum, gelation time and end of cure in this study. Dielectric sensor is applicable to most composite processing methods, such as oven curing, autoclave processing, RTM etc. The sensors can be embedded into any locations within the part. Multiple sensors can be implanted into the specimen and monitored by a single multi-channel DAQ system. It can perform the measurement even on thin parts with a thickness as small as 1 micron (D. D. Shepard et al. (43)). However, implantable sensors may act as defects and influence the integrity of composites. Due to the small size of the sensor, it measures the local properties, but not global properties, bulk property measurement in a relatively thick part using a single sensor is not possible. The measured data could be difficult to analyze because of the interference due to high level of ionic conductivity, electrode polarization and interfacial polarization. It may also be affected by cure reaction byproducts, such as ammonia, water etc., containing ionic species that mask the curing reaction. Dielectric monitoring also cannot be performed in conductive resin systems.

Ultrasonic sensor can monitor nondestructively the curing process. It can be used to perform bulk property inspection. The ultrasonic response is not affected by reaction byproducts. The sensor may be mounted on the tool permanently. On the other hand, ultrasonic transducers must be carefully aligned and installed for both the pulse/echo and transmission modes. Measurement can only be carried out at the location where the sensor is mounted. Appropriate part thickness is required. If the part has high damping or has inserts and honeycomb cores structures, it would create a problem in obtaining

ultrasonic signals. The part must maintain contact with tool during processing. Loss of contact will cause loss of signals. For quality control, part thickness and density changes must be accurately monitored during curing. Selecting the more appropriate cure monitoring technique depends on the specific applications.

5.3.2.2 Experimental Issues

5.3.2.2.1 Influence of Resin Flow on Dielectric Monitoring

Sensors with filters were used to monitor the curing of composite specimens. The filter layers of the sensor must prevent the sensing element from coming in contact with the conductive fiber reinforcement, while allow the resin reaching the sensing element. Good resin flows are required to flow through these filter layers and wet the sensing surface. It was proven in this study when the composite was processed with poor resin flow, the specimen cannot be well consolidated. On the other hand, the resin cannot reach the sensing element. Hence no dielectric data can be obtained. Good resin flow should be obtained by applying proper vacuum, pressure and heating rate during processing.

5.3.2.2.2 Fundamental Relationship

The fundamental molecular theories of dielectric change in chemically reactive systems are yet to be developed. The major limitation of dielectric sensor for online monitoring of composite curing is lack of fundamental correlations between the dielectric data (dipole contribution) and degree of cure, viscosity, etc. In this study, the ionic conductivity (ionic viscosity) and dlog IV/dt were used to quantitatively and empirically monitor the material parameters, such as viscosity, gel point etc. However, the ionic contribution results from

impurity ions present in the resin, which could be by-products generated in the manufacturing procedure, reactants in curing process, and absorbed moisture etc, and also may vary from batch to batch. Hence, this cannot have any direct relationship with mobility of polymer chains. Despite of this, some researchers (20, 21, 24) have tried to correlate ionic conductivity data to the degree of cure and T_g of the material. However, because no fundamental relationship can be established, these models are purely empirical and are only valid for a specific material and for a specific experimental environment. Dipoles exist in a dielectric material at the molecular level. Hence the material properties can be directly related to dipole changes during curing. Establishing a quantitative model based on the dipole contribution in monitoring work is highly desired.

As mentioned in previous chapters, experiments at higher frequencies will yield pure dipole contributions, and the fundamental model relating of ϵ' (or ϵ'') to degree of cure could be established. Recent researches (29, 30) showed that at microwave frequencies, the dielectric behavior was dominated by the disappearance of epoxy groups, allowing for a direct correlation between the dielectric response and the degree of cure. Further studies along these directions should be pursued.

5.3.2.3 Data Processing Issues

5.3.2.3.1 Result Analysis

As described in last chapter, the data interpretation was influenced by a number of factors. Hence, the fundamental relationship between the dielectric response and material parameters, such as degree of cure, could not be established. Efforts were made to

account for these factors by performing isothermal experiments. The temperature effect on dielectric response hence was eliminated. However, the complete reaction curves for permittivity and loss factor could not be obtained due to the fast reaction of the material at the cure temperature. The high level of ionic conductivity and electrode polarization still had significant effects on dielectric response. The parameters related to dipole contribution such as relaxed permittivity, unrelaxed permittivity, dipole relaxation time etc. could not be determined using the Cole-Cole plots in this study. Hence it was not possible to establish the relationship between the dipole contribution and material properties. Experiments performed at lower temperatures should be pursued in the future work.

5.3.2.3.2 Data Processing

The dielectric monitoring data is acquired and stored by the Eumetric software system in ASCII format. The information including process time, temperature, permittivity, loss factor, frequency, gain and phase can be easily retrieved from the data file. Parameters such as ionic conductivity, ionic viscosity and dlog IV/dt can be calculated and displayed by the Eumertric software system in real time. The software worked well for determining the ionic conductivity. However, measurement accuracy is unknown. In addition, it did not account for the ion contribution for permittivity, and dipole contribution for loss factor data. The electrode polarization correction function provided by the software is limited and could not work properly and reliably for data interpretation. An algorithm is required to determine crucial event in dielectric signals on-line, such as the process time corresponding to the minimum value, inflection and plateau values of ionic conductivity,

peak and zero values of dlog IV/dt. It also needs to be able to take the sensing data for APCS, make decisions based on the monitored material parameters and communicate with the autoclave controller.

5.3.3 Issues Related to Use of FBG Sensor

5.3.3.1 Sensor and Installation Issues

5.3.3.1.1 FBG Sensors

Sensor manufacturers could not provide a sensor with high temperature protecting sheath for use at high temperature applications. This forces the user to use bare sensors, which are very brittle and delicate to handle. Over stretching or bending during embedment within the material could break the sensor. The most vulnerable locations are feed throughs in the mold and vacuum bag. Reinforcement in this region is recommended.

5.3.3.1.2 Alignment of FBG sensor

It has been proven that placing the sensor in a direction parallel to the reinforcing fibers is the optimal orientation to minimize the effect that the embedded optical fiber has on the surrounding host material (51). Figure 5.6 shows a FBG sensor embedded in a composite specimen used in this study. It was observed that the sensor introduced heterogeneity in the host composite structure. Since the diameter of the sensor is much larger than that of the carbon fiber, and the prepregs are in fabric form with the fibers in both directions, a resin rich region around the sensor is inevitable as shown in Figure 5.6. In this resin rich layer, the volume fraction of carbon fibers is different from other locations. This raises a

concern that the FBG sensor may be measuring local strain in the resin rich region instead of measuring the global strain in the composite.

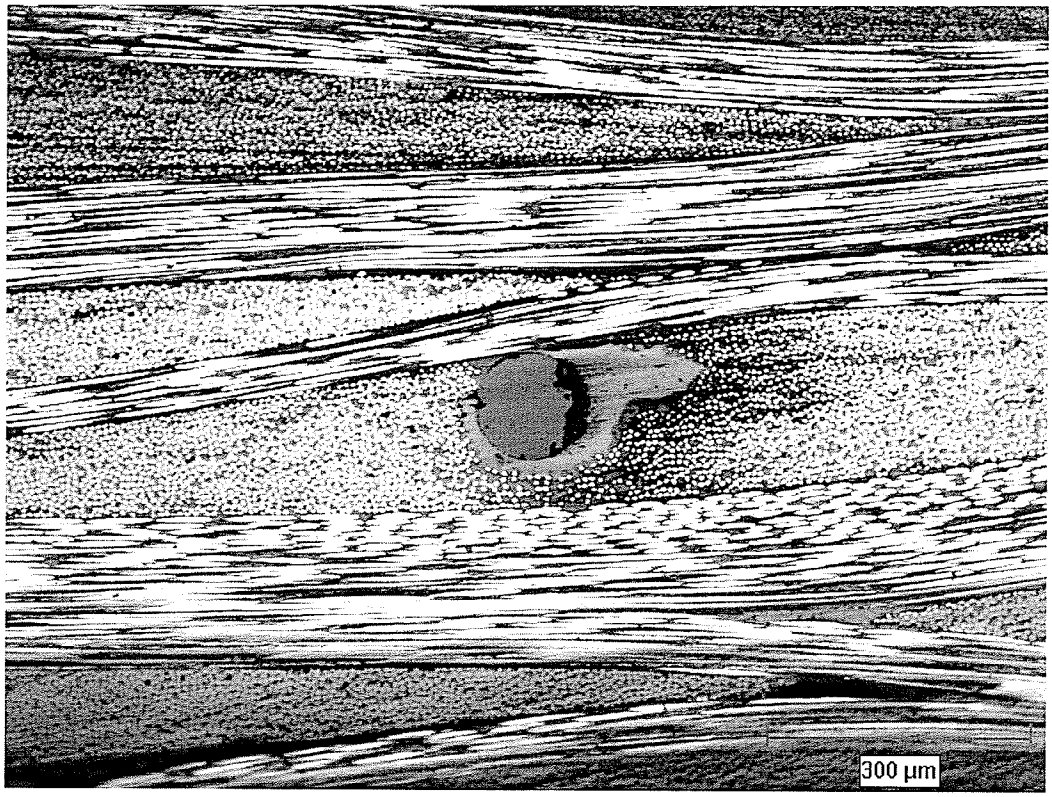

Figure 5.6 The FBG sensor embedded in a composite specimen

5.3.3.1.3 Effects of Transverse Strains and Thermal Response of FBG Sensors

The application of the vacuum and pressure resulted in a significant response from FBG sensor during curing of the composite specimen (HMF T-25, Cure Cycle 11), since Bragg gratings are also sensitive to transverse loading caused by vacuum and pressure, and resin shrinkage. The strains induced by the vacuum and pressure cannot be simply compensated as a constant value, because the state of the bonding of the optical fiber with the resin changes with process time and temperature, from no bonding to good bonding.

This would result in a change of strain-optic and photoelastic coefficients during curing. The sensitivity of FBG sensor to transverse loads could be evaluated by comparing with the response of an extrinsic Fabry-Perot interferometric (EFPI), which is not sensitive to transverse strains. A cure cycle without vacuum and pressure could also be helpful in studying the effects of non-axial strains to the sensor response. However, a cure cycle without vacuum and pressure may affect resin flow and wetting of the sensor.

As discussed in Chapter 4, the coefficient of thermal expansion of Bragg grating changed due to the change in the state of bonding to the resin. In addition, tooling effect could have affected the measurement of the thermal expansion of the FBG sensor. Precise compensation for the thermal expansion/contraction of the sensor was difficult since the thermal sensitivity changed with process time. This is an important issue that needs to be addressed before this sensor can be used in the real industrial environment. Since the single Bragg grating sensor could not separate the thermal and mechanical strains, this effect could not be isolated and analyzed. Future work should focus on separating the thermal and mechanical strain components.

5.3.3.1.4 The Advantages and Limitations of FBG sensors

FBG sensors have high sensitivity to cure induced shrinkage strains with minimum intrusion on host structure's integrity. The measurement is wavelength-based and independent of intensity variations and losses from the light source. Multiple sensors can be constructed as network to monitor the bulk properties of the material, and used in the subsequent in-service health monitoring.

The brittle nature of the sensor is a problem in a real industrial environment, which might cause difficulties when it is used in the autoclave processing. The effect of temperature on the sensor response must be compensated. The high cost of sensor and instrumentation and skill requirements could limit it to be applied in high volume, mid to low value product industries.

5.3.3.2 Data Processing Issues

As described in Chapter 3, the computer is connected with the SHM 5100A system via a RJ-45 networking cable. The Shmget software developed by the manufacturer communicates with the SHM 5100 system and downloads the sensing data every 5 minutes (this time interval can be determined by the operator). Each set of 5000 sampled readings, collected at a 50 or 100 Hz sampling rate, is stored in one file in a special format and cannot be retrieved and analyzed directly. Software is also provided by the manufacturer to convert the raw data files to text or Excel files. All the converted files are combined into one Excel file manually and thus the measured strains can be analyzed. Hence for monitoring the cure strain on-line, a program is required to convert and pick up the measured data and calculate the cure induced strains.

CHAPTER 6

CONCLUSIONS AND RECOMMENDATIONS

6.1 Introduction

This chapter contains the conclusions and recommendations for further study.

6.2 Conclusions

The objectives of this thesis have been successfully realized. Three types of commercially available sensors, namely ultrasonic sensor, dielectric sensor, and FBG sensor, have been found to be promising – yet, further research and development is required before use for on-line monitoring of autoclave processing of polymer composites in industries.

Both the ultrasonic sensor and dielectric sensor can be used to determine the time when the viscosity minimum and gelation occurs during processing. The sensors used in this study could determine these within an error of 10 minutes for composites. However, these sensors could not measure the absolute value of viscosity and degree of cure. In addition, these sensors could not be used to determine the time for completion of cure and vitrification. No fundamental relationships could be established between the sensor response and various material parameters of interest. Due to experimental difficulties, the moduli of the specimen could not be measured during curing at high temperature though they could be measured at room temperature, using the ultrasonic sensor.

The ability of a FBG sensor to quantitatively measure the process induced strains has been demonstrated. However, its temperature and transverse strain sensitivities are significant, and they must be properly accounted to improve the accuracy of the measurement.

The analysis software that comes with these sensors and their instrumentation does not yield the material parameters directly. Significant data conversion and manipulation are required. As such, these sensors are not readily suitable for industrial applications yet.

Firsthand knowledge and experience in sensors, sensor installations, data acquisition, processing and analysis of data have been gained through this study. Issues regarding sensor and installation, experimental and data processing have been identified and their importance has been highlighted through this study. Based on this, it is concluded that application of these sensors for on-line monitoring is not straightforward. Significant amount of user training in application and maintenance of these sensors as well as data interpretation is needed.

Based on this study, a number of advantages and disadvantages of using sensors became evident. There are listed below:

1) Ultrasonic sensors

Advantages:

- The sensors are easy to handle and install;
- The sensors with pulse/echo mode may be mounted on the tool permanently.

Disadvantages:

- The ultrasonic couplants that are able to work stably at elevated temperatures are not available in the market;
- An effective cooling system is required for the sensor to work in the autoclave processing environment;
- The quality of ultrasonic signals are sensitive to a number of factors, including the installation of the sensors, ultrasonic couplant, thickness of samples, consolidation and surface quality of samples, etc.;
- Difficulties in moduli measurement during curing using ultrasonic sensors;
- Data processing is complicated and time consuming.

2) Dielectric sensors

Advantages:

- The sensors are robust and easy to be embedded into the host composite structures;
- The sensors are easy to be fed through the vacuum bag and the mold;
- The sensor signals are less affected by the part quality. However, good resin flow is required.

Disadvantages:

- Sensor response is affected by high level ionic conductivity contribution and the electrode polarization effect;
- Certain level of knowledge is required for data processing.

3) FBG sensors

Advantages:

- The sensors are able to perform absolute measurements;
- The size of the sensors is small compared to the host composite structures.

Disadvantages:

- The sensors are brittle and difficult to handle. They are difficult to be embedded into host composite structures;
- The sensors are sensitive to thermal and transverse strains, which significantly affect the accuracy of the measurement. Obtaining correct data for thermal expansion of the sensor is a big issue;
- The fitting for the FBG sensor is difficult to design and machine. Pressurization gas leakage at the fitting is a big issue for application of the sensor. The sensor is difficult to be safely removed from the mold after curing;
- Data processing is complicated and time consuming;
- The sensors are expensive.

6.3 Recommendations

Based on the results from this study, a number of recommendations for further work were developed. They are:

1. Ultrasonic transducers with lower center frequencies should be evaluated. Theoretically, the ultrasonic waves with lower frequencies can travel through a thicker specimen and thus stronger signals can be obtained. In order to measure

the modulus during cure, single mode transducers for longitudinal wave and transverse wave should be used. Since no suitable ultrasonic couplant is available in the market at this time, it is recommended to bond the transducer with the buffer rod permanently. For anisotropic materials, such as carbon fiber reinforced composites, the ultrasonic response of transverse wave is related to both the lay up sequence and polarization direction of the wave. Hence the transverse wave transducer should be carefully aligned to the desired direction. A feasible method is also needed to monitor the thickness and density changes of the specimens during curing.

2. For dielectric monitoring technique, the ionic conductivity data (ionic viscosity) was used in this work. As mentioned above, the ionic contribution is due to impurity ions, while dipole relaxation contribution relates directly to material property changes. Hence establishing a fundamental relationship between dipole contribution and degree of cure is highly recommended. According to current results, the need to eliminate or correct for the ionic conduction and electrode polarization is a key factor in obtaining acceptable dipole response data. To establish the relationship between dipole contribution and degree of cure, experiments at lower isothermal temperature or at microwave frequencies are recommended.

3. Cure cycles without vacuum and pressure should be used to study the effects of transverse loads on FBG sensor response. The change of temperature sensitivity

of the sensor during curing should be studied for more accurate compensation of temperature sensitivity of FBG sensor. Modified sensors that are able to separate the thermal and mechanical strain components, could be used in the future work. Experiments with EFPI (Extrinsic Fabry-Perot Interferometric) sensors can also be performed to evaluate its suitability in on-line monitoring of autoclave processing of polymer composites.

4. Till now, no sensor has been used to correlate the degree of cure and the end of cure state of the composites. This is a very important material parameter required for the control of the curing process. Hence further work should focus on this.

5. Software needs to be developed to record the sensing data on-line for all the three types of sensors. The program should be able to convert the recorded data to usable formats. Intelligent algorithms are required to determine the critical information, such as the time for the maximum in time delay, the minimum in attenuation/ionic viscosity, the inflection point of time delay/ionic viscosity, the peak value of attenuation and dlog IV/dt, the zero value of dlog IV/dt, the plateau values of time delay/attenuation/ionic viscosity.

6. Currently, all the sensors are evaluated in the lab environment. In further studies, the sensors should be integrated and applied in real autoclave processing environment.

REFERENCES

1. Raghavan Jayaraman, *Aerospace Materials and Advanced Manufacturing Process*, Course Notes, University of Manitoba, (2002).

2. Michael Hudek, *Examination of Heat Transfer During Autoclave Processing of Polymer Composites*, M.Sc. Thesis, University of Manitoba, (2001).

3. Madhava Prasad Koteshwara, *Parameteric Study of Process-Induced Warpage in Composite Laminates*, M.Sc. Thesis, University of Manitoba, (2001).

4. R. Mark Shead, *Optimization of Autoclave Processing of Polymer Composites Using a Genetic Algorithm*, M.Sc. Thesis, University of Manitoba, (2001).

5. Renè Kent, "Process Control for Composite Manufacture", *Comprehensive Composite Materials*, 5 (2000), Editors: Leif Carlsson, Robert L. Crane, Kenji Uchino.

6. Josef Krautkrämer and Herbert Krautkrämer, *Ultrasonic Testing of Materials*, second edition, Springer-Verlag, New York (1977).

7. Li Che Ted Chen, *A Unique Method of Determining the Elastic and Engineering Constants of Unidirectional Fiber-Reinforced Composite Plates Using Ultrasound*, Technical Note No. 274, University of Toronto, Institute for Aerospace Studies, (1991).

8. N. Mard, C. Prèvost, and A. Johnston, " Ultrasonic Monitoring of Curing Process of Graphite/Epoxy Composites", *Proceeding of International Symposium on Polymer Composites Science Technology, SPE*, Quebec, Canada (1999), pp. 251 – 264.

9. J. –Y. Chen, S. V. Hoa, C. –K. Jen and H. Wang, "Fiber-optic and ultrasonic measurements for in-situ cure monitoring of graphite/epoxy composites", *Journal of Composite Materials*, 33 (1999), pp. 1860-1881.

10. Paul J. Biermann and Joan H. Cranmer, "End-of-Cure Sensing Using Ultrasonics for Autoclave Fabrication of Composites", *Proceeding of Society of Photo-Optical Instrumentation Engineers (SPIE)*, 2948 (1996), pp. 72 – 83.

11. M. Rath, J. Döring, W. Stark, G. Hinrichsen, "Process Monitoring of Moulding Compounds by Ultrasonic Measurements in a Compression Mould", *NDT and Einternational – Non Destructive Testing and Evaluation*, 33 (2000), pp. 123 – 130.

12. T. Saliba, S. Saliba, J. Lanzafame, and L. Gudeman, "In-Situ Cure Monitoring of Advanced Composite Materials", *Proceeding of International SAMPE Symposium and Exhibition*, Anaheim, CA, 37 (1992), pp. 1445 – 1454.

13. J. N. Prassianakis, N. Kompoti and J. Varakis, "Curing Effects on the Acoustical Properties of Epoxy Polymers", *Experimental Mechanics*, 33 (1993), pp. 77 – 80.

14. Susan S. Saliba, Tony E. Saliba and John F. Lanzafame, "Acoustic Monitoring of Composite Materials During The Cure Cycle", *Proceeding of International SAMPE Symposium*, Covina, CA, 34 (1989), pp. 397 – 406.

15. Donald E. Yuhas and Bruce Isaacson, "Elevated Temperature Measurements of Elastic Constants in Polymer Composites", *Proceeding of International SAMPE Symposium and Exhibition*, 43 (1998), pp. 498 – 510.

16. M. Frigione and A. Maffezzoli, "Nondestructive and In-Situ Monitoring of Mechanical Property Buildup in Epoxy Adhesive for Civil Application by Propagation of Ultrasonic Waves", *Polymer Engineering and Science*, 40(3) (2000), pp. 656 – 664.

17. Edward R. Kolesor, "Dielectric Measurements for Monitoring the Cure of Epoxies and Composite Materials", *Comprehensive Composite Materials*, 5 (2000). Editors: Leif Carlsson, Robert L. Crane, Kenji Uchino.

18. J. Mijović, J. M. Kenny, A. Maffezzoli, A. Trivisano, F. Bellucci, and L. Nicolais, "The Principles of Dielectric Measurements for In Situ Monitoring of Composite Processing", *Composites Science and Technology*, 49 (1993), pp. 277 – 290.

19. A. Wall, *Technical Notes and Operation Manual of EUMETRIC Software*, Micromet Instruments, Inc. (1999).

20. David R. Day, "Degree of Cure in 3501-6 Epoxy Graphite: a Comparison of Dielectric Cure Index With Model Predictions", *Proceeding of International SAMPE Symposium and Exhibition*, Anaheim, CA, 35 (1990), pp. 2289 – 2297.

21. D. Day, D. D. Shepard and A. S. Wall, "The Determination of Glass Transition Temperature During Real Time Cure", *Proceeding of Technical Sessions of 43rd Annual Conference, Composite Institute*, Cincinnati, OH, (1988), pp. 11D.1 – 11D.4.

22. D. R. Day, D. D. Shepard, and Kelly J. Craven, "In-Process Endpoint Determination of Hercules 3501-6", *Proceeding of International SAMPE Symposium and Exhibition*, Covina, CA, 36(1) (1991), pp. 571 – 581.

23. D. Abraham and R. Mcllhagger, "Glass Fiber Epoxy Composite Cure Monitoring Using Parallel Plate Dielectric Analysis in Comparison with Thermal and Mechanical Testing Techniques", *Composites* – Part A, 29A (1998), pp. 811 – 819.

24. F. Stèphan, A. Fit, and X. Duteurtre, "In-Process Control of Epoxy Composite by Microdielectrometric Analysis", *Polymer Engineering and Science*, 37(2) (1997), pp. 436 – 448.

25. G. M. Maistros and I. K. Partridge, "Dielectric Monitoring of Cure in a Commercial Carbon-Fiber Composite", *Composites Science and Technology*, 53 (1995), pp. 355 – 359.

26. G. M. Maristros and C. B. Bucknall, "Modeling the Dielectric Behavior of Epoxy Resin Blends During Curing", *Polymer Engineering and Science*, 34(20) (1994), pp. 1517 – 1528.

27. A. Ajji, P. Sammut, M. M. Dumoulin, E. Bellefleur and L. Boutin, " Simultaneous Dielectrometry and Rheology of Model Epoxy Resins", *Proceeding of Annual Technical Conference ANTEC 94*, San Francisco, CA, Part 1 (1994), pp. 918 – 922.

28. J. O. Simpson and S. A. Bidstrup, "Modeling Conductivity and Viscosity Changes during Epoxy Cure Using DEA, DMA and DSC", *Polymeric Materials Science and Engineering, Proceedings of the ACS Division of Polymeric Materials Science and Engineering*, Chicago, IL, 69 (1993), pp. 451 – 452.

29. J. Jow, M. C. Hawley, M. Finzel, and T. Kern, "Dielectric Analysis of Epoxy/Smine Resins Using Microwave Cavity Technique", *Polymer Engineering and Science*, 28(22) (1988), pp. 1450 – 1454.

30. S. Carrozzino and G. Levita, "Calorimetric and Microwave Dielectric Monitoring of Epoxy Resin Cure", *Polymer Engineering and Science*, 30(6) (1990), pp. 366 – 373.

31. N. Mrad, "Fiber Optic Sensor Technology: Technology Introduction and Evaluation", *Report - LTR-ST-2260 of Institute for Aerospace Research*, NRC, Ottawa, (2000).

32. J. Chen, A. Johnston, N. Mrad, and L. Petrescue, "On-Line Resin Flow and Cure Monitoring in Liquid Composites Moulding", *Report - LTR-SMPL-2002-0015 of Institute for Aerospace Research*, NRC, Ottawa, (2002).

33. K. T. Slattery, K. Corona-Bittick, and D. J. Dorr, "Composite Cure Monitoring With Bragg Grating Sensors", *Proceedings of The International Society for Optical Engineering*, San Antonio, TX, 3399 (1998), pp. 114 – 121.

34. C. M. Lawrence, D. V. Nelson, J. R. Spingarn, and T. E. Bennett, "Measurement of Process-induced Strains in Composite Materials Using Embedded Fiber Optic Sensors", *Proceedings of The International Society for Optical Engineering*, San Diego, CA, 2718 (1996), pp. 60 – 68.

35. J. S. Leng and A. Asundi, "Real-time Cure Monitoring of Smart Composite Materials Using Extrinsic Fabry-Perot Interferometer and Fiber Bragg Grating Sensors", *Smart Mater. Struct.*, 11 (2002), pp. 249 – 255.

36. V. Dewynter-Marty and P. Ferdinand, "Embedded Fiber Bragg Grating Sensors for Industrial Composite Cure Monitoring", *Journal of Intelligent Material Systems and Structures*, 9 (1998), pp. 785 – 787.

37. H. Kang, D. Kang, H. Bang, C. Hong, and C. Kim, "Cure Monitoring of Composite Laminates Using Fiber Optic Sensors", *Smart Materials and Structures*, 11 (2002), pp. 279 – 287.

38. M. G. Xu, J. –L. Archambault, L. Reekie, and J. P. Dakin, "Discrimination between strain and Temperature Effects Using Dual-Wavelength Fiber Grating Sensors", *Electronics Letters*, 30(13) (1994), pp. 1085 – 1087.

39. B. Guan, H. Tam, H. L. W. Chan, C. Choy, and M. S. Demokan, "Discrimination Between Strain and Temperature With a Single Fiber Bragg Grating", *Microwave and Optical Technology Letters*, 33 (2002), pp. 200 – 202.

40. P. Sivanesan, J. Sirkis, V. Venkat, Y. Shi, C. J. Reddy, S. Sankaran, and H. Singh, "Simultaneous Measurement of Temperature and Strain Using a Single Bragg Grating", *Proceedings of the Smart Structures and Materials*, Newport Beach, CA, 3670 (1999), pp. 92 – 103.

41. C. M. Lawrence and D. V. Nelson, "An Embedded Fiber Optic Sensor Method for Determining Residual Stress in Fiber-Reinforced Composite Materials", *Journal of Intelligent Material Systems and Structures*, 9 (1999), pp. 788 –799.

42. M. J. O'Dwyer, G. M. Maistros, S. W. James, R. P. Tatam and I. K. Partridge, "Relating the State of Cure to the Real-time Internal Strain Development in a Curing Composite Using In-fiber Bragg Gratings and Dielectric Sensors", *Measurement Science and Technology*, 9(8) (1998), pp. 1153 – 1158.

43. D. D. Shepard, K. R. Smith and L. H. Thibodeau, "A Comparison of Dielectric and Ultrasonic Cure Monitoring of Advanced Composites", *Technical Notes of Micromet Instruments, Inc.*

44. J. –Y. Chen, S. V. Hoa, C. K. Jen and H. Wang, "In-situ Monitoring of Graphite/Epoxy Cure Using Optical Fiber and Ultrasonic Sensors", *Proceeding of 12th Technical Conference of the American Society for Composite*, Dearborn, Michigan, (1997), pp. 872 – 881.

45. Chailleux E., Salvia M., Jaffrezic-Renault N., Jayet Y., Maazouz A., Seytre G. and Kasik I., "Process Monitoring of Composites Using Multidetection Techniques", *Proceeding of the SPIE – The International Society for Optical Engineering*, Newport Beach, CA, 4336 (2001), pp. 204 – 210.

46. M. –T. Ton-That, K. C. Cole, C. –K. Jen and D. R. Franca, "Polyester Cure Monitoring by Means of Different Techniques", *Polymer Composite*, 21(4) (2000), pp. 605 – 618.

47. J. David N. Cheeke, *Fundamentals and Applications of Ultrasonic Waves*, CRC Press LLC (2002).

48. William D. Callister, JR., *Materials Science and Engineering, An Introduction*, fourth edition, John Wiley & Sons, Inc. (1997).

49. M. A. Balachander, *On prediction of creep in multidirectional polymer composites*, MSc. Thesis, University of Manitoba, (2001).

50. David R. Day, "Cure Control: Strategies for Using Dielectric Sensors", *Review of Progress in Quantitative Nondestructive Evaluation*, 7B (1988), pp. 1573 – 1579.

51. G. P. Carman and G. P. Sendeckyj, "Review of the Mechanics of Embedded Optical Sensors", *Journal of Composites Technology and Research*, 17 (1995), pp. 183 – 193.

APPENDIX A

THEORY OF OPERATIONAL PRINCIPLES FOR VARIOUS SENSORS

A.1 Ultrasonic Sensors

A.1.1 Frequency, Period, Wavelength and Velocity of Ultrasonic Wave

Unlike light waves, ultrasonic waves cannot travel in vacuum (empty space). There must be a certain medium, such as a solid, liquid and a gas to support the sound waves. The relation between the period (T) and the frequency (f) of ultrasonic waves is:

$$f = \frac{1}{T} \tag{A.1}$$

The velocity of the ultrasonic wave in a solid is related to the type of the wave, the density and elastic constants of the solid. The velocity (c) in a solid at a given temperature and pressure is constant. The relation between c, f, λ, and T are

$$\lambda = \frac{c}{f} \text{ and } \lambda = cT \tag{A.2}$$

A.1.2 Types of Ultrasonic Waves

Longitudinal Waves

An ultrasonic wave is called a longitudinal wave when the particle motion of the medium is along the direction of propagation of the wave, as shown in Figure A.1. It is also called a pressure or compression wave because compressional and dilatational forces are active in it. It is also known as a density wave because the particle density of the medium fluctuates as waves propagate. Longitudinal waves can propagate in any kinds of media,

including solids, liquids and gases. It is the most important and commonly used wave in ultrasonic testing.

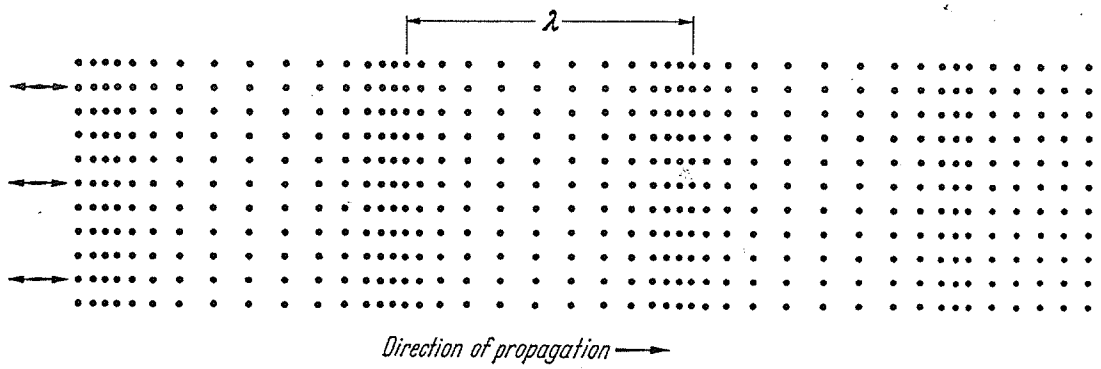

Figure A.1 Longitudinal wave (6)

Transverse Waves

Transverse wave is a wave in which the particle oscillation is perpendicular to the direction of the propagation, as shown in Figure A.2. The direction of the particle oscillation is the direction of polarization, and the plane determined by the particle oscillation direction and wave propagation direction is the plane of polarization. Transverse waves can only be propagated in the media where there is shear elasticity. That is, it can only propagate in solids. The transverse wave is more important in testing of anisotropic media, such as fiber reinforced composites.

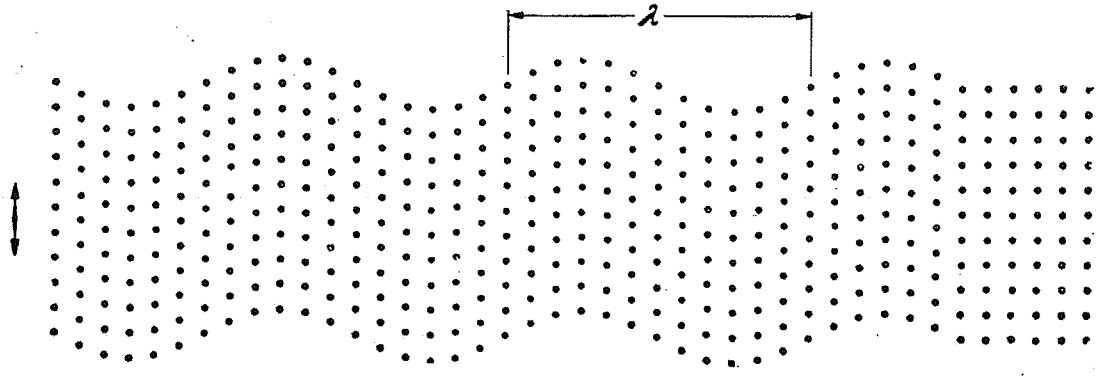

Figure A.2 Transverse wave (6)

There are other types of waves that are more specialized, and not very commonly used in ultrasonic monitoring of curing of composites, such as surface waves and Lamb waves, which will not be discussed here.

A.1.3 Attenuation of Ultrasonic Waves

Ultrasonic wave will continuously lose energy due to internal friction and scattering from the microscopic grain interfaces within the material during its propagation. Hence, the sound pressure will decrease exponentially with distance, and the attenuation can be expressed as

$$p = p_0 e^{-\tau_p d} \tag{A.3}$$

where p_0 is the sound pressure at distance $d = 0$, p is the sound pressure at distance d and τ_p is the attenuation coefficient. It can also be expressed in the form of intensity:

$$I = I_0 e^{-\tau d} \tag{A.4}$$

The attenuation coefficient is related to the properties of the medium and the frequency of the ultrasonic wave. At lower frequencies, the attenuation is mainly caused by internal friction. At higher frequencies, the wavelength is close to the grain size of the material. The sound wave is partially reflected at each grain interface in all directions because of the irregular shape of the grains. More details about ultrasonic attenuation can be found in 2.2.1.

A.1.4 Acoustic Impedance

The acoustic impedance of the medium in which the ultrasonic waves are traveling is defined as a ratio of:

Z_{ac} = sound pressure/volume velocity (A.5)

The volume velocity is the velocity imparted on the particles of the medium by the sound wave multiplied by the area over which the pressure is considered to be acting. Another commonly used expression is the one for the characteristic impedance or the acoustic resistance:

$$Z = \rho c \tag{A.6}$$

where ρ is the density of the medium and c is the sound velocity.

The characteristic impedance is related to the dissipation of energy. It can be seen from the equation for solids, there are several values of impedance Z, corresponding to the types of the waves propagating in the media, e.g. longitudinal waves, transverse waves etc. Because liquids and gases can only support longitudinal waves, there is only one Z value corresponding to longitudinal waves.

A.1.5 Reflection and Transmission of Ultrasonic Waves at a Boundary

Normal incidence

When an ultrasonic wave is incident normally to the smooth boundary between two media, part of its energy will be reflected back and part will be transmitted across the boundary along the same direction as the incident wave. As required by the law of conservation of energy, the energy is balanced along the incident wave, the reflected wave, and the transmitted wave.

$$J_e = J_r + J_d \tag{A.7}$$

where J_e is the incident wave energy, J_r is the reflected wave energy and J_d is the transmitted wave energy.

Effects of a boundary on ultrasonic can be expressed in terms of sound pressure. Consider a wave incident on the boundary between two medias as shown in Figure A.3. Let p_e, p_r and p_d be pressure of incident, reflected and refracted waves respectively; ρ_1 and c_1 be the density of and sound velocity in material 1, ρ_2 and c_2 be the density of and sound velocity in material 2. Then R and D are the coefficients of reflection and transmission, respectively, can be defined as

$$R = \frac{p_r}{p_e} = \frac{Z_2 - Z_1}{Z_2 + Z_1} = \frac{\rho_2 c_2 - \rho_1 c_1}{\rho_2 c_2 + \rho_1 c_1} \tag{A.8}$$

$$D = \frac{p_d}{p_e} = \frac{2Z_2}{Z_2 + Z_1} = \frac{2\rho_2 c_2}{\rho_2 c_2 + \rho_1 c_1} \tag{A.9}$$

Both of them are dimensionless numerical values.

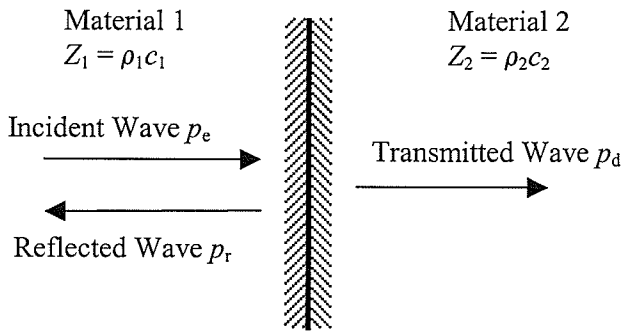

Figure A.3 Reflection and transmission of ultrasonic waves at a boundary

When $Z_2 > Z_1$, the sound pressure of the reflected wave has the same sign as that of the incident wave. If $Z_2 < Z_1$, there will be a 180° phase shift. It can be seen from the equation that the reflection coefficient is large when the ultrasonic wave passes from a medium with larger impedance to the medium with smaller impedance (e.g. the sound wave travels from a solid or liquid to a gas), and vice versa. For example, in the case that sound

wave travels from water to steel at normal incidence, $R = 0.935$, $D = 1.94$. If the sound wave travels from steel to water, $R = -0.935$ and $D = 0.061$.

Generally, if there is a significant difference between the impedance of the two mediums, complete reflection will occur at the boundary. Ultrasonic couplants are used at the interface of ultrasonic transducer and the material under test in order to fill in any air gaps to ensure that maximum energy can be transmitted in to the material.

Oblique Incidence

It is very common to encounter the situation where the sound wave strikes the boundary obliquely at an angle of α_e. Longitudinal or transverse waves are reflected and refracted (transmitted) at the boundary between two different materials as in optics, as shown in Figure A.4. The angles of the reflected wave α_r and refracted wave α_d depend on the angle of incident wave α_e and the velocity of the waves in two materials. The directions of the reflected and refracted waves are determined by the Snell's law of refraction:

$$\frac{\sin\alpha_I}{\sin\alpha_{II}} = \frac{c_I}{c_{II}} \quad \text{or} \tag{A.10}$$

$$\frac{c_1}{\sin\alpha_e} = \frac{c_2}{\sin\alpha_d} = \frac{c_1}{\sin\alpha_r} \tag{A.11}$$

The equation is applicable to the longitudinal, transverse and surface waves.

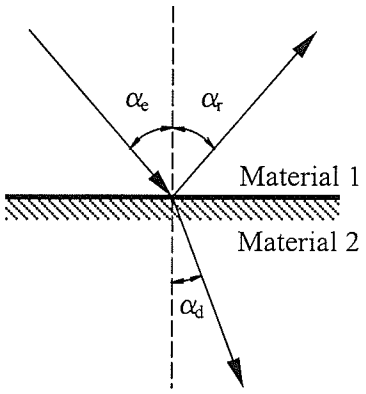

Figure A.4 Reflection and transmission of an ultrasonic wave at oblique incidence

The incident wave may be converted into another mode of vibration after reflection or refraction occurs, i.e. mode conversion. For example, a longitudinal wave traveling into a solid medium at certain incident angle would generate a refracted longitudinal wave and a refracted transverse wave. Here, the general law of refraction is again applicable. Mode conversion can also happen to the reflected wave.

A.1.6 Generation of Ultrasonic Waves

There are several methods to generate ultrasonic waves, such as the piezoelectric effect, mechanical shock, thermal shock, electrostatic effects, and electrodynamic effects. The most commonly used method in NDE applications is the piezoelectric effect.

If a mechanical stress is applied to a piezoelectric material, electric charges will be generated at its surfaces. This is the direct piezoelectric effect, which is used for detecting and measuring the ultrasonic wave. Alternatively, when a voltage is applied across a piezoelectric material, a mechanical strain will be generated. This is the inverse

piezoelectric effect and it is used for the generation of ultrasonic waves. It is a linear relation between the applied voltage and the strain, up to a few thousand volts.

All piezoelectric materials are crystalline in nature. The most commonly used material in ultrasonic transducers is lead zirconate-titanate (PZT) known for its stability, good electrical properties and lower production cost. The material has the piezoelectric effect because of asymmetrical crystal structure. By cutting a piezoelectric quartz crystal in different orientations (axes), longitudinal and transverse waves can be generated. The frequency of oscillations (the frequency of the transducer) is dependant on the input signal (input voltage). However, it is necessary to optimize the thickness of the cut crystal plate for a given frequency. Due to the Poisson's ratio effect, there will always have unwanted longitudinal, transverse or surface waves generated along with the required longitudinal or transverse wave, either along the same direction or in other directions. Whether or not these by-product waves can be ignored in an application should be considered carefully.

A.2 Dielectric Sensors

A.2.1 Classic Debye Equations of Dielectric Response

Dielectric measurement is performed by placing the dielectric materials between the two electrically conducting parallel plates (electrodes), applying a time-varying voltage $v(t)$ between the electrodes, and measuring the response current $i(t)$ and the phase difference between $v(t)$ and $i(t)$.

The dipole polarization and ion migration are the most important response of a dielectric material. Electrode polarization is always occurred during the curing of the polymers. The dipole and ionic contribution can be modeled as a circuit illustrated in Figure A.5.

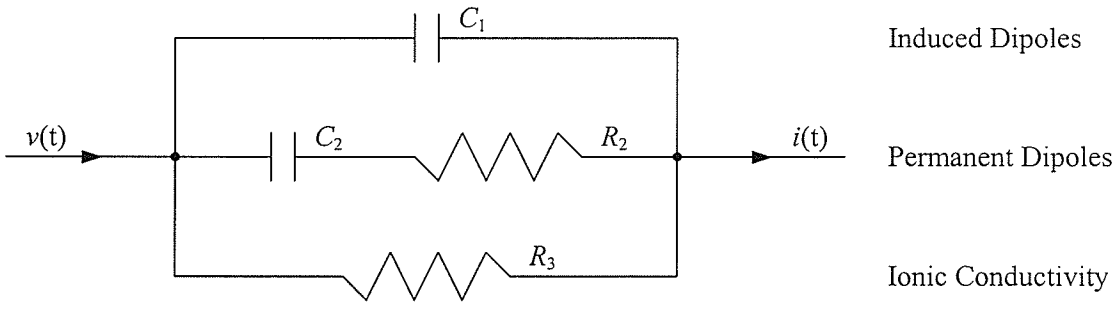

Figure A.5 Model of a polymeric material under test (19)

Because of the frequency independent nature of the induced dipoles, they are modeled as a capacitor C_1 in the circuit. The permanent dipoles are modeled as a capacitor C_2 in series with a resistor R_2 due to their frequency dependent. The capacitor is fully charged at low frequencies. At high frequencies, C_2 is almost not charged due to the current limiting resistor R_2. The relaxation time τ is the product of C_2R_2. The ionic conduction contribution to the dielectric response is modeled as a parallel resistor R_3.

To simplify the modeling of dielectric response, the dielectric measurement will deal with the circuit as a capacitor in parallel with a resistor, with the excitation sinusoidal voltage $v(t)$ with an angular frequency ω, the corresponding output sinusoidal current $i(t)$. At each frequency, the electrical admittance, $Y(\omega)$, can be expressed as:

$$Y(\varpi) = \frac{I}{V} \tag{A.12}$$

where V and I are the complex amplitudes of $v(t)$ and $i(t)$, respectively.

There will be a phase difference θ of the output current from the input signal, when polymeric materials exhibit both time dependent dipole polarization and conduction effects.

$$v(t) = V_0 \cos(\varpi t) \tag{A.13}$$

$$i(t) = I_0 \cos(\varpi t + \theta) \tag{A.14}$$

V_0 and I_0 are the amplitudes of $v(t)$ and $i(t)$. Expressing the above equations in complex form format, i.e.

$$v(t) = \mathrm{Re}\{Ve^{j\varpi t}\} \tag{A.15}$$

$$i(t) = \mathrm{Re}\{Ie^{j\varpi t}\} \tag{A.16}$$

and $V = V_0$, $I = I_0 e^{j\theta}$. (A.17), (A.18)

Thus the admittance becomes

$$Y(\varpi) = \frac{1}{Z(\varpi)} = j\varpi C(\varpi) + \frac{1}{R(\varpi)} = j\varpi C_1 + \frac{1}{R2 + \dfrac{1}{j\varpi C_2}} + \frac{1}{R_3} \tag{A.19}$$

where $C(\varpi) = \dfrac{I_0 \sin\theta}{\varpi V_0}$, $R(\varpi) = \dfrac{V_0}{I_0 \cos\theta}$ (A.20), (A.21)

Substitute that $C_2 R_2 = \tau$, the admittance becomes (A.22)

$$Y(\varpi) = j\varpi C_1 + \frac{j\varpi C_2 + \varpi^2 \tau C_2}{1 + (\varpi\tau)^2} + \frac{1}{R_3} \tag{A.23}$$

Define a general dielectric permittivity function ϵ^*, which has both of the real and imaginary components, corresponding to the capacitive and conductive contributions, i.e.

$$\varepsilon^* = \varepsilon' - j\varepsilon'' \tag{A.24}$$

The admittance becomes

$$Y(\varpi) = j\varpi C^* = j\varpi C_o(\varepsilon' - j\varepsilon'')$$

$$= j\varpi C_o\varepsilon' + \varpi C_o\varepsilon'' \tag{A.25}$$

where C^* is the complex capacitance

C_o is the capacitance of the free space

ϵ' is the permittivity (or dielectric constant) of the material under test

ϵ'' is the loss factor of the material under test

Separate the real and imaginary parts of the admittance equation yield:

$$j\varpi C_o\varepsilon' = j\varpi C_1 + \frac{j\varpi C_2}{1+(\varpi\tau)^2} \tag{A.26}$$

$$\varpi C_o\varepsilon'' = \frac{\varpi^2\tau C_2}{1+(\varpi\tau)^2} + \frac{1}{R_3} \tag{A.27}$$

Hence, the permittivity and the loss factors are:

$$\varepsilon' = \frac{C_1}{C_o} + \frac{j\varpi C_2}{C_o(1+(\varpi\tau)^2)} \tag{A.28}$$

$$\varepsilon'' = \frac{\varpi\tau C_2}{C_o(1+(\varpi\tau)^2)} + \frac{1}{\varpi C_o R_3} \tag{A.29}$$

The expressions for the capacitance are

$$C_o = \frac{\varepsilon_o A}{d} \tag{A.30}$$

$$C^* = \varepsilon^* C_o = \frac{\varepsilon^*\varepsilon_o A}{d} \tag{A.31}$$

Hence

$$\varepsilon^* = \frac{C^*}{C_o} \tag{A.32}$$

where ϵ_o is the permittivity of the free space

ϵ^* is the complex permittivity of the material under test

A is the area of parallel plate electrode

D is the separation of parallel plate electrodes

Combine the above equations, the permittivity and loss factor can be expressed as:

$$\varepsilon' = \varepsilon_1 + \frac{\varepsilon_2}{1+(\varpi\tau)^2} \tag{A.33}$$

$$\varepsilon'' = \frac{D}{\varpi\varepsilon_o AR} + \frac{\varepsilon_2\varpi\tau}{1+(\varpi\tau)^2} = \frac{\sigma}{\varpi\varepsilon_o} + \frac{\varepsilon_2\varpi\tau}{1+(\varpi\tau)^2} \tag{A.34}$$

where $\sigma = \frac{D}{AR} = \frac{1}{G(\varpi)}$ is the bulk ionic conductivity. $G(\omega)$ is the frequency dependent conductance and σ is the dielectric material's conductivity ($ohm^{-1}m^{-1}$). (A.35)

In the dielectric measurement, when the polymeric system is under high (infinite) frequencies, the permanent dipoles and ions are not able to respond to the varying electric field in such short time interval, only the induced dipoles will have contribution to the dielectric permittivity. The induced dipole polarization provides the background values (the base line) for dielectric monitoring. Therefore the unrelaxed permittivity is:

$$\varepsilon_\infty = \varepsilon_1 \tag{A.36}$$

At low scanning frequencies, there is sufficiently long time for dipole reorientation. The system will reach a maximum permittivity value, termed as relaxed permittivity. Both the induced dipoles and permanent dipoles contribute to the relaxed permittivity:

$$\varepsilon_s = \varepsilon_1 + \varepsilon_2 \tag{A.37}$$

Combine the above two equations, there is

$$\varepsilon_2 = \varepsilon_s - \varepsilon_1 = \varepsilon_s - \varepsilon_\infty \tag{A.38}$$

Substituting ϵ_2 into equation, the permittivity and loss factor can be expressed as:

$$\varepsilon' = \varepsilon_\infty + \frac{\varepsilon_s - \varepsilon_\infty}{1 + (\varpi\tau)^2} \tag{A.39}$$

$$\varepsilon'' = \frac{\sigma}{\varpi\varepsilon_o} + \frac{(\varepsilon_s - \varepsilon_\infty)\varpi\tau}{1 + (\varpi\tau)^2} \tag{A.40}$$

and the loss tangent is

$$\tan\delta = \frac{\varepsilon''}{\varepsilon'} = \frac{(\varepsilon_s - \varepsilon_\infty)\varpi\tau}{\varepsilon_s + \varepsilon_\infty(\varpi\tau)^2} \tag{A.41}$$

The above equations for ϵ', ϵ'' and tan δ are the classic Debye equations of dielectric response.

As the curing process proceeded, the dielectric material changes from a liquid to a gel state, and finally becomes a solid. The dipole relaxation time will increase because of the decreased mobility of the polymeric molecules. The permittivity ϵ' and loss factor ϵ'' are functions of ω and τ, and they will change corresponding to the product of $\omega\tau$, as shown in Figure A.6.

Another commonly used representation of dielectric data is the Cole-Cole plot or the arc diagram, shown in Figure A.7, which has been discussed in 3.3.1. The plot in Figure A.7 is for ideal condition with the assumption that there is just one single dipole relaxation time (τ) for the material. In most of polymeric systems, the relaxation time will change as dipole mobility changes, which depend on molecular weight, and the

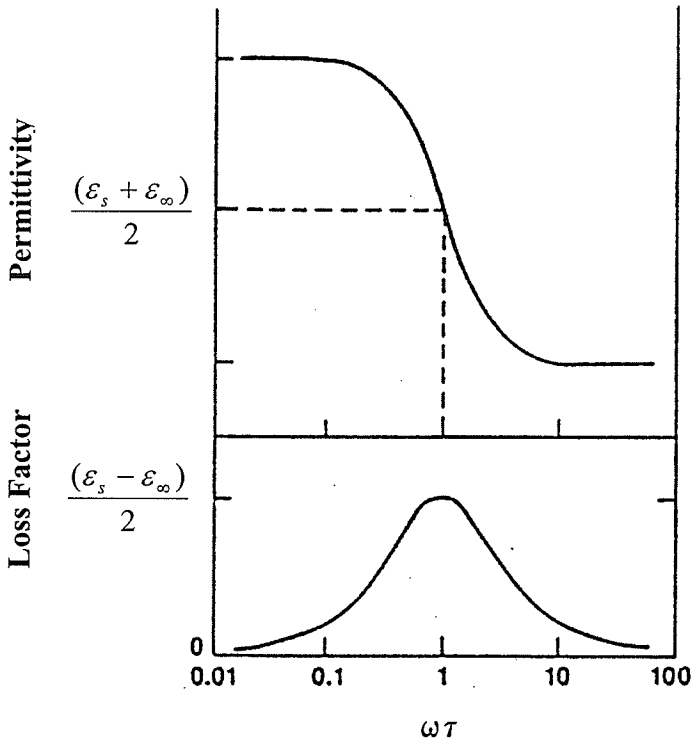

Figure A.6 The Debye response as a function of $\omega\tau$

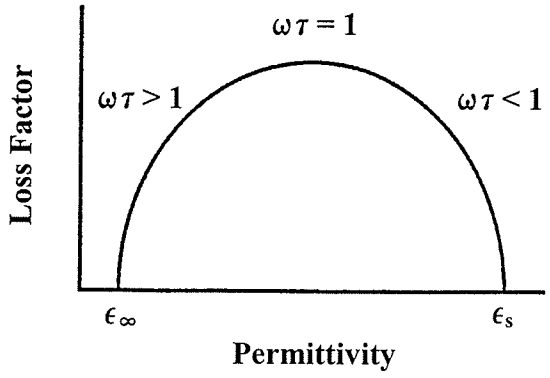

Figure A.7 The Cole – Cole plot or arc diagram

surrounding environment. A parameter β is induced to approximately model the distribution of the relaxation time τ. Thus ϵ' and ϵ'' can be expressed as:

$$\varepsilon' = \varepsilon_\infty + \frac{\varepsilon_s - \varepsilon_\infty}{1 + (\varpi\tau)^{2\beta}} \tag{A.42}$$

$$\varepsilon'' = \frac{\sigma}{\varpi\varepsilon_o} + \frac{(\varepsilon_s - \varepsilon_\infty)\varpi\tau^{\beta}}{1 + (\varpi\tau)^{2\beta}} \tag{A.43}$$

where β is between 0 and 1.

There have been a number of research done in the past on a more precise relaxation time distribution based modeling of dielectric data. Because of this distribution in the relaxation time, the Cole-Cole plot is often squashed or skewed.

A.2.2 Division of Dielectric Sensors

Dielectric sensors can be divided into surface (or fringe) measurement sensors and bulk (or through-the-part) sensors. As shown in Figure A.8, surface (fringe) measurement sensors are comprised of two planar interdigitated comb electrodes on an inert substrate. The electrode line width and the spacing between the electrodes determines approximately how far into the material the fringe field will penetrate. For example, a sensor with line width and electrode spacing of 25 microns, will measure the change in perhaps within approximately 25 microns into the material. Bulk measurement sensors are like parallel plate sensors and consist of one electrode and typically use the mold wall as the other electrode. More details about dielectric sensors used in this study can be found in 3.4.2.

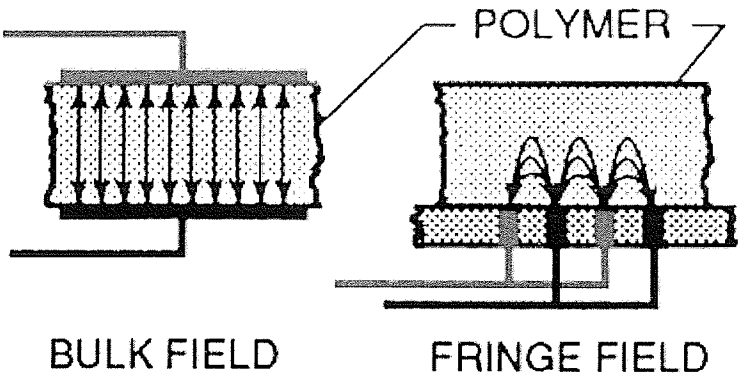

Figure A.8 Bulk and fringe measurement sensors

A.3 Optical Fiber Sensors

A.3.1 Mode of Optical Fibers

An optical fiber consists of an inner core lightwaves guide (usually made by silica), a surrounding cladding (silica), coating and a protective jacket (polymeric or metallic coating). The refractive index of the inner core n_{co} is made large than that of the cladding n_{cl}, and thus the light is kept within the core and propagated. The optic fiber can be classified as single mode and multimode. The number of modes, M, propagating inside the core is dependent on the wavelength of the incident light, the waveguide geometry and distribution of its refractive indices.

$$M = \frac{V^2}{2} = \frac{1}{2}\left[r\pi \left(\frac{2}{\lambda_0} \right) \sqrt{n_{co}^2 - n_{cl}^2} \right]^2 \tag{A.44}$$

where λ_0 is the light wavelength in vacuum

r is the fiber core radius

V is the dimensionless standardized structure constant

Three types of optical fibers are currently commonly used. They are multimode stepped index, multimode graded index and single mode stepped or graded index waveguide transmitting optical fibers. The single mode fiber has a narrow step or graded refractive index. It has a core diameter of 2 to 9 μm, and produces a sharp output pulse and essentially eliminates intermodal dispersion. Multimode graded index fibers have a core diameter of 20 to 90 μm. The multimode stepped index fiber has a homogeneous core diameter of 50 to 150 μm or greater, and a cladding with a diameter of 100 to 250 μm. The multimode stepped index fiber is the least effective transmitting medium, but also the least expensive fiber. It has higher dispersion, thus the higher traveling time and distance. Comparing the multimode stepped index fibers, the multimode graded index fibers can have transit properties with reduced drawbacks and intermediate price. Figure A.9 shows the properties of three types of fibers. The single mode and multimode stepped index fibers are the most commonly used optical fibers in sensor development and sensing applications.

A.3.2 Classification of Optical Fiber Sensors

Figure A.10 illustrates the classification of optical fiber sensors. Optical fiber sensors can be divided into two classes, the short and long gauge length optical fiber sensors. The short gauge length sensors are also referred to as point or discrete sensors. They can be used to measure the physical parameters at a distance range of several millimeters to 20 mm. The long gauge length sensors are known as distributed, spatially distributed, distributed-effect, integrating and averaging sensors. They have a gauge length of several centimeters to hundreds of meters. They can be used to measure the physical parameters

at a distance range of 40 cm to 5 m. Short gauge length sensors can be aligned to compose a quasi-distributed, multiplexed, multi-point array sensor system or a distributed sensor system.

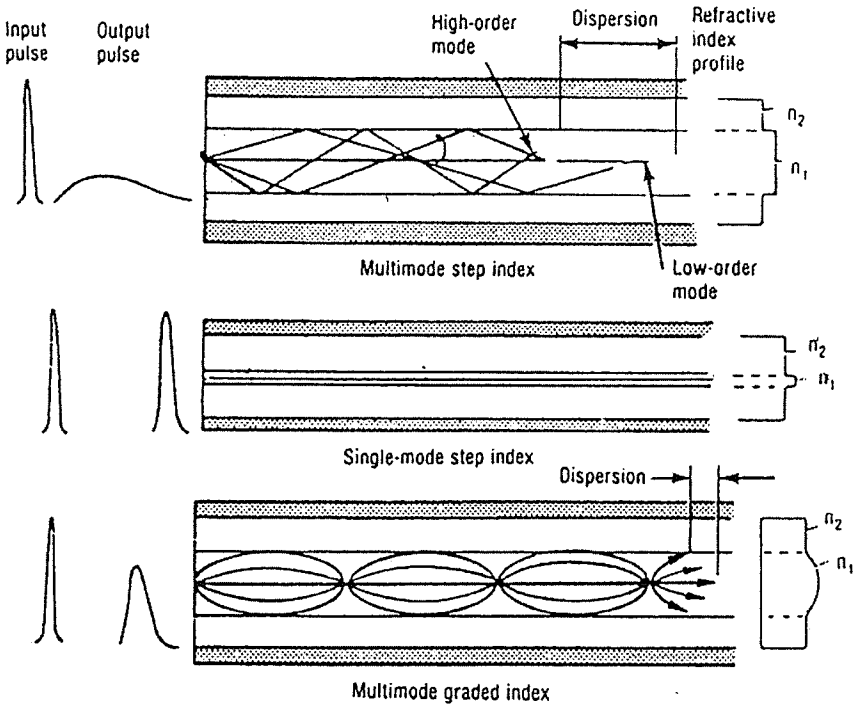

Figure A.9 Three basic types of optical fiber waveguides (31)

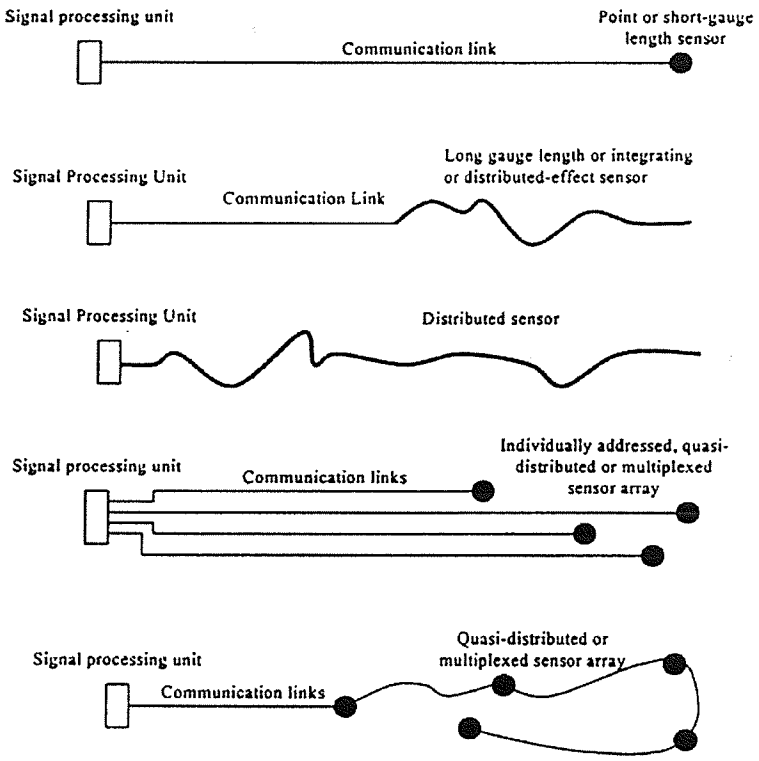

Figure A.10 Classification of optical fiber sensors (31)

A.3.3 Sensor Interrogation Techniques

Several interrogation techniques have been developed and used in fiber optic sensing systems. They are:

Optical Time-Domain Reflectometry (OTDR)

Polarization OTDR (POTDR)

Optical Frequency-Domain Reflectometry (FMCW)

Step Frequency Method (SFM)

Time Delay Multiplexing (TDM)

Wavelength Domain Multiplexing (WDM)

They have been used in structural monitoring, damage assessment, nondestructive evaluation and physical variables measurement including temperature, pressure, strain etc.

Different types of fiber optic sensors will have different sensing mechanisms, depending on the changes in the light propagation, induced by perturbations in environment, such as intensity, phase, polarization state and wavelength.

APPENDIX B

MORE INFORMATION FOR EXPERIMENTAL DETAILS

B.1 FEM Analysis Results for Processing Mold

Finite element analysis was performed to confirm that that the processing mold was capable of withstanding the applied pressure. The analysis results for the top plate and bottom plate of the mold are shown in Figure B.1 and B.2, respectively.

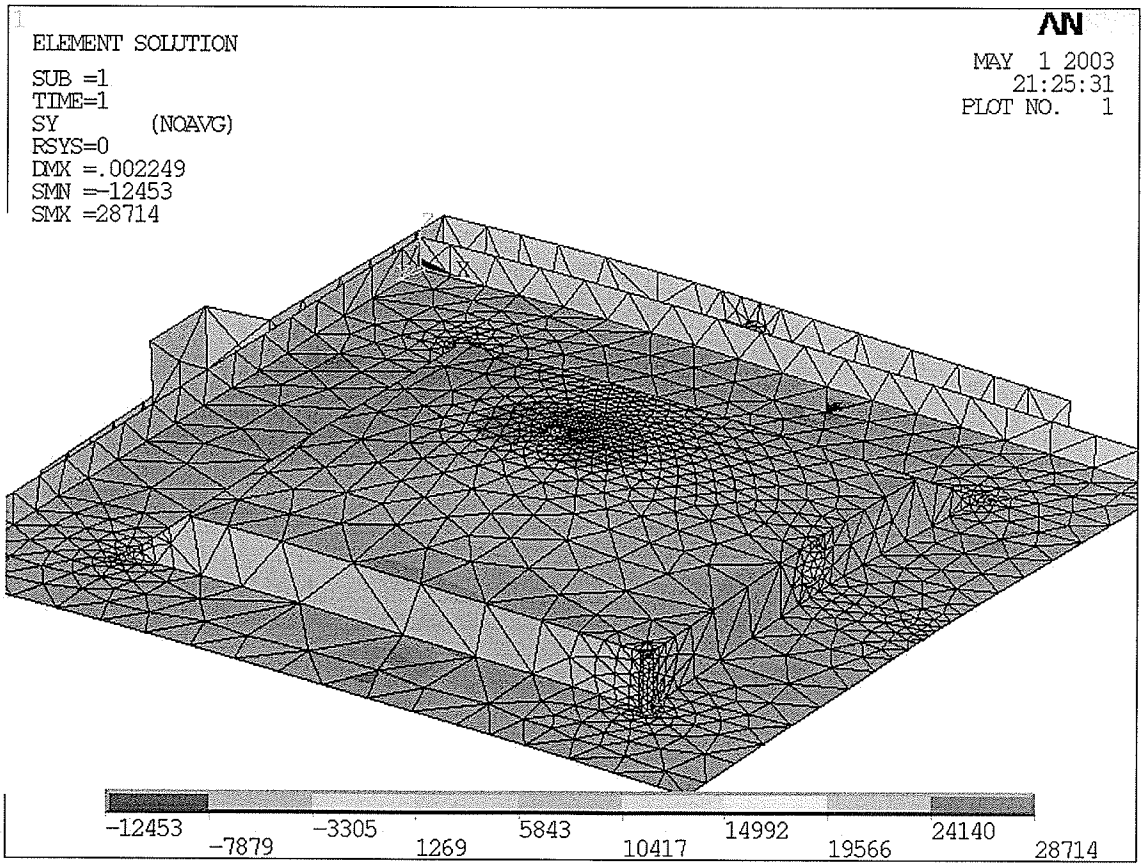

Figure B.1 FEM analysis for top plate

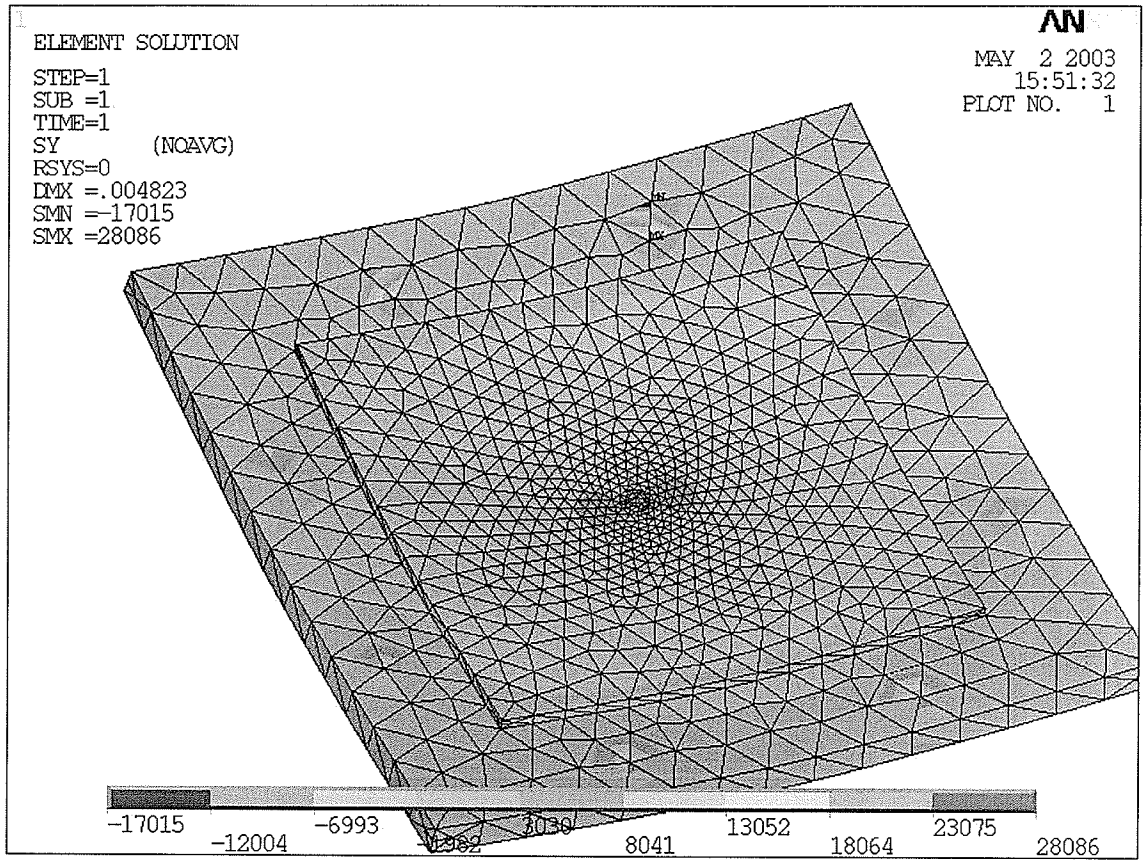

Figure B.2 FEM analysis for bottom plate

B.2 Determination of Ultrasonic Time Delay and Amplitude Using Sensing Data

B.2.1 Ultrasonic Time Delay

The ultrasonic signals were recorded in the A-Scan mode. A waveform at certain process time is shown in Figure B.3. The number of digitized sample points (pts) on the acquired analog waveform, since the generation of ultrasonic waves to the traveling of the waves through the specimen thickness direction and being reflected back from the specimen

surface, is plotted in x-axis. The ultrasonic time delay is calculated using this number of points and the sampling rate. It can be observed from the figure that the number of points at the main bang is about 31 pts, while at the 1st echo is about 127 pts. Thus the time delay can be determined using the equation:

$$\text{Time Delay} = \text{Number of Points} / \text{Sampling Rate}$$

$$= (127 - 31)\ \text{pts} / 50\ \text{MHz} = 1.92\ \mu\text{s} \qquad \text{(B.1)}$$

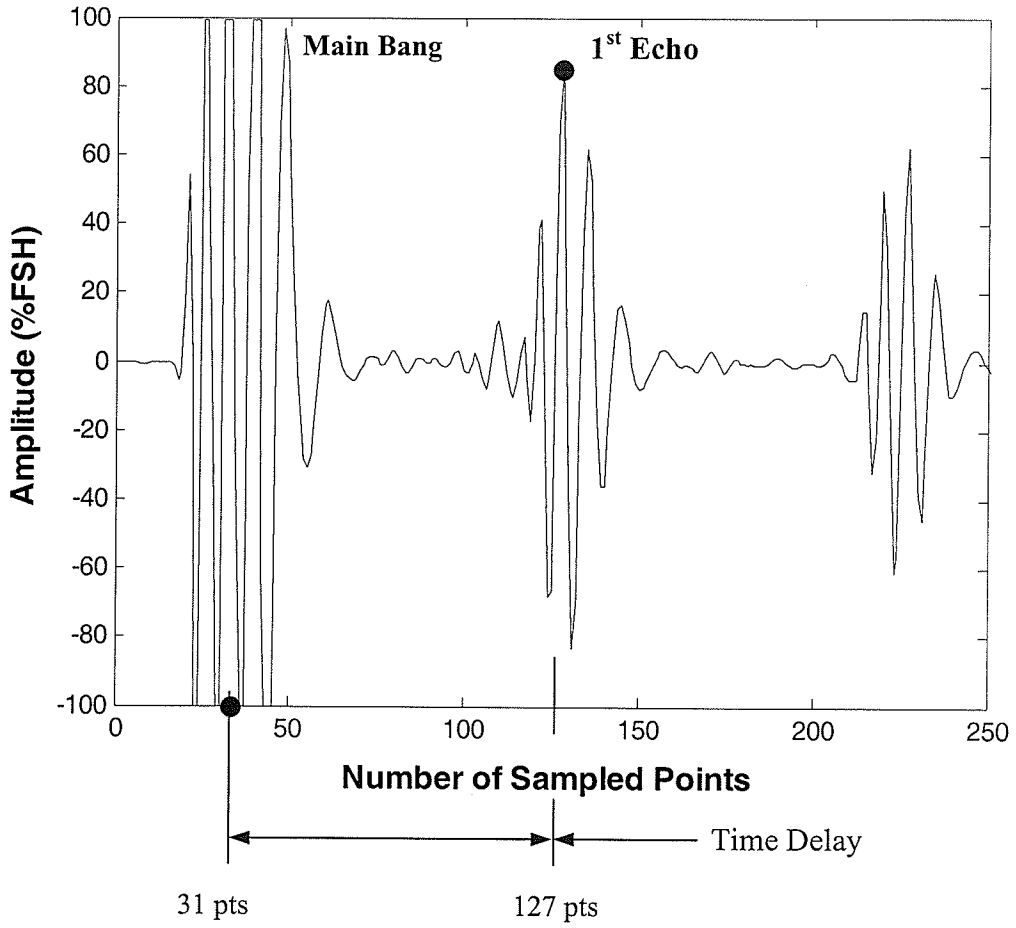

Figure B.3 Determination of ultrasonic time delay

B.2.1 Ultrasonic Amplitude

The ultrasonic waveform is displayed on a time versus voltage scale by ARIUS IV software system. The input reference voltage for the ultrasonic transducer is corresponding to a 100% FSH (Full Screen Height), which corresponds to an 8 Bit integer range of -128 to +127. The received ultrasonic signals in voltage hence can be converted into a ratio to the reference voltage thus the 100 % full screen height. Hence the amplitude of an ultrasonic wave can be displayed as a percentage of 100% full screen height. This is illustrated in Figure B.4, where the reference voltage is set as 1 V. The amplitude of the ultrasonic wave is plotted along the y-axis in Figure B.3, and is calculating the ultrasonic attenuation using equation (3.2).

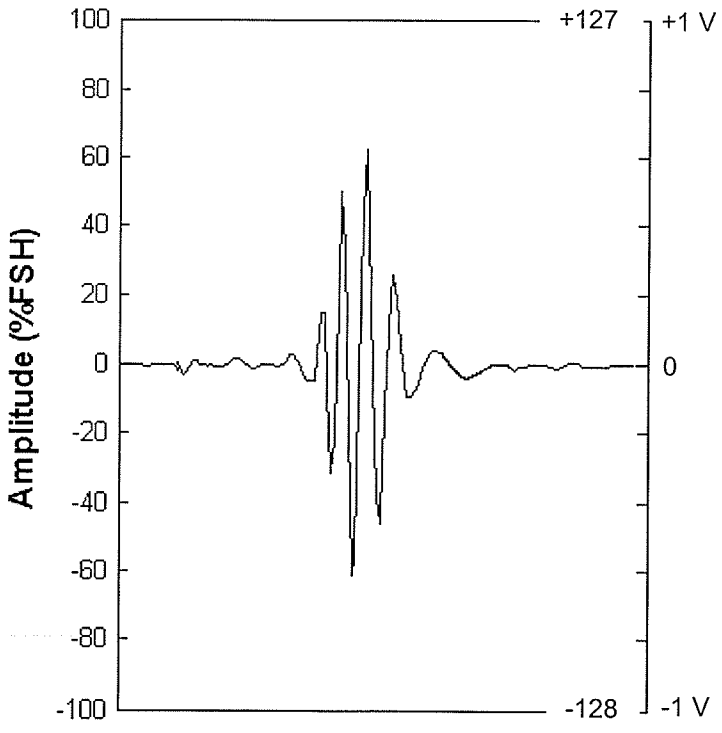

Figure B.4 Determination of ultrasonic amplitude

APPENDIX C

MORE MONITORING RESULTS

In addition to experimental results presented and discussed in Chapter 4, results obtained in other cure cycles are presented in this appendix. Various experiment and run codes used in this appendix are identified in Table 3.4.

C.1 Ultrasonic Cure Monitoring

C.1.1 Ultrasonic Response of Neat Resin Specimen

Cure Cycle 2 (R934 T-04)

The specimen was cured at 177°C for 110 minutes without postcure procedure as shown in Figure C.1. 85 psi pressure was applied at the beginning of curing, and removed after cooling.

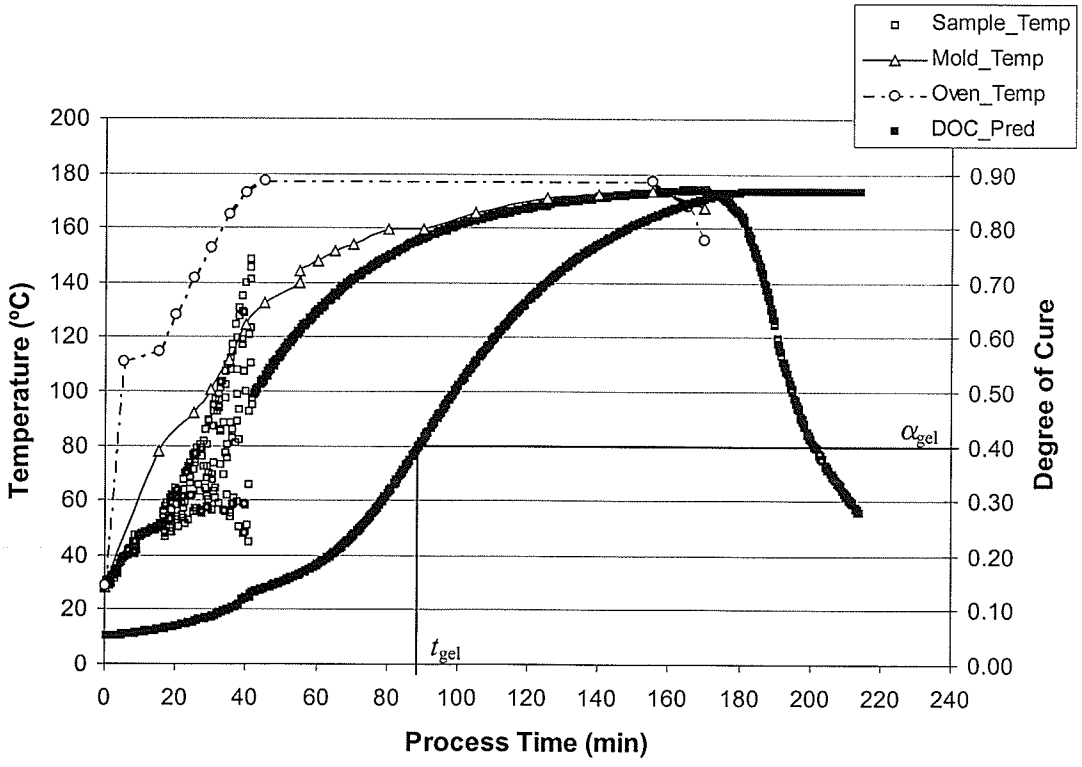

Figure C.1 Specimen temperature and predicted degree of cure for cure cycle R934 T-04

Figure C.2 shows the viscosity of the specimen, which was predicted using the model developed in reference (3). The noise in the curve is due to the noise in the temperature data. The viscosity of the resin decreased with increase in the specimen temperature until a minimum value. The time corresponding to this minimum viscosity is about t = 60 minutes. As the reaction time increased, the viscosity started to increase due to the significant curing. It took 89 minutes to gel for this imposed cure cycle.

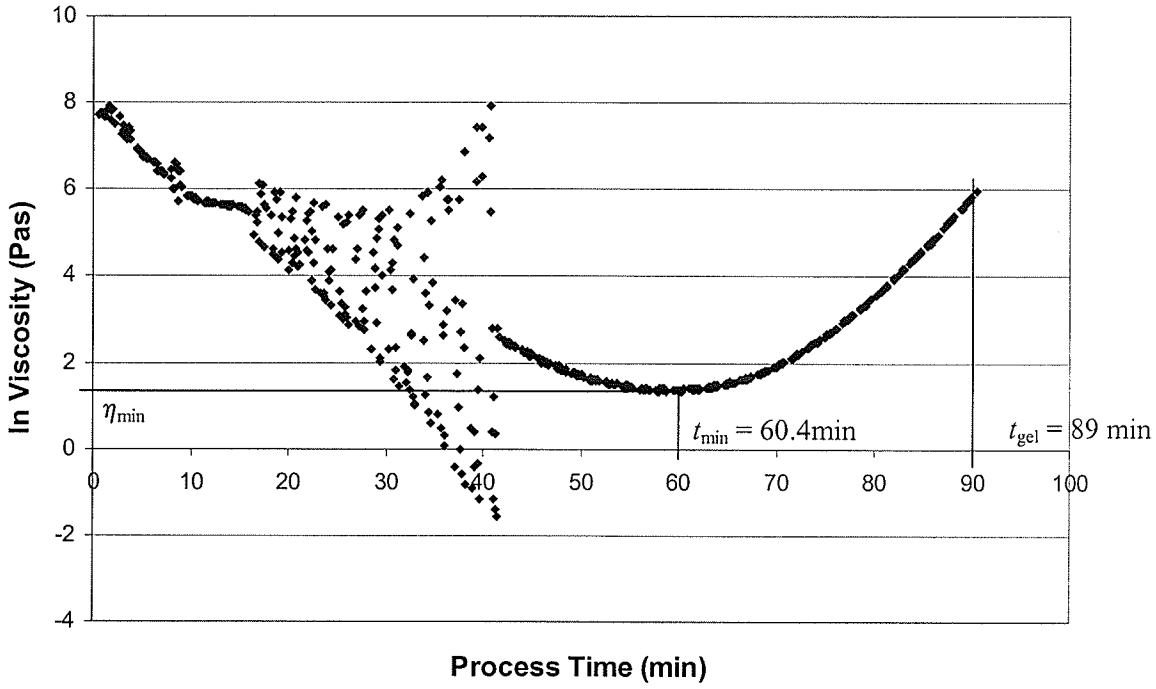

Figure C.2 Predicted viscosity for cure cycle R934 T-04

As shown in Figures C.3 and C.4, the time delay and attenuation reached their maximum and minimum values respectively at t = 42 ~ 62 minutes, while the resin reached its viscosity minimum at t = 60 minutes. When gelation occurred at t = 89 minutes, the time delay curve approached its inflection point and the attenuation started to increase sharply. A gap in the time delay and attenuation data just after gelation corresponded to the process time period of t = 95 to 115 minutes where the ultrasonic signals became too

weak to detect. Both the time delay and attenuation data did not reach a plateau value, implying that the resin did not reached its end of cure state. The second peak in attenuation was observed at $t = 128$ minutes.

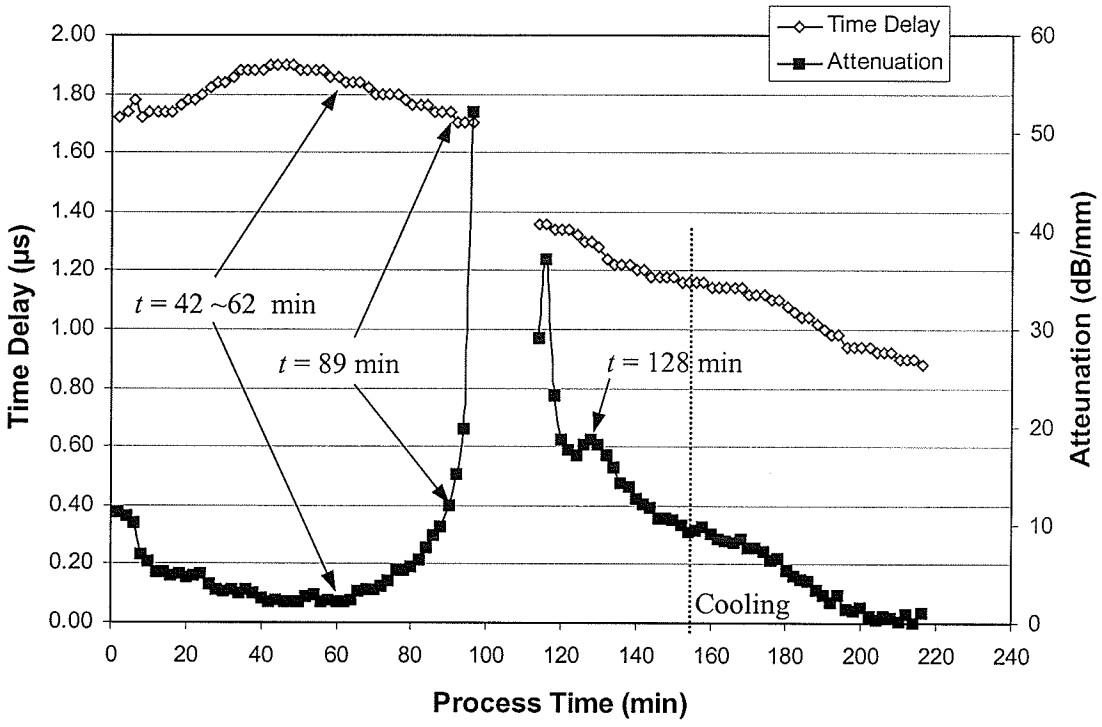

Figure C.3 Time delay and attenuation obtained for the resin specimen in cycle R934 T-04

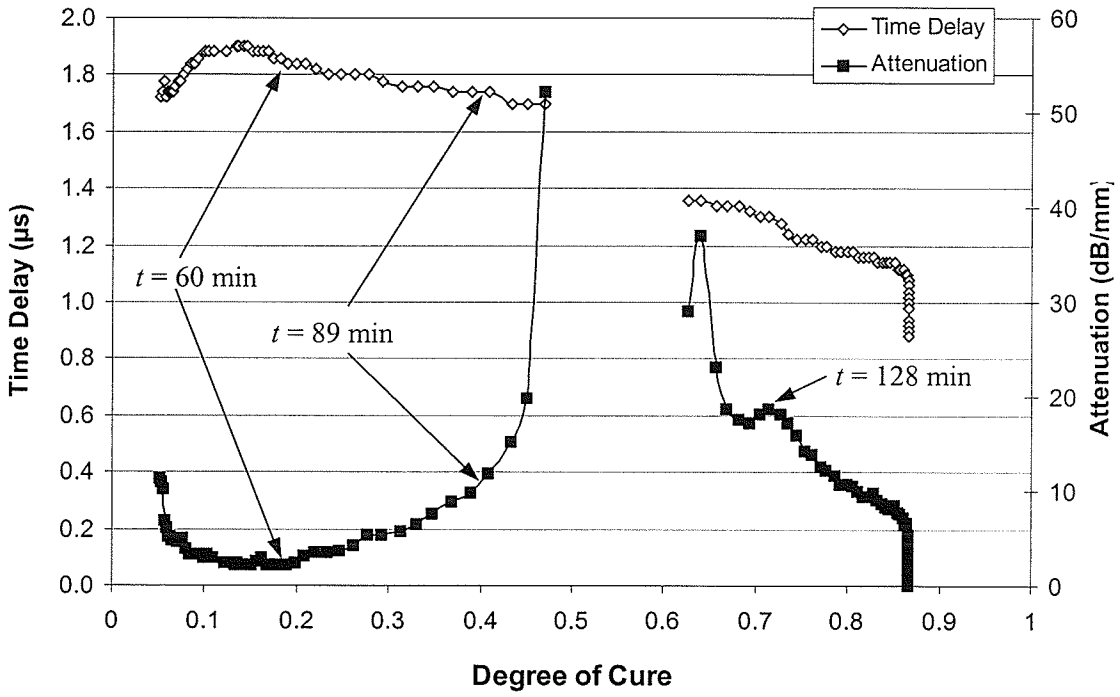

Figure C.4 Time delay and attenuation vs. DOC for the resin specimen in cycle R934 T-04

Figure C.5 shows the time delay of the echo reflected from the buffer rod/specimen interface (main bang) as a function of cure temperature. Due to the thermal expansion of the buffer rod, the main bang shifted with the change of the cure temperature. This information might be used to evaluate the temperature of the tool and processed materials during processing. However, the calibration work for this purpose is required.

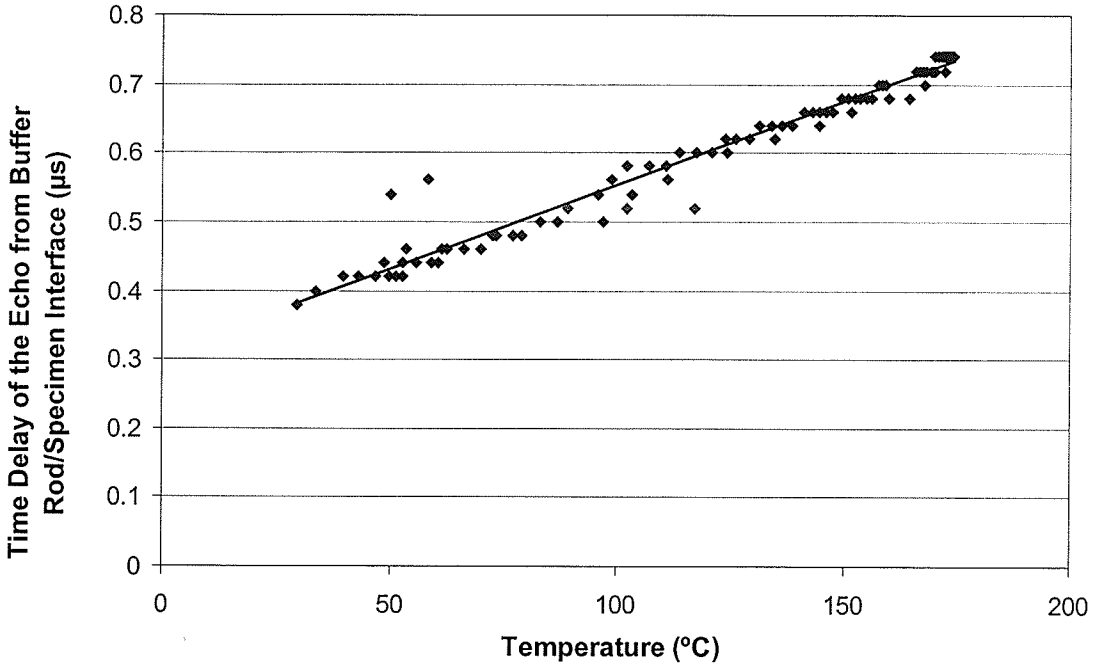

Figure C.5 Variation of the main bang with the cure temperature in cycle R934 T-04

C.1.2 Ultrasonic Response of Composite Specimen

Cure Cycle 4 (HMF T-12)

6-ply specimen was cured at 177°C for 120 minutes. The measured specimen temperature and predicted degree of cure, α, are plotted in Figure C.6. The vacuum was removed when the specimen temperature reached 90°C. After removing the vacuum, 85 psi pressure was applied till the end of cure cycle.

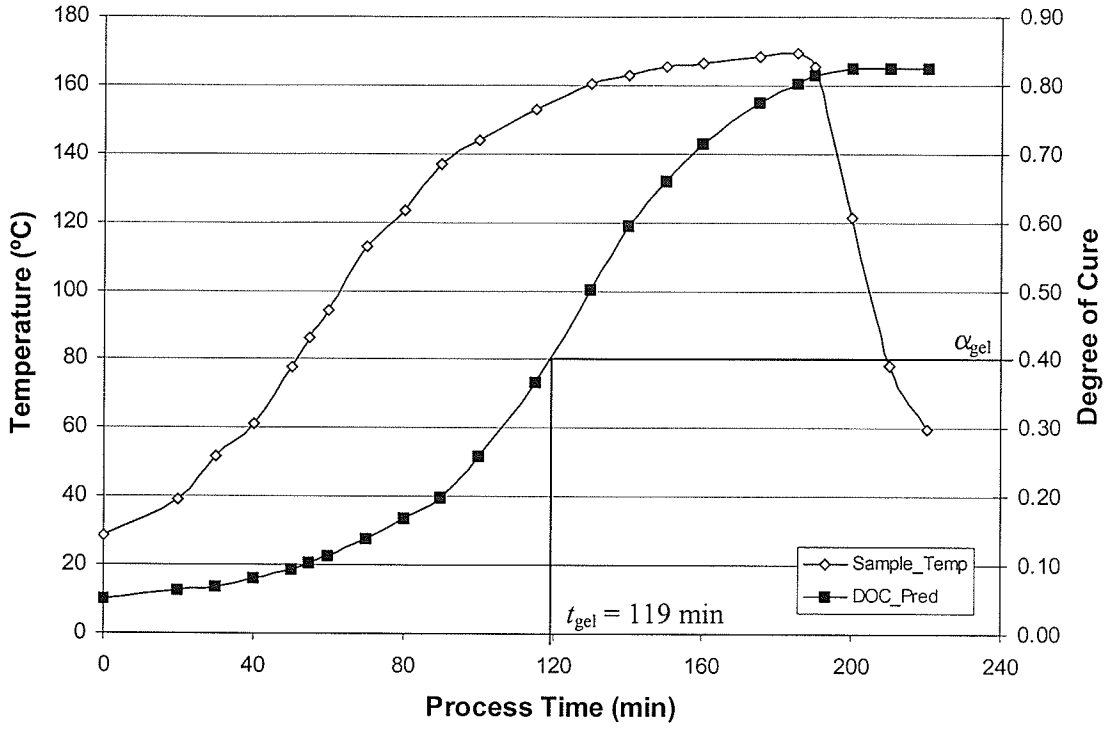

Figure C.6 Part temperature and predicted degree of cure for cycle HMF T-12

The composite specimen reached its minimum viscosity at t = 80 minutes and gelation at t = 119 minutes, respectively. The degree of cure by the end of the cure cycle was 0.83.

As shown in Figure C.7, the time delay and attenuation reached their maximum and minimum values respectively when viscosity was minimum at t = 78 minutes. When gelation occurred, at t = 118 minutes, the time delay was at its inflection point, and the attenuation reached its peak value. At the end stage of curing, both the ultrasonic time delay and attenuation reached a plateau value at t = 160 minutes. The degree of cure at this time was 0.72.

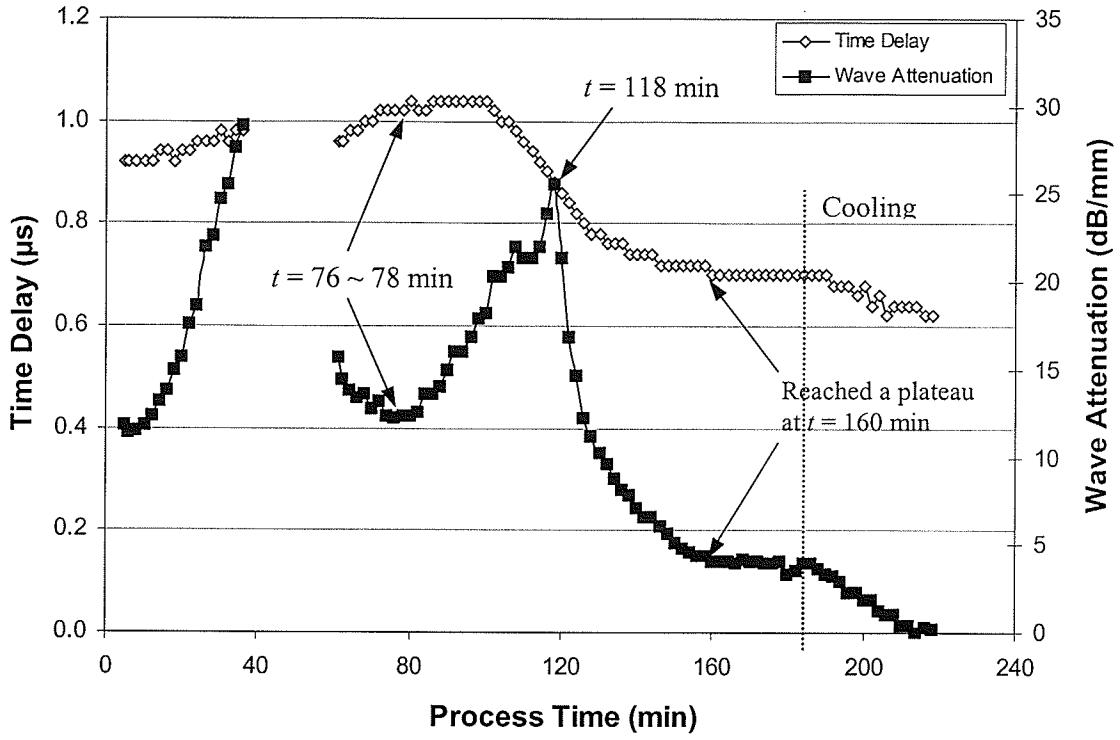

Figure C.7 Time delay and attenuation obtained from the composite specimen in cycle HMF T-12

At the beginning of the experiment, during ramping, the attenuation started to increase until the ultrasonic signals became too weak to detect and totally lost for a period from t = 37 to 60 minutes as shown in Figure C.7. The attenuation signal appeared again at t = 61 minutes when the vacuum was removed and pressure was applied.

HMF T-16 (Cure Cycle 6)

A one-hour postcure procedure at 200°C was applied after the 177°C curing. The degree of cure of the specimen was 0.96 after curing. Gelation occurred at t = 120 minutes, as shown in Figure C.8.

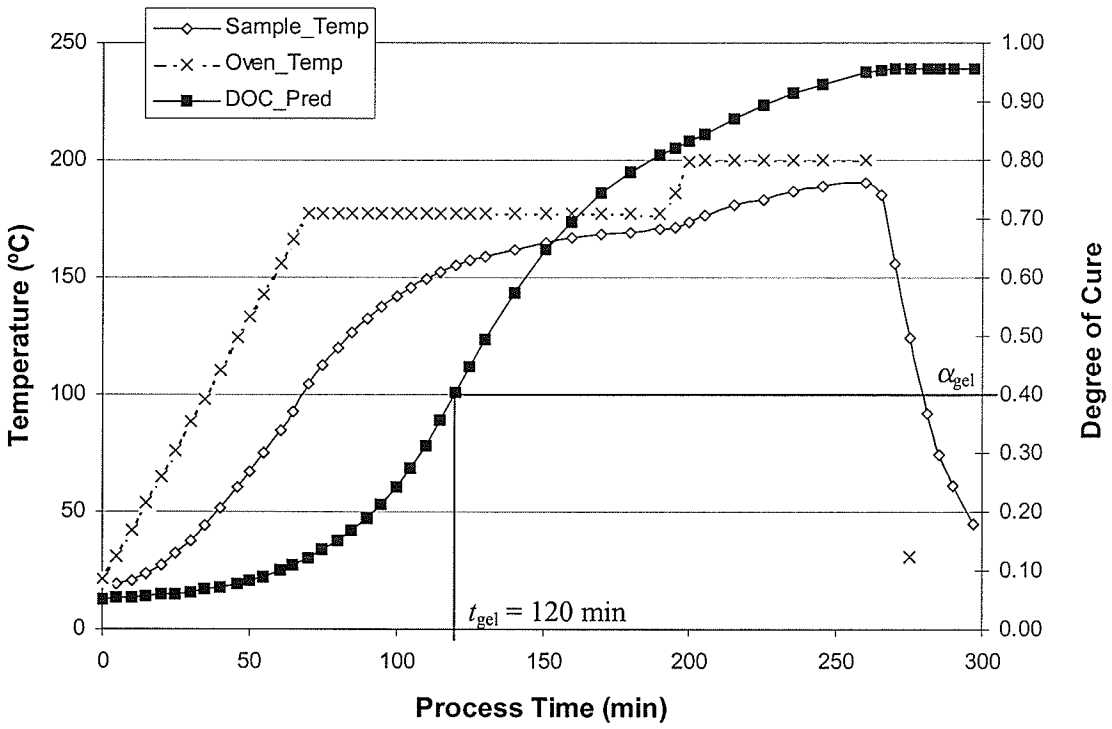

Figure C.8 Part temperature and predicted degree of cure for cure cycle HMF T-16

Both the time delay and attenuation data corresponded to the minimum viscosity and gel point very well as shown in Figure C.9. Because the signals between t = 25 minutes and t = 74 minutes were still very weak, the data in this period shown in the figure is uncertain. After the attenuation reached a peak at the gel time, a second peak appeared at t = 130 minutes, which was much smaller in magnitude. The cause for this second peak is still unclear. The attenuation decreased until it reached a plateau value at t = 162 minutes. When the temperature started to increase to the postcure temperature, the attenuation started to increase because of the increase in thickness of the specimen due to thermal expansion. The time delay was not as sensitive as the attenuation to this change in temperature because of lack of apparent increase in modulus. The ultrasonic signals were lost during ramping to the postcure temperature. The same phenomenon was also

observed in other experiments. This is believed to be due to the separation of the specimen from the mold.

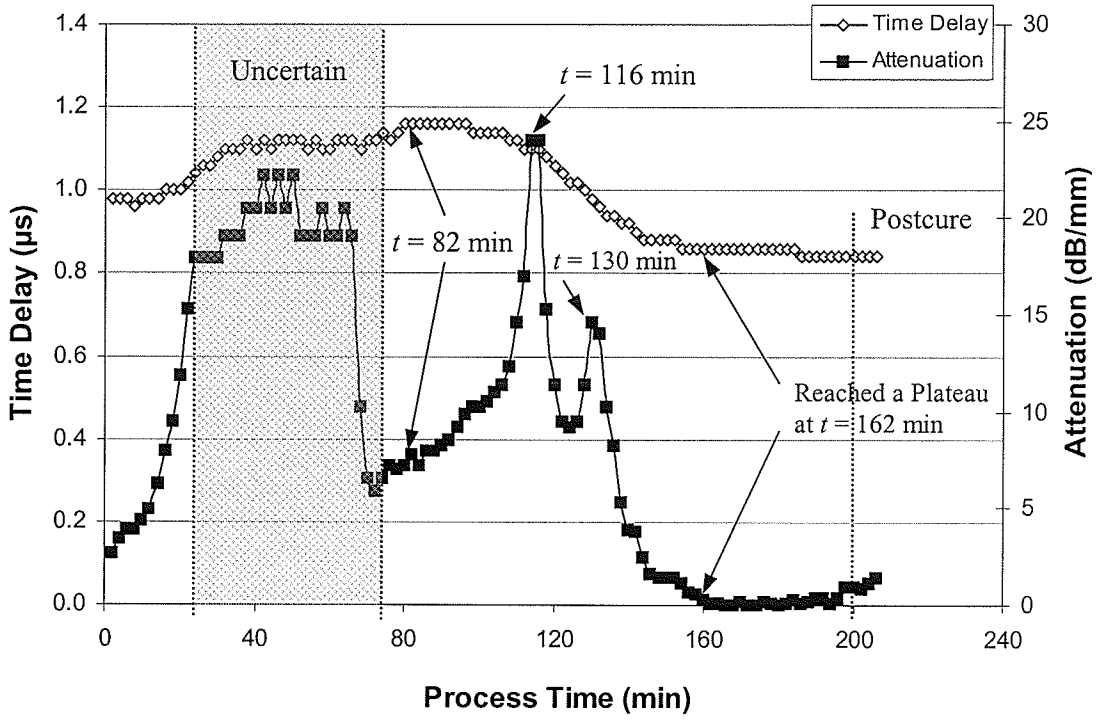

Figure C.9 Time delay and attenuation obtained from the composite specimen in cycle HMF T-16

Cure Cycle 7 (HMF T-17)

In this experiment, to obtain a cured specimen with a higher degree of cure, and avoid the signal loss during the postcure procedure, the specimen was cured at 190°C for 180 minutes, as shown in Figure C.10. The vacuum was removed at t = 90 minutes and the nitrogen pressure was applied. The final degree of cure of the specimen was 0.94. The minimum viscosity and gel point was appeared at t = 80 and t = 108 minutes, respectively.

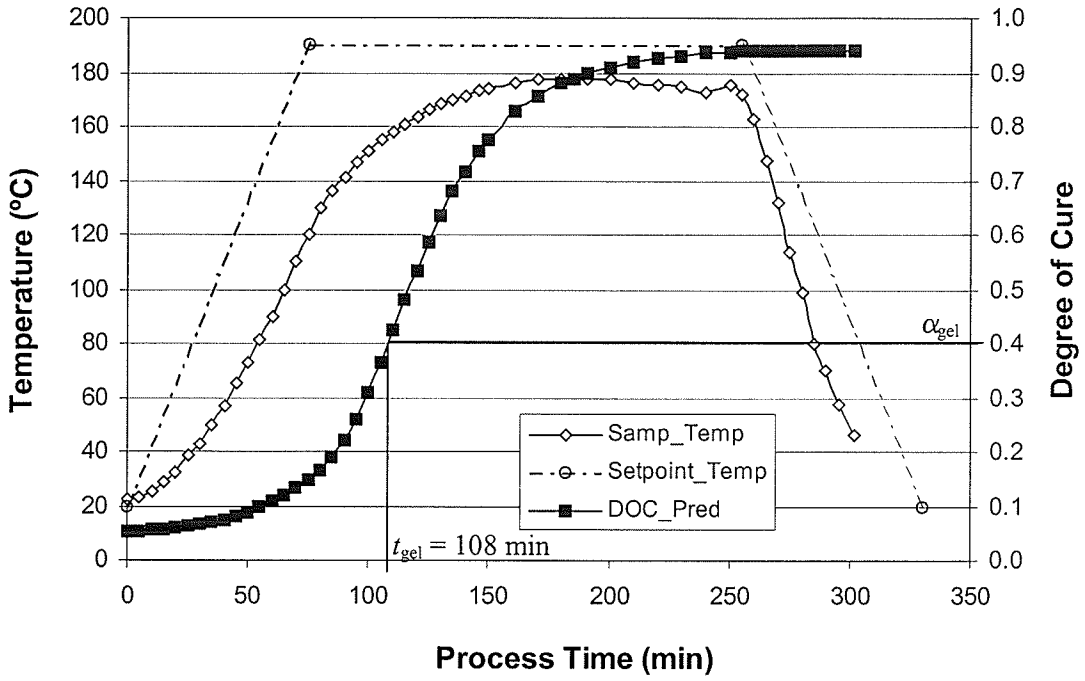

Figure C.10 Part temperature and predicted degree of cure in cycle HMF T_17

As observed in previous experiments, the minimum viscosity and gelation can be clearly determined from the ultrasonic time delay and attenuation data, as shown in Figure C.11. The second peak of attenuation curve occurred at t = 170 minutes. However, it did not correspond to the vitrification, which was predicted to be occurred at t = 191 minutes. The time delay stopped decreasing at t = 144 minute. The attenuation reached the plateau at t = 212 minutes with the degree of cure of 0.92, which was very close to the fully cured state of the specimen.

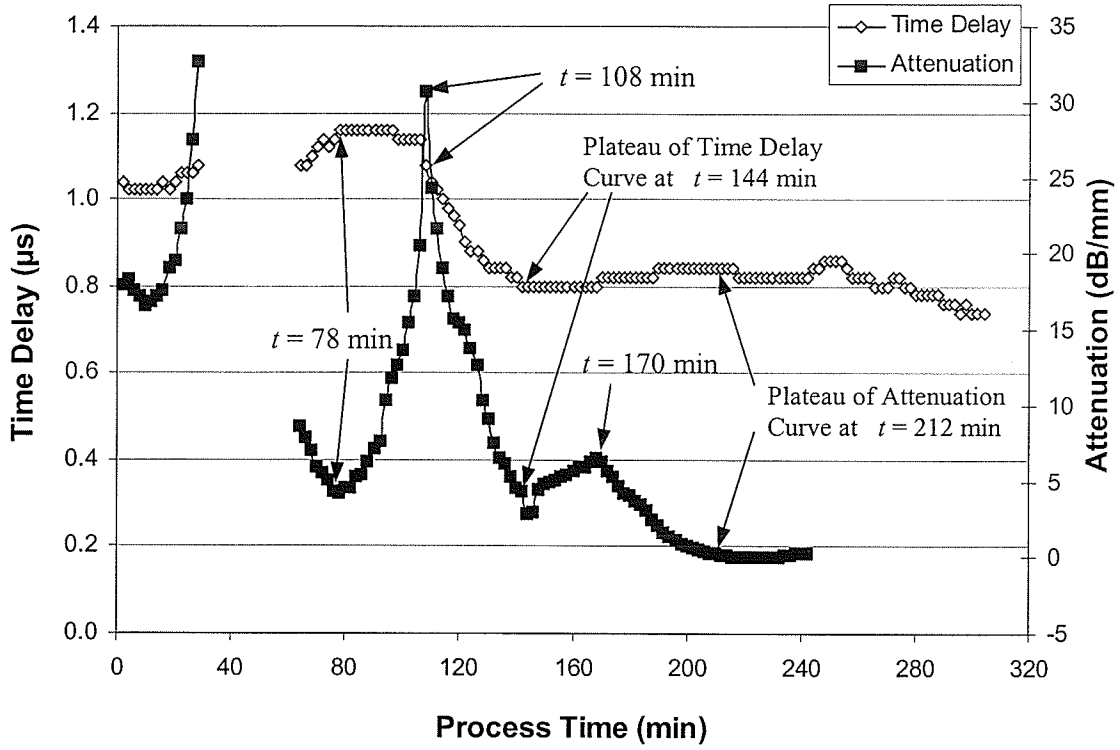

Figure C.11 Time delay and attenuation obtained from the composite specimen in cycle HMF T-17

C.2 Dielectric Cure Monitoring

C.2.1 Dielectric Response of Neat Resin Specimen

Cure Cycle 3 (R934 T-05)

The cure cycle for R934 T-05 has been described in ultrasonic monitoring experiments. 85 psi pressure was applied during the entire cycle. The minimum viscosity and gelation occurred at t = 76.4 minutes and t = 107.3 minutes, respectively. At the end of curing, the degree of cure of the specimen was 0.965.

As shown in Figure C.12, the ionic viscosity reached its minimum value at t = 74 minute. At this time, dlog IV/dt passed through zero value. When the gelation happened, the ionic

viscosity started to increase sharply but had not yet reached the inflection point. dlog IV/dt approached zero at about t = 190 minute, when the ionic viscosity reached a local minimum value. At the end of the holding stage, the specimen temperature was 175°C and the degree of cure was 0.862. The ionic viscosity increased as the ion mobility increased with the increase in specimen temperature during postcure procedure. At the cooling stage, the ionic viscosity data extracted at different frequencies did not superimpose. The reason could be due to the thermal expansion difference between the sensor and specimen, a certain extent of contact change at the interface occurred, which affected the dielectric response.

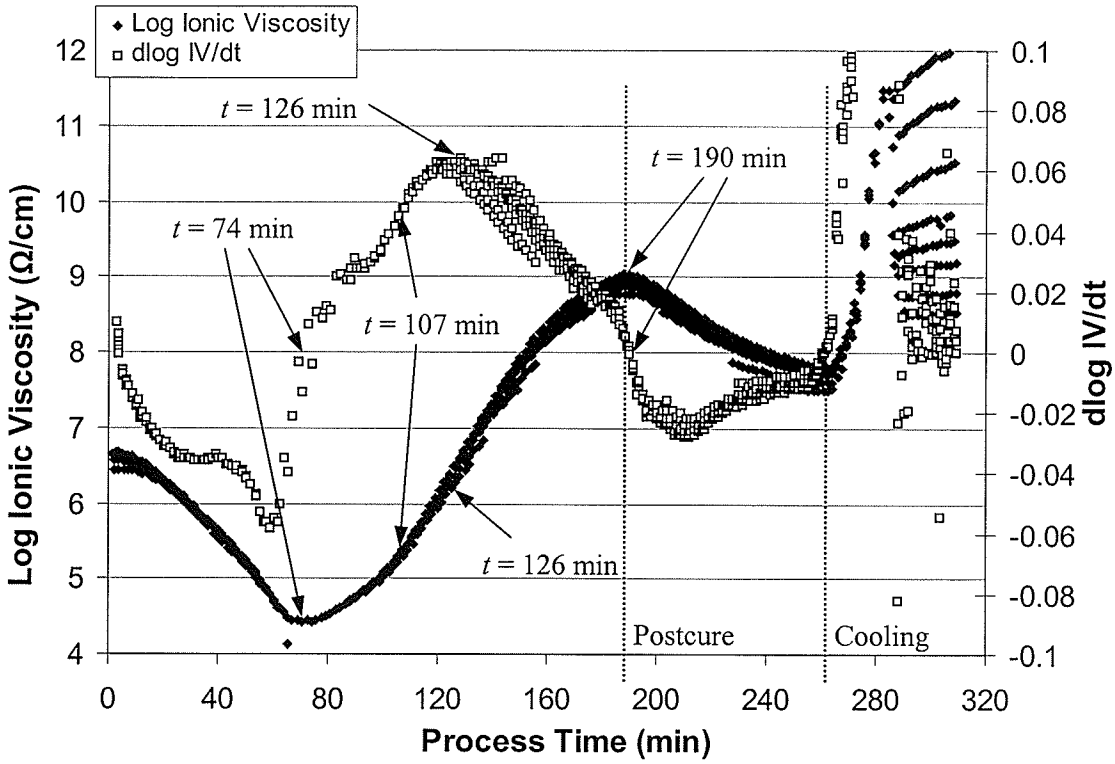

Figure C.12 log Ionic Viscosity and dlog IV/dt obtained in cycle R934 T-05

C.2.2 Dielectric Response of Composite Specimen

Cure Cycle 5 (HMF T-13)

The MRC (Manufacturer Recommended Cycle) plus a 1-hour's postcure procedure and a 6-ply composite specimen was applied in this experiment. The specimen's degree of cure was 0.962 after curing. The minimum viscosity and gelation occurred at t = 85 minutes and t = 119.2 minutes, respectively, as shown in Figure C.13.

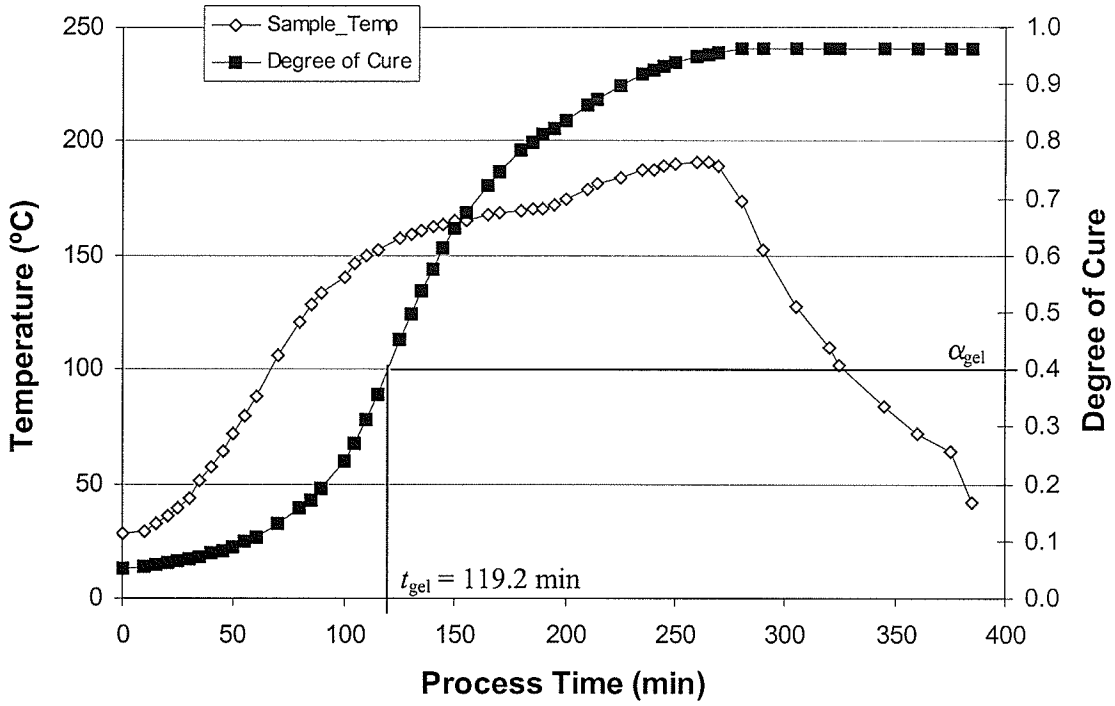

Figure C.13 Part temperature and predicted degree of cure for cure cycle HMF T-13

As shown in Figure C.14, the ionic viscosity reached its minimum value at t = 82 minutes, which corresponded well to the time for the minimum viscosity. When the gelation happened at t = 119.2 minutes, the ionic viscosity approached its inflection point, where dlog IV/dt reached a peak value. In the postcure stage, because of the elevated temperature, the ionic viscosity increased. A slight scatter in the ionic viscosity data was observed during postcure, which could have been caused by the changes at the

interface of the sensor and specimen. dlog IV/dt approached zero value at about t = 189.3 minutes.

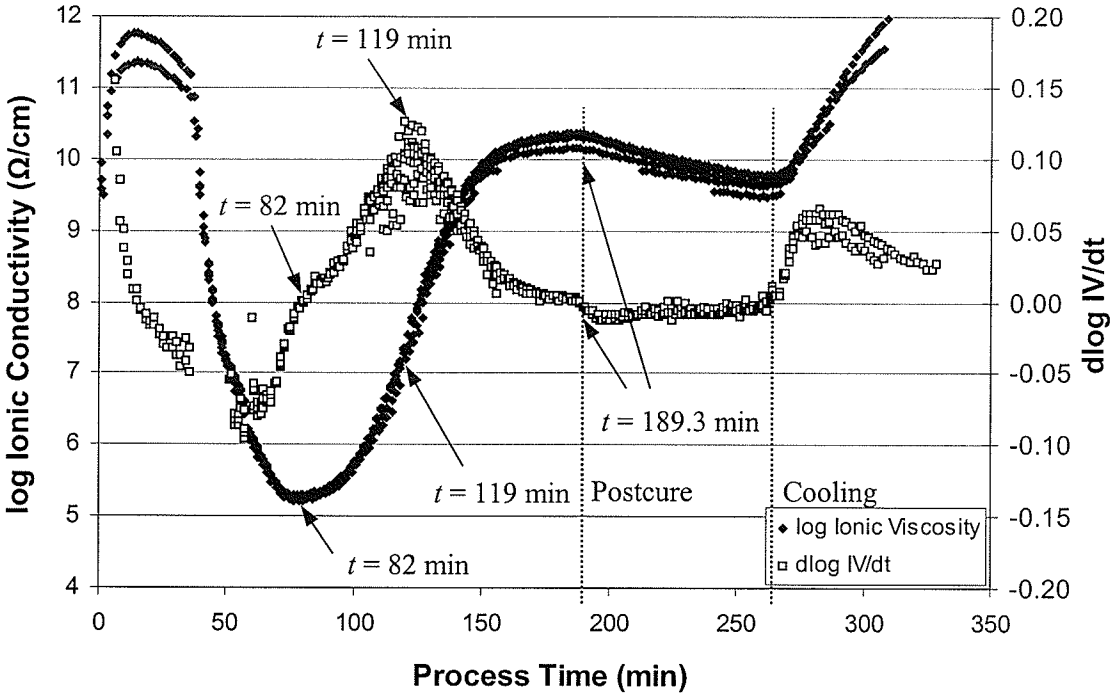

Figure C.14 log Ionic Viscosity and dlog IV/dt data for cycle HMF T-17

C.2.3 Dielectric Response of Neat Resin Specimens in Isothermal Experiments

Isothermal experiments at 164, 176 and 190°C were performed. The figure for temperature and degree of cure of these experiments can be found in 4.2.2.4. All experiments used the same procedure. The mold was pre-heated to the pre-determined isothermal temperature. The resin was subsequently poured over the sensor bonded to the bottom of the mold and the oven door was closed within half a minute. It took about 5 minutes for the resin to return to the pre-determined temperature. Since the mold had to be left open, to enable pouring the resin, the vacuum and pressure could not be applied. In the experiment conducted at 164°C, the specimen temperature was stable at about

162.5°C and was cured for 5 hours. The predicted degree of cure by the end of the cycle was 0.88. The gelation was predicted to occur at t = 10.3 minutes. Since the resin cured faster at this temperature, the minimum viscosity occurred during the time for stabilizing of the temperature after pouring the resin. Hence signals corresponding to minimum viscosity were rarely obtained. The results for experiments performed at 176°C and 190°C can be found in Table 4.6.

As shown in Figures C.15 and C.16, as the resin cured at 164°C, the ionic viscosity increased rapidly until it reached a plateau value at around t = 247 minutes, when dlog IV/dt was equal to zero with a DOC of 0.86. It was not easy to determine the gel time by dielectric monitoring data in this case because of the high rate of reaction. The gelation occurred during the heat-up procedure to the cure temperature.

Log Ionic Viscosity and dlog IV/dt data of specimens cured at 164°C, 176°C and 190°C are compared in Figures C.15 and C.16. As expected, the specimen processed at a higher temperature cured faster. It is observed that the log Ionic Viscosity of the specimens cured at 164°C, 176°C and 190°C reached plateau values at t = 244.6, 78.8 and 35.2 minutes, respectively. The DOC of specimens at this time was 0.86, 0.89 and 0.87, respectively. It is very close to the process time when the predicted vitrification occurred at t = 244, 78.2 and 57.2 minutes. However, as discussed in previous chapters, the specimens did not reach the end of cure state.

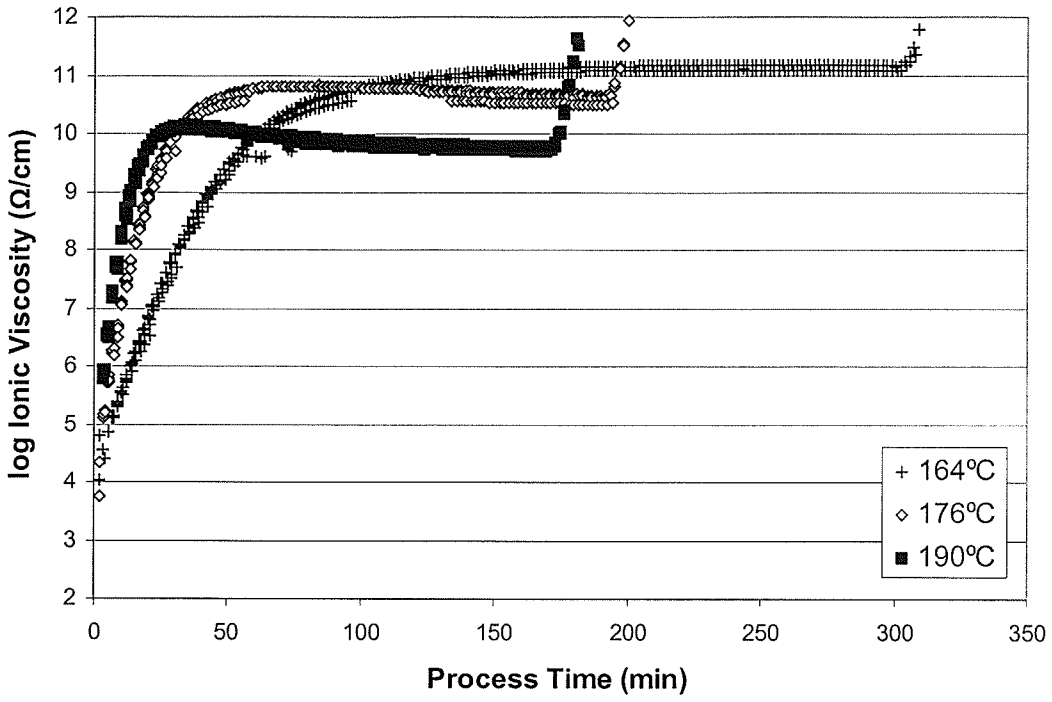

Figure C.15 log Ionic Conductivity data obtained in isothermal experiments with 934 neat resin system

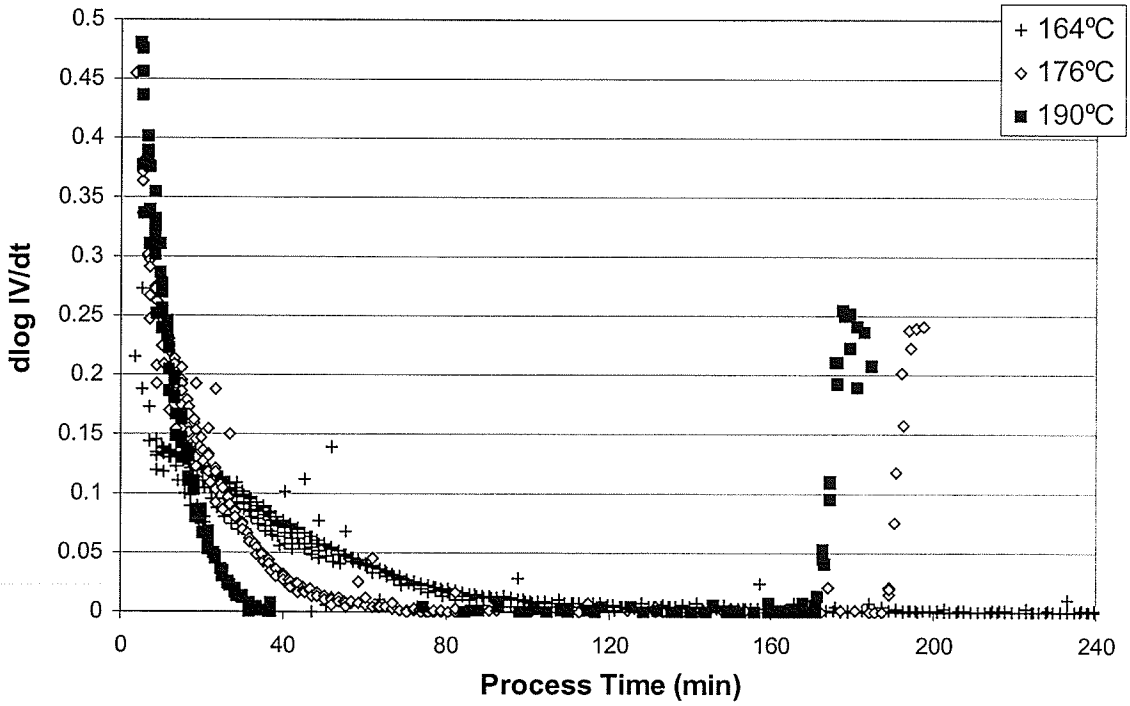

Figure C.16 dlog IV/dt data obtained in isothermal experiments with 934 neat resin system

Efforts on correlation of vitrification with permittivity data

Log Loss Factor and log Permittivity for the neat resin specimen cured at 164°C are plotted in figures, which can be found in 4.2.2.4. Although the temperature effect on the dielectric response was eliminated by performing isothermal experiment, a high level of log Permittivity values were still observed at the beginning stage of the cure and low frequencies. No dipolar loss peak could be observed. The relationship between the dipole contribution and material parameters still cannot be obtained.

As discussed in Chapter 2, G. M. Maistros et al. (25) reported that the vitrification time correlated approximately with time corresponding to the dipolar loss peak at a frequency of 1 Hz. The frequency of the dielectric loss peak is the frequency at which permittivity is half-way between the static (ϵ_s) and infinite frequency values (ϵ_∞). A plot of ϵ' vs. $\log f$ of a DGEBA (diglycidyl ether of bisphenol A) polymer as a function of process time in an isothermal experiment is shown in Figure C.17. The high value at low frequencies can be deemed as relaxed permittivity ϵ_s, and the low value at high frequency end is the unrelaxed (infinite frequency) permittivity ϵ_∞ Thus the midpoints of curves at different time points between ϵ_s and ϵ_∞ can be determined. Because few researches tried to correlate the dipole contribution to material parameters, it is also desirable to verify its observation in this study, although this method still cannot be used to establish the correlation of dipole item with other parameters than vitrification, such as degree of cure and T_g.

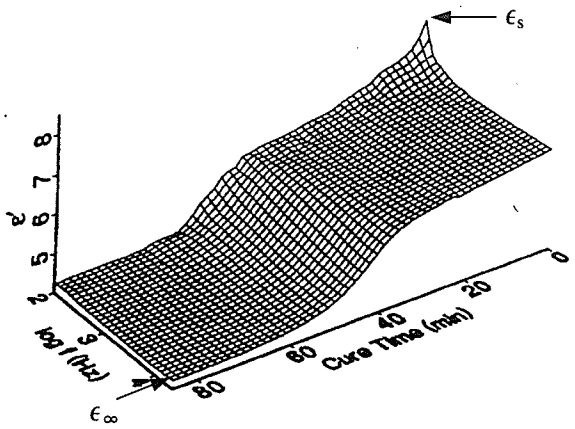

Figure C.17 Permittivity vs. log frequency of a DGEBA polymer in an isothermal experiment (G. M. Maristros et al. (26))

The permittivity data of the specimen cured at 164°C is shown in Figure C.18. Following the same method as used in reference (25), high values at 0.1 Hz was selected as ϵ_s, while low values at 100,000 Hz was deemed as ϵ_∞. Hence the midpoint between ϵ_s and ϵ_∞ for each frequency can be decided. The time corresponding to the midpoint of 1 Hz scanning data was determined as t = 65.1 minutes as shown in the figure. However, this value is not correct since the predicted vitrification occurred at t = 244 minutes. As shown in the Cole-Cole plot in Figure C.19, from which it is difficult to determine the relaxed and unrelaxed permittivity values, the relaxation time etc. Hence the raw data of dielectric response cannot be used in correlation of vitrification.

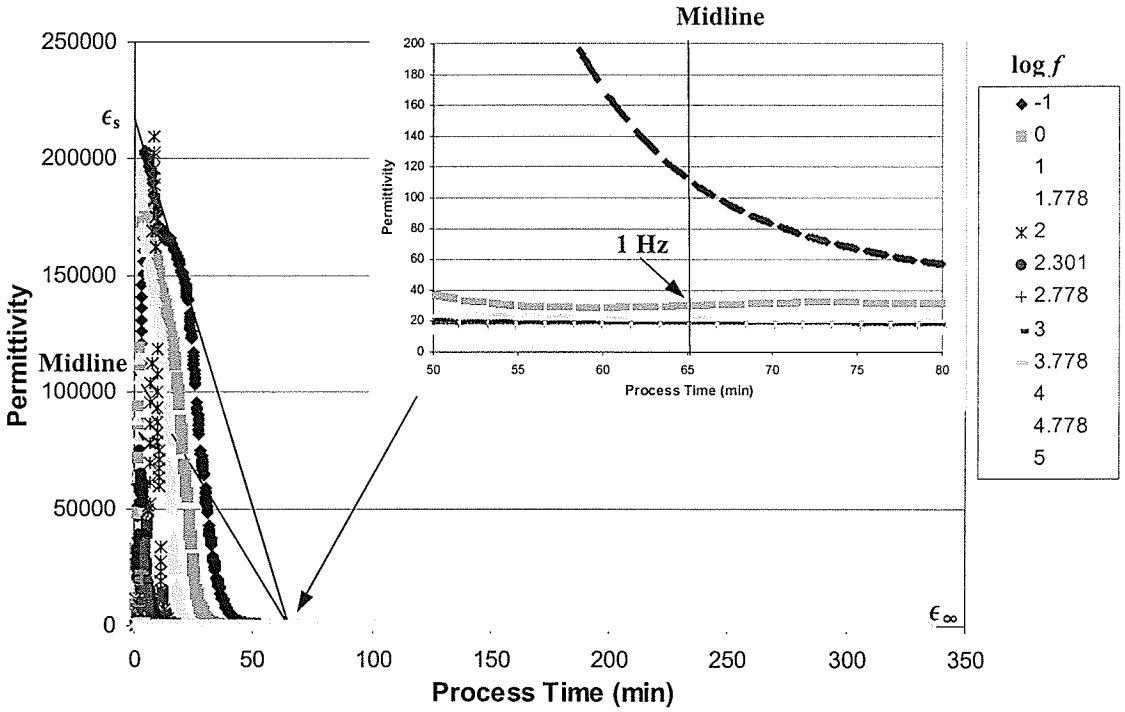

Figure C.18 Method of estimating the time when the loss peak occurred at each frequency

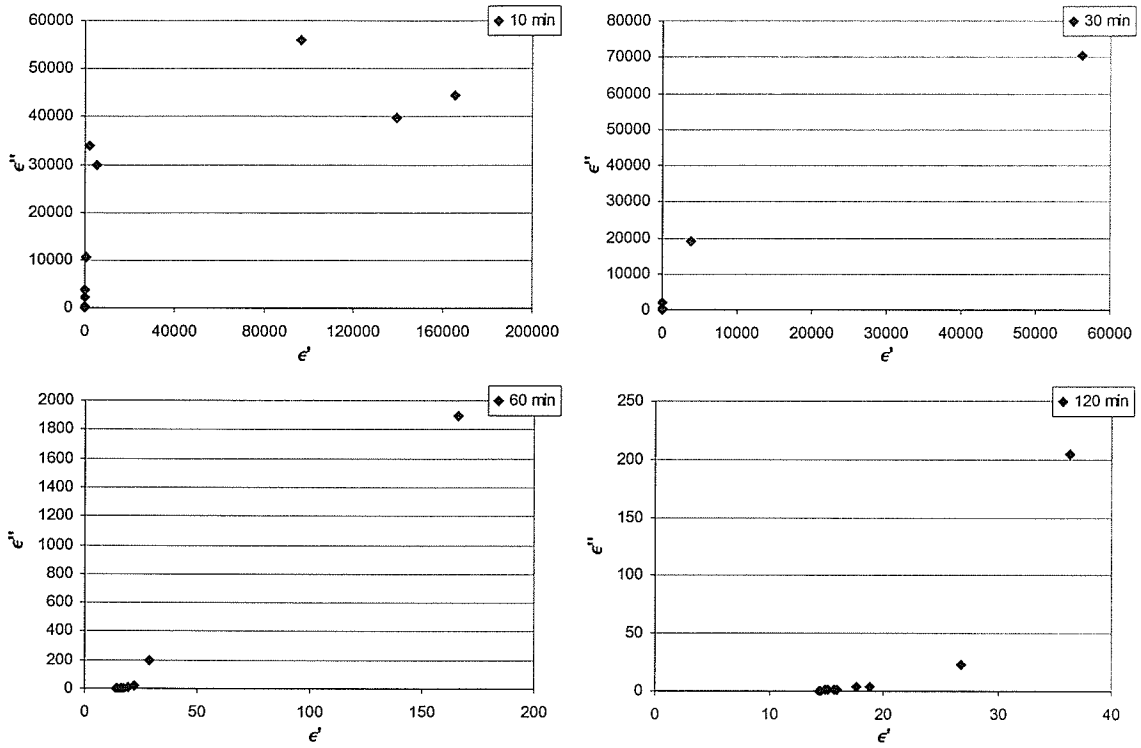

Figure C.19 Cole-Cole plot at different process time of cycle R934 T-08

Efforts for correction of electrode polarization effect

All the results shown above are extracted from the raw data without removing the effects of the electrode polarization and hence, efforts were made to eliminate its influence.

The EPC (Electrode Polarization Correction) function has been built in EUMETRIC, the control and data acquisition software for DEA 230/1. This routine assigns the user defined relaxed permittivity value to any measured data, which has a higher value than the defined one. The software corrects the loss factor values based on the modified permittivity values. The corrected loss factor and permittivity data are shown in Figures C.20 and C.21.

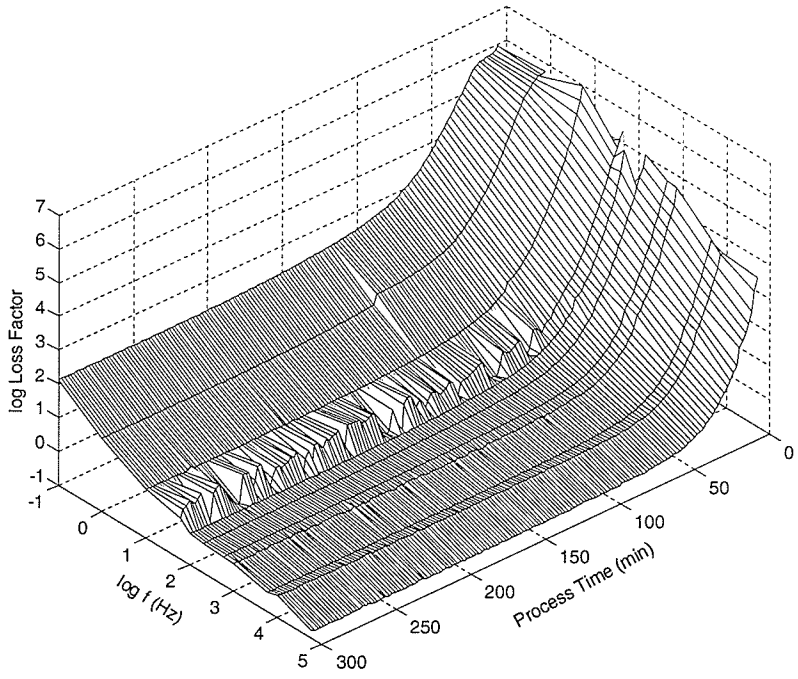

Figure C.20 log Loss Factor after EPC by software for cycle R934 T-08

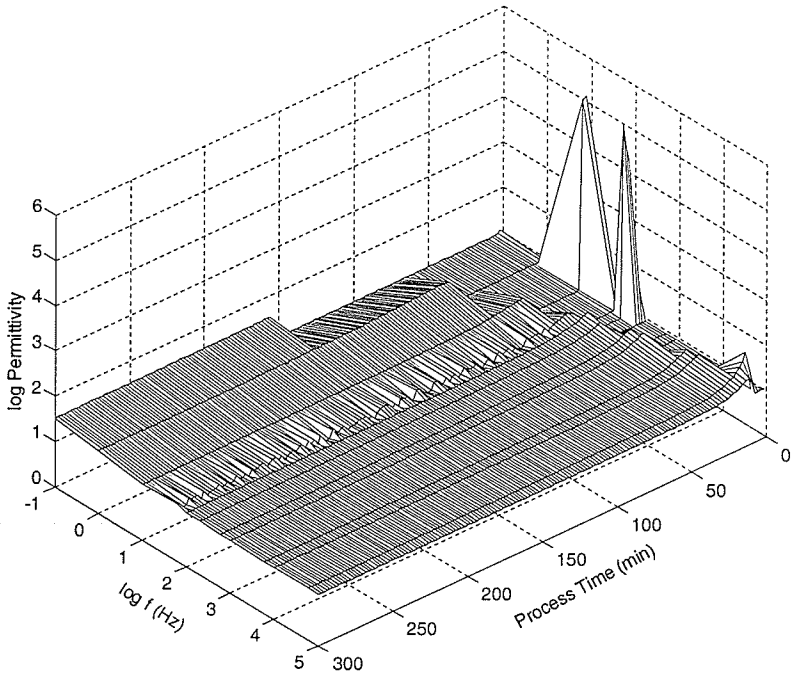

Figure C.21 log Permittivity after EPC by software for cycle R934 T-08

As the software dose not really correct the electrode polarization effect to permittivity data based on calculations, this work can be conducted using the following equations:

$$\varepsilon'_x = \varepsilon' R\left[\frac{\left(\frac{\varepsilon''}{\varepsilon'}\right)^2 + R}{\left(\frac{\varepsilon''}{\varepsilon'}\right)^2 + R^2}\right] \tag{C.1}$$

$$\varepsilon''_x = \varepsilon'' R\left[\frac{R-1}{\left(\frac{\varepsilon''}{\varepsilon'}\right)^2 + R^2}\right] \tag{C.2}$$

where ϵ'_x is the experimentally measured permittivity

ϵ''_x is the experimentally measured loss factor

ϵ' is the actual permittivity

ϵ'' is the actual loss factor

$R = \frac{L}{2t_b}$ (L is the plate separation (electrode spacing), and t_b is the blocking layer thickness) (C.3)

One problem with the EPC is that it requires one additional resin system constant as the input. The constant is referred to as ϵ'_o or the low frequency dielectric constant, or relaxed permittivity, i.e. ϵ_s, which for most epoxy systems is about 10. As the EPC is not a critically strong function of ϵ'_o, in many cases if ϵ'_o is not known, a value of 10 works well. In this study, the ϵ'_o value was selected from the real experiment data for ϵ_s. In order to solve the equations, the R value must be calculated. On a Cole-Cole plot the electrode polarization phenomenon appears as a semicircle whereas in the absence of electrode

polarization, only a vertical line due to high loss factor is obtained, as shown in Figure 2.4. The Cole-Cole plot for R934 T-08 at different processing time is plotted in Figure 4.19. As shown in Figure C.22, in theory, the right ϵ' axis intercept of the electrode polarization semicircle is equal to $\epsilon'_o R$. The left intercept is equal to ϵ'_o. The left intercept point could be known from plot, one point on the semicircle (ϵ'_x and ϵ''_x), and the fact that the center of the circle is on the ϵ'_x axis, the right intercept and therefore R can be calculated. The expression for R is:

$$R = \frac{L}{2t_b} = \left(\frac{\varepsilon'^{\,2}_x + \varepsilon''^{\,2}_x - \varepsilon'^{\,2}_o}{\varepsilon'_x - \varepsilon'_o} - \varepsilon'_o \right) \frac{1}{\varepsilon'_o} \tag{C.4}$$

Substituting ϵ'_o for ϵ' into equation (4.3), since ϵ' theoretically equals to ϵ'_o in regions of high molecular mobility, which is also where electrode polarization occurs:

$$\varepsilon'' = \varepsilon'_o \left(\frac{R^2(\varepsilon'_o - \varepsilon'_x)}{\varepsilon'_x - \varepsilon'_o R} \right)^{\frac{1}{2}} \tag{C.5}$$

Thus ϵ'' can be calculated from ϵ'_x and ϵ''_x.

To correct ϵ' values, use the formulation derived from the above equations:

$$\varepsilon' = \varepsilon'' \sqrt{\frac{\varepsilon''_x}{\varepsilon'' R(R-1) - \varepsilon''_x R^2}} \tag{C.6}$$

The calculated ϵ' and ϵ'' are shown in Figure C.23 and C.24.

http

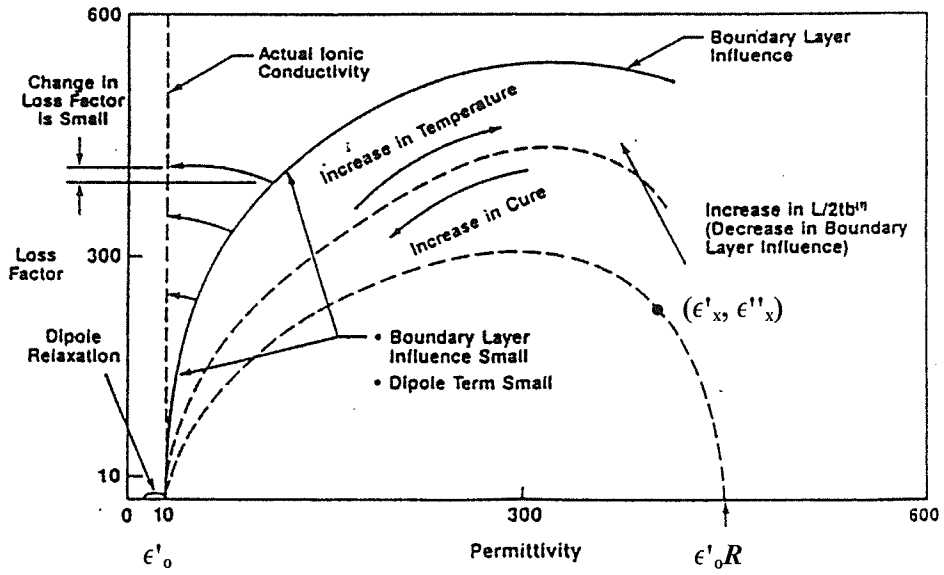

Figure C.22 Parameters for electrode polarization correction

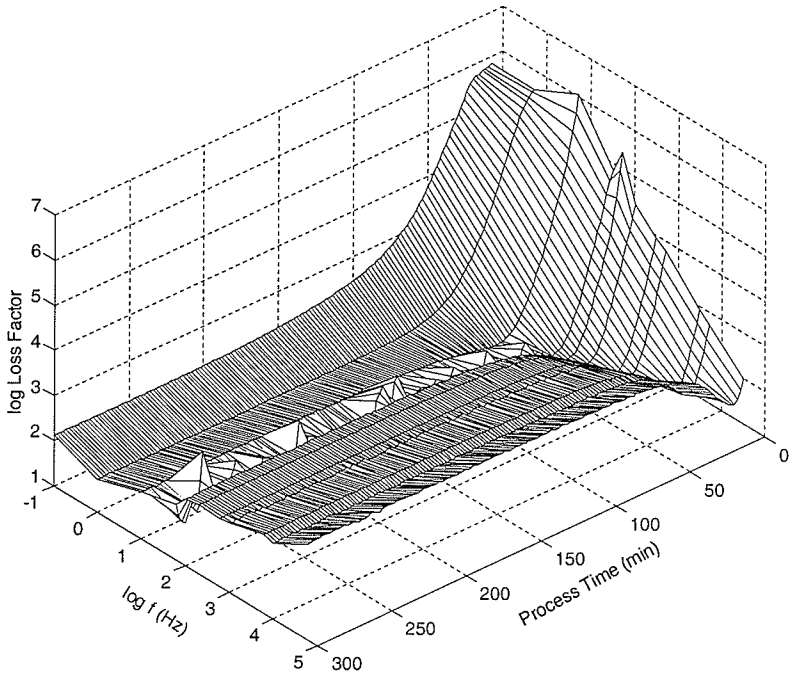

Figure C.23 log Loss Factor after EPC by calculation for cycle R934 T-08

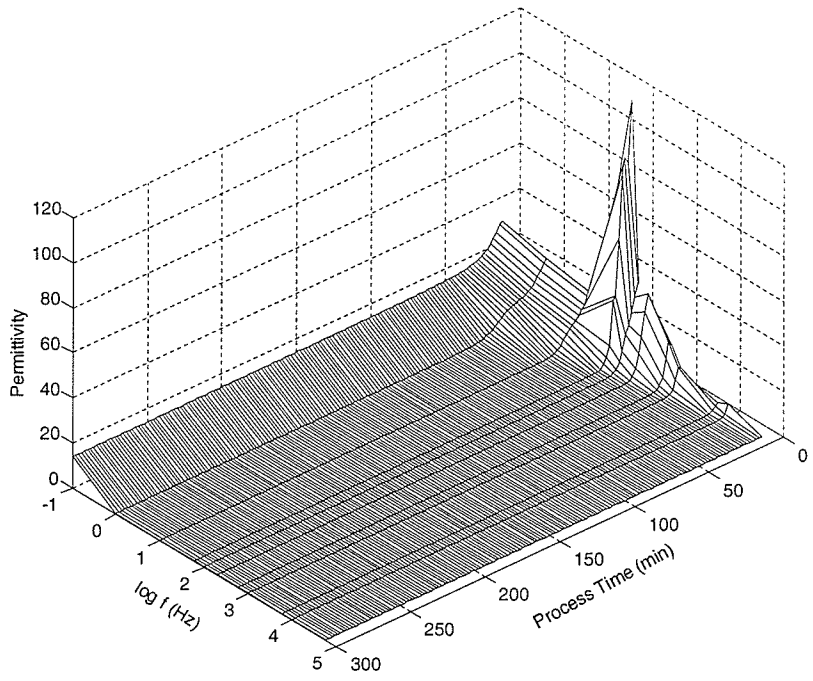

Figure C.24 Permittivity after EPC by calculation for cycle R934 T-08

From both the ϵ" plots obtained by the software or calculations, it can be seen that the dipole relaxation peak still cannot be observed. The same condition occurred in the room temperature cured fiberglass resin system. This could be due to the difference between dielectric properties of materials and equipment used in current experiments and in other research works.

The Cole-Cole plot after EPC by calculation of R934 T-08 is shown in Figure C.25. Unfortunately, the plots still significantly deviated from the typical shapes and the relevant parameters are difficult to determine.

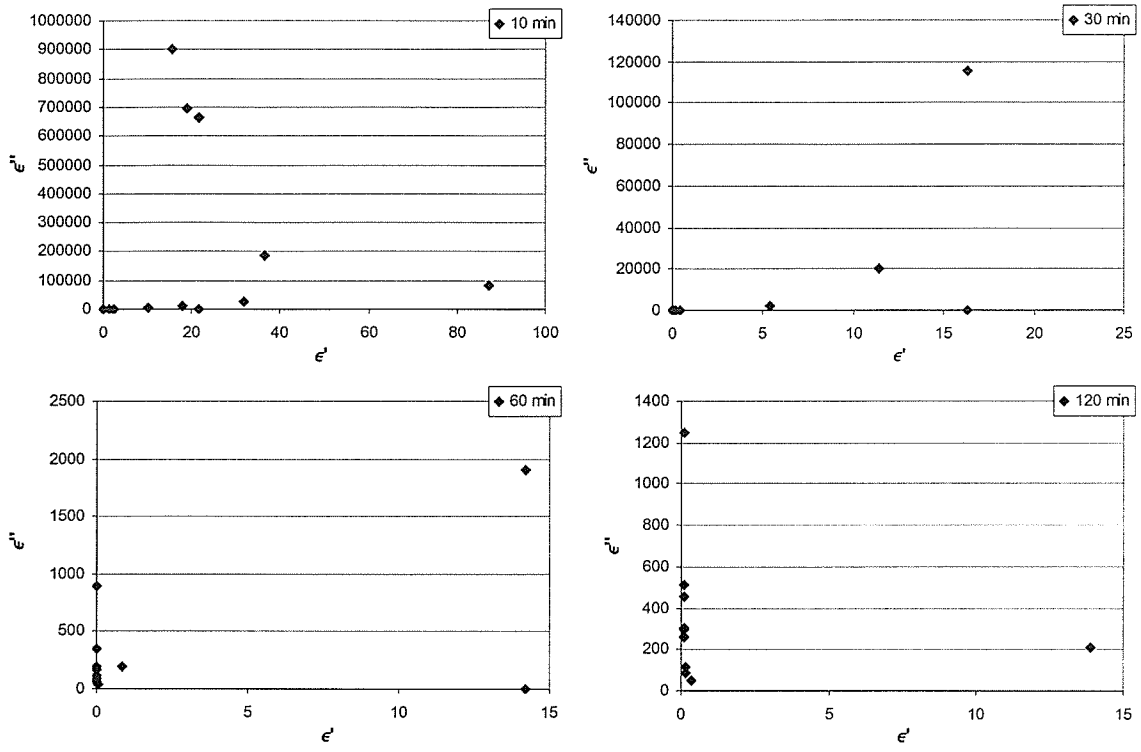

Figure C.25 Cole-Cole plot after EPC by calculation for cycle R934 T-08

The plot of corrected permittivity as a function of log frequencies also shows incomplete reaction curves at each frequency, and the determination of vitrification becomes impossible, as illustrated in Figure C.26. The same condition is observed in the room temperature cured fiberglass resin system. Hence the method reported in the research work of G. M. Maistros et al. (25) is not applicable for the equipment and materials used in current studies. The dipole contribution could not be extracted from the measured permittivity and loss factor data in this study, and the fundamental relationship between the dielectric response and material parameters could not be established.

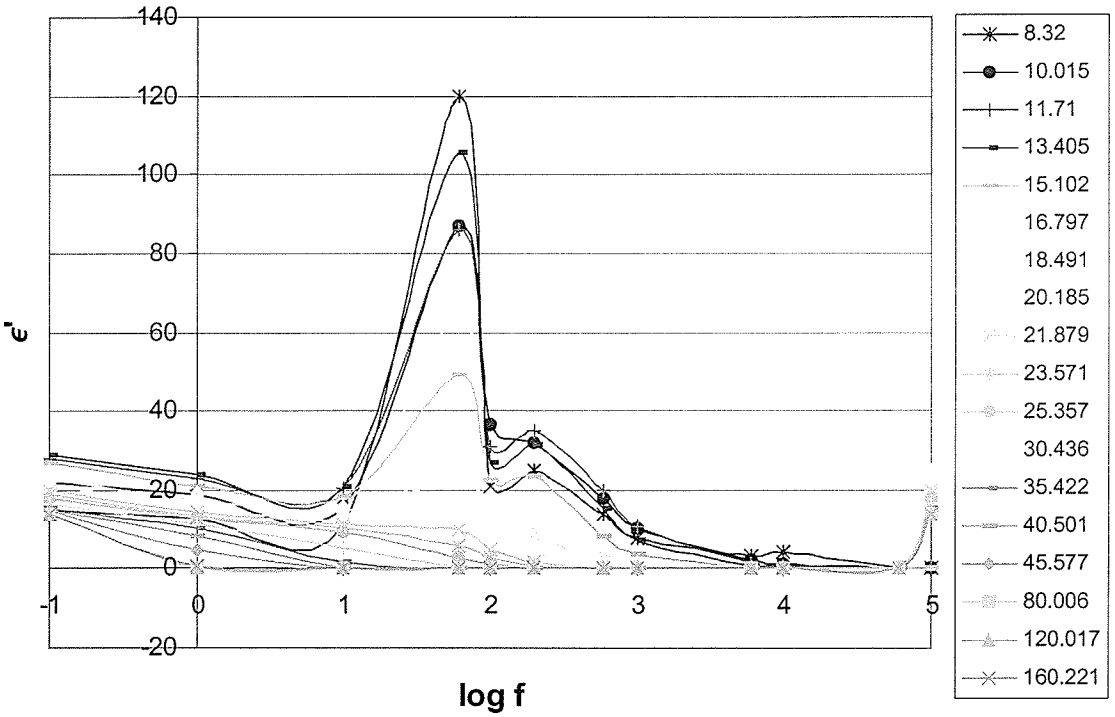

Figure C.26 Permittivity vs. log frequency after EPC for cycle R934 T-08

C.3 FBG Sensor Cure Monitoring

Cure Cycle 11 (HMF T-25)

As discussed in 4.2.3, if the sensitivity coefficient of the FBG sensor to temperature is assumed to be a constant value of 11.25×10^{-6} /°C, the actual strain (cure induced strain) can be calculated after compensating for the thermal expansion of the sensor using the assumption that the effects of strain and temperature could be separated by:

$$\varepsilon_{total} = \varepsilon_{actual} + \varepsilon_{sensor\ \ thermal\ \ expansion} \tag{C.7}$$

However, this assumption may be invalid for low degrees of cure values when the sensor has not bonded to the resin. The calculated actual strain is shown in Figure C.27.

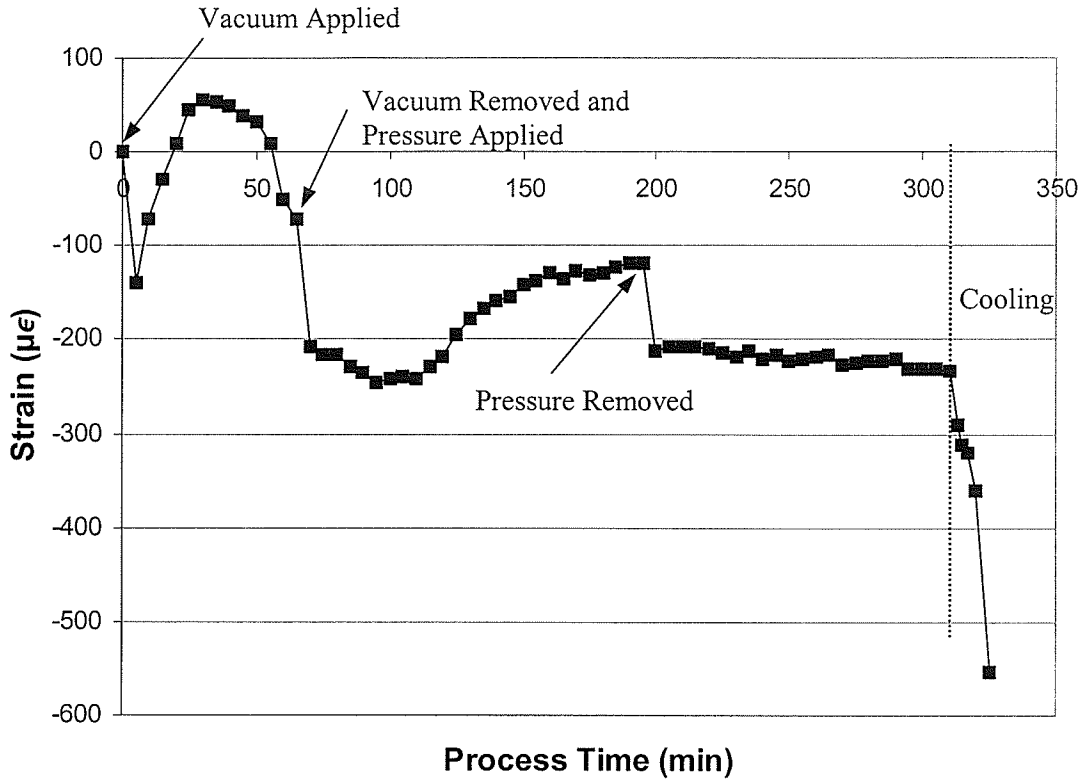

Figure C.27 Actual strain obtained after compensating for the thermal effect of the sensor

The actual strain (cure induced strain) results from two contributions: the thermal expansion of the specimen at elevated temperature and the chemical cure shrinkage induced in the resin during the processing, i.e.

$$\varepsilon_{actual} = \varepsilon_t + \varepsilon_c \tag{C.8}$$

where ϵ_t is the strain induced by thermal expansion of the specimen and ϵ_c is the strain caused by cure shrinkage. ϵ_t can be represented as:

$$\varepsilon_t = \alpha(T - T_0) \tag{C.9}$$

where T_0 is the room temperature (reference temperature, which is set at 20°C) and T is temperature at any instant during curing.

Hence the strain due to cure shrinkage can be calculated as:

$$\varepsilon_c = \varepsilon_{actual} - \varepsilon_t \tag{C.10}$$

The coefficient of thermal expansion (CTE) of the woven prepreg had been calculated using the model established in 4.2.3 and lamination theory to be

$$\alpha_{11} = \alpha_{22} = 5.354 \times 10^{-6} /^{\circ}C \tag{C.11}$$

The cure shrinkage obtained based on the experiment data is shown in Figure C.28.

To verify the measurement results, the cure shrinkage was also calculated based on the model developed by reference (3). The cure shrinkage of the unidirectional lamina was experimentally determined to be a function of degree of cure as:

$$\varepsilon_{11}^c = -6.924 \times 10^{-4} \alpha + 9.122 \times 10^{-6} \quad (37\% < \alpha < 71\%) \tag{C.12}$$

and $$\varepsilon_{22}^c = \varepsilon_{33}^c = -4.1882 \times 10^{-2} \alpha + 1.3005 \times 10^{-2} \quad (37\% < \alpha < 100\%) \tag{C.13}$$

The total cure shrinkage in the longitudinal and transverse directions for 100% cured unidirectional laminate was determined experimentally to be

$$\epsilon^c_{11} = -0.048\% \tag{C.14}$$

$$\epsilon^c_{22} = \epsilon^c_{33} = -2.49\% \tag{C.15}$$

The cure shrinkage of the woven composite specimen with a degree of cure of 0.90 was calculated to be

$$\epsilon^c_{11} = \epsilon^c_{22} = -0.186\% \tag{C.16}$$

The measured cure shrinkage and calculated values using the model are compared in Figure C.28.

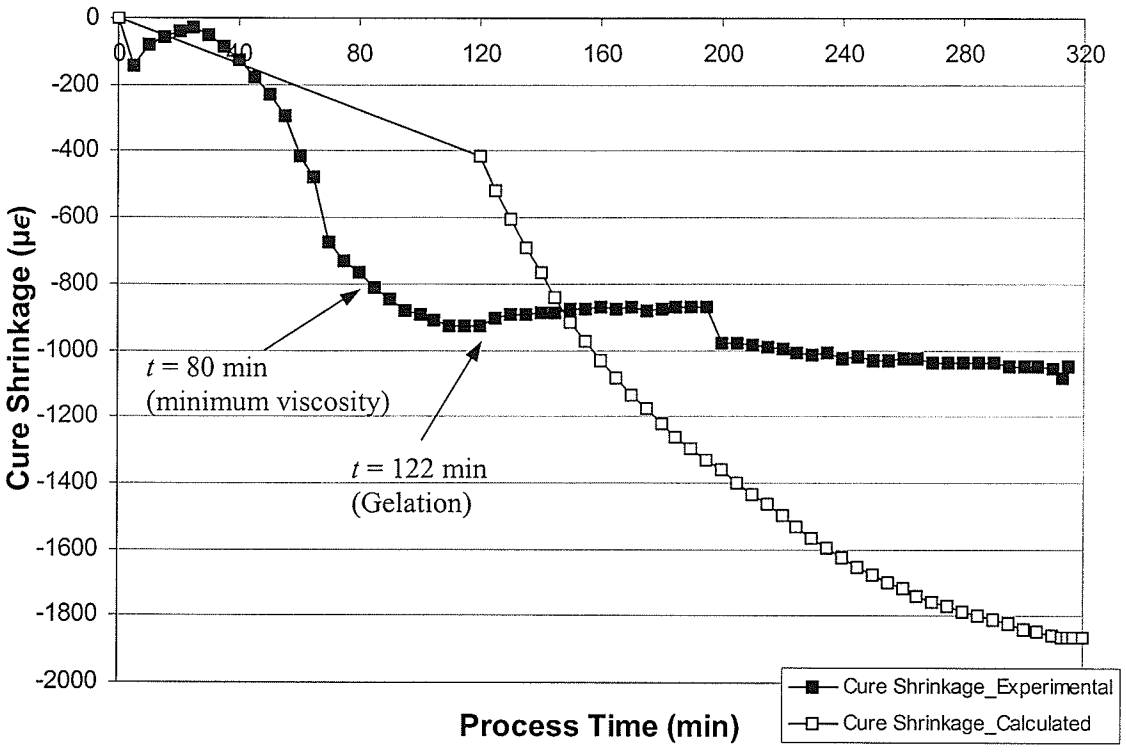

Figure C.28 Cure shrinkage of the composite part in cycle HMF T-25

As expected, the result is found to be not correct comparing with the value predicted by the model. The reason has been discussed in 4.2.3, and will not be repeated in this appendix.